

ISSN 1881-7815 Online ISSN 1881-7823

BST

BioScience Trends

Volume 12, Number 4
August, 2018



www.biosciencetrends.com

BST

BioScience Trends



ISSN: 1881-7815
Online ISSN: 1881-7823

CODEN: BTIRCZ

Issues/Year: 6

Language: English

Publisher: IACMHR Co., Ltd.

BioScience Trends is one of a series of peer-reviewed journals of the International Research and Cooperation Association for Bio & Socio-Sciences Advancement (IRCA-BSSA) Group and is published bimonthly by the International Advancement Center for Medicine & Health Research Co., Ltd. (IACMHR Co., Ltd.) and supported by the IRCA-BSSA and Shandong University China-Japan Cooperation Center for Drug Discovery & Screening (SDU-DDSC).

BioScience Trends devotes to publishing the latest and most exciting advances in scientific research. Articles cover fields of life science such as biochemistry, molecular biology, clinical research, public health, medical care system, and social science in order to encourage cooperation and exchange among scientists and clinical researchers.

BioScience Trends publishes Original Articles, Brief Reports, Reviews, Policy Forum articles, Case Reports, News, and Letters on all aspects of the field of life science. All contributions should seek to promote international collaboration.

Editorial Board

Editor-in-Chief:

Norihiro KOKUDO
National Center for Global Health and Medicine, Tokyo, Japan

Co-Editors-in-Chief:

Xue-Tao CAO
Nankai University, Tianjin, China
Rajendra PRASAD
University of Delhi, Delhi, India
Arthur D. RIGGS
Beckman Research Institute of the City of Hope, Duarte, CA, USA

Chief Director & Executive Editor:

Wei TANG
National Center for Global Health and Medicine, Tokyo, Japan

Senior Editors:

Xunjia CHENG
Fudan University, Shanghai, China
Yoko FUJITA-YAMAGUCHI
Beckman Research Institute of the City of Hope, Duarte, CA, USA
Na HE
Fudan University, Shanghai, China
Kiyoshi KITAMURA
The University of Tokyo, Tokyo, Japan
Misao MATSUSHITA
Tokai University, Hiratsuka, Japan
Munehiro NAKATA
Tokai University, Hiratsuka, Japan
Takashi SEKINE

Toho University, Tokyo, Japan
Ri SHO
Yamagata University, Yamagata, Japan
Yasuhiko SUGAWARA
Kumamoto University, Kumamoto, Japan
Ling WANG
Fudan University, Shanghai, China

Managing Editor:

Jianjun GAO
Qingdao University, Qingdao, China

Web Editor:

Yu CHEN
The University of Tokyo, Tokyo, Japan

Proofreaders:

Curtis BENTLEY
Roswell, GA, USA
Christopher HOLMES
The University of Tokyo, Tokyo, Japan
Thomas R. LEBON
Los Angeles Trade Technical College, Los Angeles, CA, USA

Editorial Office

Pearl City Koishikawa 603,
2-4-5 Kasuga, Bunkyo-ku, Tokyo 112-0003, Japan
Tel: +81-3-5840-8764 Fax: +81-3-5840-8765
E-mail: office@biosciencetrends.com

BioScience Trends

Editorial and Head Office

Pearl City Koishikawa 603, 2-4-5 Kasuga, Bunkyo-ku,
Tokyo 112-0003, Japan

Tel: +81-3-5840-8764, Fax: +81-3-5840-8765
E-mail: office@biosciencetrends.com
URL: www.biosciencetrends.com

Editorial Board Members

Girdhar G. AGARWAL <i>(Lucknow, India)</i>	Takahiro HIGASHI <i>(Tokyo, Japan)</i>	Masatoshi MAKUUCHI <i>(Tokyo, Japan)</i>	Tadatoshi TAKAYAMA <i>(Tokyo, Japan)</i>
Hirotugu AIGA <i>(Geneva, Switzerland)</i>	De-Fei HONG <i>(Hangzhou, China)</i>	Francesco MAROTTA <i>(Milano, Italy)</i>	Shin'ichi TAKEDA <i>(Tokyo, Japan)</i>
Hidechika AKASHI <i>(Tokyo, Japan)</i>	De-Xing HOU <i>(Kagoshima, Japan)</i>	Yutaka MATSUYAMA <i>(Tokyo, Japan)</i>	Sumihito TAMURA <i>(Tokyo, Japan)</i>
Moazzam ALI <i>(Geneva, Switzerland)</i>	Sheng-Tao HOU <i>(Ottawa, Canada)</i>	Qingyue MENG <i>(Beijing, China)</i>	Puay Hoon TAN <i>(Singapore, Singapore)</i>
Ping AO <i>(Shanghai, China)</i>	Yong HUANG <i>(Ji'ning, China)</i>	Mark MEUTH <i>(Sheffi eld, UK)</i>	Koji TANAKA <i>(Tsu, Japan)</i>
Hisao ASAMURA <i>(Tokyo, Japan)</i>	Hirofumi INAGAKI <i>(Tokyo, Japan)</i>	Satoko NAGATA <i>(Tokyo, Japan)</i>	John TERMINI <i>(Duarte, CA, USA)</i>
Michael E. BARISH <i>(Duarte, CA, USA)</i>	Masamine JIMBA <i>(Tokyo, Japan)</i>	Miho OBA <i>(Odawara, Japan)</i>	Usa C. THISYAKORN <i>(Bangkok, Thailand)</i>
Boon-Huat BAY <i>(Singapore, Singapore)</i>	Chunlin JIN <i>(Shanghai, China)</i>	Fanghua QI <i>(Ji'nan, Shandong)</i>	Toshifumi TSUKAHARA <i>(Nomi, Japan)</i>
Yasumasa BESSHO <i>(Nara, Japan)</i>	Kimitaka KAGA <i>(Tokyo, Japan)</i>	Xianjun QU <i>(Beijing, China)</i>	Kohjiro UEKI <i>(Tokyo, Japan)</i>
Generoso BEVILACQUA <i>(Pisa, Italy)</i>	Ichiro KAI <i>(Tokyo, Japan)</i>	John J. ROSSI <i>(Duarte, CA, USA)</i>	Masahiro UMEZAKI <i>(Tokyo, Japan)</i>
Shiuan CHEN <i>(Duarte, CA, USA)</i>	Kazuhiro KAKIMOTO <i>(Osaka, Japan)</i>	Carlos SAINZ-FERNANDEZ <i>(Santander, Spain)</i>	Junming WANG <i>(Jackson, MS, USA)</i>
Yuan CHEN <i>(Duarte, CA, USA)</i>	Kiyoko KAMIBEPPU <i>(Tokyo, Japan)</i>	Yoshihiro SAKAMOTO <i>(Tokyo, Japan)</i>	Xiang-Dong Wang <i>(Boston, MA, USA)</i>
Naoshi DOHMAE <i>(Wako, Japan)</i>	Haidong KAN <i>(Shanghai, China)</i>	Erin SATO <i>(Shizuoka, Japan)</i>	Hisashi WATANABE <i>(Tokyo, Japan)</i>
Zhen FAN <i>(Houston, TX, USA)</i>	Bok-Luel LEE <i>(Busan, Korea)</i>	Takehito SATO <i>(Isehara, Japan)</i>	Lingzhong XU <i>(Ji'nan, China)</i>
Ding-Zhi FANG <i>(Chengdu, China)</i>	Mingjie LI <i>(St. Louis, MO, USA)</i>	Akihito SHIMAZU <i>(Tokyo, Japan)</i>	Masatake YAMAUCHI <i>(Chiba, Japan)</i>
Xiaobin FENG <i>(Beijing, China)</i>	Shixue LI <i>(Ji'nan, China)</i>	Zhifeng SHAO <i>(Shanghai, China)</i>	Aitian YIN <i>(Ji'nan, China)</i>
Yoshiharu FUKUDA <i>(Ube, Japan)</i>	Ren-Jang LIN <i>(Duarte, CA, USA)</i>	Judith SINGER-SAM <i>(Duarte, CA, USA)</i>	George W-C. YIP <i>(Singapore, Singapore)</i>
Rajiv GARG <i>(Lucknow, India)</i>	Lianxin LIU <i>(Harbin, China)</i>	Raj K. SINGH <i>(Dehradun, India)</i>	Xue-Jie YU <i>(Galveston, TX, USA)</i>
Ravindra K. GARG <i>(Lucknow, India)</i>	Xinqi LIU <i>(Tianjin, China)</i>	Peipei SONG <i>(Tokyo, Japan)</i>	Benny C-Y ZEE <i>(Hong Kong, China)</i>
Makoto GOTO <i>(Tokyo, Japan)</i>	Daru LU <i>(Shanghai, China)</i>	Junko SUGAMA <i>(Kanazawa, Japan)</i>	Yong ZENG <i>(Chengdu, China)</i>
Demin HAN <i>(Beijing, China)</i>	Hongzhou LU <i>(Shanghai, China)</i>	Hiroshi TACHIBANA <i>(Isehara, Japan)</i>	Xiaomei ZHU <i>(Seattle, WA, USA)</i>
David M. HELFMAN <i>(Daejeon, Korea)</i>	Duan MA <i>(Shanghai, China)</i>	Tomoko TAKAMURA <i>(Tokyo, Japan)</i>	<i>(as of February 26, 2018)</i>

Review

- 342 - 353 **Long non-coding RNAs as emerging regulators of epithelial to mesenchymal transition in gynecologic cancers.**
Xiaojing Lin, Junjun Qiu, Keqin Hua
- 354 - 359 **Transcriptomic responses of peripheral blood cells to coronary artery disease.**
Mingshan Lin, Yuan Zhang, Zhaozhuo Niu, Yifan Chi, Qiang Huang

Original Article

- 360 - 368 **Combined biomarkers composed of environment and genetic factors in stroke.**
Yingying Wang, Jianfeng Liu, Hongyan Wu, Yunpeng Cai
- 369 - 374 **Spectroscopic methodologies and molecular docking studies on the interaction of the soluble guanylate cyclase stimulator riociguat with human serum albumin.**
Rui Ma, Zhenyu Li, Xiaxia Di, Dongxiao Guo, Jianbo Ji, Shuqi Wang
- 375 - 381 **Correlation of genetic diversity between hosts and parasites in *Entamoeba nuttalli* isolates from Tibetan and rhesus macaques in China.**
Miao Wei, Meng Feng, Yue Guan, Ce Guo, Hang Zhou, Yongfeng Fu, Hiroshi Tachibana, Xunjia Cheng
- 382 - 388 **Bolus administration of ephedrine and etilefrine induces transient vasodilation just after injection in combined epidural and general anesthesia patients: A randomized clinical study.**
Zen'ichiro Wajima, Toshiya Shiga, Kazuyuki Imanaga
- 389 - 394 **Downregulation of lncRNA TUG1 is involved in ankylosing spondylitis and is related to disease activity and course of treatment.**
Xiaoyong Lan, Haiping Ma, Zhiping Zhang, Dong Ye, Jun Min, Feng Cai, Jun Luo
- 395 - 402 **Importance of bronchoscopic lung volume reduction coil therapy in potential candidates for lung transplantation.**
Askin Gulsen
- 403 - 411 **Association between the *MVK* rs2287218 SNP and the risk of coronary heart disease and ischemic stroke: A case-control study.**
Duo-Shun Wang, Rui-Xing Yin, Kai-Guang Li, Li Lu, Yuan Su, Rong-Qin Yan
- 412 - 418 **Prognostic factors of daily blood examination for advanced melanoma patients treated with nivolumab.**
Hisako Okuhira, Yuki Yamamoto, Yutaka Inaba, Kayo Kunimoto, Naoya Mikita, Takaharu Ikeda, Chikako Kaminaka, Yoshimi Minami, Nobuo Kanazawa, Fukumi Furukawa, Masatoshi Jinnin

CONTENTS

(Continued)

- 419 - 425 **Children with *GJB2* gene mutations have various audiological phenotypes.**
Xianlei Wang, Lihui Huang, Xuelei Zhao, Xueyao Wang, Xiaohua Cheng, Yating Du, Dongxin Liu
- 426 - 431 **Surgical treatment for monolobular Caroli's disease – Report of a 30-year single center case series.**
Takamune Yamaguchi, Alessandra Cristaudi, Takashi Kokudo, Emilie Uldry, Nicolas Demartines, Nermin Halkic
- 432 - 437 **Clinical significance of respiratory compensation during exercise testing in cardiac patients.**
Rujie Qin, Akira Koike, Osamu Nagayama, Yuta Takayanagi, Longmei Wu, Isao Nishi, Yuko Kato, Akira Sato, Takeshi Yamashita, Kazutaka Aonuma, Masaki Ieda

Brief Report

- 438 - 441 **Serum cytokine profiles are altered in patients with progressive infantile hemangioma.**
Tomoka Yamashita, Masatoshi Jinnin, Katsunari Makino, Ikko Kajihara, Jun Aoi, Shinichi Masuguchi, Satoshi Fukushima, Hironobu Ihn

Letter

- 442 - 444 **Clinicopathologic characteristics of patients with tuberculosis and schizophrenia.**
Chao Han, Maoshui Wang, Yu He

Erratum

- E1 **Erratum for "The protective effects of human umbilical cord mesenchymal stem cells on damaged ovarian function: A comparative study" by Zhang J *et al.* (*BioScience Trends*. 2016; 10(4):265-276).**

Guide for Authors

Copyright

Long non-coding RNAs as emerging regulators of epithelial to mesenchymal transition in gynecologic cancers

Xiaojing Lin^{1,2,3,§}, Junjun Qiu^{1,2,3,§}, Keqin Hua^{1,2,3,*}

¹Department of Gynecology, Obstetrics and Gynecology Hospital of Fudan University, Shanghai, China;

²Shanghai Medical College, Fudan University, Shanghai, China;

³Shanghai Key Laboratory of Female Reproductive Endocrine-Related Diseases, Fudan University, Shanghai, China.

Summary

Gynecologic cancer is a vital global healthcare issue with high rates of mortality and morbidity. Tumor metastasis attributes to most of the death suffering from solid tumors. The epithelial-mesenchymal transition (EMT) plays a pivotal role in initiating metastasis. Long non-coding RNAs (lncRNAs), a well-known group of non-coding RNAs, and a prominent topic in life science research, are misregulated in many malignancies and some are EMT-associated. In the case of gynecologic cancers, several EMT-associated lncRNAs have been identified and found to be implicated in cancer aggressiveness and progression. Mechanically, these lncRNAs participate in the EMT-related metastatic process in multiple ways including interaction with polycomb repressive complex 2 (PRC2), regulation of EMT signaling networks, mediation of EMT-transcription factors (EMT-TFs) and EMT markers, and cooperation with microRNAs (miRNAs). Further studies on these EMT-associated lncRNAs and identification of more relevant lncRNAs are imperative for the lncRNAs-based clinical management of high rate of metastasis in patients with gynecologic cancers.

Keywords: Long non-coding RNA, epithelial-mesenchymal transition, metastasis, ovarian cancer, endometrial cancer, cervical cancer

1. Introduction

Gynecologic cancer is a life-threatening disorder for women due to the difficulty of early diagnosis and the high incidence of metastasis. There are five common gynecologic cancers: ovarian, cervical, endometrial (uterine), vaginal, and vulvar, the first three of which are the most frequent (1). Cancer metastasis, which is a complex multistep process regulated by multiple factors and genes, accounts for 90% of cancer-associated deaths. The epithelial mesenchymal transition (EMT), during which epithelial cells exhibit mesenchymal-like properties through cytoskeleton remodeling and morphological changes, is a crucial step in the initiation of metastasis (2). Emerging evidence has identified long non-coding RNAs (lncRNAs) as potent determinants

of gene regulation and cancerous phenotype during tumorigenesis and tumor progression. Lately, an increasing body of lncRNAs have been found to take part in tumor invasion/metastasis regulation through EMT-based mechanisms in gynecologic cancers. This review summarizes the current findings and regulatory roles of several known EMT-related lncRNAs in gynecologic cancers and lays the foundation for potential use of these lncRNAs in cancer management.

2. Key regulators of EMT in cancer

EMT, a complex and tightly regulated developmental program, triggers tumor aggressiveness and progression when this regulation is improperly controlled. The EMT process is defined by (I) an absence of baso-apical polarization; (II) a reduction in cell adhesive forces; (III) the emergence of motility; and (IV) invasive properties. Multiple signals, such as growth factors (fibroblast growth factor (FGF), epidermal growth factor (EGF), human growth factor (HGF), transforming growth factor- β (TGF- β)), differentiation factors (Wnt, Notch, sonic hedgehog(SHH), nuclear

Released online in J-STAGE as advance publication August 27, 2018.

*Address correspondence to:

Dr. Keqin Hua, Department of Gynecology, Obstetrics and Gynecology Hospital of Fudan University, 419 Fangxie Road, Shanghai 200011, China.

E-mail: huakeqin@fudan.ac.cn

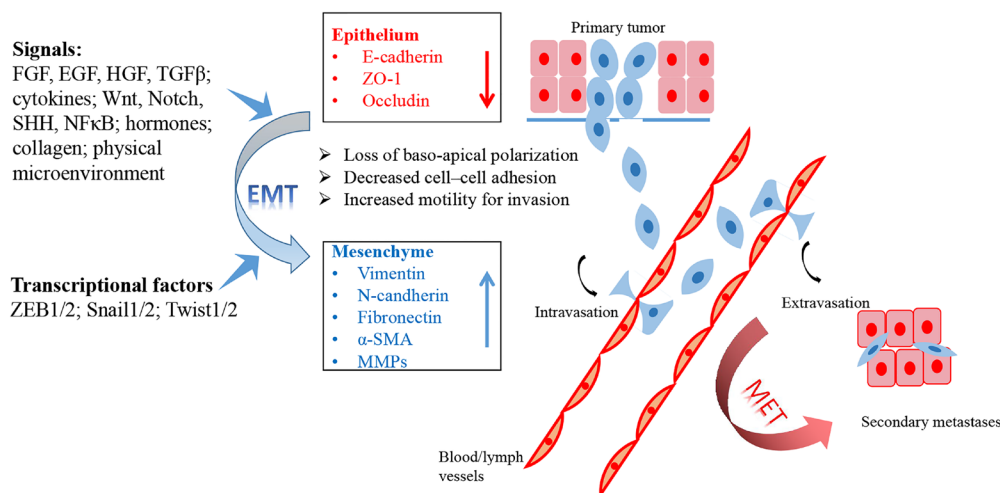


Figure 1. The regulatory network of EMT and its role in tumor metastasis. Multiple signals and factors induce EMT accompanied by alteration on EMT molecular markers, cell morphology and biological behaviors, and then trigger the primary tumor to locally infiltrate and to subsequently intravasate into nearby blood and lymphatic vessels, by which the cells are transported through the systems to extravasate into distant tissue where MET facilitates the formation of secondary metastases with epithelial characteristics.

factor kappa light-chain-enhancer of activated B cells (NF- κ B)), cytokines, and hormones (estrogen), as well as extracellular matrix components (collagen), and the physical microenvironment (hypoxia, oxidative and metabolic stress, UV light) (3) can induce various EMT-transcription factors (EMT-TFs) including the zinc finger E-box binding homeobox (ZEB1/2), the zinc finger Snail (Snail1/2) and basic helix-loop-helix families (Twist1/2). A prominent feature of the EMT is gene expression alterations in epithelial and mesenchymal markers, with decreases in the former and increases in the latter. E-cadherin (CDH1), zona occludens 1 (ZO-1), and occludin (OCLN) serve as epithelial markers while N-cadherin, vimentin, fibronectin 1 (FN1), α -smooth muscle actin (α -SMA), and some matrix metalloproteinases (MMPs) represent mesenchymal markers (4). In general, the induction of the EMT by several signals enables primary tumors to locally infiltrate, intravasate into and transport through the circulatory system, and finally extravasate into distant tissue, where mesenchymal to epithelial transition MET (MET) facilitates the formation of secondary metastases with epithelial characteristics (Figure 1).

3. Roles of lncRNAs in cancer

The growing use of high-throughput sequencing resources has revealed a great many lncRNAs, which are more than 200 nucleotides (nt) in length and constitute 76% of RNA transcripts (5). According to their location in the genome: lncRNAs are divided into five categories (I) sense, (II) antisense, (III) bidirectional, (IV) intronic and (V) intergenic. Growing evidence reveals that lncRNAs participate in cellular biological processes through diverse molecular

mechanisms, including genomic stability, epigenetic modification, transcription, post-transcription, translation and post-translational modification (6).

3.1. Genomic stability

Chromosomal instability is thought to be closely correlated with cancer initiation. lncRNAs are involved in the maintenance of chromosomal stability. For instance, noncoding RNA activated by DNA damage (NORAD) preserves fidelity of the chromosome by sequestering PUMILIO, which targets and represses messenger RNA (mRNAs) critical for accurate chromosome segregation (7). This regulatory relationship also contributes to an emerging concept that a main class of lncRNAs function as molecular decoys.

3.2. Epigenetic regulation

lncRNAs epigenetically modulate target genes *via* recruiting chromatin remodeling protein complexes, especially polycomb repressive complex 1 (PRC1) and polycomb repressive complex 2 (PRC2), and this has been demonstrated as a major regulatory mechanism (8). The details will be discussed in section 4.1.

3.3. Transcriptional regulation

Most lncRNAs described so far act by modulating transcription through recruiting proteins and/or complexes (transcription initiation factor complex) to specific target DNA sequences (9,10). In particular, promoter enhancer lncRNAs could exert enhancer-like functions and positively regulate gene expression by forming chromatin loops (11). Colorectal cancer

associated transcript 1 (CCAT1-L) is an example of an enhancer lncRNA that works to maintain myelocytomatosis oncogene (MYC) enhancer-promoter interacting structures, resulting in MYC gene transcription (12).

3.4. Post-transcriptional regulation

Post-transcription regulation includes interactions with microRNAs (miRNAs), coordination with mRNA and alternative splicing.

3.4.1. Interaction with miRNAs

lncRNA-miRNA-mRNA interactions are a significant regulatory mechanism through which lncRNAs sequester miRNA and hinder degradation of downstream RNA. The details will be discussed in section 4.4.

3.4.2. Coordination with mRNA

Several other classes of lncRNAs contribute to post-transcriptional regulation *via* coordinating specific mRNA and repressing either translation or degradation of targeted mRNA. One example is the transcription factor spi-1 proto-oncogene (PU.1) and its antisense lncRNA spi-1 proto-oncogene antisense (PU.1 AS), which form an mRNA/AS lncRNA complex and consequently represses PU.1 mRNA translation (13). In addition to translational regulation, lncRNAs may also modulate the stability of mRNA by complementarily binding with 3'-untranslated regions (3'UTRs) of mRNAs. Upon exposure to cellular stressors, the upregulation of the antisense transcript of β -secretase-1 (BACE1-AS) stabilizes BACE1 mRNA *via* a positive post-transcriptional feed-forward mechanism (14).

3.4.3. Alternative splicing

lncRNAs are also involved in the alternative splicing process. The ZEB2 natural antisense transcript (ZEB2 NAT), for instance, regulates alternative splicing by interaction with ZEB2 mRNA. It inhibits ZEB2 mRNA splicing by overlapping and binding to its alternative splice site (15).

3.5. Post-translational regulation

In some cases, there is evidence that lncRNAs are able to post-translationally modulate proteins. Signaling pathway-related lncRNAs, in particular, could alter the modification of key proteins and regulate the activation and deactivation of specific signaling pathways. For example, NF- κ B-interacting lncRNA (NKILA) hinders NF- κ B activation by affecting the phosphorylation state of the inhibitor of κ B (I κ B) (16).

3.6. Encoding small peptides

Although a majority of lncRNAs have no potential for encoding protein, some possess short open reading frames (ORFs of fewer than 100 amino acids) (17). Studies focusing on the micropeptide-coding potential of lncRNAs start from muscle-specific lncRNAs. Anderson DM *et al.* reported that one lncRNA expressed in skeletal muscle could be translated to generate a physiology-associated factor, myoregulin (MLN) (18). Other research found that the lncRNA LINC00961 encoded a new polypeptide, small regulatory polypeptide of amino acid response (SPAR), the expression level of which is altered under acute injury conditions (19). Similarly, the RNA and peptide levels of HOXB cluster antisense RNA 3 (HOXB-AS3) are decreased in highly metastatic colon (SW620 and HTC-116 high), breast (MDA-MB-231 high), nasopharyngeal (S18), and ovarian (SK-OV-3 high and OVCAR-3 high) cancer cell sublines and in primary tumor tissues in comparison with expression levels in their parental cell lines and non-tumor tissues, respectively. Moreover, as a small peptide rather than an lncRNA, HOXB-AS3 represses colorectal cancer cell biological behavior by blocking hnRNP A1-dependent PKM (pyruvate kinase M) splicing, miR-18a processing, and aerobic glycolysis (20).

Together, these findings highlight that lncRNA-encoded polypeptides are more than just translational noise but broaden the breadth and diversity of the effect of lncRNAs on gene regulation. However, few lncRNA-generating small peptides have been functionally verified. More small peptides, which have been largely overlooked in gene annotation primarily due to the difficulty of identifying functional short ORFs in lncRNAs, will be characterized in future work.

4. lncRNAs control of EMT

Numerous evidence has suggested the regulation of the EMT by lncRNAs contributes to the progression of epithelial-derived tumors *via* diverse mechanisms.

4.1. Interaction with PRC2

Myriad studies have revealed that lncRNAs can epigenetically silence gene expression through recruiting PRC2 to the promoters of target genes associated with the EMT process. PRC2 functions to trimethylate H3 lysine 27 (H3K27me3) of E-cadherin, resulting in transcriptional silencing and cancer progression (21). One well known epigenetic-related target of lncRNAs is the HOX transcript antisense intergenic RNA (HOTAIR), whose interaction with PRC2 is active in diverse cancers (22). Another example is lncRNA ubiquitin carrier protein 1 (UBC1), which alters the PRC2-mediated H3K27 trimethylation level and facilitates bladder cancer

cell invasion and metastasis (23).

4.2. Regulation of EMT signaling networks

In addition to epigenetic modification, lncRNAs are also implicated in a complex signaling pathway network.

4.2.1. TGF- β signaling pathway

TGF- β , one of the main inducers of EMT, phosphorylates cytoplasmic Smad2 and Smad3 *via* its receptors (TGF- β RI, TGF- β RII, and TGF- β RIII), thereby regulating expression of the EMT-TFs, such as Snail, ZEB, and Twist, accompanied by altered expression of the EMT markers (24). Several lncRNAs can respond to a TGF- β signal and participate in malignant transformation. For instance, lnc-ATB, a TGF- β -induced lncRNA, mediates EMT and promotes EMT-mediated metastasis in diverse kinds of cancers (25-27).

4.2.2. Wnt signaling pathway

The Wnt signaling pathway is another critical regulator of EMT. When the cell receives the Wnt signal, the membrane protein Frizzled and its low-density lipoprotein receptor form a complex, thus activating and stabilizing β -catenin, whose transfer into the nucleus triggers EMT-TF gene expression (28). Recent studies have verified that a subset of lncRNAs participate in EMT regulation *via* Wnt/ β -catenin signaling. For instance, the imprinted maternally expressed transcript H19 activates the Wnt pathway signal and blocks expression of E-cadherin *via* enhancer of zeste homolog 2 (EZH2) recruitment (29). Similarly, lncTCF7 (transcription factor 7) initiates transcription of TCF7 and thus activates the Wnt signaling pathway by recruiting the chromatin remodeling complex to the promoter site (30).

4.2.3. Hypoxia/hypoxia-inducible factor-1 α (HIF-1 α) pathway

Multiple pieces of evidence illustrate that many lncRNAs are implicated in the hypoxia/HIF-1 α -induced EMT process. For instance, H19 is triggered by both TGF- β and hypoxia, and it stimulates tumor metastasis by the induction of the EMT markers (31). In addition, tumor protein p53 pathway corepressor 1 (TP53COR1) forms a positive feedback loop with HIF-1 α under hypoxic conditions (32). In the case of gynecologic cancer, elevated levels of lncRNA plasmacytoma variant translocation 1 (PVT1) are found in response to hypoxia and are closely related to unfavorable prognosis in patients with cervical cancer (33). Mechanistically, lncRNA PVT1 silences miR-195 at the transcriptional level and modulates the EMT phenotype (34).

4.2.4. Other EMT-related pathways

Additional signaling pathways related to EMT are the mitogen-activated protein kinase (MAPK)/extracellular signal regulated protein kinase (ERK) (35), signal transducer and activator of transcription 3 (STAT3) (36), phosphatidylinositol 3 kinase (PI3K)/protein kinase (AKT) pathways (37). Collectively, the interaction of lncRNAs with various signaling pathways, some of which can crosstalk with other signaling pathways, can affect the process of EMT.

4.3. Regulation of EMT-TFs and EMT markers

Certain lncRNAs function by directly regulating the transcription of the EMT-TFs and EMT markers. For example, amine oxidase, copper containing 4 (AOC4P) binds to vimentin, facilitates its degradation, and thus suppresses the EMT process (38). Several other lncRNAs (commonly antisense lncRNAs) are reported to form duplexes with their counterparts, to either promote or prevent their translation. For example, ZEB2NAT suppresses E-cadherin expression by interacting with its mRNA counterparts called ZEB2 (39). A similar regulatory relationship exists between ZEB1 antisense 1 (ZEB1-AS1) and ZEB1 (40). Other examples of antisense transcripts include HNF1A antisense RNA 1 (HNF1A-AS1) (41) and 91H (42). Although increasing evidence supports the hypothesis that lncRNAs positively or negatively regulate EMT-related factors, thorough study is needed to determine if these effects are direct.

4.4. Interaction with miRNAs

Over the last decade, evidence has clearly shown that miRNAs are widely misregulated and play significant regulatory roles in cancer. Emerging evidence indicates that cooperation between lncRNAs and miRNAs contributes to tumor progression *via* diverse pathways.

4.4.1. miRNAs targeting lncRNAs for degradation

Numerous studies have demonstrated that miRNAs can bind to lncRNAs and trigger their decay. For example, upregulated miR-9 expression degrades metastasis-associated lung adenocarcinoma transcript 1 (MALAT1) in osteosarcoma cells and thus blocks cell migration and invasion under high doses of 17 β -estradiol (43). In addition, miR-217 post-transcriptional silencing of MALAT-1 RNA is mediated by argonaute 2 (Ago2), resulting in the mesenchymal transition of bronchial epithelial cells (44).

4.4.2. lncRNAs competitively binding to microRNA

Evidence is accumulating that lncRNAs function for a competing endogenous RNA (ceRNA) regulatory

relationship where lncRNAs are capable of sponging miRNAs and upregulating downstream mRNA expression. For example, urothelial cancer associated 1 (UCA1) could sponge miR-485-5p in epithelial ovarian cancer. The lack of UCA1 downregulates MMP14, which is targeted by miR-485-5p (45). Other examples include MALAT1 (46), colon cancer-associated transcript-1 (CCAT1) (47) and long intergenic non-protein-coding RNA, regulator of reprogramming (linc-ROR) (48).

4.4.3. lncRNAs acting as precursor RNAs

Notably, lncRNAs themselves can be precursor RNAs for miRNAs. A well-known lncRNA called H19 has been proven to be able to generate miR-675, which is an EMT-associated gene in prostate cancer (49). Another study that one lncRNA exclusively expressed in the kidney regulates EMT *via* directly encoding the miR-200 cluster, which is also evidence supporting lncRNAs as pre-miRNAs (50).

4.4.4. lncRNAs transcriptionally regulating miRNAs

Beyond the above interactions between lncRNAs and miRNAs, lncRNAs can directly transcriptionally regulate miRNAs. For example, HOTAIR can recruit PRC2 to miR34a, subsequently upregulate Snail and induce EMT-mediated metastasis of gastric cancer cells (51).

5. EMT-related lncRNAs in gynecologic cancer

Table 1 and Figure 2 illustrate the roles of the EMT-related lncRNAs in gynecologic cancer, the details of which will be discussed below.

5.1. MALAT1

MALAT1, also called NEAT2 (non-coding nuclear-enriched abundant transcript 2), is located on chromosome 11q13.1 and contains 8,000 nucleotides. MALAT1, an EMT-related lncRNA, allows epithelial cells to be malignantly transformed. In ovarian cancer, MALAT1 activates PI3K/Akt signaling and EMT induction. MALAT-1 knockdown leads to downregulation of N-cadherin, vimentin and Snail (52). In endometrial cancer (EC), miR-200c binds to MALAT1 to form the MALAT1/miR-200c sponge. When the interaction is interrupted, the cell invasive capacity is decreased and the expression of EMT markers is altered (46). In addition, MALAT1 promotes the invasive and metastatic potency of cervical cancer by altered expression of EMT markers (E-cadherin, ZO-1, β -catenin and vimentin) and EMT-TFs (Snail) (53).

5.2. H19

H19, a famous imprinted gene, is located in an

imprinted region of chromosome 11 with 2,300 nucleotides. H19 exerts oncogenic and pro-metastatic properties primarily through the H19/let-7 axis (54). In both ovarian and EC, H19 acts to antagonize let-7 and mediate the elevated level of several metastasis-related genes (c-Myc, high-mobility group AT-hook 2(HMGA2), and insulin-like growth factor 2 mRNA-binding protein 3 (IGF2BP3) (55). Furthermore, the knockdown of H19 is accompanied by Snail downregulation and E-cadherin upregulation in EC (56).

5.3. HOTAIR

HOTAIR is a lncRNA of 2158-nt length located on 12q13.13. HOTAIR has been revealed to be an EMT-related lncRNA and serves as a strong metastatic predictor in cancers (57). In cervical cancer, the expression of HOTAIR is positively correlated to a poor prognostic predictor, human papillomavirus oncogenic E7 (HPV-E7). The pro-metastatic potency of HOTAIR is partially ascribed to vascular endothelial growth factor precursor (VEGF), MMP-9, and EMT-associated genes induction (58,59). Additionally, HOTAIR regulates the malignant behavior of ovarian cancer SK-OV-3 cells partly by interacting with mitogen-activated protein kinase 1 (MAPK1), but whether EMT is regulated *via* this pathway remains to be resolved (35). Qiu JJ *et al.* demonstrated that HOTAIR facilitates epithelial ovarian cancer (EOC) cell invasion and migration by modulating MMPs and EMT-related gene expression (60).

5.4. PVT1

PVT1 is an oncogenic, intergenic lncRNA derived from 8q24.21 with multiple splicing isoforms (61). It is upregulated in various cancer types such as ovarian cancer, cervical cancer, and pancreatic cancer, among others (62). In cervical cancer cells, PVT1 can regulate EMT *via* interactions with EZH2 and the complex anchors to the miR-195 promoter region and *via* direct competitive binding with miR-195 (34). Recent studies suggest that miR-195 is an important suppressor of EMT in some cancers (63). However, the exact mechanism underlying PVT1/ miR-195 axis in cervical cancer and other gynecologic cancers is minimally understood and poorly elucidated.

5.5. ANRIL

Antisense non-coding RNA in the INK4 locus (ANRIL) is a 3800-nt long non-coding RNA located in chromosome 9p21. Numerous studies have shown that ANRIL acts as a powerful cancer progressive factor in various cancers (64). For example, in ovarian cancer, ANRIL increases migration and invasion by MET and MMP3 modulation and its expression pattern is closely

Table 1. lncRNAs related to EMT in gynecologic cancers

lncRNA	Cancer type	Expression	Potential mechanism (Ref)	Author, date
PVT1	Cervical cancer	Upregulated	Binding to EZH2; interacting with miR-195 (34).	Shen CJ <i>et al</i> , 2017
HOTAIR	Ovarian cancer	Upregulated	Interacting with MAPK1 (35); Regulating MMPs and EMT-related genes (60).	Tang YW <i>et al</i> , 2015; Qiu JJ <i>et al</i> , 2014
	Cervical cancer	Upregulated	Regulating VEGF and MMP-9 expression (58); Binding to PRC2-complex members (59).	Kim HJ <i>et al</i> , 2015; Sharma S <i>et al</i> , 2015
UCA1	Ovarian cancer	Upregulated	Binding to miR-485-5p and increasing target gene MMP14 (45).	Yang Y <i>et al</i> , 2016
MALAT1	Endometrial cancer	Upregulated	MALAT1/miR-200c sponge (46).	Li Q <i>et al</i> , 2016
	Ovarian cancer	Upregulated	Regulating N-cadherin, vimentin and Snail by the PI3K/Akt signaling pathway (52).	Jin Y <i>et al</i> , 2017
	Cervical cancer	Upregulated	Modulating E-cadherin, ZO-1, β -catenin, vimentin and Snail expression (53).	Sun R <i>et al</i> , 2016
CCAT1	Ovarian cancer	Upregulated	CCAT1-miR-152/miR-130b-ADAM17/WNT1/STAT3/ZEB1 axis (47).	Cao Y <i>et al</i> , 2017
Linc-ROR	Endometrial cancer	Upregulated	Linc-ROR/miR-145 sponge (48).	Zhou X <i>et al</i> , 2014
	Ovarian cancer	Upregulated	Wnt/ β -catenin signaling pathway (84).	Lou Y <i>et al</i> , 2017
H19	Ovarian cancer	Upregulated	H19/let7 axis (55).	Yan L <i>et al</i> , 2015
	Endometrial cancer	Upregulated	H19/let7 axis (55); Increasing Snail and decreasing E-cadherin expression (56).	Yan L <i>et al</i> , 2015; Zhao L <i>et al</i> , 2017
ANRIL	Ovarian cancer	Upregulated	Modulating MET and MMP3 (65).	Qiu JJ <i>et al</i> , 2015
AB073614	Ovarian cancer	Upregulated	Upregulating MMP-2, MMP-9, β -catenin, Twist, Snail, FN1 and E-cadherin; activating AKT and ERK (70).	Cheng Z <i>et al</i> , 2015
EBIC	Cervical cancer	Upregulated	Recruiting EZH2 and repressing E-cadherin expression (73).	Sun NX <i>et al</i> , 2014
NEAT1	Ovarian cancer	Upregulated	Affecting the expression of MMP-2, MMP-9, Snail and TGF- β -1 (76).	Li P <i>et al</i> , 2016
SPRY4-IT1	Ovarian cancer	Downregulated	Altering the expression level of N-cadherin and vimentin (78).	Yu J <i>et al</i> , 2017
TUG1	Cervical cancer	Upregulated	Upregulating fibronectin, vimentin and cytokeratin (79).	Hu Y <i>et al</i> , 2017
BANCR	Endometrial cancer	Upregulated	Increasing MMP2/MMP1 expression by activating ERK/MAPK signaling pathway (82).	Wang D <i>et al</i> , 2016
DNM3OS	Ovarian cancer	Upregulated	Regulating EMT-TFs (Snail and Slug), E-cadherin and N-cadherin; EMT-linked pathways (86).	Mitra R, 2017
SOX2OT	Ovarian cancer	Upregulated	Altering the expression of N-cadherin and E-cadherin (88).	Han L <i>et al</i> , 2018
HOXA11-AS	Ovarian cancer	Upregulated	Affecting the expression of β -catenin, Snail, Twist, vimentin, E-cadherin, invasive endothelial growth factor and MMP-9 (90).	Yim GW <i>et al</i> , 2017

lncRNA; long noncoding RNA; BANCR, BRAF-activated non-coding RNA; HOTAIR, HOX transcript antisense intergenic RNA; UCA1, urothelial cancer associated 1; MALAT1, metastasis-associated lung adenocarcinoma transcript 1; CCAT1, colon cancer-associated transcript-1; Linc-ROR, long intergenic non-protein coding RNA, regulator of reprogramming; ANRIL, antisense non-coding RNA in the INK4 locus; EBIC, EZH2-binding lncRNA in cervical cancer; NEAT1, nuclear paraspeckle assembly transcript 1; SPRY4-IT1, SPRY4 intronic transcript 1; TUG1, taurine upregulated gene 1; DNM3OS, DNM3 opposite strand RNA; SOX2OT, SOX2 overlapping transcript; HOXA11-AS, HOXA11 antisense RNA.

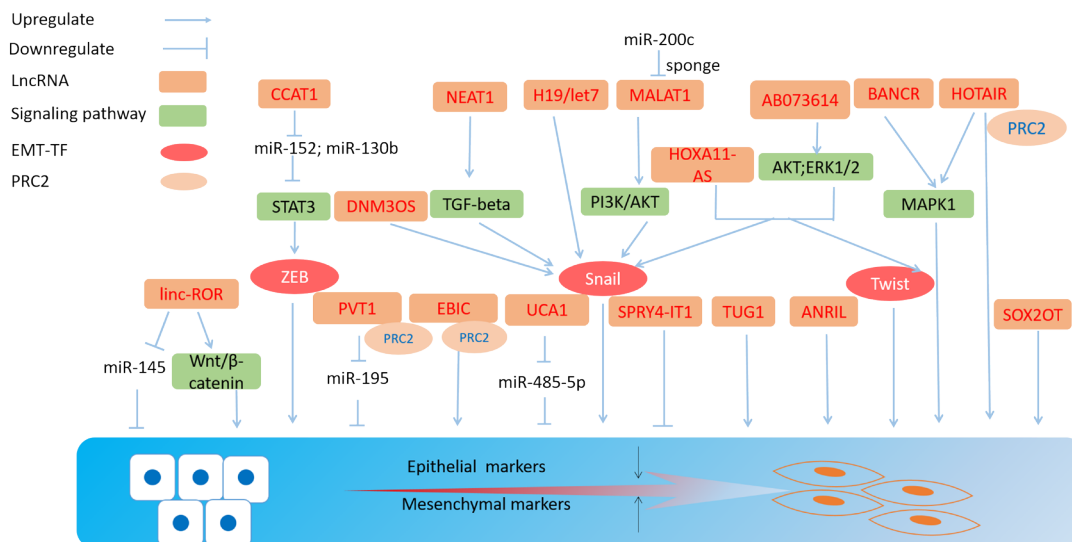


Figure 2. EMT-related lncRNAs and their regulatory network in gynecologic cancers. Schematic diagram shows several lncRNAs participate in EMT-related metastatic process in multiple ways including interaction with PRC2, regulation of EMT signaling networks, mediation on EMT-TFs and EMT markers, and cooperation with miRNAs.

linked to clinical stage, pathological grade, lymph node metastasis, and poor prognosis (65). In addition, ANRIL has been found to promote the metastatic and invasive ability of cervical cancer cells (66,67), but whether the EMT process is involved remains unclear.

5.6. UCA1

Cancer upregulated drug resistant (CUDR), also called UCA1, is located in chromosome 19p13.1 and is 2200-nt in length. It is dysregulated in cancer tissues from various malignancies (68). L Lu *et al.* reported that UCA1 is closely associated with tumor aggressiveness of EC and may serve as a prognostic predictor for EC patients (69). In EOC, UCA1 serves as a miR-485-5p "sponge" and alters downstream MMP14 expression. Moreover, the high expression level of UCA1 could be indicative of an unfavorable prognosis (45).

5.7. AB073614

AB073614 is a 1900-nt lncRNA located in the 3q24 chromosomal region. AB073614 was upregulated in ovarian cancer (70), glioma tissue(71) and colorectal cancer (72). Overexpression of AB073614 could be suggestive of tumor progression and poor prognosis. In ovarian cancer cells, downregulated p-AKT and p-ERK suggests that key signaling pathways may be implicated in AB073614-mediated tumor aggressiveness (70).

5.8. EBIC

EZH2-binding lncRNA in cervical cancer (EBIC) is a 1500-nt lncRNA located in chromosome 12q22. In cervical cancer, lncRNA-EBIC represses E-cadherin and enhances cell invasion *via* interacting with EZH2, but

the mechanism underlying this process remains to be formally demonstrated (73). In addition, it should also be determined whether EBIC is a cervical cancer-specific lncRNA or a universally expressed lncRNA in cancers.

5.9. CCAT1

CCAT1 is a 2628-nt lncRNA mapping to chromosome 8q24.21 near c-MYC, a well-known transcription factor. Upregulation of CCAT1 might be a universal rule in a variety of cancer types, suggesting that CCAT1 has oncogenic potential in development and progression of tumors (74). Cao Y *et al.* reported that in EOC, the pro-metastatic effect of CCAT1 is through interaction with miR-130b and miR-152, protecting target genes, such as ADAM17, Wnt1, STAT3 and ZEB1, from degradation (47).

5.10. NEAT1

Nuclear paraspeckle assembly transcript 1 (NEAT1) encodes two transcriptional variants, namely, NEAT1-1 and NEAT1-2, which are 3.7 kb and 23 kb in length respectively, and situated on chromosome 11. The expression level of NEAT1 is elevated in multiple types of cancers, including lung, esophageal and gastric cancers, while it is downregulated in acute promyelocytic leukemia (75). In ovarian cancer, silencing NEAT1 significantly affects the expression of cell invasion-related proteins (MMP-2, MMP-9, Snail1 and TGF-β-1) (76). Despite these findings, however, the precise role of NEAT1 remains to be characterized.

5.11. SPRY4-IT1

SPRY4 intronic transcript 1 (SPRY4-IT1) is a 687-nt

unspliced polyadenylated transcript located on human chromosome 5q31.3. Multiple studies have characterized SPRY4-IT1 as a tumor suppressor in different cancer types, such as non-small cell lung cancer, breast cancer, and endometrial cancer (77). In ovarian cancer, knockdown of SPRY4-IT1 leads cancer cells to a more aggressive phenotype, partially through regulation of N-cadherin and vimentin (78). The mechanism contributing to this dysregulation, however, is still unclear.

5.12. TUG1

Taurine upregulated gene 1 (TUG1) is a 7.1 kb lncRNA located in the 22q12 chromosomal region. Abundant studies have revealed that TUG1 promotes cancer cell invasion and radio-resistance *via* EMT (79,80). In cervical cancer, TUG1 knockdown suppresses expression of EMT related proteins (fibronectin, vimentin and cytokeratin) (79). Nonetheless, further research is required to elucidate the precise mechanism underlying TUG1 and its effects on target genes.

5.13. BANCR

BRAF-activated non-coding RNA (BANCR) derives from chromosome 9 with a length of 693-bp (81). Previous studies have reported that BANCR plays a pivotal part in malignant transformation. In EC, elevated BANCR activates the ERK/MAPK signaling pathway, upregulates MMP2/MMP1 expression and thus accelerates the progression of cancer cells (82).

5.14. linc-RoR

linc-ROR is a 2.6 kb lncRNA encoded at chromosome 18q21.31. linc-ROR is involved in cancerous cell growth and metastasis in various malignancies (83). In ovarian cancer, linc-ROR promotes EMT-mediated cancer cell metastasis *via* Wnt/ β -catenin signaling pathway activation (84). In EC, linc-RoR functions as an miR-145 "sponge" during carcinogenesis (48).

5.15. DN3OS

DNM3 opposite strand RNA (DNM3OS) is a noncoding 7.9kb fragment transcribed from 1q24.3. It was identified as an important regulator during development (85). Recent studies have pointed out that DN3OS is highly expressed in the mesenchymal subtype compared with its epithelial counterpart. In ovarian cancer, DN3OS promotes metastasis through EMT-linked genes (Snail, Slug, E-cadherin and N-cadherin) and pathways based on The Cancer Genome Atlas (TCGA) database and experimental evidence. Of note, DN3OS may be a poor prognostic predictor of ovarian cancer (86).

5.16. SOX2OT

SOX2 overlapping transcript (SOX2OT) is mapped to chromosome 3q26.3. Several studies have revealed a tumorigenic role of SOX2OT in cancers, including breast cancer, lung cancer and hepatocellular carcinoma (87). In ovarian cancer, SOX2OT silencing suppresses cell aggressiveness accompanied by decrease in N-cadherin and increase in E-cadherin (88).

5.17. HOXA11-AS

HOXA11 antisense RNA (HOXA11-AS) is located in chromosome 12q22 near the gene HOXA11 (Homeobox genes A11). In several cancers, HOXA11-AS is differentially expressed compared to normal tissues, such as glioma, uterine cervix carcinoma, and lung adenocarcinoma (89). In Serous Ovarian Cancer, the elevated level of HOXA11as promotes cell invasion and migration through EMT-associated gene alteration, including EMT-TFs (Snail and Twist), vimentin E-cadherin, invascular endothelial growth factor and MMP-9 (90).

Other EMT-associated lncRNA in gynecologic cancer detected from TCGA database include myocardial infarction associated transcript (MIAT) and maternally expressed 3 (MEG3), but more study is needed to experimentally verify its correlation with EMT (86).

6. lncRNA-based diagnostics and therapies

Numerous lncRNAs are misexpressed in human cancers and some appear to be highly cancer specific. In addition, many lncRNAs contained in body fluids can be detected by current laboratory technology. These factors contribute to lncRNAs as an attractive approach for noninvasive biomarkers and therapeutic targets. For example, in prostate cancer, prostate cancer associated 3 (PCA3) has an advantage over the current method of using serum prostate-specific antigen (PSA) as a biomarker, due to its higher specificity and sensitivity (91). In addition, the overexpression of the hepatocellular carcinoma (HCC) lncRNA HULC is detected in blood of HCC patients (92). Current studies have highlighted the role of exosome-contained lncRNAs in fields of diagnosis and prognosis. To date, exosomal transfer of lncRNAs has been increasingly verified and implicated in EMT processes. For instance, ZNF1 antisense RNA1 (ZFAS1) is found to be elevated in both tumor tissues and body fluid-derived exosomes of gastric cancer. Exosome-mediated transfer of ZFAS1 could increase the expression of ZFAS1, decrease epithelial markers and upregulate the mesenchymal markers of recipient cells, leading to enhanced proliferation and migration potential (93). Another example is HOTAIR, one of the earliest detectable and enriched lncRNAs in body fluids of patients with different types of cancer (94).

Additionally, several other EMT-related lncRNAs, including UCA1, lincRNA-p21, growth arrest specific 5 (GAS5), MALAT-1 and H19, are also secreted within exosomes (95-97). However, the concrete roles of these exosome-derived lncRNAs are rarely defined. Current advanced technologies allow therapies based on lncRNAs to be more achievable either to silence or to overexpress. For example, lung cancer metastasis could be prevented by antisense-mediated silencing of MALAT1 *in vivo* (98). Moreover, breast cancer progression can be hindered through systemic knockdown of MALAT1 using antisense oligonucleotides (99). Overall, lncRNA-targeted cancer therapies are promising; however, they are still in their infancy and require further development of experimental strategies, siRNA/antisense delivery strategies, and clinical trials.

7. Conclusions and future perspectives

Metastasis is one of the most significant factors leading to the poor outcomes of patients with gynecologic malignancies. Over the past few years, mounting evidence has linked numerous lncRNAs to the cellular EMT process in ways relevant to tumor metastasis. Despite existing advances, the accurate regulatory role of lncRNAs in the EMT process is rarely understood in the case of gynecologic cancers. For one thing, more efforts are required to know the exact underlying mechanisms. Additionally, lncRNA-based diagnostics and therapies face many challenges pertaining to application. The former includes development of effective and convenient detection technology, avoidance of degradation by body fluid components and exploration of the tissue origin of circulating lncRNAs. The later involves the need for safe and effective delivery, and minimization of off-target effects. Therefore, future studies should focus more on investigating the existing form and function of circulating lncRNA to make an efficient diagnosis, discover disease-specific lncRNAs and develop novel therapeutic agents to directly target lncRNAs. Taken together, understanding the specific role and precise mechanisms of lncRNAs in the EMT process will open up promising perspectives in disease management.

Acknowledgements

This project was supported by funding from the National Natural Science Foundation of China (81370689 and 81571404; to Keqin Hua), the National Natural Science Foundation for Young Scholars of China (81502240; to Junjun Qiu), and the Shanghai Science and Technology Development Funds for the Talents (15YF1401400; to Junjun Qiu).

References

1. Siegel R, Naishadham D, Jemal A. Cancer Statistics, 2012. *Ca-Cancer J Clin.* 2012; 62:10-29.
2. Vanharanta S, Massague J. Origins of Metastatic Traits. *Cancer Cell.* 2013; 24:410-421.
3. Moustakas A, Heldin CH. Signaling networks guiding epithelial-mesenchymal transitions during embryogenesis and cancer progression. *Cancer Sci.* 2007; 98:1512-1520.
4. Kalluri R, Weinberg RA. The basics of epithelial-mesenchymal transition. *J Clin Invest.* 2009; 119:1420-1428.
5. Di Gesualdo F, Capaccioli S, Lulli M. A pathophysiological view of the long non-coding RNA world. *Oncotarget.* 2014; 5:10976-10996.
6. Sun L, Luo HT, Liao Q, Bu DC, Zhao GG, Liu CN, Liu YN, Zhao Y. Systematic study of human long intergenic non-coding RNAs and their impact on cancer. *Sci China Life Sci.* 2013; 56:324-334.
7. Lee S, Kopp F, Chang TC, Sataluri A, Chen BB, Sivakumar S, Yu HT, Xie Y, Mendell JT. Noncoding RNA NORAD Regulates Genomic Stability by Sequestering PUMILIO Proteins. *Cell.* 2016; 164:69-80.
8. Mercer TR, Mattick JS. Structure and function of long noncoding RNAs in epigenetic regulation. *Nat Struct Mol Biol.* 2013; 20:300-307.
9. Beckedorff FC, Ayupe AC, Crocci-Souza R, Amaral MS, Nakaya HI, Soltys DT, Menck CF, Reis EM, Verjovski-Almeida S. The intronic long noncoding RNA ANRASSF1 recruits PRC2 to the RASSF1A promoter, reducing the expression of RASSF1A and increasing cell proliferation. *PLoS Genet.* 2013; 9:e1003705.
10. Sigova AA, Abraham BJ, Ji X, Molinie B, Hannett NM, Guo YE, Jangi M, Giallourakis CC, Sharp PA, Young RA. Transcription factor trapping by RNA in gene regulatory elements. *Science.* 2015; 350:978-981.
11. Kim TK, Hemberg M, Gray JM, *et al.* Widespread transcription at neuronal activity-regulated enhancers. *Nature.* 2010; 465:182-187.
12. Xiang JF, Yin QF, Chen T, Zhang Y, Zhang XO, Wu Z, Zhang SF, Wang HB, Ge JH, Lu XH, Yang L, Chen LL. Human colorectal cancer-specific CCAT1-L lncRNA regulates long-range chromatin interactions at the MYC locus. *Cell Res.* 2014; 24:1150-1150.
13. Pang WJ, Lin LG, Xiong Y, Wei N, Wang Y, Shen QW, Yang GS. Knockdown of PU.1 AS lncRNA Inhibits Adipogenesis Through Enhancing PU.1 mRNA Translation. *J Cell Biochem.* 2013; 114:2500-2512.
14. Liu T, Huang YY, Chen JL, Chi HY, Yu ZH, Wang J, Chen C. Attenuated ability of BACE1 to cleave the amyloid precursor protein *via* silencing long noncoding RNA BACE1-AS expression. *Mol Med Rep.* 2014; 10:1275-1281.
15. Beltran M, Puig I, Pena C, Garcia JM, Alvarez AB, Pena R, Bonilla F, de Herrerros AG. A natural antisense transcript regulates Zeb2/Sip1 gene expression during Snail1-induced epithelial-mesenchymal transition. *Genes Dev.* 2008; 22:756-769.
16. Liu B, Sun L, Liu Q, Gong C, Yao Y, Lv X, Lin L, Yao H, Su F, Li D, Zeng M, Song E. A cytoplasmic NF-kappaB interacting long noncoding RNA blocks IkappaB phosphorylation and suppresses breast cancer metastasis. *Cancer Cell.* 2015; 27:370-381.
17. Slavoff SA, Mitchell AJ, Schwaid AG, Cabili MN, Ma J, Levin JZ, Karger AD, Budnik BA, Rinn JL, Saghatelian A. Peptidomic discovery of short open reading frame-encoded peptides in human cells. *Nat Chem Biol.* 2013; 9:59-+.

18. Anderson DM, Anderson KM, Chang CL, Makarewich CA, Nelson BR, McAnally JR, Kasaragod P, Shelton JM, Liou J, Bassel-Duby R, Olson EN. A micropeptide encoded by a putative long noncoding RNA regulates muscle performance. *Cell*. 2015; 160:595-606.
19. Matsumoto A, Pasut A, Matsumoto M, Yamashita R, Fung J, Monteleone E, Saghatelian A, Nakayama KI, Clohessy JG, Pandolfi PP. mTORC1 and muscle regeneration are regulated by the LINC00961-encoded SPAR polypeptide. *Nature*. 2017; 541:228-232.
20. Huang JZ, Chen M, Chen, Gao XC, Zhu S, Huang H, Hu M, Zhu H, Yan GR. A Peptide Encoded by a Putative lncRNA HOXB-AS3 Suppresses Colon Cancer Growth. *Mol Cell*. 2017; 68:171-184 e176.
21. Luo HN, Jiang Y, Ma SJ, Chang HH, Yi CX, Cao H, Gao Y, Guo HL, Hou J, Yan J, Sheng Y, Ren XY. EZH2 promotes invasion and metastasis of laryngeal squamous cells carcinoma *via* epithelial-mesenchymal transition through H3K27me3. *Biochem Biophys Res Co*. 2016; 479:253-259.
22. Gupta RA, Shah N, Wang KC, *et al*. Long non-coding RNA HOTAIR reprograms chromatin state to promote cancer metastasis. *Nature*. 2010; 464:1071-U1148.
23. He W, Cai QQ, Sun FY, Zhong GZ, Wang P, Liu HY, Luo JH, Yu H, Huang J, Lin TX. linc-UBC1 physically associates with polycomb repressive complex 2 (PRC2) and acts as a negative prognostic factor for lymph node metastasis and survival in bladder cancer. *Bba-Mol Basis Dis*. 2013; 1832:1528-1537.
24. Valcourt U, Kowanzet M, Niimi H, Heldin CH, Moustakas A. TGF-beta and the Smad signaling pathway support transcriptomic reprogramming during epithelial-mesenchymal cell transition. *Mol Biol Cell*. 2005; 16:1987-2002.
25. Xiong J, Liu Y, Jiang L, Zeng Y, Tang W. High expression of long non-coding RNA lncRNA-ATB is correlated with metastases and promotes cell migration and invasion in renal cell carcinoma. *Jpn J Clin Oncol*. 2016; 46:378-384.
26. Xu S, Yi XM, Tang CP, Ge JP, Zhang ZY, Zhou WQ. Long non-coding RNA ATB promotes growth and epithelial-mesenchymal transition and predicts poor prognosis in human prostate carcinoma. *Oncol Rep*. 2016; 36:10-22.
27. Yue B, Qiu S, Zhao S, Liu C, Zhang D, Yu F, Peng Z, Yan D. LncRNA-ATB mediated E-cadherin repression promotes the progression of colon cancer and predicts poor prognosis. *J Gastroenterol Hepatol*. 2016; 31:595-603.
28. Yook JI, Li XY, Ota I, Hu C, Kim HS, Kim NH, Cha SY, Ryu JK, Choi YJ, Kim J, Fearon ER, Weiss SJ. A Wnt-Axin2-GSK3beta cascade regulates Snail1 activity in breast cancer cells. *Nat Cell Biol*. 2006; 8:1398-1406.
29. Luo M, Li Z, Wang W, Zeng Y, Liu Z, Qiu J. Long non-coding RNA H19 increases bladder cancer metastasis by associating with EZH2 and inhibiting E-cadherin expression. *Cancer Lett*. 2013; 333:213-221.
30. Wang Y, He L, Du Y, Zhu P, Huang G, Luo J, Yan X, Ye B, Li C, Xia P, Zhang G, Tian Y, Chen R, Fan Z. The long noncoding RNA lncTCF7 promotes self-renewal of human liver cancer stem cells through activation of Wnt signaling. *Cell stem cell*. 2015; 16:413-425.
31. Matouk IJ, Mezan S, Mizrahi A, Ohana P, Abu-lail R, Fellig Y, deGroot N, Galun E, Hochberg A. The oncofetal H19 RNA connection: Hypoxia, p53 and cancer. *Bba-Mol Cell Res*. 2010; 1803:443-451.
32. Yang F, Zhang H, Mei Y, Wu M. Reciprocal regulation of HIF-1alpha and lincRNA-p21 modulates the Warburg effect. *Mol Cell*. 2014; 53:88-100.
33. Iden M, Fye S, Li K, Chowdhury T, Ramchandran R, Rader JS. The lncRNA PVT1 Contributes to the Cervical Cancer Phenotype and Associates with Poor Patient Prognosis. *PLoS one*. 2016; 11:e0156274.
34. Shen CJ, Cheng YM, Wang CL. LncRNA PVT1 epigenetically silences miR-195 and modulates EMT and chemoresistance in cervical cancer cells. *J Drug Target*. 2017; 25:637-644.
35. Yiwei T, Hua H, Hui G, Mao M, Xiang L. HOTAIR Interacting with MAPK1 Regulates Ovarian Cancer skov3 Cell Proliferation, Migration, and Invasion. *Med Sci Monit*. 2015; 21:1856-1863.
36. Zhang HY, Cai K, Wang J, Wang XY, Cheng K, Shi FF, Jiang LW, Zhang YX, Dou J. MiR-7, Inhibited Indirectly by LincRNA HOTAIR, Directly Inhibits SETDB1 and Reverses the EMT of Breast Cancer Stem Cells by Downregulating the STAT3 Pathway. *Stem Cells*. 2014; 32:2858-2868.
37. Wang H, Zhang G, Zhang H, Zhang F, Zhou BH, Ning F, Wang HS, Cai SH, Du J. Acquisition of epithelial-mesenchymal transition phenotype and cancer stem cell-like properties in cisplatin-resistant lung cancer cells through AKT/beta-catenin/Snail signaling pathway. *Eur J Pharmacol*. 2014; 723:156-166.
38. Wang TH, Lin YS, Chen Y, Yeh CT, Huang YL, Hsieh TH, Shieh TM, Hsueh C, Chen TC. Long non-coding RNA AOC4P suppresses hepatocellular carcinoma metastasis by enhancing vimentin degradation and inhibiting epithelial-mesenchymal transition. *Oncotarget*. 2015; 6:23342-23357.
39. Zhuang J, Lu Q, Shen B, Huang X, Shen L, Zheng X, Huang R, Yan J, Guo H. TGFbeta1 secreted by cancer-associated fibroblasts induces epithelial-mesenchymal transition of bladder cancer cells through lncRNA-ZEB2NAT. *Sci Rep*. 2015; 5:11924.
40. Li YL, Wen XW, Wang LG, Sun XJ, Ma H, Fu Z, Li LP. LncRNA ZEB1-AS1 predicts unfavorable prognosis in gastric cancer. *Surg Oncol*. 2017; 26:527-534.
41. Cai L, Lv J, Zhang Y, Li J, Wang Y, Yang H. The lncRNA HNF1A-AS1 is a negative prognostic factor and promotes tumorigenesis in osteosarcoma. *J Cell Mol Med*. 2017; 21:2654-2662.
42. Gao T, He B, Pan Y, Xu Y, Li R, Deng Q, Sun H, Wang S. Long non-coding RNA 91H contributes to the occurrence and progression of esophageal squamous cell carcinoma by inhibiting IGF2 expression. *Mol Carcinog*. 2015; 54:359-367.
43. Fang D, Yang H, Lin J, Teng Y, Jiang Y, Chen J, Li Y. 17beta-estradiol regulates cell proliferation, colony formation, migration, invasion and promotes apoptosis by upregulating miR-9 and thus degrades MALAT-1 in osteosarcoma cell MG-63 in an estrogen receptor-independent manner. *Biochem Biophys Res Commun*. 2015; 457:500-506.
44. Lu L, Luo F, Liu Y, Liu XL, Shi L, Lu XL, Liu QZ. Posttranscriptional silencing of the lncRNA MALAT1 by miR-217 inhibits the epithelial-mesenchymal transition *via* enhancer of zeste homolog 2 in the malignant transformation of HBE cells induced by cigarette smoke extract. *Toxicol Appl Pharm*. 2015; 289:276-285.
45. Yang YJ, Jiang Y, Wan YC, Zhang L, Qiu JN, Zhou SL,

- Cheng WJ. UCA1 functions as a competing endogenous RNA to suppress epithelial ovarian cancer metastasis. *Tumor Biol.* 2016; 37:10633-10641.
46. Li QL, Zhang C, Chen RC, Xiong HZ, Qiu FM, Liu SY, Zhang MF, Wang F, Wang Y, Zhou X, Xiao GH, Wang XD, Jiang QP. Disrupting MALAT1/miR-200c sponge decreases invasion and migration in endometrioid endometrial carcinoma. *Cancer Lett.* 2016; 383:28-40.
 47. Cao Y, Shi HR, Ren F, Jia YY, Zhang RT. Long non-coding RNA CCAT1 promotes metastasis and poor prognosis in epithelial ovarian cancer. *Exp Cell Res.* 2017; 359:185-194.
 48. Zhou X, Gao Q, Wang JZ, Zhang X, Liu K, Duan Z. Linc-RNA-RoR acts as a "sponge" against mediation of the differentiation of endometrial cancer stem cells by microRNA-145. *Gynecol Oncol.* 2014; 133:333-339.
 49. Zhu MJ, Chen Q, Liu X, Sun Q, Zhao X, Deng R, Wang YL, Huang J, Xu M, Yan JS, Yu JX. lncRNA H19/miR-675 axis represses prostate cancer metastasis by targeting TGFBI. *Febs J.* 2014; 281:3766-3775.
 50. Duns G, van den Berg A, van Dijk MCRF, van Duivenbode I, Giezen C, Kluiver J, van Goor H, Hofstra RMW, van den Berg E, Kok K. The entire miR-200 seed family is strongly deregulated in clear cell renal cell cancer compared to the proximal tubular epithelial cells of the kidney. *Gene Chromosome Canc.* 2013; 52:165-173.
 51. Liu YW, Sun M, Xia R, Zhang EB, Liu XH, Zhang ZH, Xu TP, De W, Liu BR, Wang ZX. LincHOTAIR epigenetically silences miR34a by binding to PRC2 to promote the epithelial-to-mesenchymal transition in human gastric cancer. *Cell Death Dis.* 2015; 6:e1802.
 52. Jin Y, Feng SJ, Qiu S, Shao N, Zheng JH. lncRNA MALAT1 promotes proliferation and metastasis in epithelial ovarian cancer *via* the PI3K-AKT pathway. *Eur Rev Med Pharmacol Sci.* 2017; 21:3176-3184.
 53. Sun R, Qin C, Jiang B, Fang S, Pan X, Peng L, Liu Z, Li W, Li Y, Li G. Down-regulation of MALAT1 inhibits cervical cancer cell invasion and metastasis by inhibition of epithelial-mesenchymal transition. *Mol Biosyst.* 2016; 12:952-962.
 54. Ma CC, Nong KT, Zhu HD, Wang WW, Huang XY, Yuan Z, Ai KX. H19 promotes pancreatic cancer metastasis by derepressing let-7's suppression on its target HMGA2-mediated EMT. *Tumor Biol.* 2014; 35:9163-9169.
 55. Yan L, Zhou J, Gao Y, Ghazal S, Lu L, Bellone S, Yang Y, Liu N, Zhao X, Santin AD, Taylor H, Huang Y. Regulation of tumor cell migration and invasion by the H19/let-7 axis is antagonized by metformin-induced DNA methylation. *Oncogene.* 2015; 34:3076-3084.
 56. Zhao L, Li Z, Chen W, Zhai W, Pan J, Pang H, Li X. H19 promotes endometrial cancer progression by modulating epithelial-mesenchymal transition. *Oncol Lett.* 2017; 13:363-369.
 57. Zhou X, Chen J, Tang W. The molecular mechanism of HOTAIR in tumorigenesis, metastasis, and drug resistance. *Acta biochimica et biophysica Sinica.* 2014; 46:1011-1015.
 58. Kim HJ, Lee DW, Yim GW, Nam EJ, Kim S, Kim SW, Kim YT. Long non-coding RNA HOTAIR is associated with human cervical cancer progression. *Int J Oncol.* 2015; 46:521-530.
 59. Sharma S, Mandal P, Sadhukhan T, Chowdhury RR, Mondal NR, Chakravarty B, Chatterjee T, Roy S, Sengupta S. Bridging Links between Long Noncoding RNA HOTAIR and HPV Oncoprotein E7 in Cervical Cancer Pathogenesis. *Sci Rep.* 2015; 5:11724
 60. Qiu JJ, Lin YY, Ye LC, Ding JX, Feng WW, Jin HY, Zhang Y, Li Q, Hua KQ. Overexpression of long non-coding RNA HOTAIR predicts poor patient prognosis and promotes tumor metastasis in epithelial ovarian cancer. *Gynecol Oncol.* 2014; 134:121-128.
 61. Colombo T, Farina L, Macino G, Paci P. PVT1: A Rising Star among Oncogenic Long Noncoding RNAs. *Biomed Res Int.* 2015; 2015:304208
 62. You L, Chang D, Du HZ, Zhao YP. Genome-wide screen identifies PVT1 as a regulator of Gemcitabine sensitivity in human pancreatic cancer cells. *Biochem Bioph Res Co.* 2011; 407:1-6.
 63. Sun M, Song HB, Wang SY, Zhang CX, Zheng L, Chen FF, Shi DD, Chen YY, Yang CG, Xiang ZX, Liu Q, Wei C, Xiong B. Integrated analysis identifies microRNA-195 as a suppressor of Hippo-YAP pathway in colorectal cancer. *J Hematol Oncol.* 2017; 10:79.
 64. Liu FT, Zhu PQ, Luo HL, Zhang Y, Hao TF, Xia GF, Zhu ZM, Qiu C. Long noncoding RNA ANRIL: A potential novel prognostic marker in cancer: A meta-analysis. *Minerva Med.* 2016; 107:77-83.
 65. Qiu JJ, Lin YY, Ding JX, Feng WW, Jin HY, Hua KQ. Long non-coding RNA ANRIL predicts poor prognosis and promotes invasion/metastasis in serous ovarian cancer. *Int J Oncol.* 2015; 46:2497-2505.
 66. Zhang DL, Sun GX, Zhang HX, Tian J, Li YY. Long non-coding RNA ANRIL indicates a poor prognosis of cervical cancer and promotes carcinogenesis *via* PI3K/Akt pathways. *Biomed Pharmacother.* 2017; 85:511-516.
 67. Zhang JJ, Wang DD, Du CX, Wang Y. Long Noncoding RNA ANRIL Promotes Cervical Cancer Development by Acting as a Sponge of miR-186. *Oncol Res.* 2018; 26:345-352.
 68. Xue M, Chen W, Li X. Urothelial cancer associated 1: A long noncoding RNA with a crucial role in cancer. *J Cancer Res Clin.* 2016; 142:1407-1419.
 69. Lu L, Shen Y, Tseng KF, Liu WL, Duan H, Meng W. Silencing of UCA1, a poor prognostic factor, inhibited the migration of endometrial cancer cell. *Cancer Biomark.* 2016; 17:171-177.
 70. Cheng ZP, Guo J, Chen L, Luo N, Yang WH, Qu XY. A long noncoding RNA AB073614 promotes tumorigenesis and predicts poor prognosis in ovarian cancer. *Oncotarget.* 2015; 6:25381-25389.
 71. Li J, Wang YM, Song YL. Knockdown of long noncoding RNA AB073614 inhibits glioma cell proliferation and migration *via* affecting epithelial-mesenchymal transition. *Eur Rev Med Pharmacol.* 2016; 20:3997-4002.
 72. Wang YN, Kuang HY, Xue JF, Liao LY, Yin F, Zhou XJ. lncRNA AB073614 regulates proliferation and metastasis of colorectal cancer cells *via* the PI3K/AKT signaling pathway. *Biomed Pharmacother.* 2017; 93:1230-1237.
 73. Sun NX, Ye C, Zhao Q, Zhang Q, Xu C, Wang SB, Jin ZJ, Sun SH, Wang F, Li W. Long Noncoding RNA-EBIC Promotes Tumor Cell Invasion by Binding to EZH2 and Repressing E-Cadherin in Cervical Cancer. *PloS one.* 2014; 9:e100340.
 74. Guo X, Hua Y. CCAT1: An oncogenic long noncoding RNA in human cancers. *J Cancer Res Clin Oncol.* 2017; 143:555-562.
 75. Yu X, Li Z, Zheng H, Chan MT, Wu WK. NEAT1: A

- novel cancer-related long non-coding RNA. *Cell Prolif.* 2017; 50:e12329.
76. Li P, Zhang X, Lin L, Chen GL, Chen J. Silencing of the long non-coding RNA NEAT1 suppresses ovarian cancer cell proliferation, migration and invasion. *Int J Clin Exp Pathol.* 2016; 9:5138-5147.
 77. Li Z, Shen J, Chan MTV, Wu WKK. The long non-coding RNA SPRY4-IT1: An emerging player in tumorigenesis and osteosarcoma. *Cell Prolif.* 2018; 51:e12446
 78. Yu J, Han Q, Cui YL. Decreased long non-coding RNA SPRY4-IT1 contributes to ovarian cancer cell metastasis partly *via* affecting epithelial-mesenchymal transition. *Tumor Biol.* 2017; 39:1010428317709129.
 79. Hu YY, Sun XW, Mao CC, Guo GQ, Ye SS, Xu JF, Zou RM, Chen J, Wang LD, Duan P, Xue XY. Upregulation of long noncoding RNA TUG1 promotes cervical cancer cell proliferation and migration. *Cancer Med-Us.* 2017; 6:471-482.
 80. Sun JF, Ding CH, Yang Z, Liu T, Zhang XF, Zhao CL, Wang JX. The long non-coding RNA TUG1 indicates a poor prognosis for colorectal cancer and promotes metastasis by affecting epithelial-mesenchymal transition. *J Transl Med.* 2016; 14:42.
 81. Flockhart RJ, Webster DE, Qu K, Mascarenhas N, Kovalski J, Kretz M, Paul KA. BRAFV600E remodels the melanocyte transcriptome and induces BANCR to regulate melanoma cell migration. *Cancer Res.* 2012; 22:1006-1014.
 82. Wang D, Wang D, Wang N, Long Z, Ren X. Long Non-Coding RNA BANCR Promotes Endometrial Cancer Cell Proliferation and Invasion by Regulating MMP2 and MMP1 *via* ERK/MAPK Signaling Pathway. *Cell Physiol Biochem.* 2016; 40:644-656.
 83. Pan Y, Li C, Chen J, Zhang K, Chu X, Wang R, Chen L. The Emerging Roles of Long Noncoding RNA ROR (lincRNA-ROR) and its Possible Mechanisms in Human Cancers. *Cell Physiol Biochem.* 2016; 40:219-229.
 84. Lou Y, Jiang H, Cui Z, Wang L, Wang X, Tian T. Linc-ROR induces epithelial-to-mesenchymal transition in ovarian cancer by increasing Wnt/beta-catenin signaling. *Oncotarget.* 2017; 8:69983-69994.
 85. Loebel DAF, Tsoi B, Wong N, Tam PPL. A conserved noncoding intronic transcript at the mouse Dnm3 locus. *Genomics.* 2005; 85:782-789.
 86. Mitra R, Chen X, Greenawalt EJ, Maulik U, Jiang W, Zhao ZM, Eischen CM. Decoding critical long non-coding RNA in ovarian cancer epithelial-to-mesenchymal transition. *Nat Commun.* 2017; 8:1604.
 87. Shahryari A, Jazi MS, Samaei NM, Mowla SJ. Long non-coding RNA SOX2OT: Expression signature, splicing patterns, and emerging roles in pluripotency and tumorigenesis. *Frontiers in genetics.* 2015; 6:196.
 88. Han L, Zhang W, Zhang BY, Zhan LY. Long non-coding RNA SOX2OT promotes cell proliferation and motility in human ovarian cancer. *Exp Ther Med.* 2018; 15:2182-2188.
 89. Lu CW, Zhou DD, Xie T, Hao JL, Pant OP, Lu CB, Liu XF. HOXA11 antisense long noncoding RNA (HOXA11-AS): A promising lincRNA in human cancers. *Cancer Med.* 2018; 00:1-8.
 90. Yim GW, Kim HJ, Kim LK, Kim SW, Kim S, Nam EJ, Kim YT. Long Non-coding RNA HOXA11 Antisense Promotes Cell Proliferation and Invasion and Predicts Patient Prognosis in Serous Ovarian Cancer. *Cancer Res Treat.* 2017; 49:656-668.
 91. Bussemakers MJG, van Bokhoven A, Verhaegh GW, Smit FP, Karthaus HFM, Schalken JA, Debruyne FMJ, Ru N, Issacs WB. DD3: A new prostate-specific gene, highly overexpressed in prostate cancer. *Cancer Res.* 1999; 59:5975-5979.
 92. Panzitt K, Tschernatsch MMO, Guelly C, Moustafa T, Stradner M, Strohmaier HM, Buck CR, Denk H, Schroeder R, Trauner M, Zatloukal K. Characterization of HULC, a novel gene with striking up-regulation in hepatocellular carcinoma, as noncoding RNA. *Gastroenterology.* 2007; 132:330-342.
 93. Pan L, Liang W, Fu M, Huang ZH, Li X, Zhang W, Zhang P, Qian H, Jiang PC, Xu WR, Zhang X. Exosomes-mediated transfer of long noncoding RNA ZFAS1 promotes gastric cancer progression. *J Cancer Res Clin.* 2017; 143:991-1004.
 94. Berrondo C, Flax J, Kucherov V, Siebert A, Osinski T, Rosenberg A, Fucile C, Richheimer S, Beckham CJ. Expression of the Long Non-Coding RNA HOTAIR Correlates with Disease Progression in Bladder Cancer and Is Contained in Bladder Cancer Patient Urinary Exosomes. *PloS one.* 2016; 11:e0147236
 95. Conigliaro A, Costa V, Lo Dico A, Saieva L, Buccheri S, Dieli F, Manno M, Raccosta S, Mancone C, Tripodi M, De Leo G, Alessandro R. CD90+liver cancer cells modulate endothelial cell phenotype through the release of exosomes containing H19 lincRNA. *Mol Cancer.* 2015; 14:155
 96. Gezer U, Ozgur E, Cetinkaya M, Isin M, Dalay N. Long non-coding RNAs with low expression levels in cells are enriched in secreted exosomes. *Cell Biol Int.* 2014; 38:1076-1079.
 97. Xu CG, Yang MF, Ren YQ, Wu CH, Wang LQ. Exosomes mediated transfer of lincRNA UCA1 results in increased tamoxifen resistance in breast cancer cells. *Eur Rev Med Pharmacol Sci.* 2016; 20:4362-4368.
 98. Gutschner T, Hammerle M, Eissmann M, Hsu J, Kim Y, Hung G, Revenko A, Arun G, Stentrup M, Gross M, Zornig M, MacLeod AR, Spector DL, Diederichs S. The Noncoding RNA MALAT1 Is a Critical Regulator of the Metastasis Phenotype of Lung Cancer Cells. *Cancer Res.* 2013; 73:1180-1189.
 99. Arun G, Diermeier S, Akerman M, Chang KC, Wilkinson JE, Hearn S, Kim Y, MacLeod AR, Krainer AR, Norton L, Brogi E, Egeblad M, Spector DL. Differentiation of mammary tumors and reduction in metastasis upon malat1 lincrna loss. *Genes Dev.* 2016; 30:34-51.

(Received August 5, 2018 Revised August 10, 2018; Accepted August 19, 2018)

Transcriptomic responses of peripheral blood cells to coronary artery disease

Mingshan Lin, Yuan Zhang, Zhaozhuo Niu, Yifan Chi, Qiang Huang*

Department of Cardiovascular Surgery, Qingdao Municipal Hospital, Qingdao, Shandong, China.

Summary

Transcriptomic response of peripheral blood cells to coronary artery diseases (CAD) is a long recognized phenomenon. Currently, accumulating evidence indicates that such response having significant clinical utility in CAD-associated events determination. In this review, we summarized the existing data of transcriptomic biomarkers at mRNA, microRNA, long non-coding RNA, and circular RNA for the diagnosis, progression and outcome prediction and treatment response of CAD. Furthermore, we also discussed the functional significance on the gene expression patterns caused by CAD, and emphasized the importance of inflammatory pathways in CAD tissues-blood cells interaction. Based on the current knowledge, we proposed a perspective on the future strategies to further improve the robustness and reproducibility of transcriptomic biomarkers in the personalized medicine of CAD patients.

Keywords: Coronary artery diseases, transcriptome, biomarkers, peripheral blood cells, non-coding RNA

1. Introduction

Coronary artery disease (CAD) represents a major public health problem and remains the main cause of morbidity and mortality globally. Despite remarkable advances in the management, the success of prognostic and therapeutic options remains modest (1). Therefore, more personalized strategies are still needed for this condition, in particular risk-assessment strategies to detect or predict a substantial number of clinical outcome events such as recurrence and heart failure.

In the last decade, many efforts have been devoted to identify novel diagnostic or prognostic biomarkers among the entire transcriptome of peripheral blood cells of the CAD patients (2). These discovery studies are based on the assumption that gene expression profiling of circulating blood using microarrays and deep RNA sequencing technologies might reflect

physiological and pathological events occurring in different tissues of the body including CAD-related tissues. Currently, many CAD-associated RNAs confined in blood cell have been identified at mRNA, microRNA (miRNA), long non-coding RNA (lncRNA), and circular RNA (circRNA) levels. Noteworthy, based on these biomarkers, several diagnostic and predictive gene models with good performance have been developed. For example, a prospective multi-center study validated that a peripheral blood-based 23-gene expression model can provide modest but statistically significant improvement in determining the likelihood of obstructive CAD in non-diabetic patients as compared to clinical factors and other non-invasive imaging methods (3). Furthermore, another independent prospective multi-center trial demonstrated that integrating this gene signature with age and sex to calculate a diagnostic score can significantly predict near-term revascularization procedures (4). Therefore, as a new, quick, reproducible and robust method, the gene expression-based classifiers show promising clinical utility potentials in the diagnosis and prognosis prediction in CAD.

Although advances in screening, before these blood RNA biomarkers can revolutionize the clinical laboratory medicine and patient management of

Released online in J-STAGE as advance publication August 26, 2018.

*Address correspondence to:

Dr. Qiang Huang, Department of Cardiovascular Surgery, Qingdao Municipal Hospital, #1 Jiaozhou Road, Qingdao 266011, China.

E-mail: qdsslyhuangqiang@163.com

CAD, some basic concept must be addressed first, such as whether and what extent of whole blood gene expression patterns can reflect the presence, severity and prognosis of infarcted tissues? Whether transcriptomic responses of peripheral blood cells to CAD have important functional significance?

Here, we reviewed the current state of knowledge regarding CAD transcriptomic characteristics from the growing literature, and discussed the promising results in their clinical utility in CAD events prediction. In addition, we also discussed the functional significance of "bloodomics" response to CAD, and challenges and future perspective in this field.

2. Peripheral blood cells biomarkers for CAD at mRNA level

Dysregulation of a subset of genes including arachidonate 15-lipoxygenase (*ALOX15*), amphiregulin (*AREG*), BCL2 related protein A1 (*BCL2A1*), BCL2 like 1 (*BCL2L1*), carbonic anhydrase 1 (*CA1*), cytochrome c oxidase subunit 7B (*COX7B*), enoyl-CoA hydratase domain containing 3 (*ECHDC3*), interleukin 18 receptor 1 (*IL18R1*), immune response 2 (*IR2*), potassium voltage-gated channel subfamily E regulatory subunit 1 (*KCNE1*), matrix metalloproteinase 9 (*MMP9*), myosin light chain 4 (*MYL4*) and triggering receptor expressed on myeloid cells like 4 (*TREML4*) in peripheral blood cells showed a close correlation with the presence of acute coronary syndrome (ACS) at the very early stages (5). Gene annotation analysis reveals that these genes are significantly enriched in interleukins signaling, one of the key regulatory mechanisms accounting for the development of atherosclerosis. For discriminating progressive and stable CAD, an 8-gene risk prediction signature (X inactive specific transcript (*XIST*), glutathione S-transferase theta 1 (*GSTT1*), natriuretic peptide A (*NPPA*), kinesin family member 20B (*KIF20B*), *CR625615*, ankyrin 2 (*ANK2*), FLYWCH-type zinc finger 1 (*FLYWCH1*), A_24_P473972) combined with classic protein biomarkers and clinical indicators were suggested (6). Among this signature, two genes *ANK2* and *GSTT1* were independently validated using quantitative real-time PCR (6). It has been proposed that *GSTT1*, as a detoxification enzyme, is responsible for the production of oxidative stress, and may contribute to the development of CAD (7).

Kiliszek *et al.* (8) revealed that dozens of genes involved in lipid/glucose metabolism, platelet function and atherosclerotic plaque stability significantly altered among gene expression pattern in peripheral blood mononuclear cells (PBMC) in the acute phase of ST-segment elevation myocardial infarction (STEMI). In particular, suppressor of cytokine signaling 3 (*Socs3*) and golgi associated secretory pathway pseudokinase (*FAM20*) expression in PBMC were up-

regulated in the first days of myocardial infarction in the vast majority of patients (8). Another study also linked gene expression patterns in peripheral blood of peripheral blood cells with the severity of CAD (9). This study identified 160 genes significantly correlated with CAD index, a validated angiographical measure of the extent of CAD that correlates with outcome. Most interestingly, this expression pattern could also accurately separate the aorta samples according to the severity of atherosclerosis in another independent gene expression dataset (9). This finding further support the notion that gene expression changed derived from peripheral blood can reflect similar pathophysiological changes in remote disease sites such as atherosclerotic arteries.

Classic protein biomarkers are less useful in predicting the long term events of CAD. A study by Suresh *et al.* (10) identified two subsets of genes belonging to epithelial mesenchymal transition (EMT) pathway, and cholesterol transport modulation associated with long-term (18 months) recurrent events following first-time myocardial infarction. Heart failure is another occurred consequence of CAD. Maciejak *et al.* (11) revealed that the up-regulation of ribonuclease A family member 1 (*RNASE1*), formin 1 (*FMN1*), and Jun dimerization protein 2 (*JDP2*) genes on the first day of STEMI can serve as potential prognostic biomarkers for the progression of heart failure after AMI. These findings support that the transcriptomic data of the circulating blood cells may provide new clues in the prognosis prediction of CAD.

3. Peripheral blood cells biomarkers for CAD at miRNA level

As mRNA levels, miRNA profiles of whole blood cells have shown potential utility in CAD diagnosis, prediction, and monitoring. From an unbiased screen of blood cells of CAD, miR-135a expression was significantly increased compared with unaffected controls, while miR-147 decreased (12). Dong *et al.* (13) identified miR-24, miR-33, miR-103a, and miR-122 correlated with blood lipids and their combination can provide a high diagnostic accuracy of CAD. Hoekstra *et al.* (14) indicated a cluster of 3 miRNAs, miR-134, miR-198 and miR-370, which can discriminate unstable CAD cases.

Downregulation of miRNA-8059, a miRNA with unknown function, can serve as a peripheral blood biomarker for the presence and extent of coronary artery calcification (15). Except for reflecting the severity of CAD, peripheral blood cells also have prognostic significance. A miRNA regulating development of myeloid vs lymphoid, miR-23a acts as a strong predictor for clinical outcomes in CAD patients after adjustment for baseline characteristics (16).

More meaningfully, miRNA profiling is also used

Table 1. Validated transcriptomic biomarkers for coronary artery diseases

Items	Acute coronary syndrome Biomarkers	Progression biomarkers	Clinical factors-associated biomarkers	Outcome predictor	Treatment response biomarkers
mRNA	ALOX15 AREG BCL2A1 BCL2L1 CA1 COX7B ECHDC3 IL18R1 IR2 KCNE1 MMP9 MYL4 TREML4 SOCS3 FAM20	XIST GSTT1 NPPA KIF20B CR625615 ANK2 FLYWCH1 A_24_P473972		Heart failure: RNASE1 FMN1 JDP2	Renin-angiotensin system blockade and statins treatment: IRAK1 TRAF6 TLR4
microRNA	miR-135 miR-147 miR-24 miR-33 miR-103a miR-122	miR-134 miR-198 miR-370	Extent of coronary artery calcification: miRNA-8059 lipid levels: miR-24 miR-33 miR-103a miR-122	Clinical outcome: miR-23a	Resveratrol supplementation: miR-21 miR-181b miR-663 miR-30c-2 miR-155 miR-34a Renin-angiotensin system blockade and statins treatment: miR-146a/b
LncRNA	LncPPAR δ CoroMarker				
circRNA	circRNA11783-2				

to create biomarkers associated with treatments in CAD. Tomé-Carneiro *et al.* (17) found that after one-year supplementation with a grape extract containing resveratrol in CAD patients, the expression of pro-inflammatory cytokines C-C motif chemokine ligand 3 (CCL3), interleukin 1 beta (IL-1 β) and tumor necrosis factor alpha (TNF- α) was significantly reduced in peripheral mononuclear blood cells (PMBCs), while a subset of inflammatory-related miRNAs including miR-21, miR-181b, miR-663, miR-30c2, miR-155 and miR-34a was also altered. In another clinical observation, after treated with renin-angiotensin system blockade and statins, the expression of miR-146a/b, interleukin 1 receptor associated kinase 1 (*IRAK1*), TNF receptor associated factor 6 (*TRAF6*) and toll like receptor 4 (*TLR4*) genes in PMBCs of CAD were markedly decreased (18). Therefore, these findings support a possibility of transcriptomic response to CAD may also be used as potential therapeutic biomarkers.

4. Transcriptomic biomarkers for CAD at lncRNAs and circular RNAs (circRNAs) levels

Compared with mRNA and miRNA, the studies investigating in the context of lncRNA expression pattern in CAD are limited. Cai *et al.* (19,20) examined

the lncRNA profiles in PMBCs, and discovered two lncRNA (LncPPAR δ , CoroMarker) as novel biomarkers for CAD, which can enhance the diagnostic specificity and sensitivity when combined with other risk factors. They further identified monocyte CoroMarker levels independent of known CAD risk factors and other cardiovascular diseases.

As a 'miRNA sponge', circRNAs have been validated to be functionally linked with CAD progression. However, the clinical significance of circulating circRNA for CAD has seldom been evaluated. Currently, only one study investigated the circRNA profiles of whole blood cells on CAD, and they found hsa-circRNA11783-2, a functionally unknown circRNA is closely related to CAD and diabetes (21).

5. The functional significance of transcriptomic response of peripheral blood cells to CAD

Although thousands of blood cell genes dysregulated in CAD, only a minority of them were validated as diagnostic and prognostic biomarkers (Table 1). The expression patterns of peripheral blood cells indirectly reflect the remote diseases status, and are induced by cytokines cascades from CAD. Several secretory factors are indicated to be independently associated

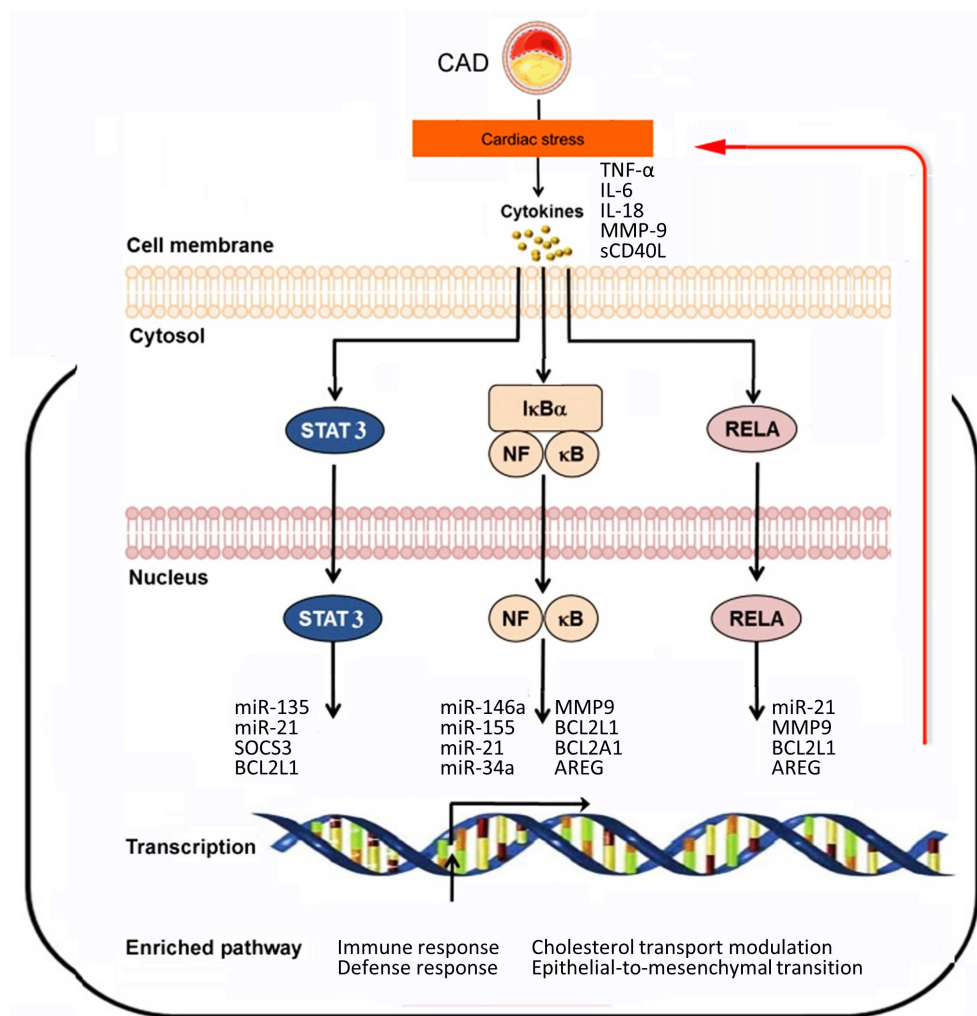


Figure 1. Functional analysis on the transcriptomic response of peripheral blood cells to coronary artery diseases.

with the severity of CAD. Among them, interleukin 6 (IL-6), interleukin 18 (IL-18), MMP-9, soluble CD40-ligand (sCD40L) and TNF α can theoretically induce the expression profiles of peripheral blood cells at all the transcriptomic levels (22). However, if these peripheral blood cells response can attribute or protect the damage of CAD has not been fully clarified.

GSTT1 is an enzyme regulating oxidative stress; its polymorphisms are associated with plasma malondialdehyde-conjugated low-density lipoprotein (MDA-LDL) levels and CAD risk (23). The overexpression of GSTT1 in PBMCs indicates that it may participate in the development of CAD through PBMCs. Significantly most of current validated peripheral blood cells mRNA and miRNA biomarkers are mediated by several important inflammatory transcription factors including signal transducer and activator of transcription-3 (STAT3), nuclear factor κ B (NF- κ B) (Figure 1). There is also strong coherence between mRNA and miRNA profiles. For example, EMT genes were enriched in CAD heart failure-related mRNA transcriptome; meanwhile some validated miRNA biomarkers also belong to EMT regulators

such as miR-23a, miR-147, and miR-122. According to the current data, transcriptomic response of peripheral blood cells significantly focuses four biological process, immune response, defense response, cholesterol transport modulation, and EMT (Figure 1). Moreover, it can be also deduced that as a result of gene expression pattern variation, some peripheral blood cells-derived cytokines and secretory proteins such as MMP-9 would also participate in the development of CAD in a positive feedback manner.

6. Future perspective

Although widely used, the current classic protein biomarkers and invasive coronary angiography to diagnose and prognostic CAD still have limitations. Current evidence has demonstrated the clinical validity and utility of "bloodomics" data to reflect CAD status. In particular, a whole blood gene expression score has been developed and validated its robustness in discriminating CAD patients from other non-cardiac conditions in two prospective multi-center trials (24). Compared with the traditional assays, blood

transcriptome-based test might be very powerful in prognosis prediction, disease and treatment monitoring.

Although the current results of the evaluation are very promising, more cautions should be paid when explain the gene expression pattern of CAD peripheral blood cells, which can be affected by many complicated abnormal conditions. Currently transcriptomic biomarkers research differs tremendously among all reported studies. Therefore, biomarkers selection and algorithm developing from blood transcriptome of CAD must be based on strict validation test in multi-center, large cohorts of trails prospectively.

Now, the present "bloodomics" studies of CAD only focus on individual levels. Considering the inherent correlation between mRNA, miRNA, lncRNA and circRNA expression pattern, discovery and evaluation of more generalized biomarkers at multiple levels of transcriptomic data would further increase the robustness of current strategies.

In the emerging field of peripheral blood cells transcriptome of CAD, increased biomarkers and models show clinical potential utility in diagnosis, outcome prediction and treatment monitoring, and with functional significance in the disease development. Before the further clinical use of transcriptomic biomarkers in personalized healthcare of CAD patients, more elaborate studies are required to improve their powers through well-designed large multicenter trial cohort studies.

Acknowledgement

This study was supported by Qingdao Medicine Research Project (2016-WJZD022).

References

- van den Hoogen PC, Feskens EJ, Nagelkerke NJ, Menotti A, Nissinen A, Kromhout D. The relation between blood pressure and mortality due to coronary heart disease among men in different parts of the world. Seven Countries Study Research Group. *N Engl J Med.* 2000; 342:1-8.
- Chen HH, Stewart AF. Transcriptomic signature of atherosclerosis in the peripheral blood: Fact or fiction? *Curr Atheroscler Rep.* 2016; 18:77.
- Rosenberg S, Elashoff MP, Daniels SE, *et al.* Multicenter validation of the diagnostic accuracy of a blood-based gene expression test for assessing obstructive coronary artery disease in nondiabetic patients. *Ann Intern Med.* 2010; 153:425-434.
- Voorra D, Coles A, Lee KL, Hoffmann U, Wingrove JA, Rhees B, Huang L, Daniels SE, Monane M, Rosenberg S, Shah SH, Kraus WE, Ginsburg GS, Douglas PS. An age- and sex-specific gene expression score is associated with revascularization and coronary artery disease: Insights from the Prospective Multicenter Imaging Study for Evaluation of Chest Pain (PROMISE) trial. *Am Heart J.* 2017; 184:133-140.
- Silbiger VN, Luchessi AD, Hirata RD, Lima-Neto LG, Cavichioli D, Carracedo A, Brión M, Dopazo J, García-García F, dos Santos ES, Ramos RF, Sampaio MF, Armaganijan D, Sousa AG, Hirata MH. Novel genes detected by transcriptional profiling from whole-blood cells in patients with early onset of acute coronary syndrome. *Clin Chim Acta.* 2013; 421:184-190.
- Nührenberg TG, Langwieser N, Binder H, Kurz T, Stratz C, Kienzle RP, Trenk D, Zohnhöfer-Momm D, Neumann FJ. Transcriptome analysis in patients with progressive coronary artery disease: Identification of differential gene expression in peripheral blood. *J Cardiovasc Transl Res.* 2013; 6:81-93.
- Kadioğlu E, Taçoş G, Özçağılı E, Okyay K, Akboğa MK, Çengel A, Şardaş S. The role of oxidative DNA damage and GSTM1, GSTT1, and hOGG1 gene polymorphisms in coronary artery disease risk. *Anatol J Cardiol.* 2016; 16:931-938.
- Kiliszek M, Burzynska B, Michalak M, Gora M, Winkler A, Maciejak A, Leszczynska A, Gajda E, Kochanowski J, Opolski G. Altered gene expression pattern in peripheral blood mononuclear cells in patients with acute myocardial infarction. *PLoS One.* 2012; 7:e50054.
- Sinnaeve PR, Donahue MP, Grass P, Seo D, Vonderscher J, Chibout SD, Kraus WE, Sketch M Jr, Nelson C, Ginsburg GS, Goldschmidt-Clermont PJ, Granger CB. Gene expression patterns in peripheral blood correlate with the extent of coronary artery disease. *PLoS One.* 2009; 4:e7037.
- Suresh R, Li X, Chiriac A, Goel K, Terzic A, Perez-Terzic C, Nelson TJ. Transcriptome from circulating cells suggests dysregulated pathways associated with long-term recurrent events following first-time myocardial infarction. *J Mol Cell Cardiol.* 2014; 74:13-21.
- Maciejak A, Kiliszek M, Michalak M, Tulacz D, Opolski G, Matlak K, Dobrzycki S, Segiet A, Gora M, Burzynska B. Gene expression profiling reveals potential prognostic biomarkers associated with the progression of heart failure. *Genome Med.* 2015; 7:26.
- Hoekstra M, van der Lans CA, Halvorsen B, Gullestad L, Kuiper J, Aukrust P, van Berkel TJ, Biessen EA. The peripheral blood mononuclear cell microRNA signature of coronary artery disease. *Biochem Biophys Res Commun.* 2010; 394:792-797.
- Dong J, Liang YZ, Zhang J, Wu LJ, Wang S, Hua Q, Yan YX. Potential role of lipometabolism-related microRNAs in peripheral blood mononuclear cells as biomarkers for coronary artery disease. *J Atheroscler Thromb.* 2017; 24:430-441.
- Hoekstra M, van der Lans CA, Halvorsen B, Gullestad L, Kuiper J, Aukrust P, van Berkel TJ, Biessen EA. The peripheral blood mononuclear cell microRNA signature of coronary artery disease. *Biochem Biophys Res Commun.* 2010; 394:792-797.
- Howlett P, Cleal JK, Wu H, Shah N, Horton A, Curzen N, Mahmoudi M. MicroRNA 8059 as a marker for the presence and extent of coronary artery calcification. *Open Heart.* 2018; 5:e000678.
- Satoh M, Nasu T, Takahashi Y, Osaki T, Hitomi S, Morino Y, Nakamura M. Expression of miR-23a induces telomere shortening and is associated with poor clinical outcomes in patients with coronary artery disease. *Clin Sci (Lond).* 2017; 131:2007-2017.
- Tomé-Carneiro J, González M, Larrosa M, Yáñez-Gascón MJ, García-Almagro FJ, Ruiz-Ros JA, Tomás-Barberán FA, García-Conesa MT, Espín JC.

- Grape resveratrol increases serum adiponectin and downregulates inflammatory genes in peripheral blood mononuclear cells: A triple-blind, placebo-controlled, one-year clinical trial in patients with stable coronary artery disease. *Cardiovasc Drugs Ther.* 2013; 27:37-48.
18. Takahashi Y, Satoh M, Minami Y, Tabuchi T, Itoh T, Nakamura M. Expression of miR-146a/b is associated with the Toll-like receptor 4 signal in coronary artery disease: Effect of renin-angiotensin system blockade and statins on miRNA-146a/b and Toll-like receptor 4 levels. *Clin Sci (Lond).* 2010; 119:395-405.
 19. Cai Y, Yang Y, Chen X, He D, Zhang X, Wen X, Hu J, Fu C, Qiu D, Jose PA, Zeng C, Zhou L. Circulating "LncPPAR δ " from monocytes as a novel biomarker for coronary artery diseases. *Medicine (Baltimore).* 2016; 95:e2360.
 20. Cai Y, Yang Y, Chen X, Wu G, Zhang X, Liu Y, Yu J, Wang X, Fu J, Li C, Jose PA, Zeng C, Zhou L. Circulating 'lncRNA OTTHUMT00000387022' from monocytes as a novel biomarker for coronary artery disease. *Cardiovasc Res.* 2016; 112:714-724.
 21. Li X, Zhao Z, Jian D, Li W, Tang H, Li M. Hsa-circRNA11783-2 in peripheral blood is correlated with coronary artery disease and type 2 diabetes mellitus. *Diab Vasc Dis Res.* 2017; 14:510-515.
 22. Rodgers GP, Kopecky S. The future of cardiovascular biomarkers. *Am Heart Hosp J.* 2006; 4:228-231.
 23. Ueno T, Watanabe H, Fukuda N, Tsunemi A, Tahira K, Matsumoto T, Takayama T, Chiku M, Saito S, Sato Y, Hirayama A, Matsumoto K, Soma M. Influence of genetic polymorphisms in oxidative stress related genes and smoking on plasma MDA-LDL, soluble CD40 ligand, E-selectin and soluble ICAM1 levels in patients with coronary artery disease. *Med Sci Monit.* 2009; 15:CR341-348.
 24. Vargas J, Lima JA, Kraus WE, Douglas PS, Rosenberg S. Use of the Corus[®] CAD Gene Expression Test for Assessment of Obstructive Coronary Artery Disease Likelihood in Symptomatic Non-Diabetic Patients. *PLoS Curr.* 2013; 5. pii: ecurrents.eogt.0f04f6081905998fa92b99593478aea.

(Received April 24, 2018; Revised July 21, 2018; Accepted August 8, 2018)

Combined biomarkers composed of environment and genetic factors in stroke

Yingying Wang¹, Jianfeng Liu², Hongyan Wu^{1,*}, Yunpeng Cai^{1,*}

¹ Research Center for Biomedical Information Technology, Shenzhen Institutes of Advanced Technologies, Chinese Academy of Sciences, Shenzhen, China;

² Department of Neurology, The First Affiliated Hospital of Harbin Medical University, Harbin, China.

Summary

It was widely accepted that stroke onset was the result of interactions between environment and genetic factors. However, the combined biomarkers covering environment and genetic factors and their interplay information in stroke were still lacking. In this study, we proposed a framework to identify the targeting or indicating role each factor played in the combined stroke biomarkers. A combined set of 36 biomarkers were identified based on evaluation and importance scores. Validations on three independent microarray data sets justified that the obtained markers were pervasively effective in discriminating stroke patients of different stages from healthy people on genetic levels. 8 and 3 genetic factors were identified as biomarkers in the acute and recovery phases of stroke, respectively. For example, the expression changing of *SERPINH1* only appeared in the acute phase of stroke showing its targeting role in the combined biomarker. Compared with this, 11 genetic factors such as *MMP9* were found to be differentially expressed in both acute and recovery phases of stroke showing their indicating roles in stroke. Functional analyses further revealed that the biomarkers could be grouped into 4 closely related processes of stroke including prevention, occurrence, processing, and recovery, respectively. These results indicated that the adoption of interactions between environment and genetic factors would be helpful in selecting robust and biologically relevant biomarkers, which cast a new insight for stroke biomarker identification.

Keywords: Combined biomarker, genetic factor, environment factor, interaction, stroke

1. Introduction

Stroke, as one of the leading causes of death and disability in the world, has attracted lots of research efforts on the analyses of its underlying mechanisms on 'Omics levels continuously since the 20th century (1). Of which, the identification framework of biomarkers that measure stroke on different molecular levels has resulted in considerable enthusiasm for their wide usage in diagnosis and prognostication. A biomarker

can be any measurement made on a biological system in theory, however, the stroke biomarkers typically refer to environment factors (EFs) and genetic factors (GFs). Many researches had been performed on EF(s) or GF(s) levels to explore the occurrence, development, and prognosis of stroke (2,3). For example, EFs such as ursolic acid (4) and GFs such as *ALOX5* (5) were shown to be closely related to the happening of stroke. Biomarkers can be generally classified into target factors and indicator factors, according to their causal relationship with the investigated disease. A target factor was one that played an important role in causing stroke, which meant that the changing of this factor would not only reflect the patient's condition, but also be a possible treatment target. In comparison, an indicator factor was one that distinguished stroke patients from healthy people, without necessarily being the cause of the disease. Usually, indicator factors were advantageous in the ability to discriminate potential

Released online in J-STAGE as advance publication August 29, 2018.

*Address correspondence to:

Dr. Hongyan Wu, and Dr. Yunpeng Cai, Shenzhen Institutes of Advanced Technologies, Chinese Academy of Sciences, 1068 Xueyuan Boulevard, University Town of Shenzhen, Xili Nanshan, Shenzhen 518055, China.

E-mail: hy.wu@siat.ac.cn; yp.cai@siat.ac.cn

patients and the ease of detection, but provided little useful information for disease treatment or prevention. On the contrary, target factors were favored for pathology or possible treatments, but may not be good for patient diagnosis or risk prediction. Ideally, a good biomarker set should contain the advantages of both types of factors and reflect the interaction(s) between them.

It was widely accepted during the past decades that the onset of stroke was the result of interactions between EFs and GFs (6). However, no combined biomarker covering both EFs and GFs on multiple omics levels were identified on stroke. The interplay(s) information between EFs and GFs under different conditions including several complex diseases were validated and stored in databases such as miREnvironment (7) and PEMDAM (8) with the development of bioinformatics which made the analyses on combined EF-GF biomarkers of stroke possible.

In this study, we proposed a framework to identify the targeting or indicating role each factor played in the combined stroke biomarkers selected based on bioinformatics analyses. The information of stroke related factors on both genetic level (including genes and miRNAs) and environment level were downloaded from several public databases. A combined set of 36 biomarkers were then chosen by an evaluation score for each candidate EF and an importance score calculated using the relationships between GFs. We further carried out validation experiments on three independent data sets with the selected biomarkers, which confirmed that the obtained markers were pervasively effective in discriminating stroke patients of different stages from healthy people. It was interesting to find out that the obtained biomarkers could further be grouped into 4 categories related to the prevention, occurrence, processing, and recovery of stroke, respectively. The classification of target and indicator factors in each combined biomarker made the relationships between environment and genetic factors clearer, which may provide a new sight for stroke prevention, treatment, and recovery.

2. Materials and Methods

2.1. Materials

Several raw data sets were built based on the data extracted from public databases as follows:

(a) Stroke-related diseases/symptoms: The following key words were used to perform the EF and GF searches according to the information from Comparative Toxicogenomics Database (CTD) (9): 'Stroke', 'Infarction, Middle Cerebral Artery', 'Cerebral Infarction', 'Brain Infarction', 'Lateral Medullary Syndrome', 'Brain Stem Infarctions', 'Infarction, Anterior Cerebral Artery', 'Infarction, Posterior Cerebral

Artery', and 'Dementia, Multi-Infarct'.

(b) Stroke-related raw EFs: 4,833 stroke EFs extracted from CTD using stroke-related diseases/symptoms (as listed in (a)) as key words.

(c) Stroke-related raw genes: 287,171 interactions were found between the 4,833 stroke-related raw EFs and 23,472 genes. These genes were marked as 'stroke-related raw genes' in the following analyses.

(d) Stroke-related raw miRNAs (SRMI): 168 miRNAs were extracted from HMDD (10), PhenomiR (11), and PEMDAM using stroke-related diseases/symptoms (as listed in (a)) as key words. Each miRNA was assigned a score calculated using the following equation:

$$W_m = S_h + S_{ph} + S_{pe},$$

Of which, if one miRNA was found to be related to stroke in HMDD or PEMDAM, the value of S_h or S_{pe} in Equation 1 was 1.0, otherwise, the value was assigned 0. Similarly, if one miRNA was found to be related to stroke in PhenomiR, S_{ph} was calculated as the product of the number of supportive literature and the number of validated types (the maximum number was 2.0, including over-regulation and down-regulation).

2.2. Candidate EFs Selections based on GFs

The relationships between EFs and miRNAs were downloaded from PEMDAM and MiREnvironment. The EFs in the 'stroke-related raw EFs' were left if at least one interaction was found. For these EFs, a score Ep , based on the interactions between GFs (including miRNAs and genes) was calculated using the following:

$$E_p = \begin{cases} \max, p \in miRTarBase \\ \sum_1^x p_x, p \notin miRTarBase \end{cases}$$

Of which, if the interaction was validated in miRTarBase (12), Ep was assigned the maximum of $p_x \cdot p_x$ represented the times the interaction predicted by 10 different miRNA target computational prediction algorithms (13).

The EFs with at least one Ep score over 0 were selected as candidate EFs (C-EF).

2.3. Evaluation Score for EF

For any C-EF i , an evaluation score was calculated as follows:

$$EE(i) = ER(i) * ES(i),$$

A higher score indicated a closer relationship between the EF and stroke. Of which, the relation score ER (EF relation score) was calculated as follows:

$$ER(i) = \sum_{i=1}^n \left(\sum_{i=1}^{n_1} E_g \sum_{i=1}^{n_2} E_m \sum_{i=1}^{n_3} E_p \right),$$

E_g was the score based on gene level, which was calculated using the interactions between EFs and genes. Of which, n_i represented the number of interactions, n_s represented the number of species, and n_l represented the number of supportive literature. E_m was the score based on miRNA level, which was calculated using the interactions between EFs and pre-miRNAs: t_n was the times each interaction between EF and miRNAs appears in the database of PEMDAM and MiREnvironment. w_m was calculated using the equation described above.

$$E_g = n_i * n_s * n_l,$$

$$E_m = \begin{cases} w_m, i \in SRMI \\ \sum_1^n t_n, i \notin SRMI \end{cases}$$

For each C-EF i , a disease specificity score ES (EF specificity score) based on the biological network analyses was calculated as follows:

$$ES(i) = \begin{cases} \text{rank}(d_i) / \max(d_i), i \in C - EF \\ 1, i \notin C - EF \end{cases}$$

Of which, d_i represents the degrees of EF i in the EF-disease network built based on the relationships between EFs and diseases from PEMDAM and miREnvironment. If the candidate EF was not included in the C-EF data set, the maximum value 1.0 was assigned for it. A higher ES score indicated a higher specificity of the EF.

2.4. Important Score for GFs

For each EF in C-EF, a network was built using its related miRNAs and genes based on the targeting information (including validated and predicted interactions between miRNAs and genes) between them.

The R package 'igraph' was used to perform the Google PageRank analyses on the miRNA-mRNA network. The PageRank score for each node in the network was used to measure the importance based on counting the number and quality of links to a node. The miRNAs and mRNAs were ranked after each of them was assigned a calculated score.

2.5. Validation based on Independent Data Sets

To validate availability of the combined biomarkers, three independent microarray data sets from NCBI GEO were chosen to check the relationships between

GFs and stroke (no such public data set for EFs were available currently) as listed in Table 1. All the samples of the three data sets were human blood. The Wilcoxon rank sum test was performed for each GF identified as a factor in any combined biomarker in this study. A GF with p -value not above the threshold we set was considered to be differentially expressed between the stroke patients and controls.

3. Results

3.1. Combined biomarkers for Stroke

There were 229 EFs in 'stroke-related raw EFs' selected as 'filtered stroke-related EFs' after the filter step based on stroke-related miRNAs. 36 EFs were finally defined as 'candidate EFs (C-EFs)'. One C-EF was thus considered as one factor of the combined biomarkers if it interacted with each C-EF with the maximum PageRank score (See Table 2 for details). The features of combined biomarkers were characterized from three aspects based on literature search results: (a) effect: the positive, negative, or dual effects on the processes of stroke; (b) structure: the role (indicator or target) EF/GF played in stroke; (c) mechanism: the interaction types (induce or inhibit) between the EF and GF(s) in the combined biomarkers. All the features were evaluated based on the target factor in each combined biomarker.

3.2. Validation Results

The expression changes of all the GFs in the combined biomarkers were checked. Any GF with at least one p -value not above 0.1 was considered as differentially expressed GFs (see details in Table 3). 8 and 3 genetic factors were identified as biomarkers in the acute and recovery phases of stroke, respectively. For example, the expression change of *SERPINH1* only appeared in the acute phase of stroke showing its targeting role in the combined biomarker. Compared with this, 11 genetic factors such as *MMP9* were found to be differentially expressed in both acute and recovery phases of stroke showing their indicated roles in stroke.

3.3. Hierarchy model of Combined bio-markers

The 36 combined biomarkers could thus be divided into 8 different groups according to the three aspects mentioned above. The biomarkers in each group were divided into sub-groups according to their features. The mean EE scores were calculated for each sub-group as shown in Figure 1. The EE mean values of sub-groups and the statistical significance were calculated using student t -test. Results showed that the differences between 'induce' and 'inhibit' sub-groups on the 'mechanism' level was significant with a p -value of 0.09605 indicating to us that 'mechanism'

Table 1. List of validated data sets used in this study

GF type	Stroke Condition	NCBI GEO ID	Number of Stroke Patients (Case)	Number of Healthy People (Controls)
Gene	Acute Phase	GSE16561	39	24
Gene/miRNA	Recovery Phase	GSE22255	20	20
miRNA	Acute Phase	GSE55937	24	24

Table 2. List of combined biomarkers

Rank	C-EF	GF(s)	Effect	Structure (target-indicator)	Mechanism
1	Dexamethasone	hsa-mir-30e	Positive, Negative	EF-GF	Induce
2	Acetaminophen	hsa-mir-122	Positive	EF-GF	Induce
3	Vitamin E	hsa-mir-15b	Positive	Unknown	Unknown
4	Cisplatin	hsa-mir-642	Negative	GF-EF	Induce
5	Cocaine	hsa-let-7d	Negative	GF-EF	Induce
6	Cadmium	hsa-mir-146a	Negative	EF-GF	Inhibit
7	Bortezomib	hsa-mir-122	Positive	EF-GF	Induce
8	Gemcitabine	hsa-mir-149	Negative	Unknown	Unknown
9	Nicotine	hsa-mir-21	Positive	EF-GF	Induce
10	Metformin	hsa-mir-21	Positive	GF-EF	Inhibit
11	Ethanol	hsa-mir-21	Positive	EF-GF	Induce
12	Nitric Oxide	hsa-mir-155	Positive	GF-EF	Induce
13	DDT	<i>NOS2, STAT3</i>	Negative	EF-GF	Inhibit, Induce
14	Docetaxel	hsa-mir-100, hsa-mir-101-1, hsa-mir-126, hsa-mir-130a, hsa-mir-16-1/2, hsa-mir-194-1, hsa-mir-195, hsa-mir-212, hsa-mir-30a, hsa-mir-34a, hsa-mir-7-1	Positive	GF-EF	Inhibit
15	Hemin	hsa-mir-126, hsa-mir-130a, hsa-mir-18b	Positive	Unknown	Inhibit, Induce
16	Letrozole	hsa-let-7f-1/2	Negative	EF-GF	Induce
17	Curcumin	<i>ALOX5</i>	Positive	EF-GF	Inhibit
18	Bromocriptine	hsa-mir-550-1	Negative	EF-GF	Induce
19	Arsenic	hsa-mir-222	Negative	EF-GF	Induce
20	Sulindac sulfide	<i>ATF3, PTGS2(COX2)</i> , hsa-mir-17, hsa-mir-21	Positive	EF-GF	Inhibit, Induce
21	Imatinib Mesylate	hsa-mir-451	Positive	GF-EF	Inhibit
22	Ursolic acid	hsa-mir-21	Positive	EF-GF	Inhibit
23	Vitamin D (VitD)	hsa-mir-22	Positive	EF-GF	Induce
24	Bleomycin	hsa-mir-21	Negative	GF-EF	Induce
25	Oxaliplatin	hsa-mir-21	Negative	GF-EF	Inhibit
26	Glucose	hsa-mir-133a-1/2, hsa-mir-146a/b, hsa-mir-451	Negative	EF-GF, GF-EF	Unknown
27	Gefitinib	hsa-mir-222, hsa-mir-30b	Negative	EF-GF	Inhibit
28	Topotecan	hsa-mir-142, hsa-mir-34b	Positive	Unknown	Unknown
29	Lead	<i>ADORA1, IGF1, IL1B</i> , hsa-mir-146a, hsa-mir-21, hsa-mir-222	Negative	Unknown	Inhibit
30	Paroxetine	hsa-mir-30a	Positive	GF-EF	Inhibit
31	Genistein	hsa-mir-151, hsa-mir-27a	Positive	EF-GF	Inhibit
32	Decitabine	hsa-mir-145	Positive	EF-GF	Induce
33	Cytarabine	<i>EDN1, F2</i> , hsa-mir-29a, hsa-mir-30c-1	Negative	GF-EF	Inhibit
34	Fludarabine	<i>MMP9</i>	Positive	EF-GF	Induce
35	Polycyclic Aromatic Hydrocarbons (PAH)	<i>CCL2</i>	Negative	Unknown	Unknown
36	Sorafenib	hsa-mir-122, <i>SERPINH1</i>	Negative	GF-EF	Induce

could be used as the first analysis level. There were 16 biomarkers in the induce group and 12 in the inhibit group (8 combined biomarkers were not included in the following analyses since their mechanism were not clear).

To explore the second analysis level, we divided the biomarkers in one sub-group into sub-sub-group according to their 'effect' and 'structure' features. EE values and PageRank scores were used to test the differences between these sub-sub-groups. For the sub-groups containing combined biomarkers with induce mechanism, significant difference was found between

two sub-sub-groups (positive and negative) according to the 'effect' feature with a p -value of 0.06137 using PageRank score. Compared with this, no significant difference was found in the 'inhibit' sub-group with p -value of 0.2826 (mean PageRank scores were 0.2588571 and 0.3178 for 'positive' and 'negative', respectively).

Similarly to the above analyses, we checked all the possible third analyses levels using statistical test. For the 8 combined biomarkers in 'Mechanism (induce)-Effect (positive)', only 1 biomarker was shown to have the structure of 'GF-EF'. The p -value of

Table 3. p-value of GFs in combined biomarkers

GF Name	P-value in Acute Phase (GSE16561, GSE55937)	P-value in Recovery Phase (GSE22255)
ADORA1	3.64E-10	2.76E-10
ALOX5	0.007267241	0.000472032
ATF3	1.43E-15	3.36E-05
CCL21	2.86E-15	0.006144956
EDN1	5.83E-06	1.69E-07
IGF1	7.16E-16	5.41E-09
IL1B	6.92E-11	0.040175085
MMP9	6.08E-10	1.34E-07
NOS2	7.16E-16	1.45E-11
PTGS2	7.97E-08	0.383413282
SERPINH1	0.000431237	0.120699706
STAT3	0.001638866	0.00513072
F2	--	0.09132
hsa-mir-145	0.000921373	--
hsa-mir-122	0.014428574	--
hsa-mir-550	0.019369559	--
hsa-mir-642	0.066476228	--
hsa-mir-30e	0.071189216	--
hsa-mir-21	0.077797772	0.06035
hsa-mir-16-2	0.092850883	--
hsa-mir-22	0.675265662	0.04298
hsa-mir-142	0.645619886	0.0675

-- Some of the GFs were not detected in all the three data sets due to the original platform, as a result, no p-value could be calculated.

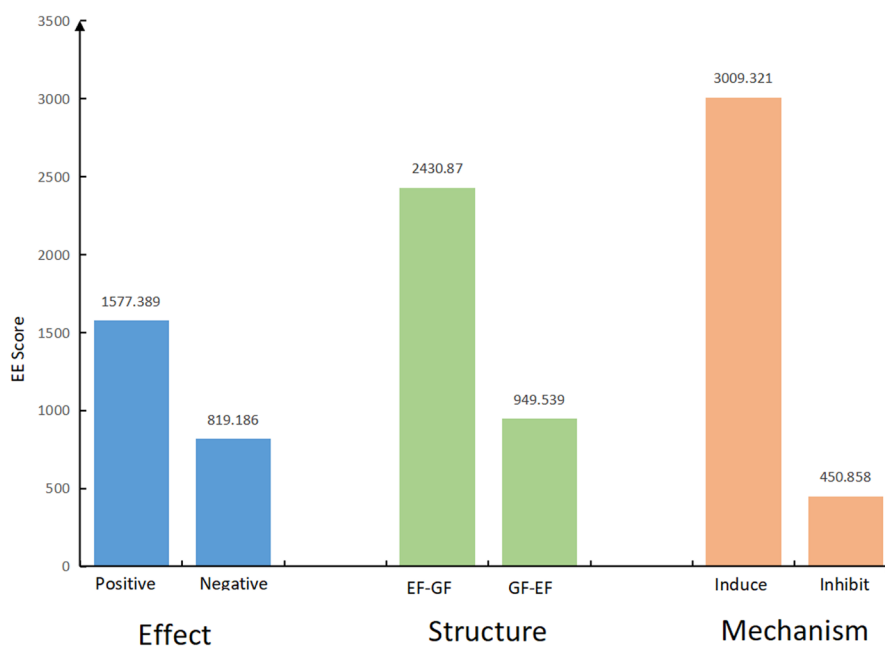


Figure 1. Comparison of mean EE scores on different levels. The mean EE scores were calculated for each sub-group.

binomial distribution analysis was 0.01563 indicating a significant difference. Analysis of the 8 combined biomarkers in 'Mechanism (induce)-Effect (negative)' showed no significant difference on structure level. Taken together, the analyses hierarchy model of the three features were then fixed as 'Mechanism-Effect'.

It was interesting to find that the significant differences were found on induce and positive level, which may indicated these combined biomarkers might play their roles in a forward way rather than feedback.

3.5. Function of Combined biomarkers

3.5.1. Combined biomarkers for Stroke Prevention and Damages Mitigation

Seven combined biomarkers in the 'Mechanism (inhibit)-Effect (positive)' model were shown to play a role in protecting against stroke or mitigating stroke-induced damages. All the EFs including curcumin, ursolic acid, genistein, metformin, docetaxel, imatinib mesylate, and

paroxetine functioned as stroke prevention or damage mitigation factors (See Table S1 of Supplemental Data for details, <http://www.biosciencetrends.com/action/getSupplementalData.php?ID=27>).

Hsa-mir-21, hsa-mir-27a, hsa-mir-151, hsa-mir-100, hsa-mir-101-1, hsa-mir-130a, hsa-mir-16-1/2, hsa-mir-194-1, hsa-mir-195, hsa-mir-212, hsa-mir-30a, hsa-mir-451, and hsa-mir-34a were shown to be over-regulated; while hsa-mir-126 and hsa-mir-7-1 were shown to be down-regulated in young stroke patients (14,15).

The relationships between EF and GF in each biomarker was inhibit, which meant that the expression or activation of indicator factor was inhibited by the target factor. For example, curcumin was shown to perform the damage mitigation role by inhibiting the catalytic activities of *ALOX5* (16), which may attenuate neuro-protection following focal cerebral ischemia (5). hsa-mir-21 was shown to be suppressed by ursolic acid in human glioblastoma cell lines U251 (17). Genistein was shown to play its roles through inhibition of mir-27a and mir-151 in different diseases (18,19). Metformin was shown to improve skeletal muscle insulin resistance by inhibiting mir-21 expression (20). Over-regulation of mir-100 could prevent docetaxel chemoresistance in patients with lung adenocarcinoma (21). Docetaxel resistance was associated with increased expression of mir-34a, and decreased expression of mir-100, mir-7, mir-16, mir-30a, and mir-126 in human breast cancer cells (22). mir-195 was a negative regulator in the resistance of *DUI45/DOC* cells to docetaxel (23). hsa-mir-451 was observed to be down-regulated in imatinib-resistant chronic myeloid leukemia patients (24). mir-30a may limit the effects of paroxetine by targeting *BDNF* (25).

3.5.2. Combined biomarkers for Causing Stroke

There were 8 combined biomarkers proved to be related to the occurrence of stroke. It was interesting to find out that all these biomarkers were in the model of 'Mechanism (induce)-Effect (negative)', of which 4 target factors were EFs while the other 4 target factors were GFs.

At least one of the EF or GF in each biomarker were proved to be a risk factor causing stroke including dexamethasone, letrozole, bromocriptine, arsenic, cisplatin, cocaine, bleomycin, sorafenib, and *SERPINH1* (26) (See Table S1 of Supplemental Data for details, <http://www.biosciencetrends.com/action/getSupplementalData.php?ID=27>).

Of all the GFs, previous studies showed that hsa-mir-30e, hsa-mir-550-1, hsa-mir-222, hsa-mir-642, hsa-mir-let-7d, hsa-mir-21, hsa-mir-122 were up-regulated while hsa-mir-7f-1, hsa-mir-7f-2, and hsa-mir-15b were down-regulated in young stroke patients (14,27,28).

The increased expression of indicator factors may

be induced by the target factor in the same combined biomarker. One study showed that dexamethasone-induced *IEC-6* cells differentiation caused a 2.5-fold increase in mir-30e expression, and upon beta-catenin siRNA transfection, mir-30e increased 1.3-fold (29). After letrozole treatment for 48 hours, all let-7 subtypes showed a trend toward increased expression (29). mir-550 was confirmed to be significantly up-regulated between the group of bromocriptine-treated and untreated prolactinomas (30). mir-222 was up-regulated in arsenic-transformed human lung epithelial *BEAS-2B* cells indicating its role in arsenic-induced tumor growth (31). The increased expression of mir-642 could increase the sensitivity of cisplatin in cell lines and advanced bladder cancer (28). Cocaine up-regulated let-7d in zebrafish embryos (32). The repressing of mir-21 could attenuate bleomycin-induced pulmonary fibrosis (33). mir-122 was shown to be up-regulated during apoptosis induced by bortezomib and sensitized hepatocellular carcinoma cells to sorafenib (27,34).

3.5.3. Combined biomarkers for Stroke Processes

Four combined biomarkers in the model of 'Mechanism (inhibit)-Effect (negative)' showed adverse effects on stroke. Gefitinib, cadmium, oxaliplatin, cytarabine, hsa-mir-146a (35), and *EDN1* (36) were proved to be negative factors of stroke (See Table S1 of Supplemental Data for details, <http://www.biosciencetrends.com/action/getSupplementalData.php?ID=27>).

hsa-mir-222, hsa-mir-21, hsa-mir-29a and hsa-mir-30c-1 were shown to be up-regulated in young stroke patients (14), while hsa-mir-30b, and hsa-mir-146a were shown to be down-regulated in young stroke patients (14,35).

mir-30b and mir-222 were shown to be down-regulated by gefitinib (37). The expression of mir-146a was negatively correlated with exposure to cadmium (38). The over-expression of mir-21 could protect CRC cells from oxaliplatin-induced apoptosis and increase the proliferative capacity (39). The deregulated expression of mir-29a and mir-30c was shown to contribute to the sensitivity to cytarabine (40).

3.5.4. Combined biomarkers for Stroke Recovery

There were 8 combined biomarkers in the 'Mechanism (induce)-Effect (positive)' model. All the GFs including hsa-mir-122, hsa-mir-21, hsa-mir-22, hsa-mir-145, hsa-mir-155, and *MMP9* in the 7 biomarkers (hsa-mir-122 and hsa-mir-21 were involved in two bio-markers) were proved to have increased expression in stroke patients (14,15,41).

Four EFs including bortezomib, nicotine, vitamin D (VitD), and fludarabine were proved to contribute to neuroprotection after stroke. The other 4 EFs including acetaminophen, ethanol, decitabine, and nitric oxide

were proved to be associated with better outcome for stroke. For example, acetaminophen was indicated to improve outcome in patients with stroke and fever without dramatically lowering body temperature in one clinical trial study. Low to moderate levels of ethanol could not only decrease the risk of stroke, but also reduce post-ischemic sequelae. Decitabine was widely used in sickle cell anemia which was closely related to stroke. Treatment with nitric oxide was shown to improve functional recovery after stroke (See Supplemental Data for details).

Most of the GFs were considered to be induced by EFs in this model based on their relationships in other conditions since their relationships were still lacking in stroke-related fields. Mir-122 was reported as a novel biomarker of acetaminophen toxicity and was shown to be up-regulated during apoptosis induced by bortezomib (27,42,43). Besides, the up-regulation of mir-21 induced by nicotine could promote EMT transforming growth factor beta ($TGF-\beta$) dependently in human esophageal cancer (44). Chronic ethanol feeding was shown to enhance mir-21 induction during liver regeneration while inhibiting proliferation in rats (45). Mir-22 was induced by VitD and contributed to its antiproliferative, antimigratory and gene regulatory effects in colon cancer cells (46). Decitabine was shown to induce the expression of mir-145 (47). *MMP9* was shown to be involved in chronic lymphocytic leukemia cell response to fludarabine (48). Knockdown of mir-155 could significantly decrease the production of nitric oxide (49), which was the indicated factor.

4. Discussion

The identification of complex diseases' biomarkers were considered to be one of the traditional topics in cardiovascular related fields. For example, the identification and evaluation of genetic biomarkers such as IL-6, TNF- α which were measured using blood as samples for heart failure had been performed which were considered to be of great importance since these results had improved the diagnosis and treatments greatly in the clinic. Compared with this, similar work performed on stroke had always been questioned since most of the samples were human blood, which may not reflect the changes of the ischemic regions due to the existence of the blood brain barrier (BBB). Considering this, the stroke related EFs attracted more and more attention since their roles could be both risk factors and/or biomarkers. These EFs could be divided into two different groups according to their features as follows: (a) risk factor (clinical environment factor): cardiovascular risk factors widely accepted in clinic such as hypertension, diabetes mellitus, smoking, alcohol consumption, and air pollution, *etc.* (b) biomarker (toxicology environment factor): chemicals, drugs, and small molecules, *etc.* However, it

was widely accepted that the occurrence of stroke was caused by both genetic and environment reasons. In recent years, research began to exploit the interplay(s) between EF(s) and GF(s). For example, one study showed that the combined effects of the *MTHFR* 3'-UTR polymorphisms and tHcy/folate levels might contribute to stroke prevalence (50). However, the relationship analyses on a systematic scale for stroke combined biomarkers were still lacking especially on multiple omics levels.

It was widely believed that genetic factors may coordinately support the influence of macro or micro environment factors. Exploring this type of genetic biomarkers would be beneficial in understanding the mechanism of disease onset and aiding the development of therapy or prevention schemes. Many mRNAs were identified as biomarkers of stroke in former studies using different frameworks such as differential analyses, network analyses, *etc.* Besides mRNAs, miRNAs were widely considered as genetic factors since they could play important roles in stroke through regulating their target genes. One miRNA might regulate hundreds to thousands of mRNAs, which made the parallel analyses performed using both mRNAs and miRNAs data sets possible. Based on these concerns, many researchers including us had constructed the combined biomarkers of stroke containing both miRNAs and mRNAs on the genetic level in previous studies. However, the close relationships between miRNAs and EFs had not been fully integrated in such studies.

In this study we demonstrated that by exploiting the environment-genetic interactions we do achieve a set of biomarkers that were robust across different data sets and with clear biological relevance. This suggested that knowledge about environment risk factors and environment-genetics would serve as a good guideline for exploring new combined biomarkers and the framework proposed in this study can be a useful tool for this purpose.

Acknowledgements

This work was supported by grants from the Basic Research Program of Shenzhen, [JCYJ20160229203627477] [JCYJ20160229193120432], National Natural Science Foundation of China, [61702496], and the Application Research and Development of Guangdong, [2015B010129012].

References

1. Markus HS, Bevan S. Mechanisms and treatment of ischaemic stroke – insights from genetic associations. *Nat Rev Neurol*. 2014; 10:723-730.
2. Wang Y, Cai Y. Obtaining human ischemic stroke gene expression biomarkers from animal models: a cross-species validation study. *Sci Rep*. 2016; 6:29693.
3. Peters JL, Perlstein TS, Perry MJ, McNeely E, Weuve J.

- Cadmium exposure in association with history of stroke and heart failure. *Environ Res.* 2010; 110:199-206.
4. Li L, Zhang X, Cui L, Wang L, Liu H, Ji H, Du Y. Ursolic acid promotes the neuroprotection by activating Nrf2 pathway after cerebral ischemia in mice. *Brain Res.* 2013; 1497:32-39.
 5. Singh DP, Chopra K. Flavocoxid, dual inhibitor of cyclooxygenase-2 and 5-lipoxygenase, exhibits neuroprotection in rat model of ischaemic stroke. *Pharmacol Biochem Behav.* 2014; 120:33-42.
 6. Szolnoki Z, Melegh B. Gene-gene and gene-environment interplay represent specific susceptibility for different types of ischaemic stroke and leukoaraiosis. *Curr Med Chem.* 2006; 13:1627-1634.
 7. Yang Q, Qiu C, Yang J, Wu Q, Cui Q. miREnvironment database: providing a bridge for microRNAs, environmental factors and phenotypes. *Bioinformatics.* 2011; 27:3329-3330.
 8. Li J, Wu Z, Cheng F, Li W, Liu G, Tang Y. Computational prediction of microRNA networks incorporating environmental toxicity and disease etiology. *Sci Rep.* 2014; 4:5576.
 9. Davis AP, Grondin CJ, Johnson RJ, Sciaky D, King BL, McMorran R, Wiegers J, Wiegers TC, Mattingly CJ. The comparative toxicogenomics database: update 2017. *Nucleic Acids Res.* 2017; 45:972-978.
 10. Li Y, Qiu C, Tu J, Geng B, Yang J, Jiang T, Cui Q. HMDD v2.0: a database for experimentally supported human microRNA and disease associations. *Nucleic Acids Res.* 2014; 42:1070-1074.
 11. Ruepp A, Kowarsch A, Schmid D, Buggenthin F, Brauner B, Dunger I, Fobo G, Frishman G, Montrone C, Theis FJ. PhenomiR: a knowledgebase for microRNA expression in diseases and biological processes. *Genome Biol.* 2010; 11:R6.
 12. Hsu SD, Tseng YT, Shrestha S, *et al.* miRTarBase update 2014: an information resource for experimentally validated miRNA-target interactions. *Nucleic Acids Res.* 2014; 42:78-85.
 13. Li J, Zhang Y, Wang Y, Zhang C, Wang Q, Shi X, Li C, Zhang R, Li X. Functional combination strategy for prioritization of human miRNA target. *Gene.* 2014; 533:132-141.
 14. Tan KS, Armugam A, Sepramaniam S, Lim KY, Setyowati KD, Wang CW, Jeyaseelan K. Expression profile of microRNAs in young stroke patients. *PloS One.* 2009; 4:e7689.
 15. Maitrias P, Metzinger-Le Meuth V, Massy ZA, M'Baya-Moutoula E, Reix T, Caus T, Metzinger L. MicroRNA deregulation in symptomatic carotid plaque. *J Vasc Surg.* 2015; 62:1245-1250.
 16. Hong J, Bose M, Ju J, Ryu JH, Chen X, Sang S, Lee MJ, Yang CS. Modulation of arachidonic acid metabolism by curcumin and related beta-diketone derivatives: effects on cytosolic phospholipase A(2), cyclooxygenases and 5-lipoxygenase. *Carcinogenesis.* 2004; 25:1671-1679.
 17. Wang J, Li Y, Wang X, Jiang C. Ursolic acid inhibits proliferation and induces apoptosis in human glioblastoma cell lines U251 by suppressing TGF- β 1/miR-21/PDCD4 pathway. *Basic Clin Pharmacol Toxicol.* 2012; 111:106-112.
 18. Xia J, Cheng L, Mei C, Ma J, Shi Y, Zeng F, Wang Z, Wang Z. Genistein inhibits cell growth and invasion through regulation of miR-27a in pancreatic cancer cells. *Curr Pharm Des.* 2014; 20:5348-5353.
 19. Chiyomaru T, Yamamura S, Zaman MS, Majid S, Deng G, Shahryari V, Saini S, Hirata H, Ueno K, Chang I, Tanaka Y, Tabatabai ZL, Enokida H, Nakagawa M, Dahiya R. Genistein suppresses prostate cancer growth through inhibition of oncogenic microRNA-151. *PLoS One.* 2012; 7:e43812.
 20. Wang J, Gao Y, Duan L, Wei S, Liu J, Tian L, Quan J, Zhang Q, Liu J, Yang J. Metformin ameliorates skeletal muscle insulin resistance by inhibiting miR-21 expression in a high-fat dietary rat model. *Oncotarget.* 2017; 8:98029-98039.
 21. Feng B, Wang R, Chen LB. MiR-100 resensitizes docetaxel-resistant human lung adenocarcinoma cells (SPC-A1) to docetaxel by targeting Plk1. *Cancer Lett.* 2012; 317:184-191.
 22. Kastl L, Brown I, Schofield AC. miRNA-34a is associated with docetaxel resistance in human breast cancer cells. *Breast Cancer Res Treat.* 2012; 131:445-454.
 23. Ma X, Zou L, Li X, Chen Z, Lin Q, Wu X. MicroRNA-195 regulates docetaxel resistance by targeting clusterin in prostate cancer. *Biomed Pharmacother.* 2018; 99:445-450.
 24. Soltani I, Douzi K, Gharbi H, Benhassine I, Teber M, Amouri H, Ben Hadj Othman H, Farrah A, Ben Lakhel R, Abbes S, Menif S. Downregulation of miR-451 in Tunisian chronic myeloid leukemia patients: potential implication in imatinib resistance. *Hematology.* 2017; 22:201-207.
 25. Angelucci F, Croce N, Spalletta G, Dinallo V, Gravina P, Bossu P, Federici G, Caltagirone C, Bernardini S. Paroxetine rapidly modulates the expression of brain-derived neurotrophic factor mRNA and protein in a human glioblastoma-astrocytoma cell line. *Pharmacology.* 2011; 87:5-10.
 26. Yagil C, Hubner N, Monti J, Schulz H, Sapojnikov M, Luft FC, Ganten D, Yagil Y. Identification of hypertension-related genes through an integrated genomic-transcriptomic approach. *Circ Res.* 2005; 96:617-625.
 27. Manfe V, Biskup E, Rosbjerg A, Kamstrup M, Skov AG, Lerche CM, Lauenborg BT, Odum N, Gniadecki R. miR-122 regulates p53/Akt signalling and the chemotherapy-induced apoptosis in cutaneous T-cell lymphoma. *PloS One.* 2012; 7:e29541.
 28. Nordentoft I, Birkenkamp-Demtroder K, Agerbaek M, Theodorescu D, Ostenfeld MS, Hartmann A, Borre M, Orntoft TF, Dyrskjot L. miRNAs associated with chemosensitivity in cell lines and in advanced bladder cancer. *BMC Med Genomics.* 2012; 5:40.
 29. Cho S, Mutlu L, Zhou Y, Taylor HS. Aromatase inhibitor regulates let-7 expression and let-7f-induced cell migration in endometrial cells from women with endometriosis. *Fertil Steril.* 2016; 106:673-680.
 30. Wang C, Su Z, Sanai N, Xue X, Lu L, Chen Y, Wu J, Zheng W, Zhuge Q, Wu ZB. microRNA expression profile and differentially-expressed genes in prolactinomas following bromocriptine treatment. *Oncol Rep.* 2012; 27:1312-1320.
 31. Wang M, Ge X, Zheng J, Li D, Liu X, Wang L, Jiang C, Shi Z, Qin L, Liu J, Yang H, Liu LZ, He J, Zhen L, Jiang BH. Role and mechanism of miR-222 in arsenic-transformed cells for inducing tumor growth. *Oncotarget.* 2016; 7:17805-17814.
 32. Gao Y, Lu J, Zhang Y, Chen Y, Gu Z, Jiang X. Baicalein attenuates bleomycin-induced pulmonary fibrosis in rats

- through inhibition of miR-21. *Pulm Pharmacol Ther.* 2013; 26:649-654.
33. Lopez-Bellido R, Barreto-Valer K, Sanchez-Simon FM, Rodriguez RE. Cocaine modulates the expression of opioid receptors and miR-let-7d in zebrafish embryos. *PLoS One.* 2012; 7:e50885.
 34. Bai S, Nasser MW, Wang B, Hsu SH, Datta J, Kutay H, Yadav A, Nuovo G, Kumar P, Ghoshal K. MicroRNA-122 inhibits tumorigenic properties of hepatocellular carcinoma cells and sensitizes these cells to sorafenib. *J Biol Chem.* 2009; 284:32015-32027.
 35. Li SH, Chen L, Pang XM, Su SY, Zhou X, Chen CY, Huang LG, Li JP, Liu JL. Decreased miR-146a expression in acute ischemic stroke directly targets the Fbxl10 mRNA and is involved in modulating apoptosis. *Neurochem Int.* 2017; 107:156-167.
 36. Zhang L, Sui R. Effect of SNP polymorphisms of EDN1, EDNRA, and EDNRB gene on ischemic stroke. *Cell Biochem Biophys.* 2014; 70:233-239.
 37. Garofalo M, Romano G, Di Leva G, *et al.* EGFR and MET receptor tyrosine kinase-altered microRNA expression induces tumorigenesis and gefitinib resistance in lung cancers. *Nat Med.* 2011; 18:74-82.
 38. Bollati V, Marinelli B, Apostoli P, Bonzini M, Nordio F, Hoxha M, Pegoraro V, Motta V, Tarantini L, Cantone L, Schwartz J, Bertazzi PA, Baccarelli A. Exposure to metal-rich particulate matter modifies the expression of candidate microRNAs in peripheral blood leukocytes. *Environ Health Perspect.* 2010; 118:763-768.
 39. Bullock MD, Pickard KM, Nielsen BS, Sayan AE, Jenei V, Mellone M, Mitter R, Primrose JN, Thomas GJ, Packham GK, Mirnezami AH. Pleiotropic actions of miR-21 highlight the critical role of deregulated stromal microRNAs during colorectal cancer progression. *Cell Death Dis.* 2013; 4:e684.
 40. Russ AC, Sander S, Luck SC, Lang KM, Bauer M, Rucker FG, Kestler HA, Schlenk RF, Dohner H, Holzmann K, Dohner K, Bullinger L. Integrative nucleophosmin mutation-associated microRNA and gene expression pattern analysis identifies novel microRNA - target gene interactions in acute myeloid leukemia. *Haematologica.* 2011; 96:1783-1791.
 41. Laterza OF, Lim L, Garrett-Engele PW, Vlasakova K, Muniappa N, Tanaka WK, Johnson JM, Sina JF, Fare TL, Sistare FD, Glaab WE. Plasma MicroRNAs as sensitive and specific biomarkers of tissue injury. *Clin Chem.* 2009; 55:1977-1983.
 42. Antoine DJ, Dear JW, Lewis PS, Platt V, Coyle J, Masson M, Thanacoody RH, Gray AJ, Webb DJ, Moggs JG, Bateman DN, Goldring CE, Park BK. Mechanistic biomarkers provide early and sensitive detection of acetaminophen-induced acute liver injury at first presentation to hospital. *Hepatology.* 2013; 58:777-787.
 43. Yang X, Salminen WF, Shi Q, Greenhaw J, Gill PS, Bhattacharyya S, Beger RD, Mendrick DL, Mattes WB, James LP. Potential of extracellular microRNAs as biomarkers of acetaminophen toxicity in children. *Toxicol Appl Pharmacol.* 2015; 284:180-187.
 44. Zhang Y, Pan T, Zhong X, Cheng C. Nicotine upregulates microRNA-21 and promotes TGF- β -dependent epithelial-mesenchymal transition of esophageal cancer cells. *Tumour Biol.* 2014; 35:7063-7072.
 45. Dippold RP, Vadigepalli R, Gonye GE, Hoek JB. Chronic ethanol feeding enhances miR-21 induction during liver regeneration while inhibiting proliferation in rats. *Am J Physiol Gastrointest Liver Physiol.* 2012; 303:733-743.
 46. Alvarez-Diaz S, Valle N, Ferrer-Mayorga G, Lombardia L, Herrera M, Dominguez O, Segura MF, Bonilla F, Hernando E, Munoz A. MicroRNA-22 is induced by vitamin D and contributes to its antiproliferative, antimigratory and gene regulatory effects in colon cancer cells. *Hum Mol Genet.* 2012; 21:2157-2165.
 47. Chinnathambi S, Wiechert S, Tomanek-Chalkley A, Winter MC, Bickenbach JR. Treatment with the cancer drugs decitabine and doxorubicin induces human skin keratinocytes to express Oct4 and the OCT4 regulator mir-145. *J Dermatol.* 2012; 39:617-624.
 48. Amigo-Jimenez I, Bailon E, Ugarte-Berzal E, Aguilera-Montilla N, Garcia-Marco JA, Garcia-Pardo A. Matrix metalloproteinase-9 is involved in chronic lymphocytic leukemia cell response to fludarabine and arsenic trioxide. *PLoS One.* 2014; 9:e99993.
 49. Zhang RL, Zhang ZG, Chopp M. Targeting nitric oxide in the subacute restorative treatment of ischemic stroke. *Expert Opin Investig Drugs.* 2013; 22:843-851.
 50. Kim JO, Park HS, Ryu CS, Shin JW, Kim J, Oh SH, Kim OJ, Kim NK. Interplay between 3'-UTR polymorphisms in the methylenetetrahydrofolate reductase (MTHFR) gene and the risk of ischemic stroke. *Sci Rep.* 2017; 7:12464.

(Received July 2, 2018; Revised August 18, 2018; Accepted August 24, 2018)

Spectroscopic methodologies and molecular docking studies on the interaction of the soluble guanylate cyclase stimulator riociguat with human serum albumin

Rui Ma¹, Zhenyu Li², Xiaxia Di³, Dongxiao Guo⁴, Jianbo Ji¹, Shuqi Wang^{1,*}

¹ School of Pharmaceutical Sciences, Shandong University, Ji'nan, Shandong, China;

² Department of Pharmacy, Shandong Provincial Hospital Affiliated with Shandong University, Ji'nan, Shandong, China;

³ Faculty of Pharmaceutical Sciences, University of Iceland, Reykjavik, Iceland;

⁴ Shandong Institute for Food and Drug Control, Ji'nan, Shandong, China.

Summary

Interaction of riociguat with human serum albumin (HSA) is extremely important in understanding the drug's disposition and efficiency. In the current study, the binding of riociguat to HSA was explored using spectroscopic methods and molecular docking. The quenching constant, the binding constant, the number of binding sites, thermodynamic parameters, and the secondary structure of protein were determined. A fluorescence study revealed that riociguat quenched HSA fluorescence via static quenching with a binding constant of $1.55 \times 10^4 \text{ L mol}^{-1}$ at 298 K. The calculated thermodynamic parameters indicated that the binding process was spontaneous and that the main interaction force was hydrophobic interaction. Site marker competitive binding experiments and molecular docking studies suggested that riociguat was inserted into the subdomain IIA (site I) of HSA. Alterations in the protein secondary structure after drug complexation were predicted. Results indicated that the protein α -helix structure increased with an increasing concentration of riociguat. This indicated that a riociguat-HSA complex was formed and that the protein secondary structure was altered by the addition of riociguat.

Keywords: Riociguat, human serum albumin (HSA), interaction, molecular docking

1. Introduction

The interaction of proteins and drugs affects the pharmacological behavior, toxicity, and metabolism of drugs. In contrast, the binding of drugs to a certain protein may lead to an alteration in the secondary structure of the protein. Only a free drug can diffuse from the blood to a target (1). Thus, binding of a drug and protein affects the metabolism and action of that drug. Examining the interaction of a protein and a drug helps to understand the pharmacokinetics and pharmacodynamics of that drug.

Riociguat (Figure 1), a stimulator of redox-sensitive

soluble guanylate cyclase, is the only drug approved for the treatment of inoperable or persistent/recurrent chronic thromboembolic pulmonary hypertension (2-4). After oral administration, riociguat is transported through the bloodstream to the tissues and organ, and the therapeutic efficacy of riociguat is directly related to its free concentration in blood plasma (5). In addition, serious adverse events have been noted after riociguat monotherapy and are associated with the plasma concentration (6). Thus, the ability of riociguat to bind to plasma proteins is critical for its metabolism and efficacy. To the extent known, the mechanism by which riociguat binds to plasma proteins has not been studied thus far.

Human serum albumin (HSA) is the prominent transport protein in human plasma, and it plays an important role in the storage and transportation of numerous compounds including drugs and other substances (7). HSA consists of three homologous domains - I, II and III - each of which is divided into two subdomains (A and B). The main binding sites

Released online in J-STAGE as advance publication August 10, 2018.

*Address correspondence to:

Dr. Shuqi Wang, School of Pharmaceutical Sciences, Shandong University, Jinan, 250012, China.

E-mail: wangsq@sdu.edu.cn

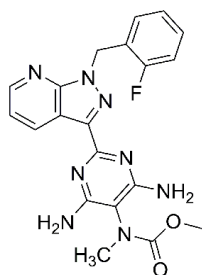


Figure 1. The structure of riociguat.

include site I (subdomain IIA), which is marked by warfarin, and site II (subdomain IIIA), which is marked by ibuprofen (8,9). The ability of a drug to bind to HSA is an important factor for its efficacy and metabolism. Examining the binding of drugs to HSA may explain the structural features that affect the pharmacokinetic and pharmacodynamics of those drugs. Therefore, the binding interaction of riociguat and HSA needs to be promptly examined.

The current study used fluorescence, Fourier-transform infrared (FT-IR) spectroscopy, circular dichroism (CD), and molecular docking to examine the intermolecular interaction between riociguat and HSA. The form of binding, the association constant, the change in the protein secondary structure, and the site where riociguat bound to were determined. Findings should have great significance in terms of studying the process of storage and transportation of riociguat in the body and its mechanism of action and pharmacokinetics.

2. Materials and Methods

2.1. Chemicals and Reagents

A reference standard of riociguat ($\geq 98\%$) was purchased from Ark Pharm, Inc. (Chi., USA). HSA was purchased from Solarbio Science & Technology Co. Ltd. (Beijing, China). Tris-(hydroxymethyl aminomethane) (Tris) ($\geq 99\%$) and sodium chloride ($\geq 99.5\%$) were purchased from Sinopharm Chemical Reagent Co., Ltd. (Shanghai, China). Ibuprofen ($\geq 99\%$) was purchased from Inno Chem Science & Technology Co., Ltd. (Beijing, China). Warfarin ($\geq 98\%$) was purchased from Adamas Reagent Co., Ltd. (Shanghai, China). Methanol (HPLC-grade) was purchased from Fisher Chemical Co., Ltd. (Shanghai, China).

2.2. Sample preparation

A stock solution of riociguat (10 mM) was prepared in methanol solution. HSA was dissolved in 0.05 M Tris-HCl buffer solution containing 0.1 M NaCl (pH = 7.4). Both warfarin and ibuprofen were dissolved in a mixture of methanol and Tris-HCl buffer solution to obtain a concentration of 1.2×10^{-4} M. All solutions were prepared at room temperature and stored at 4°C.

The final concentration of methanol in the test solutions was less than 2.4%, so the properties of HSA were not affected by methanol (10).

2.3. Fluorescence measurements

A Varian Cary Eclipse Spectrophotometer (Varian, Australia) with a 2-mm quartz cell was used to measure fluorescence spectra. The excitation wavelength for HSA-riociguat was 280 nm, and the emission spectrum was recorded from 290 to 450 nm. The widths of the excitation and emission slits were both set at 10 nm. The quenching effect of riociguat on HSA was investigated at three different temperatures of 288 K, 298 K, and 308 K. A mixture of riociguat and HSA were prepared with a constant HSA concentration of 2 μ M (11,12). The concentration of riociguat varied from 0-12 μ M. Synchronous fluorescence spectra were recorded at different scanning intervals of $\Delta\lambda$ ($\Delta\lambda = 60$ nm and 15 nm) at room temperature.

2.4. CD measurements

The CD spectra of HSA with or without riociguat were recorded using an Applied Photophysics circular dichroism spectropolarimeter (Applied Photophysics Ltd. Leatherhead, UK). The wavelength range scanned was 200-400 nm with a 1-mm quartz cell. The data were obtained with an interval of 1 nm and a scan rate of 164 nm/min.

2.5. FT-IR Measurements

FT-IR spectra were recorded using a Nicolet 6700 FT-IR spectrophotometer (Thermo Nicolet, Madison, America). The concentration of HSA was 1 mM and that of riociguat was 0.4 mM. The sample solutions were placed in a smart ITX diamond sampler. For all spectra, 100 scans recorded at a resolution of 4 cm^{-1} . Data were analyzed using Nicolet OMNIC software. The second derivative resolution enhancement was performed to determine the position of each peak when peaks overlapped, and peaks were fitted using a Gaussian peak function.

2.6. Site marker competitive binding

Site marker competitive binding experiments were conducted using warfarin (as site I marker) and ibuprofen (as site II marker). In the fluorescence experiments, the concentrations of HSA and site markers were both 2 μ M, while the concentration of riociguat gradually increased from 0 to 12 μ M.

2.7. Molecular docking

AutoDock vina 1.1.2 was used to determine how

riociguat bound to HSA (13). The three-dimensional (3D) structure of HSA (PDB ID: 2BXX) was downloaded from the Protein Data Bank (PDB) (14). The 2D structure of riociguat was drawn using ChemBioDraw Ultra 12.0 and converted to a 3D structure using the software ChemBio3D Ultra 12.0. The AutoDockTools 1.5.6 package was used to generate docking input files (15,16). A ligand was modified for docking by merging non-polar hydrogen atoms and defining rotatable bonds. The search grid of the HSA site I (subdomain IIA) was identified as center_x: 4.412, center_y: -8.174, and center_z: 8.25 with dimensions of size_x: 15, size_y: 15, and size_z: 15. The value of exhaustiveness was set to 20. The best-scoring binding mode was modeled on the software PyMol 1.7.6 (1.3r1, DeLano Scientific LLC, South San Francisco, USA) (17).

3. Results

3.1. Fluorescence measurements

Fluorescence quenching is considered to be an effective and sensitive method with which to investigate the interaction of small molecules and proteins. The intrinsic fluorescence of HSA is mainly due to tryptophan (Trp), tyrosine (Tyr), and phenylalanine (Phe) residues. Shifts in λ_{\max} and fluorescence intensity, which are mainly attributed to changes in the position of the Trp residues, were used to study HSA-riociguat interaction (18,19).

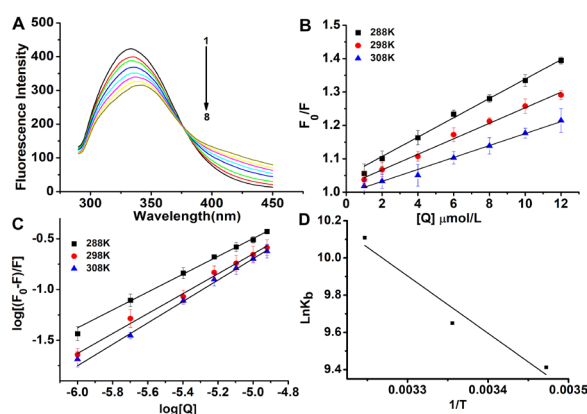


Figure 2. The fluorescence quenching spectra of HSA (2 μM) with different concentrations of riociguat at the excitation wavelength (280 nm) in Tris-HCl (pH 7.4). Riociguat solutions 1 to 8 had a concentration of 0, 1, 2, 4, 6, 8, 10, and 12 μM (A). Stern-Volmer plots for HSA (2 μM) quenched with riociguat at different temperatures (B). Plots of $\text{Log} [(F_0 - F)/F]$ vs. $\text{Log} [Q]$ for HSA (2 μM) quenched with riociguat at different temperatures (C). The van't Hoff plot for the calculation of different thermodynamic parameters (D).

As shown in Figure 2A, the fluorescence intensity of HSA decreased gradually with the increase in riociguat at around 334 nm. The fluorescence quenching data were analyzed using the Stern-Volmer equation (Eq. (1)) (20,21).

$$F_0/F = 1 + K_{SV} [Q] = 1 + K_q t_0 [Q] \quad (1)$$

In the equation, F_0 and F are the steady state fluorescence intensities in the absence and presence of a quencher, respectively. K_{SV} is the Stern-Volmer quenching constant and $[Q]$ is the concentration of the quencher (riociguat). K_q is the bimolecular quenching rate constant and t_0 is the fluorescence lifetime of HSA. The Stern-Volmer plots of the fluorescence of HSA quenched with riociguat at different temperatures are shown in Figure 2B, and the values of K_{SV} and K_q at different temperature are shown in Table 1. Results indicated that the mechanism by which riociguat quenched the fluorescence of HSA was static quenching due to the formation of a riociguat-HSA complex.

3.2. Binding constant and thermodynamic parameters

When examining the binding interaction of riociguat and HSA, the binding constant (K_b) and the number of binding sites (n) can be determined using the equation as follow (Eq. (2)) (22).

$$\log\left(\frac{F_0 - F}{F}\right) = \log K_b + n \log [Q] \quad (2)$$

where K_b is the binding constant and n is the number of binding sites for a riociguat-HSA complex. The Lineweaver-Burk plots at different temperatures are shown in Figure 2C, and the parameters are shown in Table 1. The calculated values of n were approximately equal to 1, indicating the existence of a single binding site for riociguat on HSA. The estimated value of K_b was $1.55 \times 10^4 \text{ M}^{-1}$ at 298 K, suggesting that strong interaction of riociguat and HSA.

Thermodynamic variables were calculated using the van't Hoff equation:

$$\ln K = -\frac{\Delta H}{RT} + \frac{\Delta S}{R} \quad (3)$$

$$\Delta G = \Delta H - T\Delta S \quad (4)$$

Table 1. Binding and thermodynamic parameters of an HSA-riociguat system at different temperatures

T(K)	K_{SV} 10^4 L mol^{-1}	R^2	K_q $10^{12} \text{ L mol}^{-1} \text{ s}^{-1}$	$\log K_b$	K_b 10^4 L mol^{-1}	n	R^2	ΔG KJ mol^{-1}	ΔH KJ mol^{-1}	ΔS $\text{J mol}^{-1} \text{ K}^{-1}$
288	3.01	0.995	3.01	4.09	1.22	0.92	0.997			
298	2.35	0.994	2.35	4.19	1.55	0.97	0.995	-24.11	25.62	166.88
308	1.83	0.991	1.83	4.39	2.46	1.02	0.996			

where K is the binding constant at temperature T , and the R is the gas constant. The van't Hoff plot for the interaction of riociguat and HSA is shown in Figure 2D, and the thermodynamic parameters are shown in Table 1. If the ΔH and ΔS are > 0 , then the binding force is hydrophobic interaction. A negative ΔH and ΔS usually indicates the presence of hydrogen bonding and/or van der Waals forces. If ΔH is < 0 and ΔS is > 0 , an electrostatic force is identified (23-26). In the current study, ΔG was negative, so the binding of riociguat to HSA was a spontaneous process. The positive values of both ΔH and ΔS revealed that the main force was hydrophobic interaction when riociguat bound to HSA.

3.3. Melanoma specimens

Characteristic information on Tyr and Trp residues can be obtained from synchronous fluorescence spectroscopy when the scanning interval $\Delta\lambda$ ($\Delta\lambda = \lambda_{em} - \lambda_{ex}$) is set at 15 and 60 nm (27,28). Figure 3A and 3B show the synchronous fluorescence spectra of HSA with various concentrations of riociguat, and the spectra were recorded with $\Delta\lambda = 15$ and 60 nm, respectively. A slight red shift in the maximum emission was observed at $\Delta\lambda = 60$ nm, suggesting that the hydrophobic environment surrounding Trp decreased slightly with the addition of riociguat. The intensities of both Trp and Tyr residues decreased, indicating that the quenching of HSA involved Trp and Tyr. Conformation of the protein changed upon interaction with riociguat.

3.4. CD spectroscopy

The CD spectra of HSA with and without riociguat are shown in Figure 3C. CD was calculated using the mean residue ellipticity (MRE) in $\text{deg cm}^2 \text{dmol}^{-1}$ according to the following equation:

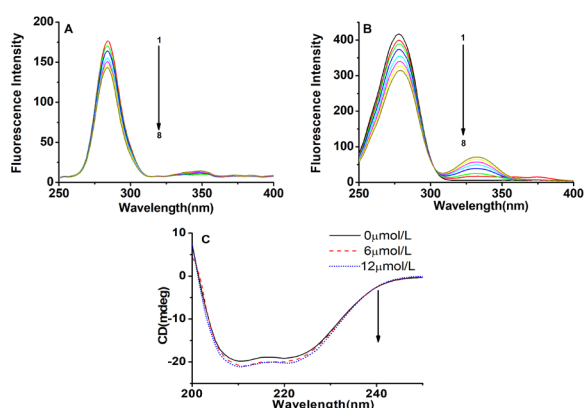


Figure 3. Synchronous fluorescence of HSA (2 μM) with different concentrations of riociguat at the excitation wavelength (280 nm) at room temperature when $\Delta\lambda = 15$ nm (A) and $\Delta\lambda = 60$ nm (B) in Tris-HCl (pH 7.4). Riociguat solutions 1 to 8 had a concentration of 0, 1, 2, 4, 6, 8, 10, and 12 μM . CD spectra of HSA (2 μM) in the presence of riociguat (12 μM) in Tris-HCl (pH 7.4) (C).

$$MER_{208} = \frac{\theta_{\text{obs}} \text{ (mdeg)}}{10 \cdot n \cdot l \cdot C_p} \quad (5)$$

$$\alpha\text{-helix}(\%) = \frac{-MER_{208} - 4000}{33000 - 4000} \quad (6)$$

where MER_{208} is the mean residue ellipticity at 208 nm, C_p is the molar concentration of HSA, n is the number of amino acid residues (585), l is the path length (0.1 cm). 4,000 is the MRE of the β -form and random coil conformation cross at 208 nm, and 33,000 is the MRE value of a pure α -helix at 208 nm. Using the above equation, the α -helicity in free HSA was 55.95%. After the addition of riociguat at 6 and 12 μM , the α -helical content increased from 55.95% to 58.01% and then to 59.49%. The structure of albumin was altered by riociguat.

3.5. FT-IR Spectra

To further investigate the changes in the structure of HSA, second derivative resolution enhancement and curve fitting were performed, as shown in Figure 4. Figure 4A and 4B show the FT-IR fitting curves of HSA in the absence and presence of riociguat in Tris-HCl buffer in the region of $1,700^{-1}, 600 \text{ cm}^{-1}$. Changes in peak positions and peak shapes indicated that riociguat induced a slight change in the secondary structure of HSA with binding toward the C=O groups. According to the quantitative analysis of the secondary structure, the α -helix content increased 8.16% as a result of the addition of riociguat. These results coincided with the CD spectra.

3.6. Site marker competitive binding

Two main specific drug-binding sites of HSA have previously been reported, including site I (subdomain IIA) and site II (subdomain IIIA). In the current study, warfarin (as site I marker) and ibuprofen (as site II marker) were used as site markers to investigate the binding site of riociguat on HSA. K_{SV} and K_b in a system of HSA and site markers were recorded as the concentration of riociguat increased, and the results are

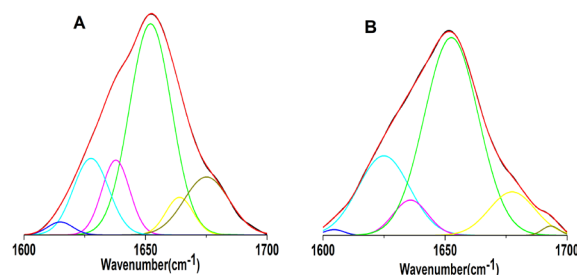
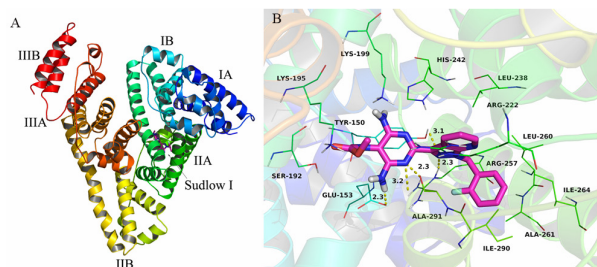


Figure 4. Second derivative resolution enhancement and curve-fitted amide I region ($1,700\text{-}1,600 \text{ cm}^{-1}$) for HSA (0.1 mM) in Tris-HCl buffer solution (pH = 7.40) in the absence (A) and presence of riociguat (B).

Table 2. Binding constants of riociguat with a mixture of HSA and site markers

System	$\log K_b$	$K_b (10^{-4} \text{L mol}^{-1})$	R^2
HSA + riociguat	4.19	1.55	0.9945
HSA + riociguat + warfarin	3.86	0.72	0.9938
HSA + riociguat + ibuprofen	4.18	1.51	0.9907

**Figure 5. Riociguat docked in the site I binding pockets of HSA (overall view) (A). Riociguat docked in the site I (subdomain IIA) binding pocket of HSA (detailed view) (B).**

shown in Table 2. K_b and K_{SV} markedly decreased in the presence of warfarin while the values were almost the same in the presence of ibuprofen. Results indicated that riociguat and warfarin competitively bound to HSA. The binding site of riociguat on HSA was primarily located on site I of HSA.

3.7. Molecular docking

Figure 5 shows the binding site of the HSA and the docking results. Riociguat docked in site I (subdomain IIA), and the overall view is shown in Figure 5A. Riociguat assumed a compact conformation to enter of the pocket of HSA, and a detailed view is shown in Figure 5B. The 2-fluorophenyl of riociguat stretched into the hydrophobic pocket that consisted of Leu-260, Ala-261, Ile-264, Ile-290, and Ala-291, forming a stable hydrophobic bond. The pyrimidine scaffold of riociguat participated in π - π stacking interaction with the residue Tyr-150. In addition, cation- π interactions between riociguat and the residues Lys-199, Arg-222, and Arg-257 were observed. Importantly, five hydrogen bond interactions were identified between riociguat and the residues Tyr-150, Glu-153, and Arg-257 of HSA. The above molecular simulations provided a good structural basis on which to explain the quenching of HSA fluorescence in the presence of riociguat.

4. Discussion

HSA is widely used in biophysical, biochemical, and physicochemical studies since it has been extensively studied with different small molecules and its primary structure is well known. The weak binding of ligands to HSA results in a short lifetime or poor distribution of compounds since strong binding leads to a decrease in the concentration of free ligands in plasma. Thus,

the interaction between a drug and HSA will affect its metabolism, distribution, toxicity, and elimination from the circulation. Riociguat is rapidly absorbed and its concentration subsequently decreases. It has a terminal half-life in the range of 5 to 10 hours, and its plasma binding rate is approximately 95% (29). The current study of the interaction between riociguat and HSA will help to understand the process of riociguat metabolism.

Fluorescence quenching is a decrease in the quantum yield of fluorescence induced by a variety of molecular interactions with a quencher molecule. Protein conformational transitions, biomolecule binding, denaturation, and other factors are responsible for the decrease in the intrinsic fluorescence of protein. Thus, fluorescence quenching is widely used to explore the binding of biomolecules and active small molecules. Fluorescence quenching can be caused by collisions or by ground-state complex formation between a fluorophore and a quencher. The former is referred to as dynamic quenching while the latter is referred to as static quenching (21). If the value of K_{SV} decreases with increasing temperature and the k_q value is much greater than the maximum diffusion collision quenching rate constant (2.0×10^{10} L/mol s) of HSA with a variety of quenchers (30,31), then the mechanism by which a compound quenches the fluorescence of albumin is static quenching due to the formation of a compound-HSA complex. In the current study, riociguat bound to HSA via static quenching.

This study used fluorescence, FT-IR spectroscopy, CD spectroscopy, and molecular docking to conduct the first detailed investigation of the interaction between riociguat and HSA. Results indicated that riociguat effectively quenched the intrinsic fluorescence of HSA via static quenching. The binding process was spontaneous, and the main force was hydrophobic interaction. Conformational results from CD and FT-IR spectra revealed that the binding of riociguat to HSA induced some micro-environmental and conformational changes. The current results will help to better understand aspects of pharmacokinetics such as drug metabolism, excretion, and distribution.

Acknowledgements

This work was supported by the Natural Science Foundation of China (81502921 and 81503251), the Key Research and Development Program of Shandong Province (2017GSF218049), and Young Scholars Program of Shandong University (2015WLJH50).

References

- Sharma R, Choudhary S, Kishore N. Insights into the binding of the drugs diclofenac sodium and cefotaxime sodium to serum albumin: Calorimetry and spectroscopy. *Eur J Pharm Sci.* 2012; 46:435-445.

2. Galie N, Humbert M, Vachiery J, *et al.* 2015 ESC/ERS Guidelines for the diagnosis and treatment of pulmonary hypertension. *Rev Esp Cardiol (Engl Ed)*. 2016; 69:177.
3. Kim NH, Delcroix M, Jenkins DP, Channick R, Darteville P, Jansa P, Lang I, Madani MM, Ogino H, Pengo V and Mayer E. Chronic thromboembolic pulmonary hypertension. *J Am Coll Cardiol*. 2013; 62:92-99.
4. Conole D, Scott LJ. Riociguat: First global approval. *Drugs*. 2013; 73:1967-1975.
5. Spreemann T, Bertram H, Happel CM, Kozlik-Feldmann R, Hansmann G. First-in-child use of the oral soluble guanylate cyclase stimulator riociguat in pulmonary arterial hypertension. *Pulm Circ*. 2018; 8:1-6.
6. Ghofrani HA, Grimminger F, Grünig E, Huang Y, Jansa P, Jing ZC, Kilpatrick D, Langleben D, Rosenkranz S, Menezes F, Fritsch A, Nikkho S, Humbert M. Predictors of long-term outcomes in patients treated with riociguat for pulmonary arterial hypertension: Data from the PATENT-2 open-label, randomised, long-term extension trial. *Lancet Respir Med*. 2016; 4:361-371.
7. Shamsi A, Ahmed A, Bano B. Probing the interaction of anticancer drug temsirolimus with human serum albumin: Molecular docking and spectroscopic insight. *J Biomol Struct Dyn*. 2018; 36:1479-1489.
8. Dockal M, Carter DC, Rüker F. Conformational transitions of the three recombinant domains of human serum albumin depending on pH. *J Biol Chem*. 2000; 275:3042-3050.
9. Dockal M, Chang M, Carter DC, Rüker F. Five recombinant fragments of human serum albumin – Tools for the characterization of the warfarin binding site. *Protein Sci*. 2000; 9:1455-1465.
10. Shi JH., Chen J, Wang J, Zhu YY, Wang Q. Binding interaction of sorafenib with bovine serum albumin: Spectroscopic methodologies and molecular docking. *Spectrochim Acta A Mol Biomol Spectrosc*. 2015; 149:630-637.
11. Yan J, Wu D, Ma X, Wang L, Xu K, Li H. Spectral and molecular modeling studies on the influence of β -cyclodextrin and its derivatives on aripiprazole-human serum albumin binding. *Carbohydr Polym*. 2015; 131:65-74.
12. Wu D, Liu D, Zhang Y, Zhang Z, Li H. Unravelling the binding mechanism of benproperine with human serum albumin: A docking, fluorometric, and thermodynamic approach. *Eur J Med Chem*. 2018; 146:245-250.
13. Trott O, Olson AJ. AutoDock Vina: Improving the speed and accuracy of docking with a new scoring function, efficient optimization, and multithreading. *J Comput Chem*. 2010; 31:455-461.
14. Ghuman J, Zunsain PA, Petitpas I, Bhattacharya AA, Otagiri M, Curry S. Structural basis of the drug-binding specificity of human serum albumin. *J Mol Bio*. 2005; 353:38-52.
15. Sanner MF. Python: A programming language for software integration and development. *J Mol Graph Model*. 1999; 17:57-61.
16. Morris GM, Huey R, Lindstrom W, Sanner MF, Belew RK, Goodsell DS, Olson AJ. Auto Dock 4 and Auto Dock Tools 4: Automated docking with selective receptor flexibility. *J Comput Chem*. 2009; 30:2785-2791.
17. Ma R, Pan H, Shen T, Li P, Chen Y, Li Z, Di X, Wang S. Interaction of flavonoids from *Woodwardia unigemmata* with bovine serum albumin (BSA): Application of spectroscopic techniques and molecular modeling methods. *Molecules*. 2017; 22:1317.
18. Klajnert B, Stanislawska L, Bryszewska M, Pałecz B. Interactions between PAMAM dendrimers and bovine serum albumin. *Biochim Biophys Acta*. 2003; 1648:115-126.
19. Lakowicz JR. Principles of Fluorescence Spectroscopy. Science Press, New York, USA, 1999; pp. 337-341.
20. Lakowicz JR, Weber G. Quenching of fluorescence by oxygen. A probe for structural fluctuations in macromolecules. *Biochemistry*. 1973; 12:4161-4170.
21. Meti MD, Gunagi SD, Nandibewoor ST, Chimatadar SA. Investigation of the interaction of the new antiarrhythmic drug procainamide hydrochloride with bovine serum albumin and the effect of some metal ions on the binding: A fluorescence quenching study. *Monatsh Chem*. 2013; 144:1253-1259.
22. Gao H, Lei LD, Liu JQ, Kong Q, Chen XG, Hu ZD. The study on the interaction between human serum albumin and a new reagent with antitumour activity by spectrophotometric methods. *J Photochem Photobiol A*. 2004; 167:213-221.
23. Forster T, Sinanoglu O. Modern Quantum Chemistry. Academic Press, New York, USA, 1996; pp. 297-318.
24. Rub MA, Khan JM, Asiri AM, Khan RH, ud-Din K. Study on the interaction between amphiphilic drug and bovine serum albumin: A thermodynamic and spectroscopic description. *J Lumin*. 2014; 155:39-46.
25. Ross PD, Subramanian S. Thermodynamics of protein association reactions: Forces contributing to stability. *Biochemistry*. 1981; 20:3096-3102.
26. Liu J, Tian J, He W, Xie J, Hu Z, Chen X. Spectrofluorimetric study of the binding of daphnetin to bovine serum albumin. *J Pharm Biomed Anal*. 2004; 35:671-677.
27. Krishnamoorthy P, Sathyadevi P, Butorac RR, Cowley AH, Bhuvanesh NS, Dharmaraj N. Variation in the biomolecular interactions of nickel (II) hydrazone complexes upon tuning the hydrazone fragment. *Dalton Trans*. 2012; 41:6842-6854.
28. Qin P, Su B, Liu R. Probing the binding of two fluoroquinolones to lysozyme: A combined spectroscopic and docking study. *Mol Biosyst*. 2012; 8:1222-1229.
29. Frey R, Muck W, Unger S, Artmeier-Brandt U, Weimann G, Wensing G. Single-dose pharmacokinetics, pharmacodynamics, tolerability, and safety of the soluble guanylate cyclase stimulator BAY 63-2521: An ascending-dose study in healthy male volunteers. *J Clin Pharmacol*. 2008; 48:926-934.
30. Zhou Q, Xiang J, Tang Y, Liao J, Yu C, Zhang H, Li L, Yang Y, Xu G. Investigation on the interaction between a heterocyclic aminated derivative, SBDC, and human serum albumin. *Colloids Surf B Biointerfaces*. 2008; 61:75-80.
31. Gerbanowski A, Malabat C, Rabiller C, Guéguen J. Grafting of aliphatic and aromatic probes on rapeseed 2S and 12S proteins: Influence on their structural and physicochemical properties. *J Agric Food Chem*. 1999; 47:5218-5226.

(Received April 26, 2018; Revised June 14, 2018; Accepted July 18, 2018)

Correlation of genetic diversity between hosts and parasites in *Entamoeba nuttalli* isolates from Tibetan and rhesus macaques in China

Miao Wei^{1,§}, Meng Feng^{1,§}, Yue Guan¹, Ce Guo¹, Hang Zhou¹, Yongfeng Fu¹, Hiroshi Tachibana^{2,*}, Xunjia Cheng^{1,2,*}

¹Department of Medical Microbiology and Parasitology, School of Basic Medical Sciences, Fudan University, Shanghai, China;

²Department of Infectious Diseases, Tokai University School of Medicine, Isehara, Kanagawa, Japan.

Summary

Entamoeba nuttalli infection is prevalent in captive and wild macaques. Recent studies have suggested that genotypes of *E. nuttalli* isolates are correlated with the geographical distribution of host macaques. Correlation of amoebic genotypes with genetic diversity of host macaques was analyzed in present study. Sixty fresh stool samples were obtained from wild Tibetan macaques living in Mount Huang (HS) of the An-hui Province in China. PCR analysis revealed that the most prevalent *Entamoeba* species was *E. chattoni* (*E. polecki* ST2) (86.7%) followed by *E. nuttalli* (58.3%) and *E. coli* (25%). Six *E. nuttalli* HS isolates were successfully cultured. The tRNA-linked short tandem repeat (STR) loci and serine-rich protein gene of *E. nuttalli* isolates from four different regions of China (Mount Long-hu, Gui-yang, Mount E-mei, and HS, the former three isolates were obtained in previous studies) were studied and high numbers of polymorphisms were detected. When genetic diversity of different populations of *E. nuttalli* isolates was compared with geographical distance, an r^2 value of 0.919 was assigned by a Mantel test based on the tRNA-STR loci. In host macaques, the mtDNA HVS-I gene was also highly polymorphic in each of the genomes. Multiple regression analysis using *E. nuttalli* tRNA-STR loci genetic, macaque mtDNA HVS-I gene, and geographic distances showed an r^2 value of 0.943, indicating that a higher relevance was demonstrated when geographic and host gene factors were considered. Analysis of genetic factor of host would benefit for better understanding of the evolution of *E. nuttalli*.

Keywords: Amoeba, host gene diversity, geographical distance

1. Introduction

Infection with *Entamoeba nuttalli*, a morphologically indistinguishable *Entamoeba* species from *E. histolytica*, is prevalent in captive and wild macaques

(1-7). There are numerous wild macaque populations in China, in which the rhesus macaque is widely distributed, but the Tibetan macaque is unique to east central China. Our recent studies have detected *E. nuttalli* infection in wild rhesus and Tibetan macaques in China (1,8), indicating that these macaques are also natural hosts of *E. nuttalli*.

In addition to the epidemiology of *E. nuttalli* in non-human primates, genetic diversity of this amoeba also needs to be studied further. To date, several polymorphic markers for genotyping *E. histolytica* isolates have been well established. Of these, the serine-rich protein (SRP) gene was the most widely used genotyping marker for *Entamoeba* isolates (4,9-15). tRNA-linked short tandem repeats (STRs) were another effective polymorphic marker (16). Recent studies on *E. nuttalli* isolate genotypes have suggested that these

Released online in J-STAGE as advance publication August 10, 2018.

§These authors contributed equally to this work.

*Address correspondence to:

Prof. Xunjia Cheng, Department of Medical Microbiology and Parasitology, School of Basic Medical Sciences, Fudan University, Shanghai 200032, China.

E-mail: xjcheng@shmu.edu.cn

Prof. Hiroshi Tachibana, Department of Infectious Diseases, Tokai University School of Medicine, Isehara, Kanagawa 259-1193, Japan.

E-mail: htachiba@is.icc.u-tokai.ac.jp

are correlated with the geographical distribution of host macaques (8,16).

In addition to geographical factors, other aspects which could be impacting *E. nuttalli* genetic diversity remain unclear. Given that more information would be advantageous in studying factors contributing to *E. nuttalli* genetic polymorphism. In the present study, we aimed to detect *Entamoeba* spp. infection in another Tibetan macaque population living in Mount Huang (HS) of the An-hui Province in China. Genetic variation of the tRNA-linked STR loci and SRP gene of *E. nuttalli* isolates from Chinese macaques were analyzed.

2. Materials and Methods

2.1. Sample collection

Sixty fresh stool samples were obtained from wild Tibetan macaques living in Mount Huang of the An-hui Province in China in May 2016 (Figure 1).

2.2. Stool examination and culture

Stool samples, PCR-positive for *E. nuttalli*, were xenically cultured in modified Tanabe-Chiba medium (17). In addition, trophozoites of two *E. nuttalli* isolates from Mount Qian-ling (GY) of the Guizhou Province and six *E. nuttalli* isolates from Mount E-mei (EM) of the Sichuan Province were axenically cultured in YIMDHA-S medium (1,8). Trophozoites from 16 *E. nuttalli* isolates from wild rhesus macaques in Mount Long-hu (LH) of the Guanxi Province were xenically cultured in modified Tanabe-Chiba medium. These isolates were used as reference strains.

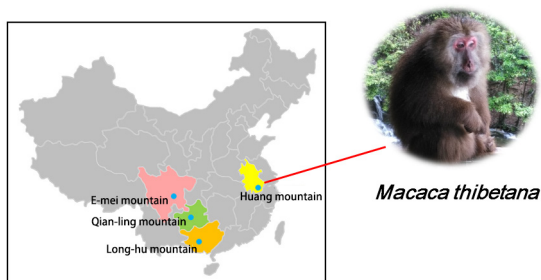


Figure 1. Geographic location of Mount Huang (HS), Mount E-mei (EM), Mount Qian-ling (GY), and Mount Long-hu (LH).

2.3. Extraction of genomic DNA and PCR amplification

PCR was used to detect various *Entamoeba* species. Genomic DNA from the 60 stool samples was extracted using a QIAamp DNA Stool Mini Kit (Qiagen, Germany) and then PCR with 35 cycles for amplification of partial 18S ribosomal RNA genes from *E. histolytica*, *E. dispar*, *E. nuttalli*, *E. coli*, and *E. chattoni* (*E. polecki* ST2) were performed as described previously (2,3,18). Genomic DNA was also extracted from cultured trophozoites using a DNeasy blood and tissue kit (Qiagen, Germany). Genomic DNA isolated from cultured trophozoites was used for amplification of amoeba genes and genomic DNA isolated from *E. nuttalli* positive stool samples were used for amplification of host genes. Complete 18S and 5.8S rRNA genes were amplified as described previously (2). The SRP gene and tRNA-linked STR fragments were amplified with Takara *Pyrobest* DNA polymerase from the genomic DNA of trophozoites using primers for five polymorphic STR loci (Locus D-A, N-K2, R-R, S-Q, and S^{TGA}-D) as described previously (16,19). The host macaque hypervariable segments I of mitochondrial DNA (mtDNA HVS-I) and partial MHC II DRB1 genes were amplified from the genomic DNA of stool samples using primers listed in Table 1. Briefly, the following PCR conditions were used: denaturation at 94°C for 15 s, annealing for 30 s, and extension at 72°C for 30 s (*Entamoeba* species diagnosis), 3 min (complete 18S and 5.8S rRNA genes), 45 s (five STR loci and SRP gene), or 1 min (mtDNA HVS-I and partial MHC II DRB1 genes). Annealing temperatures for amplifying mtDNA HVS-I and partial MHC II DRB1 genes are shown in Table 1. An initial 3-min denaturation step at 94°C and a final 7-min polymerization step at 72°C were also performed for all reactions.

2.4. Sequencing and analysis of genes

PCR products of the 2.4-kb rRNA gene, SRP gene, and five tRNA-linked STR fragments of *E. nuttalli* as well as those of mtDNA HVS-I and partial MHC II DRB1 genes of macaques were purified using an AxyPrep DNA Gel Extraction kit (Axygen, USA) and then subjected to direct sequencing by PCR primers using a BigDye Terminator v3.1 Cycle Sequencing Kit (Applied Biosystems, USA). The 2.4-kb rRNA gene were completely sequenced by primer walking. PCR products with multiple sequences were processed using a pMD[®]20-T Vector cloning kit (TaKaRa). More than

Table 1. Primers for macaque genes

Primer	Sequence (5'-3')	Annealing temperature
Macaca HVS-I-F	CTGAATTGGAAGCGAACC	55°C
Macaca HVS-I-R	CCCGTGATCCATCGAGATGTCTT	
Macaca DRB1-F	CAACCTAAGGTGACTGTGTATC	50°C
Macaca DRB1-R	CACTCCATTCCACTGTGAGAG	

10 clones of each gene were sequenced. Reactions were run on an ABI Prism 3100 Genetic Analyzer (Applied Biosystems, USA). Sequence data were analyzed using Bioedit 7.0.

2.5. Genetic variation and population analyses

Genetic distances were calculated using the SRP gene or five tRNA-STR loci using MEGA 5 software. Then, a Mantel test for isolation by distance was performed using IBD 1.5.2 software (20) with 10,000 randomizations.

A neighbor-joining (NJ) tree was constructed using the SRP gene or five of the tRNA-STR loci by MEGA 5 software.

Analysis and multiple alignments of macaque mtDNA HVSI and partial MHC II DRB1 genes were performed using Clustal X; phylogenetic trees and genetic distances were constructed using the NJ method.

SPSS 20.0 was used for preparing the 3D spot figure. Haplotype and nucleotide diversities of these gene sequences between different groups were calculated using DnaSPv5 software as described previously (21).

3. Results

3.1. Detection and isolation of *Entamoeba* spp. in stool samples

We attempted to detect the five *Entamoeba* species by

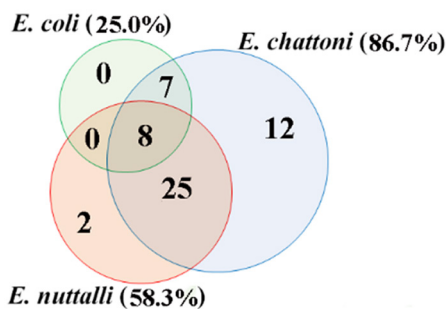


Figure 2. Detailed compositions of *Entamoeba* infections in Tibetan macaques of Mount Huang. The Venn diagram shows quantities of co-infection of *E. nuttalli*, *E. polecki* ST2, and *E. coli* in the stool samples obtained from wild Tibetan macaques of Mount Huang. Each circle represents one *Entamoeba* species. Numbers in an area overlapped by two or three circles indicate the quantity of samples of coinfections, accordingly.

PCR from all 60 stool samples. *E. chattoni* (86.7%) was the most prevalent species, followed by *E. nuttalli* (58.3%) and *E. coli* (25%) (Figure 2). In addition, mixed infections were detected in more than half of the positive samples (65%). *E. histolytica* and *E. dispar* were not detected by PCR in these samples.

Stool samples were xenically cultured in modified Tanabe-Chiba medium. Six isolates were successfully cultured and designated as follows: HS24, HS25, HS31, HS42, HS48, and HS59.

3.2. rRNA gene analysis

The 2.4-kb region containing 18S and 5.8S rRNA genes was amplified by PCR and directly sequenced. Nucleotide sequences of the Mount Huang samples indicated that the isolates were of *E. nuttalli*. Moreover, the nucleotide sequence of the rRNA gene of the isolates obtained from Tibetan macaques in Mount Huang was identical to that the rRNA gene of *E. nuttalli* isolates from wild Tibetan macaques in Mount E-mei and wild rhesus macaques in Mount Qian-ling and Mount Long-hu. The 2.4-kb region containing 18S and 5.8S rRNA genes of these Chinese *E. nuttalli* isolates were completely identical and these isolates exhibited three nucleotide differences compared with the reference strain P19-061405 (AB282657), which was obtained from a wild rhesus macaque in Kathmandu in Nepal (1,2).

3.3. SRP gene and tRNA-linked STR loci typing

Given that differentiation of STR types are indispensable for high-resolution genotyping of amoebic isolates, we analyzed the SRP gene and tRNA-linked STRs of Chinese *E. nuttalli* isolates collected from two *Macaca* species at diverse geographic locations (Table 2). Six isolates from the Tibetan macaques collected from Mount Huang shared identical STR sequence types for the SRP gene and five tRNA-linked STRs loci (Figure 3A to 3E). The newly identified sequences were deposited in the DDBJ/EMBL/GenBank database (LC379241-LC379247).

3.4. NJ tree of *E. nuttalli* isolates

Table 2. Characteristics of *E. nuttalli* isolates using SRP and tRNA-STR markers

Isolate	No. of isolates	Host macaque species	Location of collection	Genotypes of SRP gene	Genotypes of tRNA-STRs				
					N-K2	S-Q	S ^{TGA} -D	R-R	D-A
EM	6	<i>M. thibetana</i>	E-mei mountain	Cn1SRP	Cn1NK	Cn1SQ	Cn1SD	Cn1RR	Cn1DA
GY	2	<i>M. mulatta</i>	Qian-ling mountain	Cn2SRP	Cn2NK	Cn2SQ	Cn2SD	Cn2RR	Cn2DA
LH	16	<i>M. mulatta</i>	Long-hu mountain	Cn3SRP	Cn2NK	Cn3SQ	Cn2SD	Cn2RR	Cn3DA
HS	6	<i>M. thibetana</i>	Huang mountain	Cn4SRP	Cn3NK	Cn4SQ	Cn3SD	Cn3RR	Cn5DA
				Cn5SRP					
				Cn6SRP	Cn4NK	Cn5SQ	Cn4SD	Cn4RR	Cn6DA

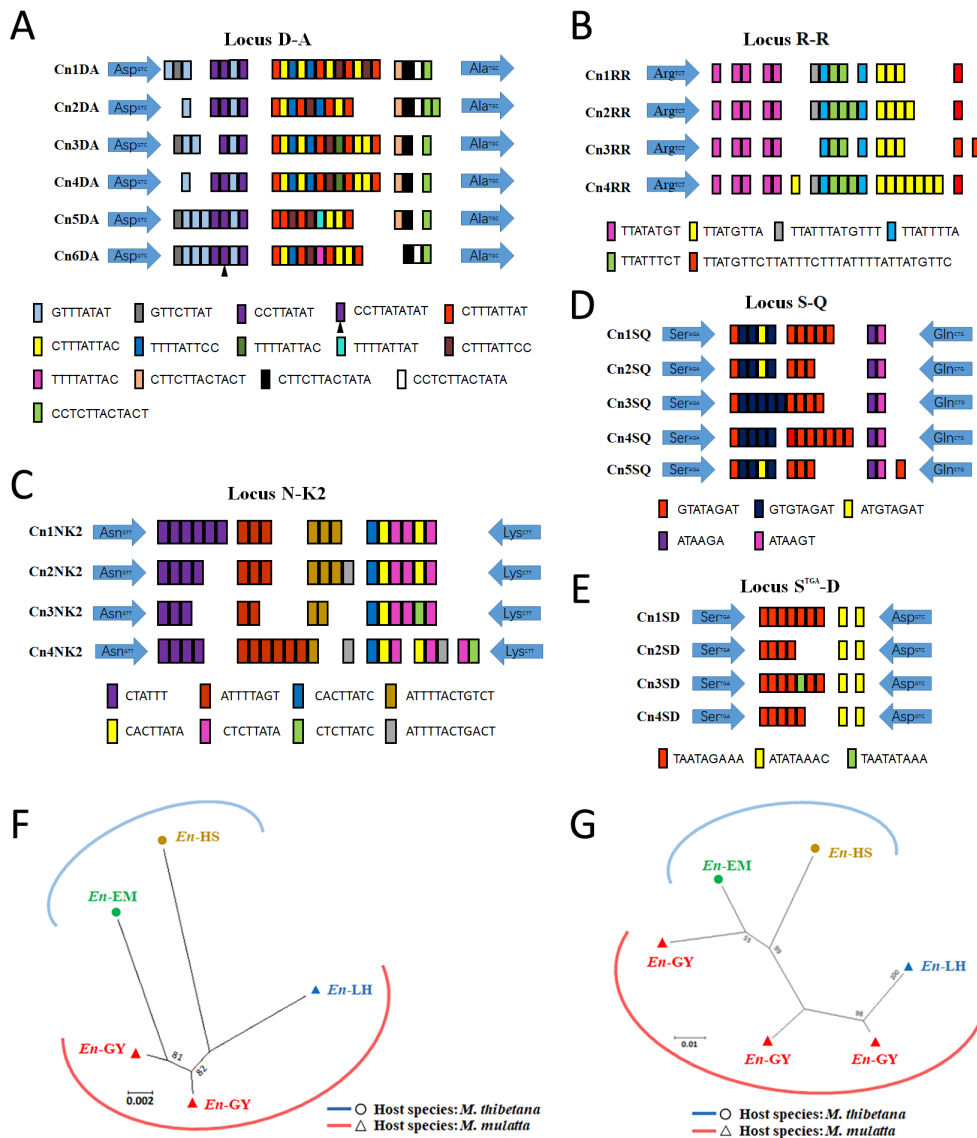


Figure 3. Schematic representation of tRNA-linked short tandem repeat types of each loci based on the nucleotide sequence and phylogenetic tree constructed using the NJ method of *E. nuttalli* isolates. Schematic representation of Locus D-A (A), R-R (B), N-K2 (C), S-Q (D), and STGA-D (E). tRNA genes and STRs are depicted as arrows and rectangles, respectively. Diagrams and sequence types are based on the study of Ali *et al.* (34). (F) NJ tree based on the tRNA-STR loci of *Entamoeba* species. (G) NJ tree based on the SRP gene of *Entamoeba* species

In the distance-based NJ tree obtained using the tRNA-STR loci (Figure 3F), *E. nuttalli* isolates were presented into five paraphyletic branches. HS, EM, and LH isolates were categorized into an independent branch and GY isolates were categorized into two branches. In the distance-based NJ tree obtained using the SRP gene (Figure 3G), *E. nuttalli* isolates were represented by six paraphyletic branches. HS and EM isolates were categorized into an independent branch, whereas GY and LH isolates were categorized within two branches.

3.5. Effect of geographical distance on genetic diversity

The genetic diversity of different populations was compared with respect to geographical distance to estimate the importance of the geographical pattern for genetic relationships among the four *E. nuttalli*

populations. Chinese *E. nuttalli* isolates were collected from four neighboring provinces (Figure 1). Results of the Mantel test gave an r^2 value of 0.919 ($P < 0.05$, for 10,000 randomizations) based on the tRNA-STR loci and an r^2 value of 0.88 ($P < 0.05$, for 10,000 randomizations) based on the SRP gene. These results indicated that a significant isolation by the distance effect was found in the populations based on the tRNA-STR loci.

3.6. Analysis of host genetic variation

The macaque mtDNA HVS-I and partial MHC II DRB1 genes were highly polymorphic in each of the genomes. In the distance-based NJ tree obtained using the mtDNA HVS-I gene (Figure 4A), different macaque populations were represented by six paraphyletic branches. HS and

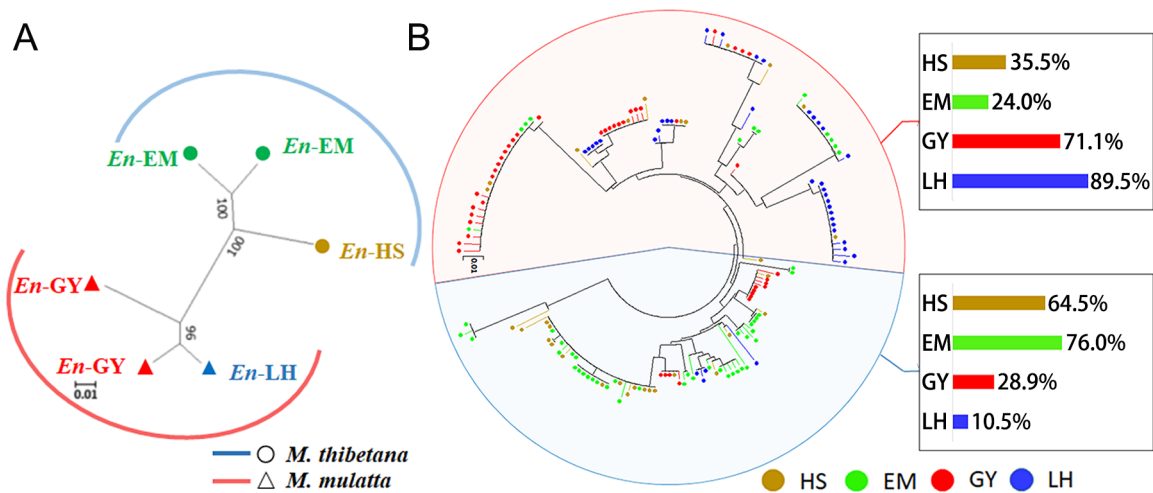


Figure 4. Phylogenetic tree constructed using the NJ method for host macaques. (A) NJ tree based on the mtDNA HVS-I gene of host macaques. **(B)** NJ tree based on the partial MHC II DRB1 gene of host macaques. Pie chart displaying the percentage of each population in the upper and lower clusters.

LH macaques were categorized into an independent branch, whereas EM and GY macaques were categorized into two branches. In the distance-based NJ tree obtained using the partial MHC II DRB1 gene (Figure 4B), different macaque populations were represented by two large clusters. The upper semi-cluster contained 89.5%, 71.1%, 35.5%, and 24% alleles of LH, GY, HS, and EM macaques, respectively, and the lower half cluster contained 76%, 64.5%, 28.9%, and 10.5% alleles of EM, HS, GY, and LH macaques, respectively. The results indicated that most alleles of LH and GY macaques were located in the upper semi-cluster and that most of the alleles of the EM and HS macaques were located in the lower half cluster. The results suggested that HVS-I gene could distinguish the four regions of macaques better than MHC II DRB1 gene. The newly identified sequences were deposited in the DDBJ/EMBL/GenBank database (LC379248- LC379253).

3.7. Effect of macaque gene diversity on *E. nuttalli* genetic diversity

Quantifiable data revealed both high haplotype (1.0) and nucleotide diversities (0.065) of tRNA-STR loci sequences from GY isolates (Figure 5A). The mtDNA HVS-I gene of macaques infected with GY isolates also indicated high haplotype (1.0) and nucleotide diversities (0.06) (Figure 5B). GY macaques and *E. nuttalli* GY isolates both had the highest genetic diversity among the four Chinese populations. The haplotype diversity and nucleotide diversity of the MHC II DRB1 gene were also calculated. But the results suggested that the MHC II DRB1 gene was too polymorphism to distinguish difference among the four regions of macaques in the present study.

Multiple regression analysis using *E. nuttalli* tRNA-STR loci genetic, macaque gene, and geographic distances indicated an r^2 value of 0.943 ($P < 0.05$, 10,000 randomizations). The results indicated that a higher

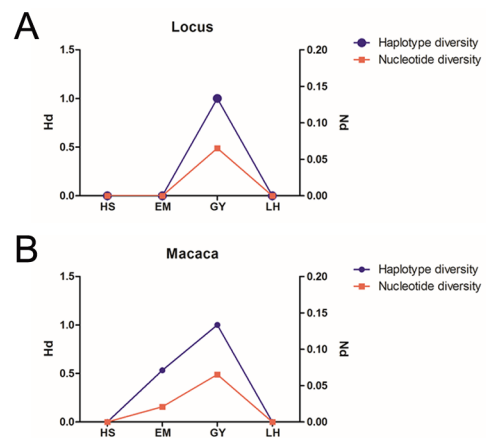


Figure 5. Gene diversity of *E. nuttalli* isolates and the macaque. (A) Haplotype and nucleotide diversities of the tRNA-STR loci of *E. nuttalli* isolates. **(B)** Haplotype and nucleotide diversities of mtDNA HVS-I gene of macaques.

relevance was shown when both geographic and host gene factors were considered.

4. Discussion

Recent studies have demonstrated high polymorphism among *E. nuttalli* SRP gene and tRNA-linked STR from Nepalese, Japanese, and Chinese isolates (1-3,6,22). The present study also demonstrated the presence of multiple genotypes in *E. nuttalli* isolates from different macaque populations. However, factors affecting polymorphism of *E. nuttalli* genes remained largely unknown. The current study attempted to provide insights into this amoeba gene polymorphism.

It has been demonstrated that genetic diversity of Chinese *E. nuttalli* isolates is associated with geographic distance based on the tRNA-STR loci (8). The importance of the geographic factor was proved by investigation of other *E. nuttalli* isolates in Nepal (16). In present study, a Mantel test indicated similar results when

the Mount Huang population was included. Geographic factors were regarded as important contributors that could explain polymorphism of *E. nuttalli* genes. However, there were exceptions, as GY isolates included in present study demonstrated separate genetic features in the NJ tree. In the distance-based NJ tree, differences in genetic distance among *E. nuttalli* HS, EM, GY, and LH isolates were demonstrated. *E. nuttalli* genes from four macaque populations could be divided into five branches, with only GY isolates being attributed to two different branches. Genetic diversity in *E. nuttalli* GY isolates was quite prominent even if the amoeba was isolated from macaques in a very close geographical range. Therefore, we could not exclude the possibility that other factors may also affect genetic polymorphism of *E. nuttalli* isolates.

Host genetic diversity or pathogen-host co-evolution have been considered as critical factors affecting pathogen genetic diversity in a number of studies (23-28). Accordingly, the host macaque species and host genetic diversity could be important factors affecting *E. nuttalli* genetic diversity. Both rhesus and Tibetan macaques were included in present study, and all the samples were examined by DNA sequence analysis to verify that they were of *Macaca* species origin. Furthermore, the hypervariable region of host mtDNA and MHC II DRB1 genes were first used to determine the possibility that the host species was correlated with the genetic diversity of the amoeba. The results indicated that mtDNA HVS-I gene was compatible for distinguishing between the four Chinese macaque populations. GY macaques contained genetic features of two clusters in the NJ tree. The high haplotype and nucleotide diversity of GY macaques was also the highest among all populations. Results were similar to the *E. nuttalli* genetic diversity of GY isolates. This may indicate that host genetic diversity could affect parasite genetic diversity and explain *E. nuttalli* genetic diversity of GY isolates.

The host factor was probably non-negligible in the study on *E. nuttalli*. Host specificity has already been proved to be an important subject in the epidemiology of *Entamoeba* (29,30). In present study, a further analysis including amoebic genetic distance, geographic distance, and host genetic distance was performed. The result gave an r^2 value of 0.943, which was higher than that obtained with the Mantel test (0.919). This higher r^2 value may have demonstrated a more reasonable fitting method to analyze *E. nuttalli* genetic features. The genetic variation of the tRNA-linked STR loci of *E. nuttalli* isolates from Chinese macaques may be partially attributable to both host geographic locations and host genetic variation.

Genetic differences between the two different macaque species included in present study could not be ignored; however, the Tibetan macaque, a unique non-human primate in China, was identified as a closely related species to the rhesus macaque (31,32). A more in-depth study involving the same species of macaque to

evaluate the relationship between host genetic variation and *E. nuttalli* genetic variation would be more powerful.

Both the SRP gene and the tRNA-linked STR genotyping systems have been commonly used to distinguish *E. histolytica* genotypes (10,19,33-36). In the five tRNA-STR loci distance-based NJ tree, HS isolates were attributed to a slightly further branch to distinguish it from the *E. nuttalli* EM and GY isolates. However, data based on the SRP gene showed slightly different results. *E. nuttalli* HS isolates were attributed to a branch closer to the EM isolates than to the GY isolates. These results suggest that genetic evolution of SRP gene has a little differences with tRNA-STR loci. Furthermore, the tRNA-STR loci had more relativity than the SRP gene when used in the Mantel test. In summary, analysis in present study was focused on data of the tRNA-STR loci of Chinese *E. nuttalli* isolates. In comparison with single-genes analysis, polygenic analysis would be better for obtaining more credible results.

In conclusion, the current study demonstrated high positive rates of *E. nuttalli* infection in Chinese macaques. These data showed that different macaque species in China were susceptible to *E. nuttalli* infection. In addition, *E. coli* and *E. chattoni* infections were commonly detected in these macaques. Present study also demonstrated that *E. nuttalli* HS isolates had unique genetic differences from other Chinese isolates based on tRNA-linked STR loci and the SRP gene. Additionally, analysis of genetic factor of host would benefit for better understanding of the evolution of *E. nuttalli*.

Acknowledgements

This work was supported by NSFC (81630057), National 163 Program of China (17-0163-15-XJ-002-003-06), and JSPS KAKENHI (16H05819).

References

1. Feng M, Cai J, Min X, Fu Y, Xu Q, Tachibana H, Cheng X. Prevalence and genetic diversity of *Entamoeba* species infecting macaques in southwest China. *Parasitol Res.* 2013; 112:1529-1536.
2. Tachibana H, Yanagi T, Pandey K, Cheng X, Kobayashi S, Sherchand J, Kanbara H. An *Entamoeba* sp. strain isolated from rhesus monkey is virulent but genetically different from *Entamoeba histolytica*. *Mol Biochem Parasitol.* 2007; 153:107-114.
3. Tachibana H, Yanagi T, Akatsuka A, Kobayashi S, Kanbara H, Tsutsumi V. Isolation and characterization of a potentially virulent species *Entamoeba nuttalli* from captive Japanese macaques. *Parasitology.* 2009; 136:1169-1177.
4. Tachibana H, Yanagi T, Lama C, Pandey K, Feng M, Kobayashi S, Sherchand J. Prevalence of *Entamoeba nuttalli* infection in wild rhesus macaques in Nepal and characterization of the parasite isolates. *Parasitol Int.* 2013; 62:230-235.
5. Tachibana H, Yanagi T, Feng M, Bandara K, Kobayashi

- S, Cheng X, Hirayama K, Rajapakse R. Isolation and molecular characterization of *Entamoeba nuttalli* strains showing novel isoenzyme patterns from wild toque macaques in Sri Lanka. *J Eukaryot Microbiol.* 2016; 63:171-180.
6. Takano J, Tachibana H, Kato M, Narita T, Yanagi T, Yasutomi Y, Fujimoto K. DNA characterization of simian *Entamoeba histolytica*-like strains to differentiate them from *Entamoeba histolytica*. *Parasitol Res.* 2009; 105:929-937.
 7. Vlčková K, Kreisinger J, Pafčo B, Čížková D, Tagg N, Hehl A, Modrý D. Diversity of *Entamoeba* spp. in African great apes and humans: An insight from Illumina MiSeq high-throughput sequencing. *Int J Parasitol.* 2018; S0020-7519:30055-9.
 8. Guan Y, Feng M, Cai J, Min X, Zhou X, Xu Q, Tan N, Cheng X, Tachibana H. Comparative analysis of genotypic diversity in *Entamoeba nuttalli* isolates from Tibetan macaques and rhesus macaques in China. *Infect Genet Evol.* 2016; 38:126-131.
 9. Feng M, Yang B, Yang L, Fu Y, Zhuang Y, Liang L, Xu Q, Cheng X, Tachibana H. High prevalence of *Entamoeba* infections in captive long-tailed macaques in China. *Parasitol Res.* 2011; 109:1093-1097.
 10. Feng M, Cai J, Yang B, Fu Y, Min X, Tachibana H, Cheng X. Unique short tandem repeat nucleotide sequences in *Entamoeba histolytica* isolates from China. *Parasitol Res.* 2012; 111:1137-1142.
 11. Fu Y, Nagakura K, Cheng X, Tachibana H. Comparison of serine-rich protein genes of *Entamoeba histolytica* isolates obtained from institutions for the mentally retarded in Kanagawa and Shizuoka Prefectures, Japan. *Parasitol Res.* 2010; 107:999-1002.
 12. Haghighi A, Kobayashi S, Takeuchi T, Masuda G, Nozaki T. Remarkable genetic polymorphism among *Entamoeba histolytica* isolates from a limited geographic area. *J Clin Microbiol.* 2002; 40:4081-4090.
 13. Haghighi A, Kobayashi S, Takeuchi T, Thammapalerd N, Nozaki T. Geographic diversity among genotypes of *Entamoeba histolytica* field isolates. *J Clin Microbiol.* 2003; 41:3748-3756.
 14. Haghighi A, Rasti S, Nazemalhosseini Mojarad E, Kazemi B, Bandehpour M, Nochi Z, Hooshyar H, Rezaian M. *Entamoeba dispar*: Genetic diversity of Iranian isolates based on serine-rich *Entamoeba dispar* protein gene. *Pak J Biol Sci.* 2008; 11:2613-2618.
 15. Zaki M, Meelu P, Sun W, Clark C. Simultaneous differentiation and typing of *Entamoeba histolytica* and *Entamoeba dispar*. *J Clin Microbiol.* 2002; 40:1271-1276.
 16. Feng M, Komiyama T, Yanagi T, Cheng X, Sherchand J, Tachibana H. Correlation between genotypes of tRNA-linked short tandem repeats in *Entamoeba nuttalli* isolates and the geographical distribution of host rhesus macaques. *Parasitol Res.* 2014; 113:367-374.
 17. Yoshimura M, Ebukuro M. A modified Tanabe-Chiba medium for detection of *Entamoeba histolytica*. *Jikken Dobutsu.* 1988; 37:321-324. (in Japanese)
 18. Verweij J, Polderman A, Clark C. Genetic variation among human isolates of uninucleated cyst-producing *Entamoeba* species. *J Clin Microbiol.* 2001; 39:1644-1646.
 19. Ali I, Zaki M, Clark C. Use of PCR amplification of tRNA gene-linked short tandem repeats for genotyping *Entamoeba histolytica*. *J Clin Microbiol.* 2005; 43:5842-5847.
 20. Jensen J, Bohonak A, Kelley S. Isolation by distance, web service. *BMC Genet.* 2005; 6:13.
 21. Liu J, Feng M, Wang X, Fu Y, Ma C, Cheng X. Unique *Trichomonas vaginalis* gene sequences identified in multinational regions of Northwest China. *Biosci Trends.* 2017; 11:303-307.
 22. Dong H, Li J, Qi M, Wang R, Yu F, Jian F, Ning C, Zhang L. Prevalence, molecular epidemiology, and zoonotic potential of *Entamoeba* spp. in nonhuman primates in China. *Infect Genet Evol.* 2017; 54:216-220.
 23. Brites D, Gagneux S. The nature and evolution of genomic diversity in the *Mycobacterium tuberculosis* complex. *Adv Exp Med Biol.* 2017; 1019:1-26.
 24. Cacciò S, Lalle M, Svärd S. Host specificity in the *Giardia duodenalis* species complex. *Infect Genet Evol.* 2017; S1567-1348:30418-5.
 25. Kabamba E, Tuan V, Yamaoka Y. Genetic populations and virulence factors of *Helicobacter pylori*. *Infect Genet Evol.* 2018; 60:109-116.
 26. Latinne A, Bezé F, Delhaes L, Pottier M, Gantois N, Nguyen J, Blasdel K, Dei-Cas E, Morand S, Chabé M. Genetic diversity and evolution of *Pneumocystis* fungi infecting wild Southeast Asian murid rodents. *Parasitology.* 2017; 9:1-16.
 27. Le Bailly M, Maicher C, Dufour B. Archaeological occurrences and historical review of the human amoeba, *Entamoeba histolytica*, over the past 6000 years. *Infect Genet Evol.* 2016; 42:34-40.
 28. Scarborough J, Paul J, Spencer J. Evolution of the ability to modulate host chemokine networks via gene duplication in human cytomegalovirus (HCMV). *Infect Genet Evol.* 2017; 51:46-53.
 29. Wilson I, Weedall G, Hall N. Host-Parasite interactions in *Entamoeba histolytica* and *Entamoeba dispar*: What have we learned from their genomes? *Parasite Immunol.* 2012; 34:90-99.
 30. Ximenez C, Moran P, Rojas L, Valadez A, Gomez A. Reassessment of the epidemiology of amoebiasis: State of the art. *Infect Genet Evol.* 2009; 9:1023-1032.
 31. Li Q, Zhang Y. Phylogenetic relationships of the macaques (Cercopithecidae: Macaca), inferred from mitochondrial DNA sequences. *Biochem Genet.* 2005; 43:375-386.
 32. Yan X, Li A, Zeng L, Cao Y, He J, Lv L, Sui L, Ye H, Fan J, Cui X, Sun Z. Identification of MHC class I sequences in four species of Macaca of China. *Immunogenetics.* 2013; 65:851-859.
 33. Ali I, Clark C, Petri W. Molecular epidemiology of amoebiasis. *Infect Genet Evol.* 2008; 8:698-707.
 34. Ali I, Haque R, Alam F, Kabir M, Siddique A, Petri W. Evidence for a link between locus R-R sequence type and outcome of infection with *Entamoeba histolytica*. *Clin Microbiol Infect.* 2012; 18:E235-237.
 35. Ali I, Mondal U, Roy S, Haque R, Petri W, Clark C. Evidence for a link between parasite genotype and outcome of infection with *Entamoeba histolytica*. *J Clin Microbiol.* 2007; 45:285-289.
 36. Jaiswal V, Ghoshal U, Mittal B, Dhole T, Ghoshal U. Association between allelic variation due to short tandem repeats in tRNA gene of *Entamoeba histolytica* and clinical phenotypes of amoebiasis. *Acta Trop.* 2014; 133:1-7.

(Received July 8, 2018; Revised July 30, 2018; Accepted August 3, 2018)

Bolus administration of ephedrine and etilefrine induces transient vasodilation just after injection in combined epidural and general anesthesia patients: A randomized clinical study

Zen'ichiro Wajima^{1,*}, Toshiya Shiga², Kazuyuki Imanaga³

¹ Department of Anesthesiology, Tokyo Medical University Hachioji Medical Center, Tokyo, Japan;

² Department of Anesthesiology and Intensive Care Medicine, International University of Health and Welfare, School of Medicine, Narita, Chiba, Japan;

³ Department of Anesthesia, Shonan Kamakura General Hospital, Kamakura, Kanagawa, Japan.

Summary

Hypotension commonly accompanies combined epidural and general anesthesia, and intravenous bolus ephedrine and etilefrine are widely used to correct hypotension. We have noticed that systemic vascular resistance (SVR) transiently decreases just after intravenous bolus administration of these drugs. The goal of the present study was to investigate whether bolus administration of these drugs decrease SVR just after intravenous administration in combined epidural and general anesthesia patients. We investigated 40 patients who were scheduled for elective abdominal surgery. Patients were chosen as subjects if their systolic arterial pressure decreased by 20% or to <100 mmHg at 30 min after the induction of general anesthesia. Baseline hemodynamic values were recorded, and after ephedrine 10 mg injection or etilefrine 2 mg injection (equipotent), the parameters were recorded again at 0.5 min and once each min for the next 5 min thereafter. The 40 patients were enrolled into the ephedrine ($n = 20$) or etilefrine ($n = 20$) treatment groups. Patient characteristics were comparable in both groups. After ephedrine injection, SVR decreased significantly at the 1-min time point, whereas after etilefrine injection, SVR decreased significantly at the 0.5- to 2-min time points compared with baseline values. SVR at the 0.5- to 1-min time points was lower in the etilefrine versus the ephedrine group. Both drugs transiently decreased SVR after intravenous injection, but etilefrine decreased SVR much more than ephedrine, indicating that more vasodilation occurred after the injection of etilefrine than after ephedrine. It is thus important to recognize the different characteristics of these drugs.

Keywords: Ephedrine, etilefrine, hemodynamics, systemic vascular resistance, vasodilation

1. Introduction

Hypotension commonly accompanies anesthesia (1), especially combined epidural and general anesthesia (2) which is a common anesthesia method, and intravenous (IV) ephedrine or etilefrine are widely used to resolve

such hypotension (2-9). We have noticed that these drugs transiently decrease systemic vascular resistance (SVR) just after bolus IV administration in combined epidural and general anesthesia patients prior to this study. To our knowledge, however, no reports have compared the very acute hemodynamic changes between ephedrine and etilefrine including those of SVR.

Therefore, in this randomized clinical study, we investigated whether the bolus administration of these drugs decreases SVR just after IV administration and also evaluated any potential differences in the very acute hemodynamics between IV ephedrine and etilefrine in combined epidural and general anesthesia patients, which have not been reported to date.

Released online in J-STAGE as advance publication August 10, 2018.

*Address correspondence to:

Prof. Zen'ichiro Wajima, Department of Anesthesiology, Tokyo Medical University Hachioji Medical Center, 1163 Tate-machi, Hachioji, Tokyo 193-0998, Japan.
E-mail: HFB01245@nifty.com

2. Materials and Methods

2.1. Study subjects

We conducted a prospective, randomized, double-blind study at the International University of Health and Welfare Shioya Hospital, Tochigi, Japan. The local hospital ethics committee approved the study protocol (protocol number 13-B-17, 2013-10-4), and the study was registered in the UMIN Clinical Trial Registry (ID: UMIN000011970). The Consolidated Standards of Reporting Trials (CONSORT) guidelines were followed. Written informed consent was obtained from all subjects. Female and male patients aged 20-75 years of American Society of Anesthesiologists' (ASA) physical classes I to II were eligible for inclusion if scheduled to undergo upper or lower abdominal surgery requiring combined epidural and general anesthesia. Patients with known diabetes mellitus, diseases of the cardiovascular (including arrhythmia), pulmonary, neurologic, endocrinologic, or autonomic systems, and diseases affecting intravascular fluid volume or balance, e.g., inflammatory diseases or obstructive diseases of the gastrointestinal tract, were excluded. Furthermore, we did not administer either ephedrine or etilefrine in tachycardic patients (HR >100) because we believe that these drugs should not be administered to such patients. All patients fasted preoperatively for at least 8 hours, and none of the patients received any premedication.

2.2. Anesthesia technique

Before the induction of general anesthesia, an epidural catheter was inserted cephaladly to a distance of 4 cm within one intervertebral space (Th8-9 to Th11-12). We use the loss-of-resistance technique with physiological saline to identify the epidural space (10,11). Anesthesia of 1% epidural lidocaine (6-12 mL) was administered, and the level of analgesia was tested with a pinprick 15 min after the epidural lidocaine was administered. We confirmed that the cephalad analgesia level was at least Th5 and the lower (caudad) analgesia level was at least L1.

General anesthesia was induced with IV administration of propofol at an initial effect-site concentration of 4 µg/mL and remifentanyl 1 µg/kg in total, along with rocuronium 0.6 mg/kg IV. Thereafter, we inserted a 23-gauge catheter into either the left or right radial artery to directly monitor arterial pressure. We used a semi-closed circle system to mechanically ventilate the patients' lungs at a fresh gas flow of 6 L/min (O₂, 2 L/min and air, 4 L/min). The controlled ventilation rate was 10 breaths/min at an inspiratory:expiratory ratio of 1:2, and a tidal volume of 8 ml/kg was used. The effect-site concentration of the propofol (administered by plasma target-controlled infusion) was later adjusted to maintain a target BIS of

40 to 60 and stable circulatory variables.

2.3. Monitoring equipment

We continuously monitored the systolic arterial pressure (SAP), mean arterial pressure (MAP), diastolic arterial pressure (DAP), heart rate (HR), pressure of end-tidal CO₂ (P_{ET}CO₂), SVV, cardiac output (CO), stroke volume index (SVI), and SVR with a CARESCAPE B850 monitor (GE Healthcare, Helsinki, Finland) and a FloTrac/Vigileo™ system (software ver. 03.06; Edwards Lifesciences, Irvine, CA, USA). We did not use a central venous catheter to directly measure the patient's central venous pressure (CVP). Instead, the SVR data was obtained using a fixed CVP of 0 mmHg by inputting this pressure value into the FloTrac/Vigileo™ (12,13).

Each patient became a subject if at 30 min after induction of general anesthesia, the systolic blood pressure had decreased by > 20% compared with that just before epidural anesthesia or had dropped to < 100 mmHg. However, if either severe hypotension (mean blood pressure < 50 mmHg) or no hypotension at all occurred, the patient was excluded as a subject (Figure 1). Furthermore, we did not administer either ephedrine or etilefrine in tachycardic patients (HR > 100) because we believe that these drugs should not be administered to such patients. Each chosen patient was randomized to receive ephedrine or etilefrine by a computer-generated list using an allocation ratio of 1:1. The baseline values of the hemodynamic parameters and those of SAP, MAP, DAP, HR, P_{ET}CO₂, SVV, CO, SVI, and SVR of the patients were recorded. Then, the patients were administered either ephedrine 10 mg or etilefrine 2 mg (the doses are equipotent (8,14)) that was prepared in identically coded syringes by a nurse not involved in the study. Because the pressure waveform is sampled by the Vigileo™ at 100 Hz over 20 s and it provides calculations at the end of each 20-s timeframe, the values of SVV, CO, SVI, and SVR were recorded 20 s after recording of the SAP, MAP, DAP, HR, and P_{ET}CO₂ (15). These values were recorded again at 0.5 min after the ephedrine or etilefrine IV administration and every 1 min for 5 min thereafter. Assessments of the recorded values were performed by a blinded assessor. We conducted all studies before the surgery began, and we administered just 100 mL of normal saline to the patients to ensure minimal change in SVV values during the induction of general anesthesia and throughout the study.

2.4. Statistical analyses

We used preliminary data obtained from 10 patients to estimate sample size, and we further assumed that a change of 200 points in the SVR between the ephedrine and etilefrine groups at 0.5 min after injection would be clinically relevant. Our power analysis indicated that a

minimum of 18 patients would be required to meet the criteria of $\beta = 0.1$ and $\alpha = 0.05$. We therefore enrolled 20 patients in each group to compensate for any potential dropouts. This analysis was conducted with GraphPad StatMate 2.00 (GraphPad Software, Inc., La Jolla, CA, USA).

Values are expressed as means \pm standard deviation (SD). Within-group differences of the recorded parameters were analysed by paired *t*-test with Bonferroni's correction to determine whether there were significant differences between the baseline values and the parameter values after injection. Between-group differences in these parameters were analysed by unpaired *t*-test. A *P* value < 0.05 was considered to indicate statistical significance. All analyses were conducted with GraphPad Prism 5.04 (GraphPad Software, Inc.).

3. Results

Details of patient recruitment and excluded participants are shown in Figure 1 (no patients showed tachycardia [HR > 100]). The 40 patients enrolled in this study were divided into the etilefrine group ($n = 20$) and the ephedrine group ($n = 20$). Patient characteristics were similar in both groups (Table 1).

After bolus injection of ephedrine, significant increases in the values of SAP, MAP, DAP, HR, $P_{ET}CO_2$, CO, and SVI at the time points of 1 to 5 min and of SVV at the time point of 1 min were noted in comparison with the baseline values (Figures 2, 3). Significant decreases were noted in comparison with the baseline values at the time point of 1 min in SVR and at the time points of 2 to 5 min in SVV (Figure 3).

After bolus injection of etilefrine, significant

increases occurred in SAP and SVI at the time points of 1 to 5 min, in MAP and DAP at the time points of 2 to 5 min, in HR at the time point of 1 min, in $P_{ET}CO_2$ at the time points of 1 to 4 min, in CO at the time points of 0.5 to 5 min, and in SVV at the time point of 0.5 min compared with the baseline values (Figures 2, 3). SVV at the time points of 2 to 5 min and SVR at the time points of 0.5 to 2 min also showed significant decreases compared with the baseline values (Figure 3).

$P_{ET}CO_2$ at the time points of 1 to 2 min and CO at the time point of 1 min were higher in the etilefrine than ephedrine group (Figures 2, 3). SVR at the time points of 0.5 to 1 min was lower in the etilefrine than ephedrine group (Figure 3).

4. Discussion

Our results showed that in combined epidural and general anesthesia patients both drugs transiently decreased SVR after bolus IV injection and that etilefrine decreased SVR much more than ephedrine did, indicating that more vasodilation occurred after the injection of etilefrine than after that of ephedrine. Furthermore, we believe that CO in the patients

Table 1 Patient characteristics

Items	Ephedrine group ($n = 20$)	Etilefrine group ($n = 20$)
Age (years)	54 \pm 16	48 \pm 15
Sex (M/F)	13/7	16/4
Body weight (kg)	59 \pm 11	61 \pm 12
Height (cm)	163 \pm 8	168 \pm 10
Body surface area (m ²)	1.63 \pm 0.18	1.69 \pm 0.19

Values are presented as means \pm standard deviation or number.

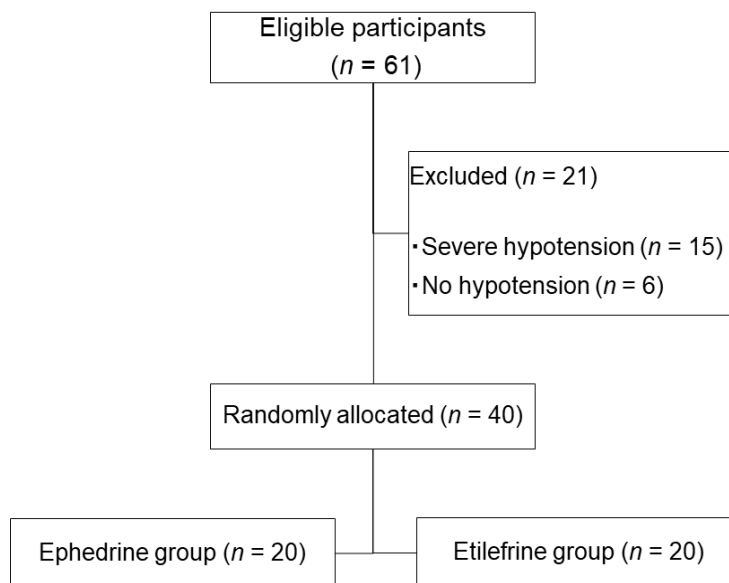


Figure 1. Selection of the study population.

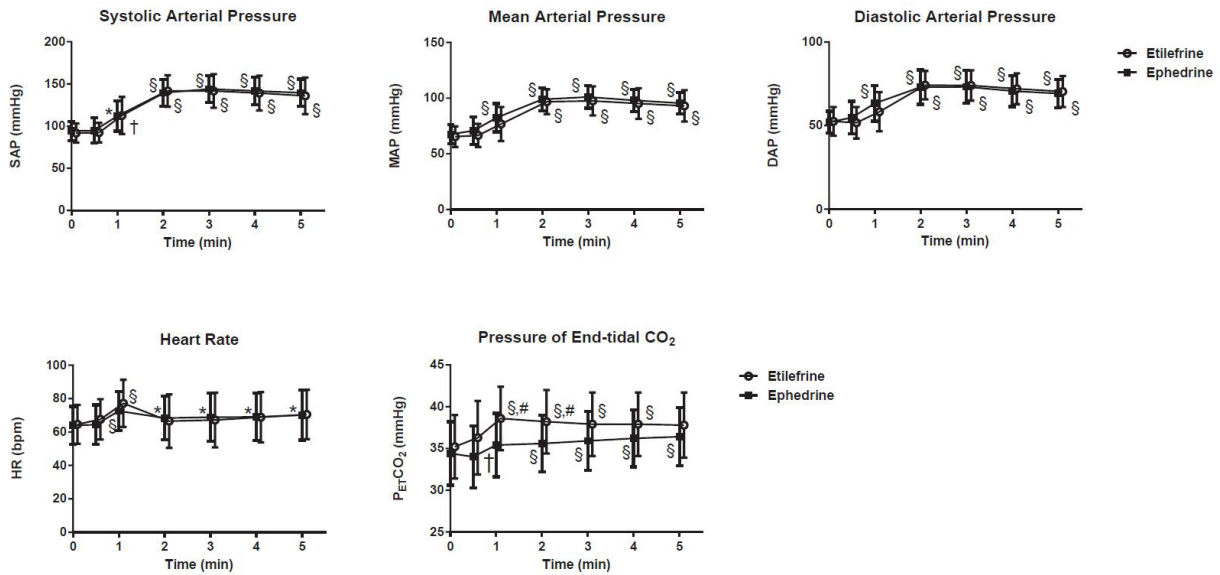


Figure 2. Sequential changes in systolic arterial pressure (SAP), mean arterial pressure (MAP), diastolic arterial pressure (DAP), heart rate (HR) and pressure of end-tidal CO₂ (P_{ET}CO₂) after IV bolus administration of etilefrine and ephedrine. Data are expressed as mean ± standard deviation. **P* < 0.05 vs baseline; †*P* < 0.01 vs baseline; ‡*P* < 0.005 vs baseline; §*P* < 0.001 vs baseline; #*P* < 0.05 compared with the ephedrine group.

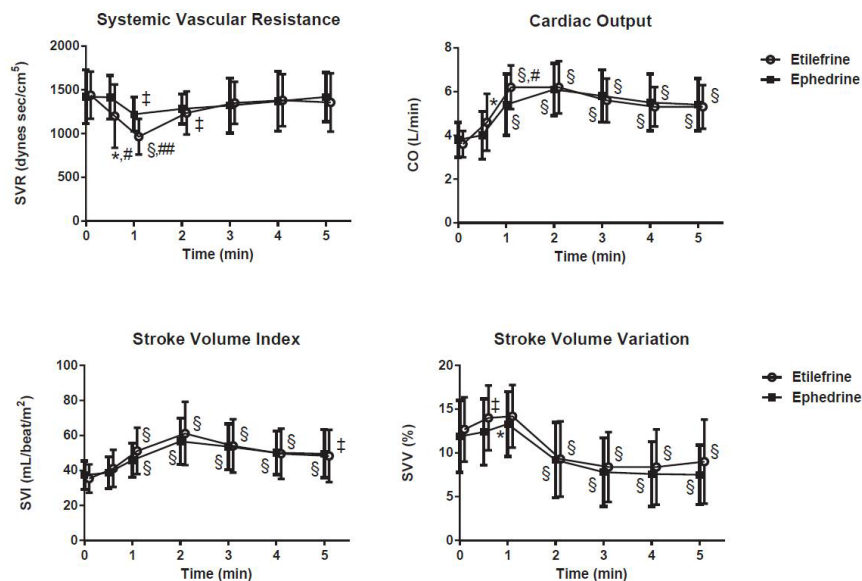


Figure 3. Sequential changes in systemic vascular resistance (SVR), cardiac output (CO), stroke volume index (SVI), and stroke volume variation (SVV) after IV bolus administration of etilefrine and ephedrine. Data are expressed as mean ± standard deviation. **P* < 0.05 vs baseline; †*P* < 0.01 vs baseline; ‡*P* < 0.005 vs baseline; §*P* < 0.001 vs baseline; #*P* < 0.05 compared with the ephedrine group; ##*P* < 0.001 compared with the ephedrine group.

receiving etilefrine was higher than that of the patients receiving ephedrine at that time because etilefrine induced more vasodilation than ephedrine did. This is new information on the action of these two drugs in combined epidural and general anesthesia patients.

Ephedrine, a commonly used vasopressor, primarily affects β -adrenergic receptors but also clearly affects α -adrenergic receptors (4). Its cardiac effects result mainly from the β -mimetic component (4), whereas vasoconstriction in capacitance vessels and an increase in venous return are the results of its α -adrenergic

effects (4). As an indirect effect, ephedrine causes the release of norepinephrine from storage granules in the postganglionic nerve endings. It also directly affects adrenergic receptors by its nonselective predominantly indirect sympathomimetic effects at both α and β receptors (ephedrine is similar in structure to amphetamine but with less blood-brain barrier penetration (16)), increases blood pressure as a result of venoconstriction, improves preload and CO, and also has some chronotropic and inotropic effects.

Etilefrine is an effective vasopressor that stimulates

α_1 - and β_1 -adrenoceptors (4,17) with a much greater affinity for β_1 - rather than for β_2 adrenoceptors (17) and also for β_1 - rather than α -adrenoceptors (17). Its molecular polarity is greater than that of ephedrine (4). In humans, previous studies showed that continuous and progressively increasing administration of IV etilefrine results in increased HR, CO, CVP, and MAP and decreased peripheral vascular resistance (18) but there have been no studies on the cardiovascular effects of the bolus administration of etilefrine, and therefore we investigated these effects in this study.

Both drugs decreased SVR transiently after bolus IV injection, but etilefrine decreased SVR much more than ephedrine did, indicating that more vasodilation occurred after the injection of etilefrine than after ephedrine. The mechanism of vasodilation of these drugs possibly operates by activating endothelial production of nitric oxide (NO) through β_2 adrenoceptors (19-22); Dabisch *et al.* (21) demonstrated that the vascular response to ephedrine in rats was modulated by NO and that NO production in response to ephedrine may be secondary to β_2 receptor stimulation. We also surmise that both drugs initially act as a β_2 -adrenoceptor agonist. Unfortunately, however, in this study, we could not explain why these drugs showed such action, and the mechanism also remains unclear. We can simply consider that both drugs initially act as a β_2 -adrenoceptor agonist, and thereafter, these drugs affect not only β_1 but also α -adrenergic receptors. In the future, measurement of the perfusion index (PI), a marker of peripheral perfusion, which is obtained by calculating the ratio of a pulsating signal to a non-pulsating signal would provide a hint to the mechanism (23-25) because PI depends on the vasomotor tone, which may affect the pulsatile absorption component in man (26,27).

Although we surmise that most anesthetists believe that both drugs simply increase blood pressure as the heart rate increases, we found that in the very short term (about 5 minutes), both drugs show characteristic hemodynamics. The present study is the first report to show that the IV bolus administration of both ephedrine and etilefrine decreases SVR (by inducing vasodilation) just after injection in combined epidural and general anesthesia patients, and no previous reports have measured SVR. Therefore, in patients with dehydration or poor cardiac function, for example, these drugs may be administered very cautiously because both drugs may first act as vasodilators, and thus, it is important to recognise the characteristics of these drugs. We believe that anesthetists should always consider using phenylephrine, which is a selective α_1 agonist, instead of ephedrine or etilefrine, which can be vasodilators in patients undergoing combined epidural and general anesthesia.

Taivainen (3) gave elderly patients bupivacaine as spinal anesthesia, and if a 25% reduction in MAP

from the preanesthetic reference value occurred, the patients were randomly chosen receive ephedrine 0.07 mg/kg or etilefrine 0.03 mg/kg by IV bolus. He found ephedrine to be slightly more potent than etilefrine in restoring MAP and DAP. However, our results were different from those of Taivainen in regard to MAP and DAP because both MAP and DAP were comparable in our present study. We surmise that the reason for this difference relates to the differences in the dose ratio of ephedrine to etilefrine and also to the anesthesia method used. The results of SAP and HR in the Taivainen study (3) are comparable and similar to ours.

Values of $P_{ET}CO_2$ at the time points of 1 to 2 min and CO at the time point of 1 min were higher in the etilefrine than ephedrine group (Figures 2, 3). This result is related to the fact that changes in CO are qualitatively reflected by changes in $P_{ET}CO_2$ during acute hemodynamic problems in anesthetized patients undergoing constant ventilation (28).

Several limitations are associated with our study. First, we compared the effects of ephedrine and etilefrine only under the combination of general anesthesia and epidural anesthesia and not separately with either epidural anesthesia or spinal anesthesia alone. Separate comparisons using these types of anesthesia should be investigated in the future. Furthermore, to investigate the early and true effects of these two vasoconstrictor drugs on SVR, we should use patients or volunteers without anesthesia. Second, we used the third-generation FloTrac/Vigileo™ (software ver. 03.06) to measure SVR. Recently, Suehiro *et al.* (29) reported that the third-generation FloTrac/Vigileo™ system can reliably measure CO only in states of normal peripheral resistance (SVR index: 1200-2500 dynes sec/cm⁵/m²), and in their clinical review, they further reported the excellent reliability of CO measurement with the third-generation FloTrac/Vigileo™ in normal patients with SVR (> 700 dynes sec/cm⁵) (30). Slagt *et al.* (31) recently reported that the third-generation system performed adequately in normotensive (surgery and general critical illness) and hypodynamic (cardiac and post-cardiac surgery) conditions but not during hyperdynamic conditions (liver surgery and sepsis). The SVR in our subjects was normal, and they were all in a normodynamic condition. Therefore, we believe that our data are clinically acceptable. However, further studies are needed in which the fourth-generation FloTrac/Vigileo™ system is used (32). Finally, as described above, we did not directly measure CVP via a central venous catheter but obtained the data for SVR by inputting a fixed CVP of 0 mm Hg into the FloTrac/Vigileo™ system (13,33). Taivainen (3) reported that although the administration of ephedrine and etilefrine tended to slightly increase the CVP, the values were basically unchanged, and we thought that the CVP value would have no bearing on the calculation of SVR by the FloTrac/Vigileo™ system.

In conclusion, in combined epidural and general anesthesia patients, the administration of both ephedrine and etilefrine transiently decreased SVR after IV bolus injection, but etilefrine decreased SVR much more than ephedrine did, indicating that more vasodilation occurred after the injection of etilefrine than after ephedrine. In patients with dehydration or severe hypotension, caution may be needed when using these two drugs, and it is thus important to recognize the individual characteristics of each drug.

Note: This work was conducted in the Department of Anesthesiology, International University of Health and Welfare Shioya Hospital, Tochigi, Japan.

References

- Desjardins G, Vezina DP, Johnson KB, Cahalan MK. Perioperative Echocardiography. In: Miller's anesthesia (Miller RD, ed.). Elsevier Saunders Philadelphia, PA, 2015; pp. 1419-1420.
- Veering BT, Cousins MJ. Epidural Neural Blockade. In: Cousins & Bridenbaugh's neural blockade in clinical anesthesia and management of pain (Cousins MJ, Carr DB, Horlocker TT, Bridenbaugh PO, eds.). Lippincott Williams & Wilkins, a Wolters Kluwer business, Philadelphia, PA, 2009; pp. 241-295.
- Taivainen T. Comparison of ephedrine and etilefrine for the treatment of arterial hypotension during spinal anaesthesia in elderly patients. *Acta Anaesthesiol Scand.* 1991; 35:164-169.
- Räsänen J, Alahuhta S, Kangas-Saarela T, Jouppila R, Jouppila P. The effects of ephedrine and etilefrine on uterine and fetal blood flow and on fetal myocardial function during spinal anaesthesia for caesarean section. *Int J Obstet Anesth.* 1991; 1:3-8.
- Eldor J. Ephedrine in the initial treatment of haemorrhagic shock. *Med Hypotheses.* 1991; 35:250-252.
- Wright PM, Fee JP. Cardiovascular support during combined extradural and general anaesthesia. *Br J Anaesth.* 1992; 68:585-589.
- Goertz AW, Seeling W, Heinrich H, Lindner KH, Rockemann MG, Georgieff M. Effect of phenylephrine bolus administration on left ventricular function during high thoracic and lumbar epidural anesthesia combined with general anesthesia. *Anesth Analg.* 1993; 76:541-545.
- Belzarena SD. Ephedrine and etilefrine as vasopressor to correct maternal arterial hypotension during elective cesarean section under spinal anesthesia. Comparative study. *Rev Bras Anesthesiol.* 2006; 56:223-229.
- Van Haren RM, Thorson CM, Valle EJ, Guarch GA, Jouria JM, Busko AM, Namias N, Livingstone AS, Proctor KG. Vasopressor use during emergency trauma surgery. *Am Surg.* 2014; 80:472-478.
- Wajima Z, Shitara T, Ishikawa G, Kaneko K, Inoue T, Ogawa R. Analgesia after upper abdominal surgery using extradural administration of a fixed dose of buprenorphine in combination with lignocaine given at two infusion rates: A comparative study. *Acta Anaesthesiol Scand.* 1997; 41:1061-1065.
- Wajima Z, Shitara T, Ishikawa G, Inoue T, Ogawa R. Analgesia after upper abdominal surgery with extradural buprenorphine with lidocaine. *Can J Anaesth.* 1998; 45:28-33.
- Wajima Z, Shiga T, Imanaga K, Inoue T. Does intravenous landiolol, a β_1 -adrenergic blocker, affect stroke volume variation? *J Anesth.* 2013; 27:890-894.
- Wajima Z, Shiga T, Imanaga K. Pneumoperitoneum affects stroke volume variation in humans. *J Anesth.* 2015; 29:508-514.
- Strümper D, Gogarten W, Durieux ME, Hartleb K, Van Aken H, Marcus MA. Effects of cafedrine/theodrenaline, etilefrine and ephedrine on uterine blood flow during epidural-induced hypotension in pregnant sheep. *Fetal Diagn Ther.* 2005; 20:377-382.
- Biais M, Vidil L, Sarabay P, Cottenceau V, Revel P, Sztark F. Changes in stroke volume induced by passive leg raising in spontaneously breathing patients: Comparison between echocardiography and Vigileo/FloTrac device. *Crit Care.* 2009; 13:R195.
- Portnoy D. Ephedrine. In: *Essence of Anesthesia Practice* (Fleisher LA, Roizen MF, eds.). Elsevier Saunders Philadelphia, PA, 2011; pp. 604.
- Offermeier J, Dreyer AC. A comparison of the effects of noradrenaline, adrenaline and some phenylephrine derivatives on alpha-, beta₁- and beta₂- adrenergic receptors. *S Afr Med J.* 1971; 45:265-267.
- Coleman AJ, Leary WP, Asmal AC. The cardiovascular effects of etilefrine. *Eur J Clin Pharmacol.* 1975; 8:41-45.
- Gray DW, Marshall I. Novel signal transduction pathway mediating endothelium-dependent β -adrenoceptor vasorelaxation in rat thoracic aorta. *Br J Pharmacol.* 1992; 107:684-690.
- Chang HY. Role of nitric oxide in vasodilator response induced by salbutamol in rat diaphragmatic microcirculation. *Am J Physiol.* 1997; 272:H2173-2179.
- Dabisch PA, Liles JT, Kadowitz PJ. Effect of inhibition of nitric oxide synthase on the vasopressor response to ephedrine. *Can J Physiol Pharmacol.* 2003; 81:966-971.
- Dessy C, Moniotte S, Ghisdal P, Havaux X, Noirhomme P, Balligand JL. Endothelial β_3 -adrenoceptors mediate vasorelaxation of human coronary microarteries through nitric oxide and endothelium-dependent hyperpolarization. *Circulation.* 2004; 110:948-954.
- Ginosar Y, Weiniger CF, Kurz V, Babchenko A, Nitzan M, Davidson E. Sympathectomy-mediated vasodilatation: A randomized concentration ranging study of epidural bupivacaine. *Can J Anaesth.* 2009; 56:213-221.
- Ginosar Y, Weiniger CF, Meroz Y, Kurz V, Bdoolah-Abram T, Babchenko A, Nitzan M, Davidson EM. Pulse oximeter perfusion index as an early indicator of sympathectomy after epidural anesthesia. *Acta Anaesthesiol Scand.* 2009; 53:1018-1026.
- Wajima Z, Shiga T, Imanaga K. Does pneumoperitoneum affect perfusion index and pleth variability index in patients receiving combined epidural and general anesthesia? *Biosci Trends.* 2018; 11:667-674.
- Lima AP, Beelen P, Bakker J. Use of a peripheral perfusion index derived from the pulse oximetry signal as a noninvasive indicator of perfusion. *Crit Care Med.* 2002; 30:1210-1213.
- Lima A, Bakker J. Noninvasive monitoring of peripheral perfusion. *Intensive Care Med.* 2005; 31:1316-1326.
- Shibutani K, Muraoka M, Shirasaki S, Kubal K, Sanchala VT, Gupte P. Do changes in end-tidal PCO₂

- quantitatively reflect changes in cardiac output? *Anesth Analg.* 1994; 79:829-833.
29. Suehiro K, Tanaka K, Funao T, Matsuura T, Mori T, Nishikawa K. Systemic vascular resistance has an impact on the reliability of the Vigileo-FloTrac system in measuring cardiac output and tracking cardiac output changes. *Br J Anaesth.* 2013; 111:170-177.
30. Suehiro K, Tanaka K, Matsuura T, Funao T, Yamada T, Mori T, Nishikawa K. The Vigileo-FloTrac system: Arterial waveform analysis for measuring cardiac output and predicting fluid responsiveness: A clinical review. *J Cardiothorac Vasc Anesth.* 2014; 28:1361-1374.
31. Slagt C, Malagon I, Groeneveld AB. Systematic review of uncalibrated arterial pressure waveform analysis to determine cardiac output and stroke volume variation. *Br J Anaesth.* 2014; 112:626-637.
32. Suehiro K, Tanaka K, Mikawa M, Uchihara Y, Matsuyama T, Matsuura T, Funao T, Yamada T, Mori T, Nishikawa K. Improved Performance of the Fourth-Generation FloTrac/Vigileo System for Tracking Cardiac Output Changes. *J Cardiothorac Vasc Anesth.* 2015; 29:656-662.
33. Wajima Z, Shiga T, Imanaga K, Inoue T. Vigilance of hemodynamic changes immediately after transferring patients is crucial. *J Anesth.* 2013; 27:521-527.
- (Received April 18, 2018; Revised July 7, 2018; Accepted July 29, 2018)

Downregulation of lncRNA TUG1 is involved in ankylosing spondylitis and is related to disease activity and course of treatment

Xiaoyong Lan¹, Haiping Ma², Zhiping Zhang¹, Dong Ye¹, Jun Min³, Feng Cai¹, Jun Luo^{4,*}

¹Department of Orthopedics, The Third Affiliated Hospital of Nanchang University, Nanchang, Jiangxi Province, China;

²Department of Neurosurgery, The Second Affiliated Hospital of Nanchang University, Nanchang, Jiangxi Province, China;

³Department of Rehabilitation, The Third Affiliated Hospital of Nanchang University, Nanchang, Jiangxi Province, China;

⁴Department of Rehabilitation, The Second Affiliated Hospital of Nanchang University, Nanchang, Jiangxi Province, China.

Summary

Long non-coding RNA taurine-upregulated gene 1 (lncRNA TUG1) promotes osteosarcoma, while its involvement in other bone diseases, such as ankylosing spondylitis (AS) is unknown. Expression of TUG1 in serum and open sacroiliac biopsies of AS patients and healthy controls was detected by real-time quantitative PCR (qRT-PCR). Ankylosing spondylitis disease activity score (ASDAS) system was used to evaluate disease activity. Receiver operating characteristic (ROC) curve analysis was performed to evaluate the diagnostic value of lncRNA TUG1 for AS. Chi-square test was performed to analyze the correlations between TUG1 expression and patients' clinicopathological data. Patients were divided into 2 groups (high and low expression groups) according to the median expression level of TUG1 and were followed-up for 5 years after discharge. Treatment courses and rehospitalization rate were compared between two groups. It was observed that TUG1 expression level was significantly lower in AS patients than in healthy controls in both serum and biopsies. Reduced expression level of TUG1 distinguished AS patients from controls. lncRNA TUG1 expression was significantly correlated with patients' smoking habits, disease activity, and course of disease. Patients in high expression group showed longer hospitalization time and higher rehospitalization rate. We therefore conclude that expression of lncRNA TUG1 was inhibited in AS patients and downregulation of lncRNA TUG1 is related to higher disease activity, longer course of treatment and higher rehospitalization rate.

Keywords: lncRNA TUG1, ankylosing spondylitis

1. Introduction

As a type of immune-mediated chronic disease characterized by new bone formation in the axial skeleton and inflammatory responses (1), ankylosing spondylitis (AS) causes deterioration of functioning, irreversible structural damage and disability, seriously affecting patients' quality of life (2). Different treatment strategies have been developed to treat AS, however most treatment therapies failed to achieve satisfactory

outcomes. Treatment with nonsteroidal anti-inflammatory drugs delays disease progression but is not sufficient to control disease symptoms (3). Anti-tumor necrosis factor (TNF) therapy now has been widely used in the treatment of active patients, but unacceptable side effects were observed in some patients (4,5). Treatment of AS is mainly challenged by the unclear pathogenesis (6), and identification of novel molecular treatment targets is always needed.

Onset, development and progression of AS is a complex process with multiple internal and environment factors involved, and genetic factors play a central role in this disease (7,8). A recent study has shown that the development of AS is also accompanied by changes in expression pattern of a large set of long non-coding RNAs (lncRNAs) (9), which is a subgroup of non-coding RNAs that play critical roles in human diseases (10). However, the roles of most lncRNAs in AS

Released online in J-STAGE as advance publication August 27, 2018.

*Address correspondence to:

Dr. Jun Luo, Department of Rehabilitation, The Second Affiliated Hospital of Nanchang University, 1 Minde Road, Donghu District, Nanchang, Jiangxi Province, China.

E-mail: rkkih54@163.com

remain unclear. LncRNA taurine-upregulated gene 1 (TUG1) has been proved to be an oncogenic lncRNA in osteosarcoma (11). In our study we observed that TUG1 was downregulated in AS and is correlated with course of treatment and re-hospitalization.

2. Materials and Methods

2.1. Specimens

Clinical data of 82 patients with AS were retrospectively reviewed. Those patients were diagnosed and treated in The Third Affiliated Hospital of Nanchang University from January 2010 to January 2012. Inclusion criteria: 1) patients diagnosed as AS and treatment for the first time; 2) patients completed treatment; 3) patients completed follow-up and have complete follow-up data; 4) patients without other severe diseases and bone disease; 5) patients and/or their families willing to participate. Exclusion criteria: 1) patients treated before admission; 2) patients transferred to other hospitals during treatment; 3) patient died during treatment or follow-up. Those patients included 44 males and 38 females, and age ranged from 12 to 44 years, with a mean age of 27.1 ± 4.4 years. Serum samples of all AS patients and open sacroiliac biopsies of 34 patients were obtained from specimen library of The Third Affiliated Hospital of Nanchang University. Besides that, our study also included 32 controls and AS were excluded from those patients through open sacroiliac biopsies. Serum samples and open sacroiliac biopsies of those controls were also obtained from specimen library of The Third Affiliated Hospital of Nanchang University. Control group included 18 males and 14 females, and age ranged from 14 to 46 years, with a mean age of 28.7 ± 5.1 years. No significant differences in age, gender and other basic clinical data were found between the two groups. This study was approved by the ethics committee of The Third Affiliated Hospital of Nanchang University and all participants and/or their families signed informed consent.

2.2. Disease activity evaluation

Ankylosing spondylitis disease activity score (ASDAS) (12) was used to evaluate disease activity. The criteria were: inactive disease, < 1.3 ; moderate disease activity, between 1.3 and 2.1; high disease activity, between 2.1 and 3.5; very high disease activity, > 3.5 .

2.3. Real-time quantitative PCR (qRT-PCR)

Trizol reagent (Invitrogen, USA) was used to extract total RNA from biopsies and serum. Biopsies were ground in liquid nitrogen before the addition of Trizol reagent to achieve complete cell lysis. Reverse transcription was performed (55°C for 15 min and 85°C for 15 min)

using SuperScript IV Reverse Transcriptase (Thermo Fisher Scientific) to synthesize cDNA, followed by PCR reaction using SYBR[®] Green Real-Time PCR Master Mixes. Sequences of primers used in PCR reactions were: 5'-CTGAAGAAAGGCAACATC-3' (sense) and 5'-GTAGGCTACTACAGGATTTG-3' (antisense) for TUG1; 5'-GACCTCTATGCCAACACAGT-3' (forward) and 5'-AGTACTTGCGCTCAGGAGGA-3' (reverse) for human β -actin. Reaction conditions of PCR: 50 s at 95°C , followed by 40 cycles of 15 s at 95°C and 40 s at 58°C . Ct values were processed using $2^{-\Delta\Delta\text{CT}}$ method, and TUG1 expression was normalized to β -actin endogenous control.

2.4. Enzyme-Linked ImmunoSorbent Assay (ELISA)

Serum levels of C-reactive protein (CRP) were measured using a human CRP quantikine ELISA Kit (DCRP00, R&D Systems). All operations were performed in strict accordance with manufacturer's instructions. Serum levels of CRP were normalized to mg/L.

2.5. Statistical analysis

All data analyses were performed using Graphpad Prism 6 software. TUG1 expression data were recorded as ($\bar{x} \pm \text{sem}$) and compared by unpaired *t* test (between 2 groups) and one way analysis of variance followed by least significant difference (LSD) test (among multiple groups). Chi-square test was used for comparisons of count data. Correlation analyses were performed by Pearson correlation analysis. $P < 0.05$ was considered to be statistically significant.

3. Results

3.1. Comparison of TUG1 expression in serum and open sacroiliac biopsies between AS patients and controls

Differential expression in patients and healthy people usually indicates the involvement of a gene in a certain disease. Therefore, we first detected the expression of TUG1 in serum and open sacroiliac biopsies of both AS patients and controls. Results showed that TUG1 expression was significantly downregulated in AS patients compared to healthy controls in both serum (Figure 1a) and open sacroiliac biopsies (Figure 1b). Therefore, downregulation of TUG1 is likely involved in the pathogenesis of AS.

3.2. Evaluation of diagnostic values of TUG1 expression for AS

Biomarkers have shown potential in assisting disease diagnosis. TUG1 expression was detected in both serum and open sacroiliac biopsies and differential expression

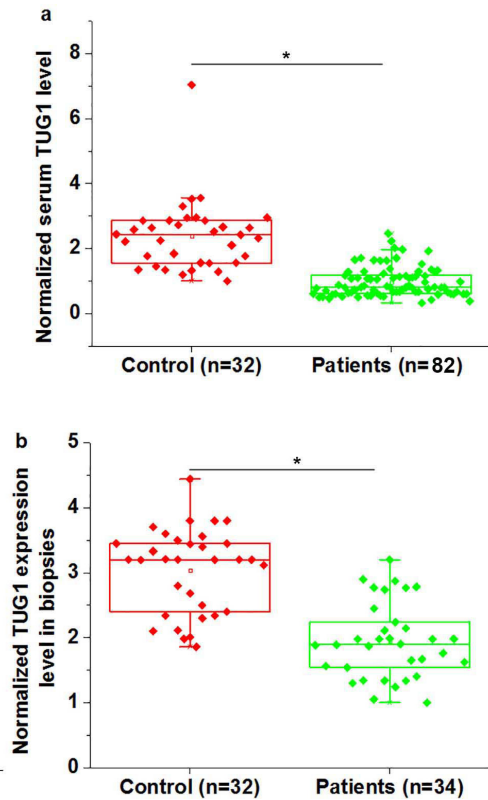


Figure 1. Comparison of TUG1 expression in serum and open sacroiliac biopsies between AS patients and controls. Normalized expression levels of lncRNA TUG1 in serum (a) and open sacroiliac biopsies (b) of AS patients and controls. Notes: *, $p < 0.05$.

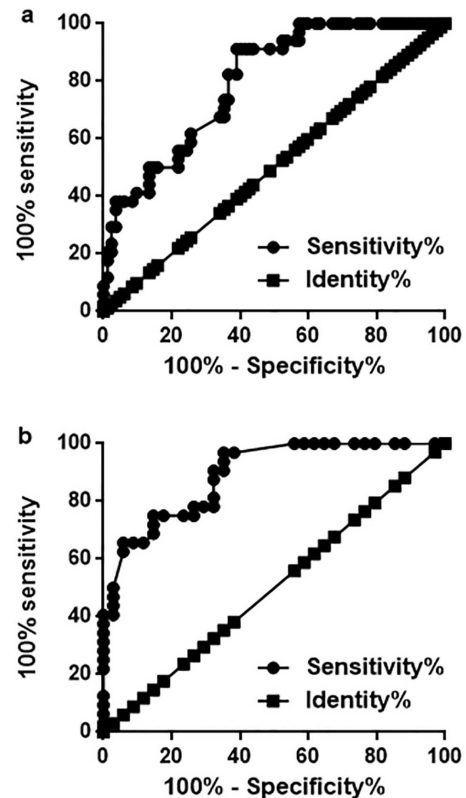


Figure 2. Evaluation of diagnostic values of TUG1 expression for AS. The ROC curve of the use of TUG1 expression in serum (a) and biopsies (b) for the diagnosis of AS.

was observed between AS patients and healthy controls. Therefore, ROC curve analysis was performed to evaluate the diagnostic values of TUG1 expression for AS. As shown in Figure 2a, area under the curve (AUC) of TUG1 expression in serum was 0.7968 with standard error of 0.04158 and 95% confidence interval of 0.7153 to 0.8783 ($p < 0.0001$). In addition, AUC of TUG1 expression in biopsies for the diagnosis of AS was 0.8911 with standard error of 0.03767 and 95% confidence interval of 0.8172 to 0.9649 ($p < 0.0001$).

3.3. Serum levels of TUG1 were negative correlated with serum levels of CRP in ankylosing spondylitis patients

Pearson correlation analysis revealed that serum levels of TUG1 were negative correlated with serum levels of CRP in ankylosing spondylitis patients ($r = -0.8091$, $R^2 = 0.6431$, $p < 0.0001$) (Figure 3).

3.4. Serum levels of TUG1 in patients with different disease activities

According to the ASDAS system, there were 22 cases of inactive disease (ID), 18 cases of moderate disease activity (MD), 28 cases of high disease activity (HD) and 14 cases of very high disease activity (VHD). As

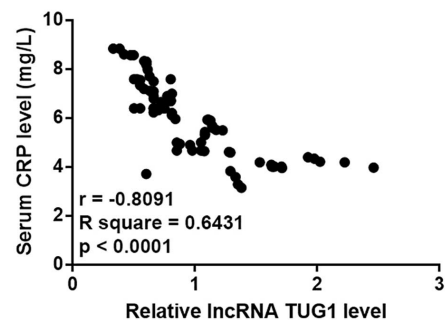


Figure 3. Pearson correlation analysis of the correlation between serum levels of TUG1 and CRP in ankylosing spondylitis patients.

shown in Figure 4, serum levels of TUG1 decreased significantly with increase of degree of disease activity ($p < 0.05$).

3.5. Correlations between TUG1 expression and patients' clinicopathological data

Patients were divided into high and low expression groups according to the median expression level of TUG1. Chi square test was performed to investigate the correlations between TUG1 expression and patients' clinicopathological data. As shown in Table 1 and 2, TUG1 expression was significantly correlated with

Table 1. Correlations between serum levels of TUG1 and patients' clinicopathological data

Items	Groups	Cases	High-expression	Low-expression	χ^2	<i>p</i> value
Gender	Male	44	20	24	0.78	0.37
	Female	38	21	17		
Age	> 25 (years)	46	21	25	0.79	0.37
	< 25 (years)	36	20	16		
Course of disease	> 5 years	40	13	27	9.57	0.002
	< 5 years	42	28	14		
Smoking	Yes	37	23	14	3.99	0.046
	No	45	18	27		
Drinking	Yes	51	24	27	0.03	0.87
	No	31	17	14		

Table 2. Correlations between TUG1 expression in biopsies and patients' clinicopathological data

Items	Groups	Cases	High-expression	Low-expression	χ^2	<i>p</i> value
Gender	Male	20	9	11	0.49	0.49
	Female	14	8	6		
Age	> 25 (years)	18	10	8	0.47	0.49
	< 25 (years)	16	7	9		
Course of disease	> 5 years	19	5	14	9.66	0.002
	< 5 years	15	12	3		
Smoking	Yes	18	12	6	4.25	0.04
	No	16	5	11		
Drinking	Yes	21	9	12	1.12	0.29
	No	13	8	5		

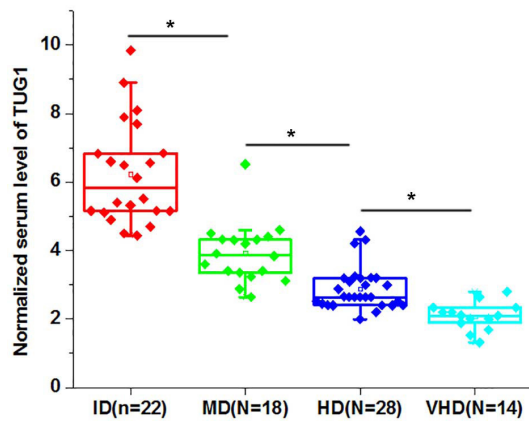


Figure 4. Serum levels of TUG1 in patients with different disease activities. Notes:*, *p* < 0.05.

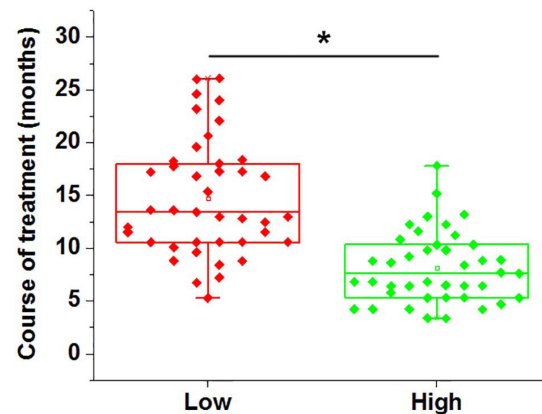


Figure 5. Comparison of course of treatment between high and low serum TUG1 groups. Notes:*, *p* < 0.05.

patients' course of disease and smoking habit (*p* < 0.05), but not gender, age as well as drinking habit (*p* > 0.05).

3.6. Comparison of course of treatment and re-hospitalization rate between high and low serum TUG1 groups

As shown in Figure 5, course of treatment is significantly longer in low expression group than in high expression group. During follow-up, re-hospitalization occurred in 18 cases of low expression group, accounting for 43.9%. In contrast, re-hospitalization only occurred in 8 cases of high expression group, accounting for 19.5%. Therefore, TUG1 is likely related to course of treatment and re-

hospitalization of AS patients.

4. Discussion

The key finding of our study is that as a lcnRNA with critical roles in human malignancies such as osteosarcoma (11), lcnRNA TUG1 is also very likely involved in the pathogenesis of AS. Low expression of TUG1 may delay patients' recovery and increase the risk of re-hospitalization.

lcnRNA plays pivotal roles in different types of human diseases (10). However, functionality of most lcnRNAs in AS still has been characterized. A recent study has shown that levels of circulating lcnRNA-

AK001085 were significantly lower in ankylosing spondylitis patients than in healthy controls (13), indicating the involvement of this lncRNA in AS. Osteoblastic differentiation plays pivotal roles in the development of AS (13). It has been shown that lncRNA TUG1 promotes osteoblast differentiation through miR-204-5p (14). Therefore, TUG1 is also likely involved in AS. In our study, significantly downregulated expression of lncRNA TUG1 was observed in AS patients compared to controls in both serum and open sacroiliac biopsies, suggesting that downregulation of TUG1 is involved in AS.

Development of human disease is usually accompanied by changes in certain substances in blood, and monitoring the content of those substances in blood may provide guidance for treatment of disease (15). In this study, TUG1 was detected in both serum and biopsies of all AS and controls. ROC curve analysis showed that low expression levels of TUG1 in serum and biopsies effectively distinguish AS patients from healthy controls. Compared with serum TUG1, the diagnostic efficacy of TUG1 expression in biopsies was much higher than that of serum TUG1. However, application of open sacroiliac biopsies is sometimes challenged by its invasive nature. Therefore, measuring serum levels of TUG1 may be used to assist the diagnosis of AS and cases of open sacroiliac biopsy is not applicable. Expression of lncRNAs is affected by many factors including aging (16), alcohol abuse (17) and tobacco consumption (18). In our study, expression of TUG1 showed no significant correlations with patients' age, gender or drinking habits. However, a significant correlation was observed between patients' smoking habit and expression of TUG1 in both serum and biopsies. Therefore, patients' smoking habit should be taken into consideration in the use of TUG1 for the diagnosis of AS.

Disease activity of AS determines its progression rate and symptoms (19). Serum levels of TUG1 were found to be significantly increased with increase of disease activities. The long treatment course and high postoperative recurrence rate bring heavy economic and mental burden on patients and their families (20,21). In our study, low serum levels of TUG1 were found to be significantly correlated with delayed recovery and increased re-hospitalization rate. Therefore, TUG1 may serve as a potential therapeutic target to inhibit the activity of AS, promote patients' recovery and reduce the risk of recurrence.

Our study is limited by its small sample size due to limited resources. Future studies with bigger sample sizes are needed to further confirm our conclusions. Mechanism of the action of TUG1 in AS is still unknown. Our further direction will focus on the molecular mechanism underlying the role of TUG1 in this disease.

In conclusion, downregulation of TUG1 is very likely involved in the pathogenesis of AS and inhibited

TUG1 expression delays patients' recovery and increases recurrence rate.

Authors' contributions

X.L, H. M, and Z.Z. designed and carried out the study. X.L, H.M, Z.Z, D.Y, J.M, and F.C. participated in experiments and statistical analysis. X.L. and J.L. wrote the manuscript. L.J. revised the manuscript. All authors read and approved the final manuscript.

References

- Jang JH, Ward MM, Rucker AN, Reveille JD, Davis JC, Jr., Weisman MH, Leach TJ. Ankylosing spondylitis: Patterns of radiographic involvement--a re-examination of accepted principles in a cohort of 769 patients. *Radiology*. 2011; 258:192-198.
- Gao X, Wendling D, Botteman MF, Carter JA, Rao S, Cifaldi M. Clinical and economic burden of extra-articular manifestations in ankylosing spondylitis patients treated with anti-tumor necrosis factor agents. *J Med Econ*. 2012; 15:1054-1063.
- Kiltz U, van der Heijde D, Mielants H, Feldtkeller E, Braun J, group PEpi. ASAS/EULAR recommendations for the management of ankylosing spondylitis: The patient version. *Ann Rheum Dis*. 2009; 68:1381-1386.
- Davis JC, Jr., Van Der Heijde D, Braun J, Dougados M, Cush J, Clegg DO, Kivitz A, Fleischmann R, Inman R, Tsuji W, Enbrel Ankylosing Spondylitis Study G. Recombinant human tumor necrosis factor receptor (etanercept) for treating ankylosing spondylitis: A randomized, controlled trial. *Arthritis Rheum*. 2003; 48:3230-3236.
- Baeten D, Baraliakos X, Braun J, et al. Anti-interleukin-17A monoclonal antibody secukinumab in treatment of ankylosing spondylitis: A randomised, double-blind, placebo-controlled trial. *Lancet*. 2013; 382:1705-1713.
- Tam LS, Gu J, Yu D. Pathogenesis of ankylosing spondylitis. *Nat Rev Rheumatol*. 2010; 6:399-405.
- Robinson PC, Brown MA. Genetics of ankylosing spondylitis. *Mol Immunol*. 2014; 57:2-11.
- Brown MA, Kenna T, Wordsworth BP. Genetics of ankylosing spondylitis--insights into pathogenesis. *Nat Rev Rheumatol*. 2016; 12:81-91.
- Zhang C, Wang C, Jia Z, Tong W, Liu D, He C, Huang X, Xu W. Differentially expressed mRNAs, lncRNAs, and miRNAs with associated co-expression and ceRNA networks in ankylosing spondylitis. *Oncotarget*. 2017; 8:113543-113557.
- Cabianca DS, Casa V, Gabellini D. A novel molecular mechanism in human genetic disease: A DNA repeat-derived lncRNA. *RNA Biol*. 2012; 9:1211-1217.
- Yun-Bo F, Xiao-Po L, Xiao-Li L, Guo-Long C, Pei Z, Fa-Ming T. LncRNA TUG1 is upregulated and promotes cell proliferation in osteosarcoma. *Open Med (Wars)*. 2016; 11:163-167.
- Lukas C, Landewe R, Sieper J, Dougados M, Davis J, Braun J, van der Linden S, van der Heijde D, Assessment of SpondyloArthritis international S. Development of an ASAS-endorsed disease activity score (ASDAS) in patients with ankylosing spondylitis. *Ann Rheum Dis*. 2009; 68:18-24.

13. Choi ST, Kim JH, Kang EJ, Lee SW, Park MC, Park YB, Lee SK. Osteopontin might be involved in bone remodelling rather than in inflammation in ankylosing spondylitis. *Rheumatology (Oxford)*. 2008; 47:1775-1779.
14. Yu C, Li L, Xie F, Guo S, Liu F, Dong N, Wang Y. LncRNA TUG1 sponges miR-204-5p to promote osteoblast differentiation through upregulating Runx2 in aortic valve calcification. *Cardiovasc Res*. 2018; 114:168-179.
15. Viereck J, Thum T. Circulating Noncoding RNAs as Biomarkers of Cardiovascular Disease and Injury. *Circ Res*. 2017; 120:381-399.
16. Nepl RL, Wu CL, Walsh K. lncRNA Chronos is an aging-induced inhibitor of muscle hypertrophy. *J Cell Biol*. 2017; 216:3497-3507.
17. Mayfield RD. Emerging roles for ncRNAs in alcohol use disorders. *Alcohol*. 2017; 60:31-39.
18. Li S, Sun X, Miao S, Liu J, Jiao W. Differential protein-coding gene and long noncoding RNA expression in smoking-related lung squamous cell carcinoma. *Thorac Cancer*. 2017; 8:672-681.
19. Poddubnyy D, Protopopov M, Haibel H, Braun J, Rudwaleit M, Sieper J. High disease activity according to the Ankylosing Spondylitis Disease Activity Score is associated with accelerated radiographic spinal progression in patients with early axial spondyloarthritis: Results from the GERman SPondyloarthritis Inception Cohort. *Ann Rheum Dis*. 2016; 75:2114-2118.
20. Boonen A, van der Heijde D, Landewe R, Guillemin F, Rutten-van Molken M, Dougados M, Mielants H, de Vlam K, van der Tempel H, Boesen S, Spoorenberg A, Schouten H, van der Linden S. Direct costs of ankylosing spondylitis and its determinants: An analysis among three European countries. *Ann Rheum Dis*. 2003; 62:732-740.
21. van Denderen JC, Visman IM, Nurmohamed MT, Suttorp-Schulten MS, van der Horst-Bruinsma IE. Adalimumab significantly reduces the recurrence rate of anterior uveitis in patients with ankylosing spondylitis. *J Rheumatol*. 2014; 41:1843-1848.

(Received May 25, 2018; Revised August 7, 2018; Accepted August 10, 2018)

Importance of bronchoscopic lung volume reduction coil therapy in potential candidates for lung transplantation

Askin Gulsen^{1,2,*}

¹Department of Pneumology, School of Medicine, Sifa University, Izmir, Turkey;

²Division of Clinical and Molecular Allergology, Research Center Borstel, Airway Research, Center North (ARCN), Member of the German Center for Lung Research, Borstel, Germany.

Summary

Bronchoscopic lung volume reduction (BLVR) coil treatment is a alternative and promising treatment modality for selected severe emphysema patients. The main indication of this treatment modality is a forced expiration volume in one second (FEV₁) of 15-45% and a residual volume (RV) > 175%. The aim of this study was to investigate the efficacy of BLVR coil therapy in patients with end-stage emphysema who were potential candidates for lung transplantation and had FEV₁ values less than 25%. Twenty-one patients who underwent bilateral BLVR coil therapy between September 2013 and May 2015 were retrospectively reviewed. We compared the changes in clinical and laboratory parameters at the baseline and 12 months after the treatment. Twelve months after the bilateral BLVR coil treatment, we observed an average increase in FEV₁ (110 mL and 4.6%), a decrease in residual volume (660 mL and 33%), and an increase in 6-minute walk tests (67 m). The most common complications were chronic obstructive pulmonary disease exacerbation (47.6%) and pneumonia (23.8%). All patients tolerated the general anesthesia and procedure very well. BLVR coil therapy is safe and effective in patients with end-stage emphysema, who are potential candidates for lung transplantation within a short to medium period. The complication rates of this treatment were not different from those of the other coil treatments, and the improvements in the clinical parameters after the treatment resulted in gaining time for lung transplantation. Future research for evaluating the long-term efficacy of BLVR coil therapy in these patients is essential.

Keywords: Lung volume reduction, coil, emphysema, lung transplantation, low FEV₁

1. Introduction

Emphysema is one of the two manifestations of chronic obstructive pulmonary disease (COPD). Chronic inflammation and permanent parenchymal damage play an important role in the progress of this disease. The loss of elastic recoil of the lungs, hyperinflation, and air-trapping also disrupt the gas-exchange in the later course of the disease (1). This results in a gradual decrease in the exercise capacity and quality of life of patients and shortness of breath. Patients with end-stage emphysema

show an increase in residual volume (RV) and respiratory muscle dysfunction due to diaphragmatic and thoracic compression (2). This condition has no definitive treatment and medical treatment options are limited, which include beta-2-mimetic and anticholinergic inhaler treatments, smoking cessation, glucocorticoids, roflumilast, mucolytics, physical and pulmonary rehabilitation for increasing the exercise capacity, and long-term supplemental oxygen therapy (3).

In the last 10 years, surgical options for the treatment of this condition have been considered because the mechanical problems of the patients cannot be treated with medications. Removal of the damaged lung area by lung volume reduction surgery contributes to the improvement of the quality of life, exercise capacity, and respiratory function in patients (4). In addition, the National Emphysema Treatment Trial emphasized the importance of patient selection due

Released online in J-STAGE as advance publication August 28, 2018.

*Address correspondence to:

Dr. Askin Gülsen, Department of Allergology, Research Center Borstel, Leibniz Lung Center Parkallee 35, 23845 Borstel, Germany

E-mail: askingulsen@hotmail.com

to the high risk of postoperative pulmonary and non-pulmonary complications and mortality (5).

In recent years, bronchoscopic lung volume reduction (BLVR) has become an alternative and promising treatment modality for selected severe emphysema patients (6). The loss of elastic recoil and hyperinflation caused by the emphysema can be treated with BLVR using the coil, valve, or thermal vapor ablation method (7-9). The main indications of this treatment modality are a forced expiration volume in one second (FEV₁) of 15-45% and an RV of more than 175% in patients with emphysema diagnosed by computed tomography (CT). Therefore, all patients are in stages 3 and 4 according to the COPD Gold classification (10). However, if the patients have interlobar collateral ventilation, the best option is BLVR coil treatment. This treatment can be applied to both heterogeneous and homogenous emphysema.

The targeted lobe is implanted with an average of 10-14 coils using a bronchoscope. This is followed by a second session of implantation of coils in the other lung, which is performed within 4-8 weeks. The goal of this treatment is to reduce the air trapping and hyperinflation, and thus reduce the RV of the lungs. Studies have shown that this treatment is useful and safe in the short and medium term (6,7). Furthermore, improvements in quality of life, 6-minute walk test (6-MWT), and pulmonary function tests (PFT) were reported in recent studies (7,11,12). In addition, these treatments were also applied to patients who were potential candidates for lung transplantation, with very low FEV₁ values. According to the guidelines published by the Pulmonary Transplantation Council of the International Society for Heart and Lung Transplantation in 2014, COPD patients with FEV₁ < 25% are candidates for lung transplantation, and those with FEV₁ < 15-20% are recommended to be included in the transplantation list (13).

The aim of this study was to investigate the efficacy of BLVR coil therapy in patients with end-stage emphysema who were potential candidates for lung transplantation and had FEV₁ values less than 25%.

2. Materials and Methods

2.1. Study design

Our study was a retrospective and observational study. Patients who were treated for BLVR coil treatment in the Department of Pneumology of the Şifa University Hospital, Bornova-Izmir, Turkey were included in the study. The inclusion and exclusion criteria were similar to those of some of the recent studies in the literature (6,7,11,12). Inclusion criteria were as follows: (i) bilateral emphysema diagnosed by CT; (ii) post-bronchodilator (salbutamol) FEV₁ of 15-45%; (iii) RV > 175%; (iv) arterial partial pressure of carbon

dioxide (PaCO₂) < 55 mmHg; (v) 6-MWT: 150-450 m; (vi) modified Medical Research Council scores ≥ 2; (vii) smoking cessation for > 8 weeks before treatment. Exclusion criteria were as follows: (i) post-bronchodilator (salbutamol) change in FEV₁ > 20% or diagnosis of asthma; (ii) COPD exacerbation (more than > 2 hospitalizations per year); (iii) bullous lesion on a single lung of more than one-third field or more than 4 cm; (iv) pulmonary artery pressure > 50 mmHg; (v) diagnosis of bronchiectasis or lung cancer; (vi) use of oral anticoagulant. The only difference in the inclusion criteria in our study with respect to the above-mentioned similar studies was the FEV₁ value of < 25%. In our study, the patients with FEV₁ between 25-45% were excluded. The flow of the study is presented in Figure 1. The study was conducted according to good clinical practice and the Declaration of Helsinki. Ethical committee approval was obtained from the local Ethics Committee in Izmir/Turkey

2.2. Data collection

Data from all patients who received BLVR coil treatment were selected from the electronic hospital data system and evaluated retrospectively, including the following: (1) epidemiological data (age, sex, smoking history, and use of long-term oxygen at home); (2) clinical data (such as symptoms, type of emphysema, and stage of COPD); (3) procedure data (target lobe, duration, number of coils, and complications); (4) laboratory data (arterial blood gas analyses, PFT parameters, and 6-MWT); (5) post-procedure data (admission to polyclinics, hospitalizations, and complications). The PFT parameters were evaluated with a Body Box 5500 Series pulmonary function testing system (Medisoft, Sorinnes, Belgium) according to ERS guidelines. The arterial blood gas samples were taken when patients were in a clinically stable condition and breathing room air. The baseline and 12-month follow-up data of the patients who underwent bilateral BLVR coil treatment between September 2013 and May 2015 were collected from the medical records.

2.3. BLVR coil procedure

Homogeneous or heterogeneous emphysema of all patients was diagnosed by CT, and the target lobe was selected under the guidance of ventilation/perfusion scintigraphy. All patients were in clinically stable conditions, under optimal medical and inhaler treatment, and were included in the necessary pulmonary rehabilitation program before the treatment. The patients also received recommendations for improving their nutritional status. All RePneu coils (PneumRx Inc., Mountain View, CA, USA) were implanted via a bronchoscopic approach with fluoroscopic guidance under general anesthesia. Each

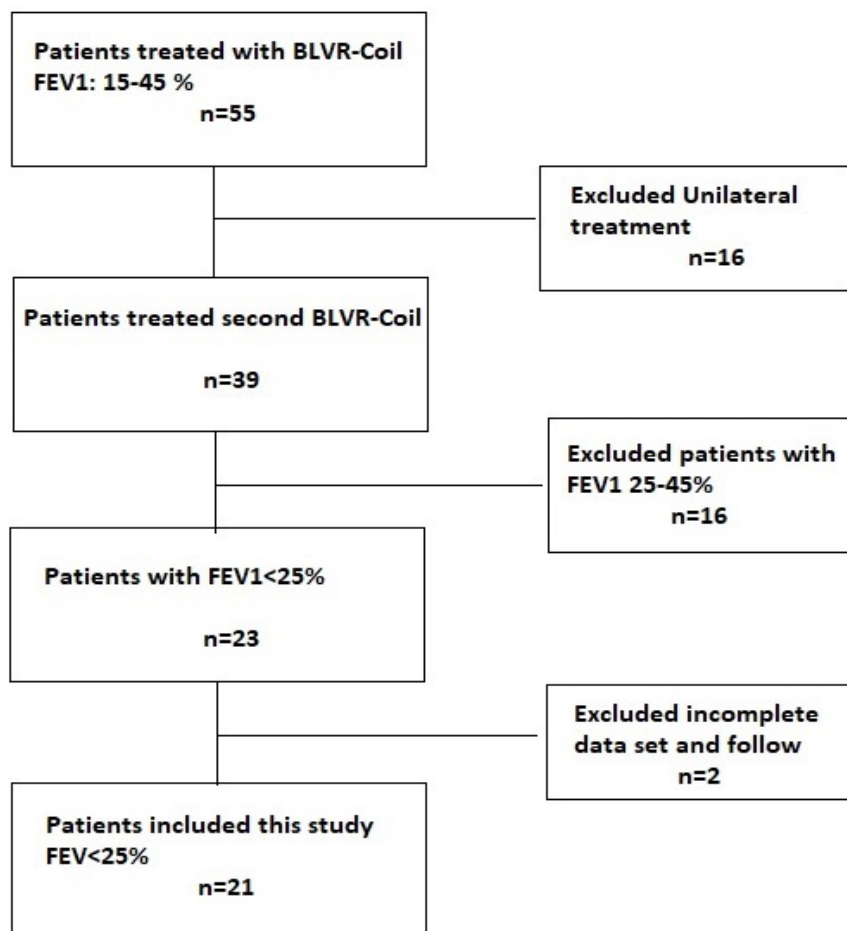


Figure 1. Case Selection Procedure. Twenty-one end-stage emphysema patients with a FEV₁ value of < 25% were included in the study.

patient received an average of 10 (range: 8-13) coils per lobe as standard treatment, and a second procedure for implantation of coils in the other lung was performed within 4 to 8 weeks.

2.4. Statistical analysis

The descriptive data are presented as the average \pm standard deviation or median (range). The categorized data are presented as absolute number with percentage. The changes between the baseline and 12-month data were analyzed using the paired *t*-test for normal distribution parameters and the Mann-Whitney *U* test for non-normal distribution parameters. The statistical significance threshold of *p* value was < 0.05 for the paired *t*-Test and < 0.01 for the Mann-Whitney *U* Test. All data were analyzed using SPSS software (version 19.0; SPSS Inc., Chicago, IL, USA).

The minimum important difference (MID) was also reported to be 100 mL and 10% for FEV₁ (14), 400 mL for RV (15), 26 m for 6-MWT (16), and four points for St. George's Respiratory Questionnaire (17) in the previous studies.

3. Results

3.1. Demographic data at baseline

A total of 42 BLVR coil procedures were performed in 21 patients. The mean age of the 21 patients (3 women and 18 men) who participated in the study was 63.76 ± 8.2 years (range: 47-83 years). Of the total patients, 62% had homogenous emphysema and 38% had heterogenous emphysema. The body mass indexes of the patients were 25.25 ± 4.5 kg/m². The average level of cigarette consumption was 30.4 packs/year. Preoperatively, six patients (28.5%) had hypoxic respiratory failure and were on long-term oxygen therapy, and 11 patients (52.3%) had mild hypercapnic respiratory failure. At the baseline before treatment, the mean FEV₁ was 0.59 ± 0.10 L, which was equal to $20.5 \pm 3.3\%$ of the predicted value. The mean RV was 5.36 ± 0.60 L, which was equal to $238 \pm 34.2\%$ of the predicted value. The mean RV/total lung capacity ratio was $66.1 \pm 4.9\%$ of the predicted value. The mean arterial partial pressure of oxygen (PaO₂) was 58.0 ± 9.3 mmHg, and the mean PaCO₂ was 45.7 ± 6.3 mmHg. The mean distance walked during

the 6-MWT was 270 ± 64 m (Table 1). A total of 422 coils were used in 42 procedures (average of 10, range: 8-13), with a mean duration of 21.7 ± 8.1 min. The most common lobes for the implantation of coils were the left upper (35.7%) and the right upper (38.0%) lobes. The

coils were implanted to the two lower lobes of the lungs in 26.1% of the patients. After the procedure, the patients stayed in the hospital for an average of 1.5 ± 0.6 days (Table 2).

Table 1. Patient demographics at baseline

Number of Patients	21
Gender F/M	3/18
Age, years	63.76 ± 8.2
Body mass index, kg/m^2	25.25 ± 4.5
Type of Emphysema	
Homogeneous	13 (62%)
Heterogeneous	8 (38%)
ASA-Status	
Group II	1 (4.7%)
Group III	11 (53.3%)
Group IV	9 (42.8%)
Pulmonary Function	
FEV_1 (l)	0.59 ± 0.1
FEV_1 (%)	20.5 ± 3.3
FVC (l)	1.31 ± 0.3
RV	5.36 ± 0.6
RV (%)	238 ± 34
RV / TLC (%)	66.1 ± 4.9
6-min walk tests (m)	270 ± 64
Blood gase	
pH	7.37 ± 0.4
PaO_2 , mmHg	58.0 ± 9.3
PaCO_2 , mmHg	45.7 ± 6.3
O_2sat , %	88.3 ± 7.6
Respiratory Failure	
Hypoxic	6 (28.5%)
Hypercapnic (mild)	11(52.3%)

FEV_1 , a forced expiration volume in 1 s; FVC, forced vital capacity; RV, residual volume; TLC, total lung capacity; PaO_2 , partial pressure of oxygen in arterial blood; PaCO_2 , partial pressure of carbon dioxide in arterial blood, LTOT, Long-term oxygen therapy; ASA, American Society of Anesthesiologists status.

Table 2. BLVR coil procedural results

Number of Procedures, <i>n</i>	42
Right upper lobe, <i>n</i>	15 (35.7%)
Right under lobe, <i>n</i>	6 (14.2%)
Left upper lobe, <i>n</i>	16 (38.0%)
Left under lobe, <i>n</i>	5 (11.9%)
Procedure time, min	21.7 ± 8.1
Number of Coils, <i>n</i>	422
Coils per procedure, <i>n</i>	10.0 (range 8-13)
Hospital stay, days	1.5 ± 0.6

3.2. Adverse events during the procedure

During the procedure, unexpected bronchial secretion was aspirated in 19.0% of the patients, and mild bleeding was observed in 9.5% patients. The mild bleeding was easily controlled by the application of saline and local adrenaline. Due to the lack of proper localization of the coils, some coils were successfully removed and repositioned in four (9.5%) patients. During this repositioning, the duration of the procedure was prolonged. Instability of vital parameters was observed in one patient, but the procedure was terminated successfully. During the procedure, pneumothorax or extrapulmonary complications were not observed. All patients tolerated the general anesthesia very well (Table 3).

3.3. Efficacy after 12 months

A significant improvements in the FEV_1 (an average increase of 110 mL, 4.6%), and RV (a average decrease of 0.66 L, 33.0%) were observed in all patients 12 months after bilateral BLVR coil procedure (Figure 2). Compared with the baseline, a significant improvement in the PaO_2 (an increase of 15.5 mmHg), arterial oxygen saturation (an increase of 5.6%), and 6-MWT results (an average increase of 67 m, 24.8%) were also observed 12 months after the BLVR coil treatment (Figure 3). However, no statistically significant improvements were observed in the arterial pH or PaCO_2 (Table 4).

Table 3. Adverse events during procedure

Aspiration of bronchial sekretion	8 (19.0%)
Mild haemorrhage	8 (19.0%)
Removal and Repositioning of Coils	4 (9.5%)
Prolonged procedure	2 (4.7%)
Instability of vital parameter	1 (2.3%)
Pneumothorax	0 (0%)

Events were scored for all 42 procedures in 21 patients.

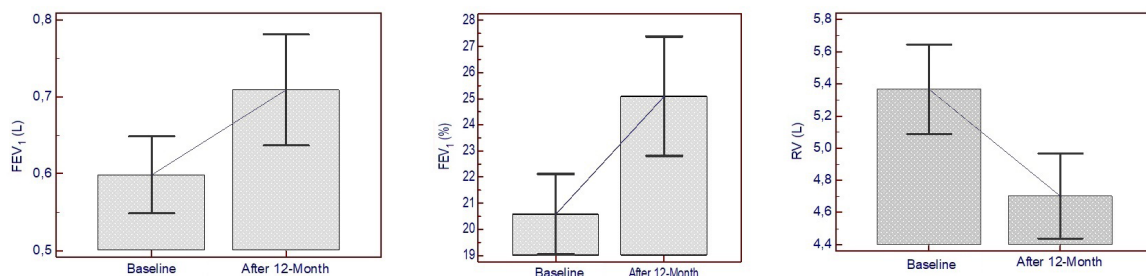


Figure 2. Comparison of baseline and 12-month pulmonary function parameters after bilateral lung volume reduction coil treatment. A significant improvements in the FEV_1 (an average increase of 110 mL, 4.6%), and RV (a average decrease of 0.66 L, 33.0%) were observed in all patients 12 months after bilateral BLVR coil procedure.

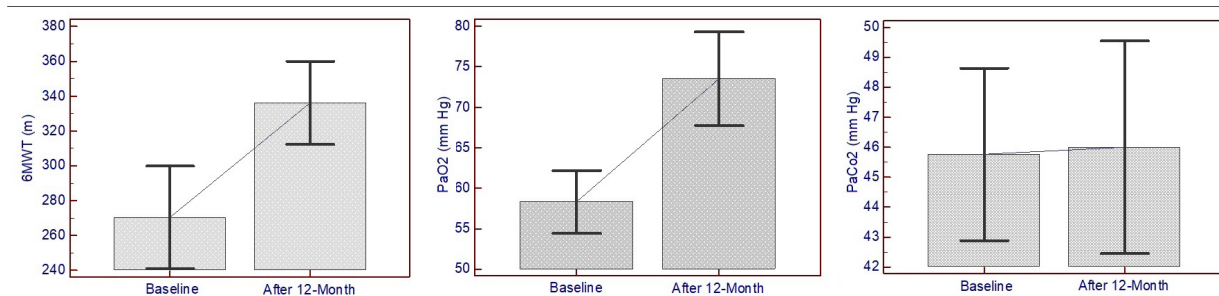


Figure 3. Comparison of baseline and 12-month 6-minute walk test (6MWT), and blood gas parameters after bilateral lung volume reduction coil treatment. A significant improvement in the PaO₂ (an increase of 15.5 mmHg), arterial oxygen saturation (an increase of 5.6%), and 6-MWT results (an average increase of 67 m, 24.8%) were also observed 12 months after the BLVR coil treatment.

Table 4. Comparison of pulmonary function parameters in 12-months follow-up

Test	Baseline	12 Months	Diff.	p-value
FEV ₁ , L	0.59 ± 0.10	0.70 ± 0.15	+ 0.11	0.001
FEV ₁ , %	20.5 ± 3.3	25.1 ± 5.0	+ 4.6	0.001
RV, L	5.36 ± 0.6	4.70 ± 0.5	- 0.66	0.001
RV, %	238 ± 34	205 ± 33.2	- 33	0.001
RV/TLC, %	66.1 ± 4.9	58.8 ± 5.0	- 7.3	0.001
6-MWT, m	270 ± 64	337 ± 49	+ 67	0.001
pH	7.37 ± 0.4	7.39 ± 0.5	+ 0.02	0.135
PO ₂ , mmHg	58.0 ± 9.3	73.5 ± 12.7	+ 15.5	0.001
PCO ₂ , mmHg	44.7 ± 6.3	46.0 ± 7.8	+ 1.3	0.896
O ₂ sat, %	88.3 ± 7.6	93.9 ± 2.4	+ 5.6	0.001

Data are presented as mean ± standard deviation. See Table 1 legend for expansion of other abbreviation.

3.4. Complications during the 12-month follow-Up

During the 12-month follow-up, mild side effects were observed in 33.3% of patients. These included cough (28.5%), mild hemoptysis (23.8%), pleuritic chest pain (9.5%), and hiccups (4.7%). Among the more serious complications, COPD exacerbations (47.6%) were the commonest. Pneumonia or procedure-related pneumonitis (23.8%) was the second most common complication. Among patients with these two major complications, 33.1% required hospitalization. None of the patients died or had pneumothorax or respiratory failure (Table 5).

4. Discussion

This retrospective study was performed on 21 patients with end-stage emphysema who were potential candidates for lung transplantation, with FEV₁ value of < 25%. Our study results indicate that BLVR coil treatment is effective and safe in this group of patients.

The main indication for BLVR coil treatment is an FEV₁ of 15-45% and RV > 175%, so all patients are at COPD Gold III and Gold IV levels. The studies conducted between in 2012-2018 show that the included patients have baseline mean FEV₁ between 0.58 and 0.91 L and between 22% and 33% predicted (Table 6) (7,11,12,18-26). Only one study was performed in

Table 5. Adverse events within 12-month follow-up

Mild events, n (%)	
Cough	6 (28.5%)
Pleuritic Pain	5 (23.8%)
Haemoptysis	2 (9.5%)
Hiccup	1 (4.7%)
Serious events, n (%)	
Exacerbation COPD	10 (47.6%)
Hospitalization, any reason	7 (33.1%)
Pneumonia, treated lung	5 (23.8%)
Pneumonia, other lung	1 (4.7%)
Pneumothorax	0 (0%)
Death	0 (0%)

Events were scored for all 42 procedures in 21 patients.

patients with FEV₁ < 20% (26). In a recent study, the 15-year survival rate of COPD Gold III patients was 5.3% and that of COPD Gold IV was 0% (27). It was also stated that in patients with an FEV₁ of less than 30%, the 2-year and 5-year survival rates were 65% and 30%, respectively (28). However, COPD patients have a lower priority for transplantation, and therefore, the time spent on the waiting list is usually very long (28). For this reason, it is necessary for these patients to gain time while waiting for transplantation. During this waiting period, besides controlling the symptoms, nutritional support, measures to increase the quality of life, and additional time-saving treatments are needed. Thus, the patient's FEV₁ value plays an important role

Table 6. Study's Baseline FEV1 in the Literature

Author	Year	n	Follow-up, M	FEV ₁ , L	FEV ₁ , % pred
Slebos <i>et al.</i> (7)	2012	16	6	0.72 ± 0.16	28.7 ± 7.1
RESET study (18)	2013	23	3	0.72	27.1
Klooster <i>et al.</i> (19)	2014	10	6	0.58	22.0
Deslee <i>et al.</i> (20)	2014	34	12	0.83 ± 0.25	30.1 ± 6.3
Hartman <i>et al.</i> (21)	2015	38	36	*	27.0
Zoumot <i>et al.</i> (22)	2015	45	12	0.76 ± 0.20	28.3 ± 8.0
Kloth <i>et al.</i> (23)	2016	30	6	0.91 ± 0.32	33.6 ± 9.0
RENEW (24)	2016	158	12	0.71 ± 0.20	25.7 ± 6.3
REVOLENS (11)	2017	50	12	0.75 ± 0.25	25.7 ± 7.5
Kontogianni (25)	2017	86	12	0.71 ± 0.21	27.0 ± 7.0
Gülksen <i>et al.</i> (12)	2017	40	6	0.68 ± 0.22	26.3 ± 9.1
Simon <i>et al.</i> (26)	2018	33	3	0.46 ± 0.12	15.0 ± 3.0
Our Study	2018	21	12	0.59 ± 0.10	20.5 ± 3.3

M, month; FEV₁, a forced expiration volume in 1 s; pred, predicted. * no data.

in determining the mortality and the BLVR treatment act as an intermediate treatment and increase the time patients have to prepare for transplantation. When the long-term efficacy of BLVR treatments is confirmed by future investigations, emphysema patients may not have any need for lung transplantation. In addition, the fewer number of donor lungs available can be used for transplantation in those with more serious diseases.

BLVR coil therapy has been increasingly used in recent years, and studies have shown improvement in 6-MWT, PFT parameters, and quality of life with this treatment (11,12,18-26). This treatment method is an alternative and effective treatment option for emphysema patients. The most recent and largest studies are the REVOLENS study and the RENEW study (11,24). In these studies, 50 patients and 158 patients were treated with BLVR coil therapy, respectively. In the REVOLENS study, the baseline mean FEV₁ value was 0.75 ± 0.25 L and 25.7 ± 7.5% predicted, and in the RENEW study, it was 0.71 ± 0.20 L and 25.7 ± 6.3% predicted. In both studies, improvements in PFT parameters, quality of life, and exercise capacity were reported (11,24). However, patients with FEV₁ of less than 25% and candidates for lung transplantation have not been studied separately. In the study involving only 33 patients by Simon *et al.* (26), a group of patients with a mean FEV₁ of 15 ± 3% was evaluated. A 100-mL increase in FEV₁, a 440-mL decrease in RV, and a 48-m increase in the 6-MWT were reported. The study concluded that BLVR coil therapy was safe in this patient group. In our study, patients with FEV₁ below 25% were investigated for 12 months. The results of our study were comparable with those of the above-mentioned studies, and it was also observed that the patients who are transplantation candidates responded well to this treatment. In addition, improvements in PaO₂ and arterial oxygen saturation values were also observed in our study. In our study, all important MID values increased significantly compared to the above-mentioned studies.

Patients with end-stage emphysema and COPD Gold IV are known to be at high risk for surgical treatments (5). Perioperative and postoperative risk increased due to low FEV₁ and diffusion capacities, restricted mobility, and increase in oxygen requirement. It has been reported that in short and medium-term studies, the BLVR coil treatments are safe with less complications. In the REVOLENS and RENEW studies, the frequencies of COPD exacerbation, pneumonia, and pneumothorax were 26%, 18%, and 2%, and 27.7%, 20%, and 9.7%, respectively (11,24). The mortality rate in the follow-up period was 8% and 6.5%, respectively (11,24). In one study, the mean complication rates of BLVR coil treatment were reported as 17-87% for COPD exacerbations, 5-46% for pneumonia, 6.0-11.6% for pneumothorax, and 0-8% for death (12). In our study, the complications during the procedure and during the follow-up time were found to be 33.3% and 61.9%, respectively. The most common complications during the procedure were mild hemoptysis (19.9%) and re-coiling (9.5%). No respiratory failure, pneumothorax, or death occurred during or after the procedure. During the 12-month follow-up period, exacerbations of COPD were found in 47.6% and pneumonia in 23.8%, and the findings were evaluated in accordance with those of similar studies in the literature. Thus, the end-stage emphysema patients who were candidates for transplantation were found to benefit from BLVR coil therapy with no serious complications, and it also provided time for these patients to prepare for lung transplantation.

The longest BLVR coil study was done by Hartman *et al.* (21). Patients with BLVR coil were followed-up for three years. The patients were classified as responders and non-responders. While BLVR coil treatment was found useful for a large group of patients one year later, it was reported that the mean of the general clinical parameters returned to baseline values at three years (21). This led to re-coiling, and a pilot study in a small patient group ($n = 8$) was conducted in

2017 by Hartmann *et al.*, in which patients got little or no benefit from re-treatment (29). However, there is a need for more extensive and larger studies to confirm these results. The results of both these studies show clearly that the patient for lung transplant gains an average time of three years with BLVR coil therapy. In our study, the FEV₁% predicted value increased from 20.1% to 25.1% at the end of first year. This result shows clearly that this group of patients has gained time for transplantation preparation.

There are several factors that limit the applicability of our study results such as, a relatively small group of patients, restricted data from only one center, and potential bias due to the nature and design of the retrospective study. Therefore, our findings cannot be generalized for all patients. However, our study results can add to the medical literature as only a few studies have been conducted on this topic. Our study showed that the BLVR coil treatment was safe and effective in this subgroup of patients with end-stage emphysema who were potential candidates for lung transplantation; this has also resulted in gaining time for lung transplantation. All other results of our study were similar to those of the few reported studies in the literature.

5. Conclusion

BLVR coil therapy is safe and effective in patients with end-stage emphysema, who are potential candidates for lung transplantation within a short to medium period. The complication rates of this treatment were not different from other coil treatments, and the improvements in clinical parameters after the treatment resulted in gaining time for lung transplantation. Future research for the evaluation of long-term efficacy of BLVR coil treatment in end-stage emphysema patients is essential.

Note: The author have stated explicitly that there are no conflicts of interest in connection with this article.

A.G. Study concept and design, data collection, analysis and interpretation of data, manuscript preparation, and drafting of the manuscript.

References

- O'Donnell DE, Webb KA. The major limitation to exercise performance in COPD is dynamic hyperinflation. *J Appl Physiol.* 2008; 105:753-757.
- Roussos C, Koutsoukou A. Respiratory failure. *Eur Respir J Suppl.* 2003; 47:3-14.
- Vogelmeier CF, Criner GJ, Martinez FJ, *et al.* Global Strategy for the Diagnosis, Management, and Prevention of Chronic Obstructive Lung Disease 2017 Report: GOLD Executive Summary. *Arch Bronconeumol.* 2017; 53:128-149.
- Ciccone AM, Meyers BF, Guthrie TJ, Davis GE, Yusef RD, Lefrak SS, Patterson GA, Cooper JD. Long-term outcome of bilateral lung volume reduction in 250 consecutive patients with emphysema. *J Thorac Cardiovasc Surg.* 2003; 125:513-525.
- Criner GJ, Cordova F, Sternberg AL, Martinez FJ. The National Emphysema Treatment Trial (NETT) Part II: Lessons learned about lung volume reduction surgery. *Am J Respir Crit Care Med.* 2011; 184:881-893.
- Herth FJF, Slebos DJ, Criner GJ, Shah PL. Endoscopic Lung Volume Reduction: An Expert Panel Recommendation - Update 2017. *Respiration.* 2017; 94:380-388.
- Slebos DJ, Klooster K, Ernst A, Herth FJF, Kerstjens HAM. Bronchoscopic lung volume reduction coil treatment of patients with severe heterogeneous emphysema. *Chest.* 2012; 142:574-582.
- Ninane V, Geltner C, Bezzi M, Foccoli P, Gottlieb J, Welte T, Seijo L, Zulueta JJ, Munavvar M, Rosell A, Lopez M, Jones PW, Coxson HO, Springmeyer SC, Gonzalez X. Multicentre European study for the treatment of advanced emphysema with bronchial valves. *Eur Respir J.* 2012; 39:1319-1325.
- Gompelmann D, Eberhardt R, Schuhmann M, Valipour A, Shah PL, Herth FJ, Kontogianni K. Lung Volume Reduction with Vapor Ablation in the Presence of Incomplete Fissures: 12-Month Results from the STEP-UP Randomized Controlled Study. *Respiration.* 2016; 92:397-403.
- Global Initiative for Chronic Obstructive Lung Disease. Global strategy for the diagnosis, management, and prevention of chronic obstructive pulmonary disease 2018. available from: https://goldcopd.org/wp-content/uploads/2017/11/GOLD-2018-v6.0-FINAL-revised-20-Nov_WMS.pdf (Accessed May 15, 2018).
- Deslée G, Leroy S, Perotin JM, *et al.* REVOLENS Study Group. Two-year follow-up after endobronchial coil treatment in emphysema: Results from the REVOLENS study. *Eur Respir J.* 2017; 50:pii:1701740.
- Gulsen A, Sever F, Girgin P, Tamci NB, Yilmaz H. Evaluation of bronchoscopic lung volume reduction coil treatment results in patients with severe emphysema. *Clin Respir J.* 2017; 11:585-592.
- Weill D, Benden C, Corris PA, Dark JH, Davis RD, Keshavjee S, Lederer DJ, Mulligan MJ, Patterson GA, Singer LG, Snell GI, Verleden GM, Zamora MR, Glanville AR. A consensus document for the selection of lung transplant candidates: 2014 – an update from the Pulmonary Transplantation Council of the International Society for Heart and Lung Transplantation. *J Heart Lung Transplant.* 2015; 34:1-15.
- Donohue JF. Minimal clinically important differences in COPD lung function. *COPD.* 2005; 2:111-124.
- Hartman JE, Ten Hacken NH, Klooster K, Boezen HM, de Greef MH, Slebos DJ. The minimal important difference for residual volume in patients with severe emphysema. *Eur Respir J.* 2012; 40:1137-1141.
- Puhan MA, Chandra D, Mosenifar Z, Ries A, Make B, Hansel NN, Wise RA, Sciurba F. NETT Research Group. The minimal important difference of exercise tests in severe COPD. *Eur Respir J.* 2011; 37:784-790.
- Jones PW. St. George's Respiratory Questionnaire. *MCID. COPD.* 2005; 2:75-79.
- Shah PL, Zoumot Z, Singh S, Bicknell SR, Ross ET, Quiring J, Hopkinson NS, Kemp SV. Endobronchial coils for the treatment of severe emphysema with

- hyperinflation (RESET): A randomised controlled trial. *Lancet Respir Med.* 2013; 1:233-240.
19. Klooster K, Ten Hacken NH, Franz I, Kerstjens HA, van Rikxoort EM, Slebos DJ. Lung volume reduction coil treatment in chronic obstructive pulmonary disease patients with homogeneous emphysema: A prospective feasibility trial. *Respiration.* 2014;88:116-125.
 20. Deslee G, Klooster K, Hetzel M, Stanzel F, Kessler R, Marquette CH, Witt C, Blaas S, Gesierich W, Herth FJ, Hetzel J, van Rikxoort EM, Slebos DJ. Lung volume reduction coil treatment for patients with severe emphysema: A European multicentre trial. *Thorax.* 2014; 69:980-986.
 21. Hartman JE, Klooster K, Gortzak K, ten Hacken NH, Slebos DJ. Long-term follow-up after bronchoscopic lung volume reduction treatment with coils in patients with severe emphysema. *Respirology.* 2015; 20:319-326.
 22. Zoumot Z, Kemp SV, Singh S, Bicknell SR, McNulty WH, Hopkinson NS, Ross ET, Shah PL. Endobronchial coils for severe emphysema are effective up to 12 months following treatment: Medium term and cross-over results from a randomised controlled trial. *PLoS One.* 2015; 10:e0122656.
 23. Kloth C, Thaiss WM, Hetzel J, Ditt H, Grosse U, Nikolaou K, Horger M. Impact of endobronchial coiling on segmental bronchial lumen in treated and untreated lung; lobes: Correlation with changes in lung volume, clinical and pulmonary function tests. *Eur Radiol.* 2016; 26:2176-2183.
 24. Sciruba FC, Criner GJ, Strange C, *et al.* RENEW study research group. Effect of endobronchial coils vs Usual care on exercise tolerance in patients with severe emphysema: The RENEW randomized clinical trial. *JAMA.* 2016; 315:2178-2189.
 25. Kontogianni K, Gerovasili V, Gompelmann D, Schuhmann M, Hoffmann H, Heussel CP, Herth FJ, Eberhardt R. Coil therapy for patients with severe emphysema and bilateral incomplete fissures - effectiveness and complications after 1-year follow-up: A single-center experience. *Int J Chron Obstruct Pulmon Dis.* 2017; 12:383-394.
 26. Simon M, Harbaum L, Oqueka T, Kluge S, Klose H. Endoscopic lung volume reduction coil treatment in patients with very low FEV(1): An observational study. *Ther Adv Respir Dis.* 2018; 12:1753466618760133.
 27. Van Hirtum PV, Sprooten RTM, van Noord JA, van Vliet M, de Kruif MD. Long term survival after admission for COPD exacerbation: A comparison with the general population. *Respir Med.* 2018; 137:77-82.
 28. Lane CR and Tonelli AR. Lung transplantation in chronic obstructive pulmonary disease: Patient selection and special considerations. *Int J Chron Obstruct Pulmon Dis.* 2015; 10:2137-2146.
 29. Hartman JE, Klooster K, Ten Hacken NHT, Slebos DJ. The Safety and Feasibility of Re-treating Patients with Severe Emphysema with Endobronchial Coils: A Pilot Study. *COPD.* 2017; 14:339-343.

(Received June 19, 2018; Revised August 15, 2018; Accepted August 17, 2018)

Association between the *MVK* rs2287218 SNP and the risk of coronary heart disease and ischemic stroke: A case-control study

Duo-Shun Wang, Rui-Xing Yin*, Kai-Guang Li, Li Lu, Yuan Su, Rong-Qin Yan

Department of Cardiology, Institute of Cardiovascular Diseases, the First Affiliated Hospital, Guangxi Medical University, Nanning, Guangxi, China.

Summary

The association between the mevalonate kinase gene (*MVK*) single nucleotide polymorphism (SNP) and serum lipid levels has been detected in several previous genome-wide association studies, but the results are inconsistent. In addition, it is still unclear whether the loci identified exert the similar effect on the susceptibility of coronary heart disease (CHD) or ischemic stroke (IS). Therefore, the present study was undertaken to detect the association between the *MVK* rs2287218 SNP and serum lipid levels, the susceptibility of CHD and IS in a Southern Chinese Han population. The genotypes of the SNP in 1764 unrelated subjects (CHD, 583; IS, 555; and healthy controls, 626) were determined by the Snapshot technology. The genotypic and allelic frequencies were different between CHD and control subjects ($P \leq 0.013$ for each), or between IS and control groups ($P < 0.01$ for each). The T allele carriers had an increased risk of CHD and IS (CHD: OR = 1.674, 95% CI = 1.25-2.25, $P = 0.001$ for CT/TT vs. CC genotypes; OR = 1.595, 95% CI = 1.23-2.07, $P < 0.001$ for T vs. C alleles; IS: OR = 1.890, 95% CI = 1.36-2.47, $P = 0.001$ for CT/TT vs. CC genotypes; OR = 1.829, 95% CI = 1.38-2.42, $P < 0.001$ for T vs. C alleles). The T allele carriers in healthy controls had lower serum high-density lipoprotein cholesterol (HDL-C) levels than the T allele non-carriers ($P = 0.013$). These findings suggest that the *MVK* rs2287218 SNP is likely to increase the risk of CHD and IS by decreasing serum HDL-C levels in our study populations.

Keywords: Coronary heart disease, ischemic stroke, mevalonate kinase gene, rs2287218, single nucleotide polymorphism, serum lipid levels

1. Introduction

Among the non-communicable disease, cardiovascular and circulatory disease primarily made up by ischemic heart disease (5.2%), hemorrhagic stroke (2.5%), ischemic stroke (IS, 1.6%), and hypertensive heart (0.6%), accounted of 11.8% of global disability-adjusted life years (DALYS) (1). More than 2.5 and 1 million persons suffered from the stroke and heart attack, resulting in more than 2 million deaths each year in China (2). The location of coronary heart

disease (CHD) and IS was different, but they may share the common risk factors such as hypertension, dyslipidemia and metabolic syndrome (3), and the same pathophysiological basis: atherosclerosis (4). Dyslipidemia such as low concentration of high-density lipoprotein cholesterol (HDL-C), high levels of low-density lipoprotein cholesterol (LDL-C), total cholesterol (TC) and triglyceride (TG) was one of the most important risk factors for CHD (5,6) and IS (7,8). It is well-known that the disorder of lipid metabolism is a complex characteristic, resulted from multiple environmental and genetic factors and their interactions (9,10). Twins and family studies indicated that disorder of lipid metabolism was influenced by genetic and environmental factors, which might contribute to the individual discrepancy in the serum lipid profiles (11).

Previous genome-wide association studies (GWASes) have found the association of several novel loci in the mevalonate kinase gene (*MVK*, also as: *MK*; *LRBP*; *MVLK*; *POROK3*) and serum lipid levels

Released online in J-STAGE as advance publication August 12, 2018.

*Address correspondence to:

Dr. Rui-Xing Yin, Department of Cardiology, Institute of Cardiovascular Diseases, the First Affiliated Hospital, Guangxi Medical University, 22 Shuangyong Road, Nanning 530021, Guangxi, China.

E-mail: yinruixing@163.com

(12,13). The *MVK* was located at chromosome 12q24 (12,13) and encoded the mevalonate kinase (MVK) (14). MVK was a key early enzyme in isoprenoid and sterol synthesis metabolism, which implicated to affect HDL-C levels (12,15). Mutations in the *MVK* gave rise to hyperimmunoglobulinemia D syndrome (HIDS), in which low HDL-C levels could be found (16), in accordance with the latest GWAS findings (12,13). Several novel loci in *MVK* were confirmed to be associated with serum HDL-C levels (17-19) and an increased risk of CHD and IS (19). But no significant association between the *MVK* rs2287218 SNP and serum lipid levels was conducted by Sun *et al.* in a Northern Chinese Han population (20). To our knowledge, the genetic evidence on the associations between the *MVK* rs2287218 SNP and serum lipid levels, and the susceptibility of CHD or IS in a Southern Chinese Han population has not been reported previously. Therefore, the present study was undertaken to detect the association between the *MVK* rs2287218 SNP and serum lipid levels, and the susceptibility of CHD and IS in a Southern Chinese Han population.

2. Materials and Methods

2.1. Study patients

A total of 1138 patients with CHD ($n = 583$) and IS ($n = 555$) were recruited from the First Affiliated Hospital, Guangxi Medical University. The age of these patients ranged from 23 to 87 years with a mean age of 62.26 ± 10.51 years in CHD and 62.85 ± 12.32 years in IS. All of enrolled CHD patients were evaluated by coronary angiography. The coronary angiograms were analyzed by two experienced interventional cardiologist. CHD was defined as severe coronary stenosis ($\geq 50\%$) in at least either one of the three main coronary arteries or their major branches (branch diameter ≥ 2 mm). Subjects with congenital heart disease and type 1 diabetes mellitus (T1DM) were excluded in the study. All of enrolled IS patients received a strict neurological examination and brain magnetic resonance imaging. The diagnosis of IS was according to the International Classification of Diseases (9th Revision). Patients with a transient ischemic attack, embolic brain infarction, stroke caused by inflammatory disease, or serious chronic diseases were excluded from the study. The CHD patients who had a past history of IS, or the IS cases who had a past history of CHD were also excluded from the study (21).

2.2. Controls

A control group of 626 subjects matched by age, gender, and nationality was also included in the study. They were randomly selected from the healthy adults who underwent periodical check-up at our hospital during the same period when CHD and IS patients

recruited. The average age of the participants was 61.95 ± 10.01 years. They were free from CHD and IS at time of history taking, clinical, biochemical, and image examinations such as 64-slice computed tomographic coronary angiography. Information on demography, medical history and lifestyle was collected with standardized questionnaires. This study design was approved by the Ethics Committee of the First Affiliated Hospital, Guangxi Medical University (No. Lunshen 2009-Guike-018). Informed consent was obtained from all participants before the study.

2.3. Biochemical measurements

A fasting venous blood sample of 5 ml was obtained from the participants. A part of the sample (2 mL) was collected into glass tubes and used to determine serum lipid levels. Another part of the sample (3 mL) was transferred to tubes with anticoagulants (4.80 g/L citric acid, 14.70 g/L glucose and 13.20 g/L tri-sodium citrate) and used to extract deoxyribonucleic acid (DNA). Measurements of serum TC, TG, HDL-C, and LDL-C levels in the samples were performed by enzymatic methods with commercially available kits (RANDOX Laboratories Ltd., Ardmore, Diamond Road, and Crumlin Co. Antrim, United Kingdom, BT29 4QY; Daiichi Pure Chemicals Co, Ltd., Tokyo, Japan). Serum apolipoprotein (Apo) A1 and ApoB levels were detected by the immunoturbidimetric immunoassay using a commercial kit (RANDOX Laboratories Ltd.). All determinations were performed with an auto-analyzer (Type 7170A; Hitachi Ltd., Tokyo, Japan) in the Clinical Science Experiment Center of the First Affiliated Hospital, Guangxi Medical University (22).

2.4. Genotyping

Genomic DNA was extracted from peripheral blood leukocytes using the phenol-chloroform method. Genotyping of the *MVK* rs2287218 SNP was performed by the Snapshot technology platform in the Center for Human Genetics Research, Shanghai Genesky Bio-Tech Co. Ltd., China (23). The restriction enzyme for the *MVK* rs2287218 SNP was SAP (Promega) and Exonuclease I (Epicentre). The sense and antisense primers were 5'-CTGCGGGAGAGTCACGTTTCAC-3' and 5'-GAGGGACACTGGCCAGGTAAGG-3', respectively.

2.5. Diagnostic criteria

The normal values of serum TC, TG, HDL-C, LDL-C, ApoA1, ApoB levels and the ApoA1/ApoB ratio in our Clinical Science Experiment Center were 3.10-5.17, 0.56-1.70, 0.91-1.81, 2.70-3.20 mmol/L; 1.00-1.78, 0.63-1.14 g/L; and 1.00-2.50; respectively (24). The individuals with TC > 5.17 mmol/L and/or TG

> 1.70 mmol/L were defined as hyperlipidemic (25). LDL-C \geq 3.20 mmol/L was defined as high low-density lipoproteinemia (26). Hypertension was diagnosed according to the 1999 and 2003 criteria of the World Health Organization-International Society of Hypertension Guidelines for the management of hypertension (27). The diagnostic criteria of overweight and obesity were according to the Cooperative Meta-Analysis Group of China Obesity Task Force. Normal weight, overweight and obesity were defined as a body mass index (BMI) < 24, 24-28 and > 28 kg/m², respectively (28).

2.6. Statistical analyses

The statistical analyses were performed with the statistical software package SPSS 21.0 (SPSS Inc., Chicago, Illinois). The quantitative variables were presented as mean \pm standard deviation (serum TG levels were presented as medians and interquartile ranges). Allelic frequency was determined via direct counting, and the Hardy-Weinberg equilibrium was verified with the standard goodness-of-fit test. The sex ratio and genotypic distribution between the two groups were analyzed by the chi-square test. General characteristics between patients and controls were compared by the Student's unpaired *t*-test. The association between genotypes and serum lipid parameters was tested by

covariance analysis (ANCOVA). Unconditional logistic regression was used to assess the correlation between the risk of CHD or IS and genotypes. Gender, age, BMI, blood pressure, alcohol consumption and cigarette smoking were adjusted for the statistical analysis. Odds ratio (OR) and 95% confidence interval (CI) were calculated by using unconditional logistic regression. Results were considered to be statistically significant if two-sided *P* value was less than 0.05.

3. Results

3.1. Clinical characteristics of the subjects

The clinical characteristics of the subjects are described in Table 1. The male to female ratio, mean age, serum LDL-C and ApoB levels were not different between the control and experimental groups (*P* > 0.05 for all). As compared with the CHD and IS patients, the control subjects had higher serum TC, HDL-C, ApoA1 levels and the ApoA1/ApoB ratio (*P* < 0.05). The body height, weight, average BMI, systolic blood pressure, pulse pressure, the prevalence of hypertension, TG levels and the percentages of subjects who smoked cigarettes and did not drink alcohol were lower in the control than in CHD and IS groups (*P* < 0.05). In addition, the control subjects had lower diastolic blood pressure levels than the IS patients (*P* < 0.01).

Table 1. Comparison of the clinical characteristics and serum lipid levels between the controls and patients

Parameter	Control	CHD	IS	<i>P</i> _{CHD}	<i>P</i> _{IS}
Number	626	583	555	-	-
Male/female	457/169	431/152	401/154	0.716	0.773
Age (years)	61.95 \pm 10.01	62.26 \pm 10.51	62.85 \pm 12.32	0.599	0.175
Height (cm)	155.04 \pm 7.87	164.15 \pm 6.83	163.74 \pm 7.14	0.000	0.000
Weight (kg)	54.51 \pm 9.04	64.57 \pm 10.60	62.96 \pm 11.11	0.000	0.000
Body mass index (kg/m ²)	22.60 \pm 2.81	23.89 \pm 3.21	23.42 \pm 3.49	0.000	0.000
Cigarette smoking [<i>n</i> (%)]					
Non-smoking	382 (61.0)	328 (56.2)	324 (58.4)		
\leq 20 cigarettes per day	189 (30.2)	99 (17.0)	162 (29.1)		
> 20 cigarettes per day	55 (8.8)	156 (26.8)	69 (12.4)	0.000	0.124
Alcohol consumption [<i>n</i> (%)]					
Non-drinker	354 (56.6)	449 (77.0)	400 (72.1)		
\leq 25 g per day	200 (31.9)	81 (13.9)	122 (22.0)		
> 25 g per day	72 (11.5)	53 (9.1)	33 (5.9)	0.000	0.000
SBP (mmHg)	128.00 \pm 19.60	133.03 \pm 23.21	147.72 \pm 22.03	0.000	0.000
DBP (mmHg)	80.49 \pm 11.35	79.17 \pm 14.17	83.78 \pm 12.90	0.077	0.000
Pulse pressure (mmHg)	47.52 \pm 14.73	53.85 \pm 17.50	63.94 \pm 17.80	0.000	0.000
Total cholesterol (mmol/L)	4.90 \pm 1.02	4.53 \pm 1.18	4.52 \pm 1.13	0.000	0.000
Triglycerid (mmol/L)	1.01 (0.66)	1.36 (0.94)	1.37 (0.91)	0.000	0.000
HDL-C (mmol/L)	1.92 \pm 0.50	1.14 \pm 0.34	1.23 \pm 0.40	0.000	0.000
LDL-C (mmol/L)	2.73 \pm 0.78	2.71 \pm 0.99	2.68 \pm 0.89	0.701	0.349
ApoA1 (g/L)	1.41 \pm 0.27	1.04 \pm 0.52	1.02 \pm 0.22	0.000	0.000
ApoB (g/L)	0.90 \pm 0.21	0.91 \pm 0.27	0.89 \pm 0.24	0.779	0.450
ApoA1/ApoB	1.65 \pm 0.52	1.38 \pm 2.45	1.25 \pm 0.58	0.011	0.000
Hypertension [<i>n</i> (%)]	210 (33.5)	419 (71.9)	379 (68.3)	0.000	0.000

CHD, coronary heart disease; IS, ischemic stroke; TC, total cholesterol; TG, triglyceride; HDL-C, high-density lipoprotein cholesterol; LDL-C, low-density lipoprotein cholesterol; ApoA1, apolipoprotein A1; ApoB, apolipoprotein B; ApoA1/ApoB, the ratio of apolipoprotein A1 to apolipoprotein B; SBP, systolic blood pressure; DBP, diastolic blood pressure. *P*_{CHD}: CHD vs. control; *P*_{IS}: IS vs. control. The value of triglyceride was presented as median (interquartile range); the difference among the genotypes was determined by the Wilcoxon-Mann-Whitney test. The remaining characteristics between patients and controls were tested by the Student's unpaired-test.

3.2. Genotypic and allelic frequencies

The genotypic and allelic frequencies of the rs2287218 SNP are presented in Figure 1. The genotypic and allelic frequencies were different between the CHD/IS and control groups ($P < 0.05$). The C and T allele frequencies were 88.7% and 11.3% in controls, 84.8% and 15.2% in CHD, and 84.1% and 15.9% in IS patients; respectively. The CC, CT and TT genotype frequencies were 78.4%, 20.6% and 1.0% in controls; 72.0%, 25.6% and 2.4% in CHD; and 71.0%, 26.1% and 2.9% in IS patients; respectively. The genotypic distribution was in accordance with the Hardy-Weinberg equilibrium in the three groups ($P > 0.05$).

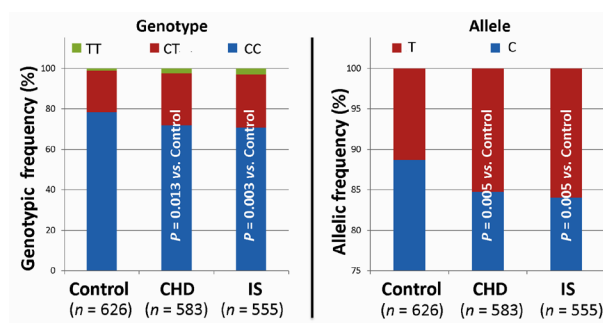


Figure 1. Genotypic and allelic frequencies of the MVK rs2287218 SNP in controls, coronary heart disease (CHD) and ischemic stroke (IS) patients. The genotypic and allelic distribution in the three groups was analyzed by the chi-square test.

3.3. The rs2287218 SNP and the risk of CHD or IS

The T allele carriers had an increased risk of CHD and IS (CHD: OR = 1.674, 95% CI = 1.25-2.25, $P = 0.001$ for CT/TT vs. CC genotypes; OR = 1.595, 95% CI = 1.23-2.07, $P < 0.001$ for T vs. C alleles; IS: OR = 1.890, 95% CI = 1.36-2.47, $P = 0.001$ for CT/TT vs. CC genotypes; OR = 1.829, 95% CI = 1.38-2.42, $P < 0.001$ for T vs. C alleles) after adjusting for age, gender, BMI, smoking status, alcohol consumption and hypertension.

3.4. Gene-environment interactions on the risk of CHD or IS

Stratified analysis showed that an increased risk of CHD and IS was found in subjects with CT/TT genotypes, especially in those who belonged to one of the following categories: females, elder (> 60 years), low BMI (< 24 kg/m²), nonsmokers and nondrinkers (Table 2).

3.5. Related risk factors for CHD and IS

As shown in Table 3, multivariate logistic analysis showed that the incidence of CHD and IS was positively correlated with smoking, high BMI (≥ 24 kg/m²), hypertension and CT/TT genotypes, whereas it was negatively associated with alcohol consumption. There was also a positive association between the incidence of CHD and hyperlipidemia, but not between the incidence of IS and hyperlipidemia.

Table 2. The MVK rs2287218 SNP and the risk of CHD and IS according to gender, age, body mass index, smoking status and alcohol consumption

Factor	Genotype	OR (95%CI) _{CHD}	P_{CHD}	P_1	OR (95%CI) _{IS}	P_{IS}	P_1
Gender	CC	1			1		
	CT + TT	1.332 (0.943-1.880)	0.104		1.324 (0.927-1.890)	0.123	
Female	CC	1		0.000	1		0.000
	CT + TT	8.002 (3.397-18.852)	0.000		6.366 (2.691-15.060)	0.000	
Age	CC	1			1		
	CT + TT	1.505 (0.928-2.442)	0.097		1.643 (0.991-2.725)	0.054	
	CC	1		0.161	1		0.121
> 60 years	CT + TT	1.917 (1.304-2.818)	0.001		1.848 (1.221-2.797)	0.004	
BMI	CC	1			1		
	CT + TT	1.656 (1.130-2.426)	0.010		2.048 (1.387-3.025)	0.000	
	CC	1		0.584	1		0.678
≥ 24 kg/m ²	CT + TT	1.006 (0.97-1.10)	0.028		1.469 (0.857-2.518)	0.162	
Smoking	CC	1			1		
	CT + TT	2.844 (1.869-4.327)	0.000		3.092 (1.969-4.854)	0.000	
	CC	1		0.000	1		0.000
Smoking	CT + TT	1.235 (0.704-2.165)	0.462		0.916 (0.581-1.446)	0.708	
Drinking	CC	1			1		
	CT + TT	2.578 (1.753-3.791)	0.000		3.068 (1.995-4.719)	0.000	
	CC	1		0.000	1		0.000
Drinking	CT + TT	0.945 (0.473-1.889)	0.873		0.759 (0.457-1.262)	0.288	

OR and 95% CI were obtained from unconditional logistic regression model after adjusting for age, gender, body mass index, smoking status, alcohol consumption, hypertension. P_1 , the value of interaction between the SNP and factors

Table 3. Related risk factors for CHD and IS

Factor	OR (95%CI) _{CHD}	<i>P</i> _{CHD}	OR (95%CI) _{IS}	<i>P</i> _{IS}
Nonsmoking	1		1	
Smoking	1.586 (1.186-2.121)	0.003	1.468 (1.075-2.004)	0.016
Nondrinking	1		1	
Drinking	0.214 (0.156-0.295)	0.000	0.388 (0.281-0.535)	0.000
BMI < 24 kg/m ²	1		1	
BMI ≥ 24 kg/m ²	2.260 (1.739-2.937)	0.000	1.622 (1.213-2.167)	0.001
rs2287218CC	1		1	
rs2287218CT/TT	1.658 (1.232-2.231)	0.001	1.890 (1.378-2.592)	0.000
Normotensive	1		1	
Hypertension	4.298 (3.046-6.066)	0.000	1.709 (1.239-2.358)	0.001
Normal blood lipids	1		1	
Hyperlipidemia	1.833 (1.411-2.383)	0.000	0.804 (0.575-1.123)	0.201

OR and 95% CI were obtained from unconditional logistic regression model after adjusting for age, gender, body mass index (BMI), smoking status, alcohol consumption, hypertension.

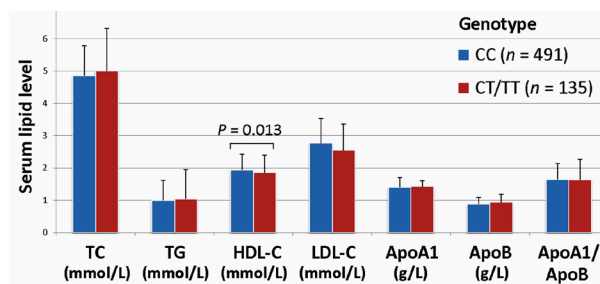


Figure 2. Association between the *MVK* rs2287218 SNP and serum lipid levels in the controls. TC, total cholesterol; TG, triglyceride; HDL-C, high-density lipoprotein cholesterol; LDL-C, low-density lipoprotein cholesterol; ApoA1, apolipoprotein A1; ApoB, apolipoprotein B; ApoA1/ApoB, the ratio of apolipoprotein A1 to apolipoprotein B. The value of TG was presented as median (interquartile range), and the difference between the genotypes was determined by the Wilcoxon-Mann-Whitney test. The association between genotypes and the remaining serum lipid parameters was tested by analysis of covariance (ANCOVA).

3.6. Genotypes and serum lipid levels

As shown in Figure 2, the subjects with CT/TT genotypes in control group had lower serum HDL-C levels than those with CC genotype ($P = 0.013$). There was no difference in the remaining lipid parameters between the CT/TT and CC genotypes ($P > 0.05$ for all).

4. Discussion

A considerable amount of literatures showed that blood lipid metabolism was closely related to the occurrence and development of atherosclerosis and cardiovascular disease (CVD) (29,30). As a significant monitoring indicator of CVD, dyslipidemia is a complex and multifactorial disease, resulting from multiple environmental factors, including age, sex, obesity, abnormal glucose, hypertension, lifestyle and daily exercise (31,32), genetic factors, and their interactions (33,34). The SNP was the most abundant genetic variation in the human genome, which was

manifested in the substitution mutation of a single base. SNP could be used to explain the individual phenotypic discrepancy and the susceptibility of different groups and individuals to some diseases. So, to identify the gene mutations regulating the serum lipid profiles and increasing the risk of CHD or IS has received considerable critical attentions, especially in the development of new markers for risk stratification assessment, diagnosis, treatment and prognosis of CVD.

The principal finding of the present study was a significant association between the *MVK* rs2287218 SNP and serum HDL-C levels in a Southern Chinese Han population. The subjects with CT/TT genotypes in healthy controls had lower serum HDL-C levels than the subjects with CC genotype ($P = 0.013$). Recent GWASes have found that several novel loci in *MVK* could influence HDL-C concentrations (12,13). The subjects with GG genotype (the major homozygote) of the *MVK* S52N had lower HDL-C levels than the subjects with AA genotype (17). The associations between the *MVK* rs2338104 SNP and HDL-C levels were definitive ($P < 0.001$) and consistent (18,35). In addition, the *MVK* rs3759387AA genotype had lower HDL-C levels than the rs3759387AC/CC genotypes (19). Furthermore, *MVK* (i85G→T and S52NG→A) had low HDL-C levels linked to dietary habit, especially in carbohydrates intakes (17). These studies suggested that the *MVK* rs2287218 SNP, as a member of *MVK*, may be linked to HDL-C levels. In the present study, our results in accordance with the latest GWAS findings (12,13) may be reasonable. But Sun *et al.* showed that there was no significant association between the *MVK* rs2287218 SNP and serum lipid levels in a Northern Chinese Han population (20). The precise reason for these conflicting results was unknown. Because blood lipid metabolism genes were multilocus and multivariate, the locations and properties of different populations may be diverse. The relationships between the same genetic frequency and serum lipid levels may not be the same in different ethnic groups or geographic

areas (36). On one hand, in addition to sample size and different statistical methods, they were different in exposed environments. It was reported that serum lipid levels and the prevalence of dyslipidemia were influenced by multiple environmental factors, such as dietary habit (37), lifestyle (38), daily exercise (39). Junyent *et al.* found that *MVK* (i85G→T and S52NG→A) had low HDL-C levels linked to dietary habit, especially in carbohydrates intakes (17). On the other hand, their genetic background was not similar, which may contribute to the discrepancies between our and the other studies in different populations. In the present study, we showed that the *MVK* rs2287218T allele frequency was 14.0% in the Guangxi Han population. According to the International 1000 Genomes data-base (<https://www.ncbi.nlm.nih.gov/variation/tools/1000genomes/>), the *MVK* rs2287218T allele frequency was 10.7% in Han Chinese in Beijing, China (CHB); 13.9% in Japanese in Tokyo, Japan (JPT); 21.9% in African Caribbeans in Barbados (ACB); 17.2% in Americans of African ancestry in SW USA (ASW); and 17.2% in Mexican ancestry from Los Angeles USA (MXL). These results showed that the prevalence of the *MVK* rs2287218T allele was higher in North American or in European than in Asian. The minor allele frequency of the *MVK* rs2287218 SNP was also different between Southern and Northern Chinese populations. These findings revealed that the *MVK* rs2287218 SNP has a racial/ethnic and geographic specificity.

The *MVK* exists in a wide range of organisms from bacteria to human and is a key early enzyme in isoprenoid and sterol synthesis metabolism (12,15). The *MVK* was modified by sterol-responsive element-binding protein 2 (SREBP2) by sharing a promoter, which was a transcription factor that played a vital role in controlling cholesterol homeostasis (40). Moreover, it was also reported that *MVK* took part in metabolic pathways and had an effect on HDL-C metabolism in the previous study. *MVK* mutations, especially in homozygosity, or the *MVK* deficiency caused hyperimmunoglobulinemia D syndrome (HIDS), in which the basic symptoms were recurrent episodes of fever and high concentrations of immunoglobulin (Ig) D and A in blood (16). When the patients suffered from HIDS, low HDL-C levels could be found, in accordance with the latest GWAS findings (12,13). In some previous studies, the increased immunoglobulin containing IgD and IgA contributed to the low levels of HDL-C (41,42). It was likely that the immunoglobulin synthesis took a lot of nutrients, such as albumin and cholesterol, resulting in decreased HDL-C levels. It was worth mentioning that the statins were reported to be applied in the treatment of HIDS by inhibiting the 3-hydroxy-3-methylglutaryl coenzyme A (HMG-CoA) reductase and the pro-inflammatory cytokines (43). These results indicated

that the *MVK* rs2287218 SNP could influence serum HDL-C levels. However, the precise mechanism of *MVK* on serum lipid metabolism remains to be explored.

Another important finding in the current study was that the *MVK* rs2287218 SNP was strongly associated with the risk of CHD and IS in the Guangxi Han population. The frequencies of the TT/CT genotypes and T allele were associated with an increased risk of CHD and IS after adjusting for potential confounding factors. Multivariate analysis showed that the known factors, such as cigarette smoking, high BMI (≥ 24 kg/m²), hypertension, hyperlipidemia and the TT/CT genotypes were dependently associated with CHD. Meanwhile, the occurrence of IS was positively correlated with cigarette, high BMI, hypertension and the TT/CT genotypes. Both CHD and IS were negatively correlated with the *MVK* rs2287218 CC genotype and alcohol consumption. We also found that the drinkers, especially moderate alcohol, had a lower risk of CVD than non-drinkers (44). The effects of alcohol on lipid metabolism, especially the HDL-C-elevating effects (45), were considered to greatly promote the cardio-protective action of alcohol (46). In the stratified analysis, the increased risk of CHD and IS in subjects with the CT and TT genotypes was mainly observed in females, age > 60 years, BMI < 24 kg/m², nonsmokers and nondrinkers. Significant interactions between the *MVK* rs2287218 SNP and environmental factors on the risk of CHD or IS were observed in those of females, nonsmokers and nondrinkers. The subjects with CT/TT genotypes of the *MVK* rs2287218 SNP contributed to the increased risk of CHD and IS. A previous study confirmed that the *MVK* rs3759387 AC/CC genotypes interacted with some environmental exposures (such as males, elder), resulting in increasing the risk of CHD and IS (19), which suggested gene-environment interactions contributed to higher risk of CHD and IS. It was reported that the *MVK* variants displayed low HDL-C levels and an activity decline of the *MVK*. The high levels of HDL-C could regulate monocytes proliferation and activation, changing the composition of the myeloid cell lineage, which was thought to generate beneficial anti-inflammatory and athero-protective effects to prevent CVD (47,48). In addition, the activity of the *MVK* played a key role in controlling cholesterol homeostasis (13) and HDL-C metabolism. Elimination of the *MVK* activity caused low HDL-C levels in HIDS and increased atherosclerosis. It has been demonstrated that the abnormal blood lipid metabolism is closely related to the occurrence and development of atherosclerosis and CVD (29,30). Therefore, the *MVK* rs2287218 SNP was likely to increase the risk of CHD and IS by reducing serum HDL-C levels without anti-inflammatory and athero-protective effects. Besides, the frequencies of genotype

and allele were statistically significant between the CHD or IS and control groups. The frequency of the *MVK* rs2287218T allele was higher in the CHD (15.2%) and IS (15.9%) patients than in the controls (11.3%, $P = 0.005$). According to the International 1000 Genomes data-base, the frequency of the *MVK* rs2287218T allele was diverse in different racial groups and geographic areas. We also showed that the frequencies of TT/CT genotypes were higher in the CHD (28.0%) and IS (29.0%) patients than in the controls (21.6%, $P \leq 0.01$ for each). In addition, a previous study indicated that the *MVK* expression levels were different in some tissues (49). These findings suggested that the *MVK* rs2287218 SNP may be a susceptibility to CHD and IS. It was likely to increase the risk of CHD and IS by decreasing the serum HDL-C levels. However, large genetic association studies or meta-analyses are necessary to further explore these associations between them.

The present study had several potential limitations. Firstly, the number of involved patients was relatively small compared to many previous GWASs and replication studies. Therefore, further studies with larger sample sizes are needed to confirm our findings. Secondly, a number of patients with CHD or IS took anti-atherosclerotic drugs, such as statins, angiotensin-converting enzyme inhibitors, beta blockers, and aspirin when they were enrolled in the study, whereas the controls did not take any medicine. The levels of TC and LDL-C were lower in the patients with CHD or IS than in the healthy controls. However, the drug information was missing for some IS and CHD patients. Finally, only one *MVK* SNP was studied in this study. The interaction of the *MVK* SNP-SNP on serum lipid profiles and the susceptibility of CHD and IS was not observed. Therefore, the observed associations need further replications to avoid spurious associations.

5. Conclusion

The *MVK* rs2287218 SNP was associated with serum HDL-C levels and the susceptibility of CHD and IS in a Southern Chinese Han population. The T allele carriers had an increased risk of CHD and IS. The T allele carriers in healthy controls had lower serum HDL-C levels than the T allele non-carriers. These findings suggest that the *MVK* rs2287218 SNP is likely to increase the risk of CHD and IS by decreasing serum HDL-C levels.

Acknowledgements

This study was supported by the Science Foundation of Guangxi Returned Oversea Scholars (No. 0991004) and the National Natural Science Foundation of China (No. 81460169).

References

- Murray CJ, Vos T, Lozano R, *et al.* Disability-adjusted life years (DALYs) for 291 diseases and injuries in 21 regions, 1990-2010: A systematic analysis for the Global Burden of Disease Study 2010. *Lancet*. 2012; 380:2197-2223.
- Ding H, Xu Y, Wang X, Wang Q, Zhang L, Tu Y, Yan J, Wang W, Hui R, Wang CY, Wang DW. 9p21 is a shared susceptibility locus strongly for coronary artery disease and weakly for ischemic stroke in Chinese Han population. *Circ Cardiovasc Genet*. 2009; 2:338-346.
- Fruchart JC, Nierman MC, Stroes ES, Kastelein JJ, Duriez P. New risk factors for atherosclerosis and patient risk assessment. *Circulation*. 2004; 109:115-19.
- Pasternak RC, Criqui MH, Benjamin EJ, Fowkes FG, Isselbacher EM, McCullough PA, Wolf PA, Zheng ZJ. Atherosclerotic Vascular Disease Conference: Writing Group I: Epidemiology. *Circulation*. 2004; 109:2605-2612.
- Castelli WP, Garrison RJ, Wilson PW, Abbott RD, Kalousdian S, Kannel WB. Incidence of coronary heart disease and lipoprotein cholesterol levels. The Framingham Study. *JAMA*. 1986; 256:2835-2838.
- Gordon DJ, Probstfield JL, Garrison RJ, Neaton JD, Castelli WP, Knoke JD, Jacobs DR, Jr., Bangdiwala S, Tyroler HA. High-density lipoprotein cholesterol and cardiovascular disease. Four prospective American studies. *Circulation*. 1989; 79:8-15.
- Tanne D, Yaari S, Goldbourt U. High-density lipoprotein cholesterol and risk of ischemic stroke mortality. A 21-year follow-up of 8586 men from the Israeli Ischemic Heart Disease Study. *Stroke*. 1997; 28:83-87.
- Soyama Y, Miura K, Morikawa Y, Nishijo M, Nakanishi Y, Naruse Y, Kagamimori S, Nakagawa H. High-density lipoprotein cholesterol and risk of stroke in Japanese men and women: The Oyabe Study. *Stroke*. 2003; 34:863-868.
- Yin RX, Li YY, Wu JZ, Pan SL, Liu CW, Lin WX, Yang DZ. Interactions between the apolipoprotein A1/C3/A5 haplotypes and alcohol consumption on serum lipid levels. *Alcohol Clin Exp Res*. 2013; 37:234-243.
- Yin RX, Wu DF, Wu JZ, Cao XL, Aung LH, Miao L, Long XJ, Liu WY, Zhang L, Li M. Interactions of several lipid-related gene polymorphisms and cigarette smoking on blood pressure levels. *Int J Biol Sci*. 2012; 8:685-696.
- Dursun S, Cuhadar S, Koseoglu M, Atay A, Aktas SG. The anti-inflammatory and antioxidant effects of pravastatin and nebivolol in rat aorta. *Anadolu Kardiyol Derg*. 2014; 14:229-233.
- Willer CJ, Sanna S, Jackson AU, *et al.* Newly identified loci that influence lipid concentrations and risk of coronary artery disease. *Nat Genet*. 2008; 40:161-169.
- Deodato F, Boenzi S, Santorelli FM, Dionisi-Vici C. Methylmalonic and propionic aciduria. *Am J Med Genet C Semin Med Genet*. 2006; 142c:104-112.
- Schafer BL, Bishop RW, Kratunis VJ, Kalinowski SS, Mosley ST, Gibson KM, Tanaka RD. Molecular cloning of human mevalonate kinase and identification of a missense mutation in the genetic disease mevalonic aciduria. *J Biol Chem*. 1992; 267:13229-13238.
- Kuijk LM, Beekman JM, Koster J, Waterham HR, Frenkel J, Coffey PJ. HMG-CoA reductase inhibition

- induces IL-1beta release through Rac1/PI3K/PKB-dependent caspase-1 activation. *Blood*. 2008; 112:3563-3573.
16. Klasen IS, Goertz JH, van de Wiel GA, Weemaes CM, van der Meer JW, Drenth JP. Hyper-immunoglobulin A in the hyperimmunoglobulinemia D syndrome. *Clin Diagn Lab Immunol*. 2001; 8:58-61.
 17. Junyent M, Parnell LD, Lai CQ, Lee YC, Smith CE, Arnett DK, Tsai MY, Kabagambe EK, Straka RJ, Province M, An P, Borecki I, Ordovas JM. Novel variants at KCTD10, MVK, and MMAB genes interact with dietary carbohydrates to modulate HDL-cholesterol concentrations in the Genetics of Lipid Lowering Drugs and Diet Network Study. *Am J Clin Nutr*. 2009; 90:686-694.
 18. Sing CF, Davignon J. Role of the apolipoprotein E polymorphism in determining normal plasma lipid and lipoprotein variation. *Am J Hum Genet*. 1985; 37:268-285.
 19. Miao L, Yin RX, Huang F, Chen WX, Cao XL, Wu JZ. The effect of MVK-MMAB variants, their haplotypes and G × E interactions on serum lipid levels and the risk of coronary heart disease and ischemic stroke. *Oncotarget*. 2017; 8:72801-72817.
 20. Sun J, Qian Y, Jiang Y, Chen J, Dai J, Jin G, Wang J, Hu Z, Liu S, Shen C, Shen H. Association of KCTD10, MVK, and MMAB polymorphisms with dyslipidemia and coronary heart disease in Han Chinese population. *Lipids Health Dis*. 2016; 15:171.
 21. Wu DF, Yin RX, Cao XL, Chen WX, Aung LH, Wang W, Huang KK, Huang P, Zeng XN, Wu J. Scavenger receptor class B type 1 gene rs5888 single nucleotide polymorphism and the risk of coronary artery disease and ischemic stroke: A case-control study. *Int J Med Sci*. 2013; 10:1771-1777.
 22. Guo T, Yin RX, Lin QZ, Wu J, Shen SW, Sun JQ, Shi GY, Wu JZ, Li H, Wang YM. Polymorphism of rs873308 near the transmembrane protein 57 gene is associated with serum lipid levels. *Biosci Rep*. 2014; 34:69-81.
 23. Zhou YJ, Yin RX, Hong SC, Yang Q, Cao XL, Chen WX. Association of the HNF1A polymorphisms and serum lipid traits, the risk of coronary artery disease and ischemic stroke. *J Gene Med*. 2017; 19:UNSP e2941.
 24. Cao XL, Yin RX, Huang F, Wu JZ, Chen WX. Chromosome 9p21 and ABCA1 genetic variants and their interactions on coronary heart disease and ischemic stroke in a Chinese Han population. *Int J Mol Sci*. 2016; 17:586.
 25. Li WJ, Yin RX, Huang JH, Bin Y, Wu-Xian Chen WX, Cao XL. Association between the *PPP1R3B* polymorphisms and serum lipid traits, the risk of coronary artery disease and ischemic stroke in a southern Chinese Han population. *Nutrition & Metabolism*. 2018; 15:27.
 26. Wellcome Trust Case Control Consortium. Genome-wide association study of 14,000 cases of seven common diseases and 3,000 shared controls. *Nature*. 2007; 447:661-678.
 27. Whitworth JA. 2003 World Health Organization (WHO)/International Society of Hypertension (ISH) statement on management of hypertension. *J Hypertens*. 2003; 21:1983-1992.
 28. Zhou BF, Cooperative Meta-Analysis Group of the Working Group on Obesity in China. Predictive values of body mass index and waist circumference for risk factors of certain related diseases in Chinese adults – study on optimal cut-off points of body mass index and waist circumference in Chinese adults. *Biomed Environ Sci*. 2002; 15:83-96.
 29. Puranik R, Celermajer DS. Smoking and endothelial function. *Prog Cardiovasc Dis*. 2003; 45:443-458.
 30. Gastaldelli A, Folli F, Maffei S. Impact of tobacco smoking on lipid metabolism, body weight and cardiometabolic risk. *Curr Pharm Des*. 2010; 16:2526-2530.
 31. Hata Y, Nakajima K. Life-style and serum lipids and lipoproteins. *J Atheroscler Thromb*. 2000; 7:177-197.
 32. Barnard RJ. Effects of life-style modification on serum lipids. *Arch Intern Med*. 1991; 151:1389-1394.
 33. Ordovas JM, Shen AH. Genetics, the environment, and lipid abnormalities. *Curr Cardiol Rep*. 2002; 4:508-513.
 34. Ordovas JM, Robertson R, Cleirigh EN. Gene-gene and gene-environment interactions defining lipid-related traits. *Curr Opin Lipidol*. 2011; 22:129-136.
 35. Law SW, Lackner KJ, Fojo SS, Hospattankar A, Monge JC, Brewer HB, Jr. The molecular biology of human apoA-I, apoA-II, apoC-II and apoB. *Adv Exp Med Biol*. 1986; 201:151-162.
 36. Verdugo RA, Zeller T, Rotival M, Wild PS, Munzel T, Lackner KJ, Weidmann H, Ninio E, Tregouet DA, Cambien F, Blankenberg S, Tiret L. Graphical modeling of gene expression in monocytes suggests molecular mechanisms explaining increased atherosclerosis in smokers. *PLoS One*. 2013; 8:e50888.
 37. Bermudez OI, Velez-Carrasco W, Schaefer EJ, Tucker KL. Dietary and plasma lipid, lipoprotein, and apolipoprotein profiles among elderly Hispanics and non-Hispanics and their association with diabetes. *Am J Clin Nutr*. 2002; 76:1214-1221.
 38. Erem C, Hacıhasanoglu A, Deger O, Kocak M, Topbas M. Prevalence of dyslipidemia and associated risk factors among Turkish adults: Trabzon lipid study. *Endocrine*. 2008; 34:36-51.
 39. Slentz CA, Houmard JA, Johnson JL, Bateman LA, Tanner CJ, McCartney JS, Duscha BD, Kraus WE. Inactivity, exercise training and detraining, and plasma lipoproteins. STRRIDE: A randomized, controlled study of exercise intensity and amount. *J Appl Physiol* (1985). 2007; 103:432-442.
 40. Holleboom AG, Vergeer M, Hovingh GK, Kastelein JJ, Kuivenhoven JA. The value of HDL genetics. *Curr Opin Lipidol*. 2008; 19:385-394.
 41. Aixala M, Sarandria CN, Speroni JG. Hypocholesterolemia in hematologic neoplasms. *Sangre (Barc)*. 1997; 42:7-10. (in Spanish)
 42. Musolino C, Calabro L, Bellomo G, Cincotta M, Di Giacomo V, Pezzano C, Loteta B, Rizzo V, Guglielmo S, Alonci A. Lipid profile in hematologic neoplasms. *Recenti Prog Med*. 2002; 93:298-301. (in Italian)
 43. Naruto T. MVK gene abnormality and new approach to treatment of hyper IgD syndrome and periodic fever syndrome. *Nihon Rinsho Meneki Gakkai Kaishi*. 2007; 30:86-89. (in Japanese)
 44. Corrao G, Rubbiati L, Bagnardi V, Zamboni A, Poikolainen K. Alcohol and coronary heart disease: A meta-analysis. *Addiction*. 2000; 95:1505-1523.
 45. Brinton EA. Effects of ethanol intake on lipoproteins and atherosclerosis. *Curr Opin Lipidol*. 2010; 21:346-351.
 46. Ellison RC, Zhang Y, Qureshi MM, Knox S, Arnett DK,

- Province MA. Lifestyle determinants of high-density lipoprotein cholesterol: The National Heart, Lung, and Blood Institute Family Heart Study. *Am Heart J.* 2004; 147: 529-535.
47. Murphy AJ, Westerterp M, Yvan-Charvet L, Tall AR. Anti-atherogenic mechanisms of high density lipoprotein: Effects on myeloid cells. *Biochim Biophys Acta.* 2012; 1821:513-521.
48. Norata GD, Pirillo A, Catapano AL. HDLs, immunity, and atherosclerosis. *Curr Opin Lipidol.* 2011; 22:410-416.
49. Fogarty MP, Xiao R, Prokunina-Olsson L, Scott LJ, Mohlke KL. Allelic expression imbalance at high-density lipoprotein cholesterol locus MMAB-MVK. *Hum Mol Genet.* 2010; 19:1921-1929.

(Received June 26, 2018; Revised July 25, 2018; Accepted July 30, 2018)

Prognostic factors of daily blood examination for advanced melanoma patients treated with nivolumab

Hisako Okuhira, Yuki Yamamoto*, Yutaka Inaba, Kayo Kunimoto, Naoya Mikita, Takaharu Ikeda, Chikako Kaminaka, Yoshimi Minami, Nobuo Kanazawa, Fukumi Furukawa, Masatoshi Jinnin

Department of Dermatology, Wakayama Medical University, Wakayama, Japan.

Summary

Biomarkers to distinguish patients with advanced melanoma responsive to nivolumab are of great interest. Therefore, we examined the possibility that laboratory data of daily blood examination become novel biomarkers. Laboratory data of 16 melanoma patients who were treated with nivolumab were retrospectively analyzed. Patients were classified as responder group or non-responder group. Examined were: white blood cell count (WBC), absolute lymphocyte counts (ALC), absolute neutrophil count (ANC), absolute monocyte count (AMC), absolute eosinophil count (AEC), and absolute basophil count (ABC), as well as levels of lactate dehydrogenase (LDH), C-reactive protein (CRP), one hour value of erythrocyte sedimentation rate (ESR), and 5-S-cysteinydopa (5-S-CD). Responder group showed significantly higher baseline levels of ESR or CRP and significantly lower ALC level before nivolumab treatment. Additionally, nivolumab treatment decreased the levels of CRP, ESR, and ANC, while it increased ALC level in the responder group. CRP was the most effective in distinguishing responder group from non-responder group both before and during treatment, according to the receiver operating characteristic (ROC) curve. We firstly showed that ESR is also the baseline biomarker of the efficacy of nivolumab. Furthermore, we confirmed that CRP is useful to predict the efficacy both before and during the treatment, and suggested that CRP is the most effective biomarker among daily blood examination by using ROC curve analysis. There is a possibility that nivolumab treatment may be more effective for malignant melanoma with stronger inflammation.

Keywords: Absolute lymphocyte counts, absolute neutrophil counts, biomarker, malignant melanoma, PD-1

1. Introduction

Until recently, dacarbazine chemotherapy was mainly used for treatment of advanced malignant melanoma. Its effect was limited; however, the five-year survival rate was around 10% (1). In 2014, anti-programmed cell death protein 1 (PD-1) monoclonal antibody, nivolumab, was released in Japan, ahead of other countries. PD-1

is an immunosuppressive receptor belonging to the CD28 family and expressed on activated T cells to suppress T cell proliferation and effector function (2). An immune checkpoint, PD-1 is thought to play an important role in controlling adaptive immune response under physiological conditions (3). Nivolumab has been utilized for the treatment of advanced malignant melanoma and improves median overall patient survival. According to NCCN guideline version 2018, the combination of anti-PD-1 antibodies (nivolumab/pembrolizumab) or immunecheckpoint inhibitors (nivolumab/ipilimumab) is recommended as the first line immunotherapy for metastatic/unresectable melanoma. Nivolumab has also become available for non-small cell lung carcinoma (4,5), renal cell carcinoma (6), Hodgkin's lymphoma (7), squamous cell carcinoma of the head and

Released online in J-STAGE as advance publication August 29, 2018.

*Address correspondence to:

Dr. Yuki Yamamoto, Department of Dermatology, Wakayama Medical University, 811-1 Kimiidera, Wakayama 641-0012, Japan.

E-mail: yukiy@wakayama-med.ac.jp

neck (8), and will be used for treatment of additional cancers in the future.

On the other hand, in patients with advanced stage melanoma, objective response rates of nivolumab were 43.7% and median progression-free survival was 6.9 months (9). Overall mortality and recurrence rates, however, remain high in the patients treated with immune checkpoint inhibitors. There is great interest in identifying biomarkers that will allow the selection of patients who would respond to nivolumab because of the associated substantial side effects and treatment costs. We therefore examine the possibility of daily blood examination laboratory data as new biomarkers.

2. Materials and Methods

2.1. Patient material

Enrolled in this study were sixteen patients with unresectable malignant melanoma, who were treated with nivolumab in Department of Dermatology, Wakayama Medical University, between September 2014 and March 2017. Excluded were patients with single nivolumab treatment and those with inflammatory diseases, such as rheumatoid arthritis, which could affect laboratory data. Nivolumab dose was fixed at 2 mg/kg every three weeks in 13 patients or 3 mg/kg every two weeks in the remaining three patients.

Patient characteristics are summarized in Table 1. Mean age was 71.3 years (range, 48-87), and 43.8% ($n = 7$) were male. Performance status (PS) was 0 to 1 in 93.8% ($n = 15$) of patients, while 56.3% ($n = 9$) of patients had stage IV disease. According to Curtin classification (10), clinical subtypes of primary lesions were as follows: 43.8% ($n = 7$) of mucosal melanoma, 25% ($n = 4$) of acral melanoma, 18.8% ($n = 3$) of melanoma arising from non-chronically sun-damaged (non-CSD), 6.3% ($n = 1$) of melanoma arising from chronically sun-damaged (CSD), and 6.3% ($n = 1$) of unknown. Metastasis was found in lymph node ($n = 10$, 62.5%), lung ($n = 5$, 31.3%), skin ($n = 3$, 18.8%), mesenterium ($n = 3$, 18.8%), liver ($n = 2$, 12.5%), digestive tract ($n = 2$, 12.5%), or other sites (bone, brain, kidney and adrenal glands). As prior treatment, primary lesions were surgically removed in 81.3% patients ($n = 13$). Additional treatment, including dacarbazine chemotherapy ($n = 7$, 43.8%), interferon (IFN)- β local injection ($n = 2$, 12.5%), and radiotherapy, ($n = 2$, 12.5%) was performed in 50% ($n = 8$) of patients.

2.2. Clinical assessment

Response assessment based on response evaluation criteria in solid tumor (RECIST) v1.1 was performed, and patients were classified into responder groups (Partial Response: PR) + Stable Disease: SD) or non-responder groups (Progressive Disease: PD). Laboratory data in

Table 1. Clinical features of 16 melanoma patients treated with nivolumab

Factor/Category	<i>n</i> (%)
Age	
< 65	5 (31.3)
≥ 65	11 (68.8)
Median age (range)	71.3 (48-87)
Gender	
Male	7 (43.8)
Female	9 (56.3)
Stage	
III	7 (43.8)
IV	9 (56.3)
ECOG performance status	
0	14 (87.5)
1	1 (6.3)
2	1 (6.3)
3	0 (0)
4	0 (0)
Primary lesion	
Mucosal	7 (43.8)
Acral	4 (25.0)
non-CSD	3 (18.8)
CSD	1 (6.3)
Unknown	1 (6.3)
Prior therapy	
Surgery	13 (81.3)
Chemotherapy	7 (43.8)
Adjuvant IFN- β (local injection)	2 (12.5)
Radiotherapy	2 (12.5)

ECOG: Eastern Cooperative Oncology Group, Non-CSD: melanoma arising from non-chronically sun-damaged, CSD: melanoma arising from chronically sun-damaged, IFN- β : interferon- β .

this study was obtained before nivolumab treatment and approximately one month before first imaging assessment (average 77.4 days after first administration of nivolumab). Examined were: white blood cell count (WBC, by electric resistance method), absolute lymphocyte counts (ALC, by flow cytometry method), absolute neutrophil count (ANC, by flow cytometry method), absolute monocyte count (AMC, by flow cytometry method), absolute eosinophil count (AEC, by flow cytometry method), and absolute basophil count (ABC, by flow cytometry method), as well as levels of lactate dehydrogenase (LDH, by JSCC standardization compliance law), C-reactive protein (CRP, by latex immunization turbidity method), one hour value of erythrocyte sedimentation rate (ESR, by light beam detection method), and 5-S-cysteinydopa (5-S-CD, by HPLC method). This study protocol was approved by the Wakayama Medical University Ethical Committee.

2.3. Statistical analysis

Statistics were calculated using single-factor analysis of variance (ANOVA) and repeated measure ANOVA for comparison of median. $p < 0.05$ was considered statistically significant. Receiver operating characteristic (ROC) curve analysis was also performed using GraphPad Prism software®.

3. Results

3.1. Side effects and clinical responses

Immunology-related adverse events that occurred in our patients were as follows: vitiligo ($n = 3$), psoriaform rash ($n = 2$), interstitial pneumonia ($n = 1$, grade 3), hypothyroidism ($n = 1$, grade 2), thrombocytopenia ($n = 1$, grade 3), stomatitis ($n = 1$, grade 3), and nausea ($n = 1$, grade 3). Laboratory data abnormalities including liver enzymes and renal function were also found, although they were all grade 1 and asymptomatic. In three patients, nivolumab administration was discontinued after experience of grade 3 interstitial pneumonia, grade 2 hypothyroidism, or grade 3 nausea.

The best response rates were PD in nine patients (56.3%), SD in five patients (31.3%) and PR in two patients (12.5%). Most patients showed no change in the response after the first evaluation, except for one patient whose response changed from SD into PD after about one year.

3.2. Baseline levels of candidates for biomarkers

First, we examined whether baseline laboratory data before treatment can predict response to nivolumab. Blood counts, LDH, CRP, ESR, and 5-S-CD were regarded as candidates. Patients were classified into responder groups (PR+SD) and non-responder groups (PD), according to RECIST v1.1. In the responder

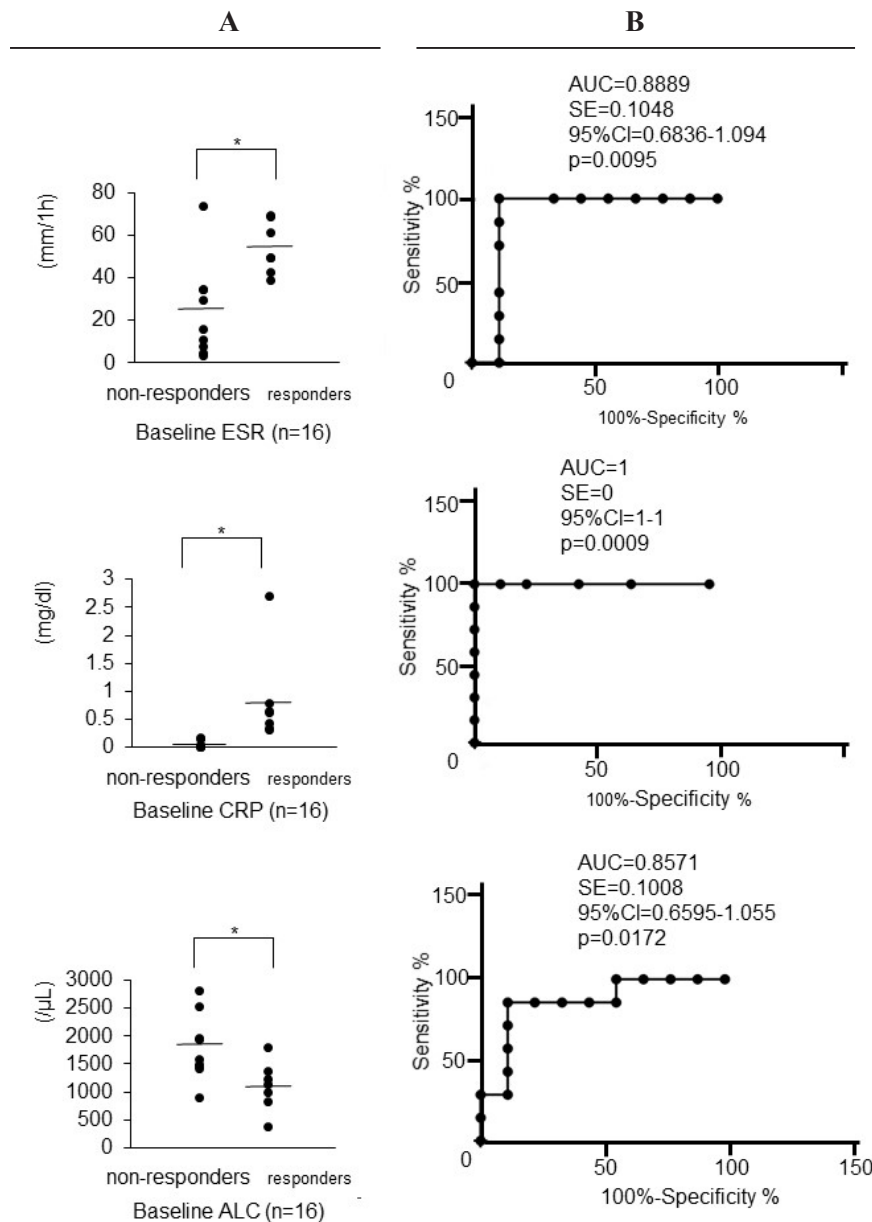


Figure 1. Baseline levels of candidates for biomarkers. (A) Baseline levels of ESR, CRP, and ALC were compared between responders (PR+SD) and non-responders (PD). Bars show means. $*p < 0.05$. (B) Receiver operating characteristic (ROC) curve for each laboratory data to distinguish responders from non-responders. AUC: areas under curves, SE: standard error, CI: confidence interval.

Table 2. Baseline levels of candidates for biomarkers in responders (PR+SD) and non-responders (PD)

Items	responders (<i>n</i> = 7)	non-responders (<i>n</i> = 9)	<i>p</i>
WBC [μ L]	5,620	5,190	0.552
ALC [μ L]	1,110	1,800	0.023*
ANC [μ L]	3,930	2,940	0.098
AMC [μ L]	359	312	0.444
AEC [μ L]	158	114	0.727
ABC [μ L]	22.9	24.4	0.932
LDH [IU/L]	211	196	0.595
CRP [mg/dL]	0.835	0.058	0.014*
ESR [mm/1h]	54.7	24.2	0.006*
5-S-CD [nmol/L]	11.0	17.2	0.213

WBC: white blood cell, ALC: absolute lymphocyte counts, ANC: absolute neutrophil count, AMC: absolute monocyte count, AEC: absolute eosinophil count, ABC: absolute basophil count, LDH: lactate dehydrogenase, CRP: C-reactive protein, ESR: erythrocyte sedimentation rate one hour value, 5-S-CD: 5-S-cysteinindopa. Mean values of each laboratory data are shown. **p* < 0.05.

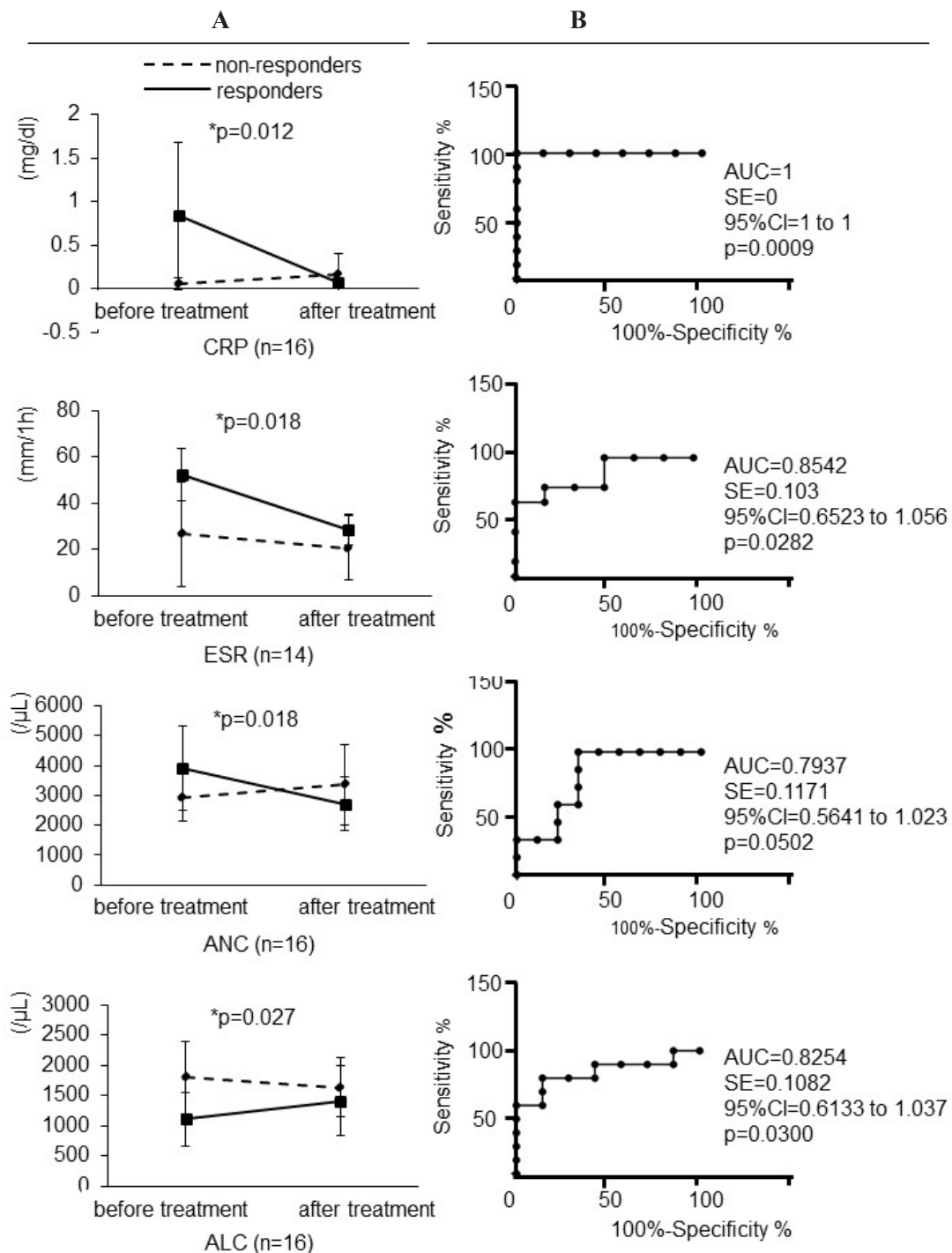


Figure 2. Changes of candidates for biomarkers before and during nivolumab treatment. (A) Graphs show mean \pm standard deviation. **p* < 0.05. **(B)** Receiver operating characteristic (ROC) curve for each laboratory data to distinguish responders (PR+SD) from non-responders (PD). AUC: areas under curves, SE: standard error, CI: confidence interval.

group, we found significantly higher ESR level ($p = 0.006$), higher CRP level ($p = 0.014$), and lower ALC level ($p = 0.023$), compared with non-responder group (Figure 1, left). There were no other significant differences between these groups (Table 2).

We then performed ROC curve analysis to compare the clinical usefulness of above baseline biomarkers for nivolumab treatment (Figure 1, right). Areas under curve (AUC) of baseline ESR, CRP, or ALC were 0.89 (95% CI, 0.68 to 1.09), 1.00 (95% CI, 1.00 to 1.00) or 0.86 (95% CI, 0.66 to 1.06), respectively. AUC of baseline CRP level was higher than those of other markers.

3.3. Changes of levels of biomarker candidates in the responder group during treatment

Increase or decrease of candidate levels after nivolumab treatment as novel biomarkers for response rate prediction were then evaluated. Laboratory data was obtained approximately one month before the first

imaging assessments. In the responder group (PR+SD), there were significant differences in the levels of CRP, ESR, ANC, and ALC; ALC levels were significantly increased, while other levels were decreased after nivolumab treatment compared with the baseline ($p = 0.027, 0.012, 0.018, \text{ and } 0.018$, respectively) (Figure 2, left). Changes of other laboratory data are shown in Table 3.

In ROC curve analysis, AUC of CRP, ESR, ANC, or ALC was 1.00 (95% CI, 1.00 to 1.00), 0.85 (95% CI, 0.65 to 1.06), 0.79 (95% CI, 0.56 to 1.02), or 0.83 (95% CI, 0.61 to 1.04), respectively (Figure 2, right). Accordingly, AUC for CRP level was higher than those for the other biomarkers.

3.4. Case presentation of a representative patient

In a patient with typical PR course, baseline ESR levels and CRP levels were elevated, and ALC level was reduced before nivolumab treatment (Figure 3A). After

Table 3. Changes of values of candidates for biomarkers in responders (PR+SD) and non-responders (PD)

Items	responders		non-responders		p
	before treatment	during treatment	before treatment	during treatment	
WBC [μL]	5,620 (n = 7)	4,680	5,190 (n = 9)	5,570	0.105
ALC [μL]	1,110 (n = 7)	1,410	1,800 (n = 9)	1,640	0.027*
ANC [μL]	3,930 (n = 7)	2,720	2,940 (n = 9)	3,350	0.018*
AMC [μL]	359 (n = 7)	319	312 (n = 9)	333	0.421
AEC [μL]	158 (n = 7)	169	114 (n = 9)	222	0.242
ABC [μL]	22.9 (n = 7)	61.4	24.4 (n = 9)	25.6	0.123
LDH [IU/L]	211 (n = 7)	181	197 (n = 9)	211	0.073
CRP [mg/dL]	0.835 (n = 7)	0.07	0.058 (n = 9)	0.16	0.012*
ESR [mm/1h]	52.2 (n = 6)	28.5	26.6 (n = 8)	20.6	0.018*
5-S-CD [nmol/L]	17.5 (n = 2)	6.85	14.7 (n = 5)	24.8	0.080

WBC: white blood cell, ALC: absolute lymphocyte counts, ANC: absolute neutrophil count, AMC: absolute monocyte count, AEC: absolute eosinophil count, ABC: absolute basophil count, LDH: lactate dehydrogenase, CRP: C-reactive protein, ESR: erythrocyte sedimentation rate (one hour value), 5-S-CD: 5-S-cysteinyl-dopa. Mean values of each laboratory data are shown. * $p < 0.05$.

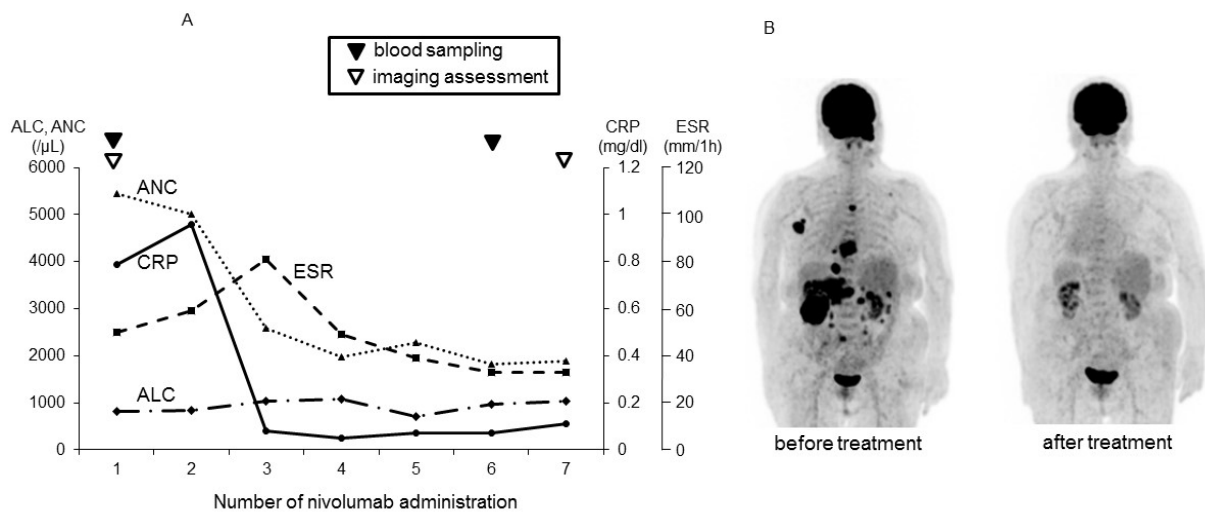


Figure 3. Case presentation of a patient with typical PR course. (A) ESR, CRP, ANC, and ALC levels before and during nivolumab treatment. Black arrowheads indicate the timing of blood sampling, and while arrowheads indicate the timing of imaging assessment. **(B)** PET imaging before and during treatment. After seven nivolumab treatments, the primary tumor of left buccal mucosa and metastatic lesions showed almost complete remission.

five courses of nivolumab, levels of CRP, ESR, and ANC were decreased, and ALC level was increased from the baseline. Positron emission tomography (PET) imaging showed the patient's tumor was markedly diminished by nivolumab (Figure 3B).

4. Discussion

Predictive biomarkers for the efficacy of nivolumab treatment against malignant melanoma have been investigated vigorously in recent years. For example, soluble CD73 levels (11) or Th9 cell number (12) in peripheral blood, expression levels of PD-L1 (13) or MHC-II (14) in tumor cells, as well as number of CD8 positive T cells (15) or specific inflammation and IFN- γ related mRNA-based signatures in infiltrating immune cells have been reported as clinically useful biomarkers. Furthermore, Nakamura *et al.* described serum LDH and CRP levels to be baseline prognostic markers in patients with advanced melanoma treated with nivolumab (16). They also indicated that patients with increased ALC and decreased ANC during nivolumab therapy had significantly better overall survival.

In this study, we determined the possibility that treatment efficacy of nivolumab can be predicted by daily blood examination. Responder group showed significantly higher baseline levels of ESR or CRP and significantly lower ALC level before the nivolumab treatment. In addition, nivolumab treatment decreased the levels of CRP, ESR, and ANC, while it increased ALC level in responder group. According to the ROC curve, CRP was most effective of these to distinguish responder group from non-responder group both before and during treatment. Patients with elevated baseline CRP levels before treatment will respond to nivolumab, and normalization of the elevated CRP by nivolumab indicates that the patients are the responder before the first imaging assessment.

Taken together, we firstly reported ESR is also the baseline biomarker of the efficacy of nivolumab. We confirm that CRP is also useful to predict efficacy both before and during treatment. CRP is suggested to be the most effective biomarker in daily blood examination using ROC curve analysis. There is a possibility that inflammation responses, reflected by elevated CRP and ESR, may be activated in the responder group before nivolumab treatment, and they are normalized during the treatment. Nivolumab treatment may therefore be more effective for malignant melanoma with strong inflammation.

Link between inflammation and cancer has been reported for over 150 years. Virchow firstly reported the association by observing white blood cells around the cancer cells in 1881 (17). Increased CRP has been reported to be an independent prognostic marker for malignant melanoma (18), correlating with the number of lymph node metastases (19). Indication of

the association of elevated ESR with short survival has also been reported (20). PD-1 is expressed on effector T cells only after an immune response, such as infection or inflammation (15). Especially, its expression is especially remarkable on effector T cells invading the peripheral inflamed tissues. The extent of the immune response against malignant tumors usually varies depending on general condition of the patients or type of malignant tumors. Considering the inflammatory markers (CRP and ESR) in the responder group were higher before treatment, these patients have more baseline PD-1 expression due to strong immune response. Our study also suggests the synergistic effect of nivolumab therapy combined with existing treatments that causes inflammation (such as IFN- β local injection or radiation therapy).

Our study also showed increased ALC and decreased ANC levels during nivolumab therapy correlated with the better response. Neutrophil-lymphocyte ratio (NLR) is a known marker of systemic host inflammation, and it is reported that the increased NLR is associated with poor prognosis in several malignant tumors, including malignant melanoma (21,22), consistent with the previous paper and current study. On the other hand, lower baseline ALC before the treatment in the responder group, which was found in this study, is contradictory to this hypothesis, and may be because of the small number of patients. As the limitation, this study is retrospective study of only 16 patients. For earlier and more efficient prediction of the efficacy, the clinical significance of the combination of levels of CRP/ESR and other inflammatory markers should be evaluated in larger number of patients.

References

1. Garbe C, Eigenhler TK, Keiljolz U, Hauschild A, Kirkwood JM. Systematic review of medical treatment in melanoma: Current status and future prospects. *Oncologist*. 2011; 16:15-24.
2. Freeman GJ, Long AJ, Iwai Y, *et al.* Engagement of the PD-1 immunoinhibitory receptor by a novel B7 family member leads to negative regulation of lymphocyte activation. *J Exp Med*. 2000; 192:1027-1034.
3. Seidel JA, Otsuka A, Kabashima K. Treating tumors with immune checkpoint inhibitors: Rationale and limitations. *Trends in Immunotherapy*. 2017; 1:2-9.
4. Kazandjian D, Suzman DL, Blumenthal G, Mushti S, He K, Libeg M, Keegan P, Pazdur R. FDA approval summary: Nivolumab for the treatment of metastatic non-small cell lung cancer with progression on or after platinum-based chemotherapy. *Oncologist*. 2016; 21:634-642.
5. Borghaei H, Paz-Ares L, Horn L, *et al.* Nivolumab versus docetaxel in advanced nonsquamous non-small-cell lung cancer. *N Engl J Med*. 2015; 373:1627-1639.
6. Motzer RJ, Escudier B, McDermott DF, *et al.* Nivolumab versus everolimus in advanced renal-cell carcinoma. *N Engl J Med*. 2015; 373:1803-1813.
7. Younes A, Santoro A, Shipp M, *et al.* Nivolumab for

- classical Hodgkin's lymphoma after failure of both autologous stem-cell transplantation and brentuximab vedotin: A multicentre, multicohort, single-arm phase 2 trial. *Lancet Oncol.* 2016; 17:1283-1294.
8. Ferris RL, Blumenschein G Jr, Fayette J, *et al.* Nivolumab for recurrent squamous-cell carcinoma of the head and neck. *N Engl J Med.* 2016; 375:1856-1867.
 9. Larkin J, Chiarion-Sileni V, Gonzalez R, *et al.* Combined nivolumab and ipilimumab or monotherapy in untreated melanoma. *N Engl J Med* 2015; 373:23–34.
 10. Curtin JA, Fridlyand J, Kageshita T, Patel HN, Busam KJ, Kutzner H, Cho KH, Aiba S, Bröcker EB, LeBoit PE, Pinkel D, Bastian BC. Distinct sets of genetic alterations in melanoma. *N Engl J Med.* 2005; 353: 2135-2147.
 11. Morello S, Capone M, Sorrentino C, Giannarelli D, Madonna G, Mallardo D, Grimaldi AM, Pinto A, Ascierto PA. Soluble CD73 as biomarker in patients with metastatic melanoma patients treated with nivolumab. *J Transl Med.* 2017; 15:244.
 12. Nonomura Y, Otuka A, Nakashima C, *et al.* Peripheral blood Th9 cells are a possible pharmacodynamic biomarker of nivolumab treatment efficacy in metastatic melanoma patients. *Oncoimmunology.* 2016; 5:e1248327.
 13. Gandini S, Massi D, Mandala M. PD-L1 expression in cancer patients receiving anti PD-1/PD-L1 antibodies: A systematic review and meta-analysis. *Crit Rev Oncol Hematol.* 2016; 100:88-98.
 14. Johnson DB, Estrada MV, Salgado R, *et al.* Melanoma-specific MHC-II expression represents a tumour-autonomous phenotype and predicts response to anti-PD-1/PD-L1 therapy. *Nat Commun.* 2016; 7:10582.
 15. Erdag G, Schaefer JT, Smolkin ME, Deacon DH, Shea SM, Dengel LT, Patterson JW, Slingluff CL Jr. Immunity and immunohistologic characteristics of tumor-infiltrating immune cells are associated with clinical outcome in metastatic melanoma. *Cancer Res.* 2012; 72:1070-1080.
 16. Nakamura Y, Kitano S, Takahashi A, Tsutsumida A, Namikawa K, Tanese K, Abe T, Funakoshi T, Yamamoto N, Amagai M, Yamazaki N. Nivolumab for advanced melanoma: Pretreatment prognostic factors and early outcome markers during therapy. *Oncotarget.* 2016; 7:77404-77415.
 17. Virchow R. An address on the value of pathological experiments. *Br Med J.* 1881; 2:198-203.
 18. Fang S, Wang Y, Sui D, *et al.* C-reactive protein as a marker of melanoma progression. *J Clin Oncol.* 2015; 33:1389-1396.
 19. Neuss H, Koplín G, Raue W, Reetz C, Mall JW. Analysing the serum levels of tumour markers and primary tumour data in stage III melanoma patients in correlation to the extent of lymph node metastases – a prospective study in 231 patients. *Acta Chir Belg.* 2011; 111:214-218.
 20. Tas F, Erturk K. Elevated erythrocyte sedimentation rate is associated with metastatic disease and worse survival in patients with cutaneous malignant melanoma. *Mol Clin Oncol.* 2017; 7:1142-1146.
 21. Lino-Silva LS, Salcedo-Hernández RA, García-Pérez L, Meneses-García A, Zepeda-Najar C. Basal neutrophil-to-lymphocyte ratio is associated with overall survival in melanoma. *Melanoma Res.* 2017; 27:140-144.
 22. Templeton AJ, Knox JJ, Lin X, *et al.* Change in neutrophil-to-lymphocyte ratio in response to targeted therapy for metastatic renal cell carcinoma as a prognosticator and biomarker of efficacy. *Eur Urol.* 2016; 70:358-364.

(Received July 9, 2018; Revised August 14, 2018; Accepted August 17, 2018)

Children with *GJB2* gene mutations have various audiological phenotypes

Xianlei Wang¹, Lihui Huang^{1,*}, Xuelei Zhao¹, Xueyao Wang¹, Xiaohua Cheng¹, Yating Du², Dongxin Liu¹

¹ Beijing Tongren Hospital, Capital Medical University; Beijing Institute of Otolaryngology; Key Laboratory of Otolaryngology, Head and Neck Surgery, Ministry of Education, Beijing, China;

² Department of Anesthesiology, Peking University First Hospital, Beijing, China.

Summary

The current study retrospectively investigated variations in audiological phenotypes in children with *GJB2* gene mutations. Subjects were 128 infants and young children who were seen as outpatients by Otolaryngology at Beijing Tongren Hospital from 2012 to 2018. Of the 128 subjects, 99 had biallelic truncating (T/T) mutations and 29 had truncating/nontruncating (T/NT) mutations. Genotypes, results of universal newborn hearing screening (UNHS), and the degree and symmetry of hearing loss were examined in the two groups. Twenty-two subjects (20.37%, 22/128) passed UNHS, including 13 children with T/T mutations and 9 with T/NT mutations. Of the 128 subjects, 22 had normal hearing, 2 had unilateral hearing loss, and 115 had bilateral hearing loss. Severe-to-profound hearing loss was the most prevalent phenotype in children with T/T mutations (73.23%), while normal hearing was prevalent in children with T/NT mutations (41.38%). Symmetrical hearing loss was the main phenotype in both groups, and the number of subjects with symmetrical hearing loss did not differ significantly between the two groups. Therefore, children with *GJB2* gene mutations have phenotypic variability in terms of their results of UNHS and their degree and symmetry of hearing loss. Subjects with T/NT mutations of the *GJB2* gene were more likely to pass UNHS and had milder hearing loss compared to those with T/T mutations. Symmetrical hearing loss was the main phenotype in the two groups, but 36.53% of children had bilateral asymmetric hearing loss. Parents of all subjects with sensorineural hearing loss were informed that their children may have a *GJB2* mutation.

Keywords: *GJB2* gene, screening, Genotype

1. Introduction

Hearing loss is the most common congenital sensory disorder, with studies describing an incidence of neonatal congenital deafness of approximately 0.1-0.3%, 50% of which is caused by genetic factors (1). Hereditary deafness is divided into nonsyndromic hearing loss

(NSHL) and syndromic hearing loss (SHL).

The *GJB2* gene that encodes connexin26 (Cx26) is the gene that most often causes NSHL (2). There are ethnic differences in *GJB2* gene mutations. In Caucasians in Europe and the US, c.35delG is the most common mutation (3), while c.235delC is most commonly found in Chinese with an allele frequency of approximately 11.90%, followed by c.299delAT with a frequency of approximately 2.22%, c.176del16 with a frequency of approximately 0.65%, and c.35delG with a frequency of approximately 0.27% (4). A recent study been found that the p.V37I mutation is also highly prevalent in Chinese, with a carrier frequency of 6.2% (5).

GJB2-associated hearing loss can result in congenital severe-to-profound bilateral hearing loss, and the severity of hearing loss guides the clinical management

Released online in J-STAGE as advance publication August 27, 2018.

*Address correspondence to:

Dr. Lihui Huang, Beijing Tongren Hospital, Capital Medical University; Beijing Institute of Otolaryngology; Key Laboratory of Otolaryngology, Head and Neck Surgery, Ministry of Education, No.17 Hougou Lane, Chongnei Street, Beijing 100005, China.

E-mail: huangpub@126.com

of a mutation (6). There has been a growing recognition of phenotypic diversity associated with various *GJB2* genotypes. The degree of *GJB2*-associated hearing loss depends on the degree of damage to the coding protein connexin26. Truncating mutations, which create a premature stop codon and result in the absence of any functional connexin 26 protein, constitute nonsense mutations. The functions of nontruncating mutations, which result in altered proteins that may or may not be impaired, constitute missense mutations. Most *GJB2* gene mutations can be classified as truncating mutations (T) and nontruncating mutations (NT). Snoeckx *et al.* studied patients ages 0-26 with *GJB2* biallelic alleles; the most common mutation was c.35delC and the degree of hearing loss was related to the genotype (7). In those patients, the degree of hearing loss was most severe with a T/T mutation, followed by a T/NT mutation and an NT/NT mutation. In a previous study of *GJB2* mutations among Chinese ages 0-68, Dai *et al.* found that the degree of hearing loss was mild-to-profound and proposed detection of the *GJB2* gene for all patients with sensorineural hearing loss (8).

As a result of the promotion of "newborn screening for deafness genes," many patients with *GJB2*-associated hearing loss have been identified at a young age. Therefore, one aim of the current study was to classify children with *GJB2*-associated hearing loss depending on mutations in that gene. A second aim of this study was to examine genotypes, the results of universal newborn hearing screening (UNHS), and the degree of hearing loss in order to provide a basis for clinical genetic counseling.

2. Materials and Methods

Written informed consent was obtained from parents of all subjects. This study was in accordance with the principles of the Declaration of Helsinki and it was approved by the Ethics Committee of Beijing Tongren Hospital, Capital Medical University.

2.1. Subjects

Subjects were 128 children with *GJB2*-associated hearing loss who were seen by Otolaryngology and Head and Neck Surgery at Tongren Hospital (Beijing, China) between 2012 and 2018. All subjects were screened for nine loci in four genes, including *GJB2* c.235delC, c.299delAT, c.176delI6, and c.35delG; *GJB3* c.538C>T; *SLC26A4* c.IVS7-2A>G and c.2168A>G; and mitochondrial *12S rRNA* m.1555A>G and m.1494C>T. Subjects with *GJB2* heterozygous mutations were screened for all exons and flanking splice sites of the *GJB2* gene. Exclusion criteria were as follows: carriers of *GJB3* c.538C>T, *SLC26A4* c.IVS7-2A>G, or c.2168A>G, or mitochondrial *12S rRNA* m.1555A>G or m.1494C>T mutations; familial

segregation of hearing loss in an autosomal dominant, maternally transmitted, or X-linked manner; and individuals with syndromic hearing loss, conductive deafness, or secretory otitis media. Based on *GJB2* gene mutations, the subjects were divided into two groups, those with biallelic truncating (T/T) mutations and those with compound heterozygous truncating/nontruncating (T/NT) mutations.

2.2. Clinical evaluation

The following demographic information was collected for each subject: sex, date of birth and birth history, date of initial otolaryngological consultation, and major comorbidities.

2.3. DNA analysis

Genomic DNA was extracted from 2 mL of whole blood from each subject using the Blood DNA kit (Tiangen Biotech, Beijing, China). All exons and flanking splice sites of the *GJB2* genes were screened for mutations through amplification with PCR and bidirectional sequencing.

2.4. Auditory evaluation

Subjects underwent universal newborn hearing screening and a physical examination, including an otoscopic examination, with special attention to hearing. Comprehensive audiological evaluation included auditory brainstem response (ABR), 40-Hz auditory event-related potential, distortion product otoacoustic emission, auditory steady-state response (ASSR), acoustic immittance, and pediatric behavioral audiometry. The hearing threshold was calculated as the average hearing level at 0.5, 1.0, 2.0, and 4.0 kHz according to the 1997 standards of the World Health Organization. The severity of hearing impairment was defined as mild (26-40 dB), moderate (41-60 dB), severe (61-80 dB), or profound (> 80 dB). Owing to the subjects' young age, the ABR threshold and/or ASSR were recorded, and mean thresholds at frequencies in the 0.5-4 kHz range were averaged to obtain an approximation for directional conditioned reflex. For children lacking behavioral thresholds and ASSR results, the ABR threshold was considered the high-frequency auditory threshold (9,10). Subjects with normal hearing and unilateral hearing loss were excluded, and asymmetrical hearing loss was defined as a difference in HL > 10 dB between the ears for at least two frequencies (11).

2.5. Statistical analysis

The statistical software SPSS21.0 was used to analyze data with the chi-squared (χ^2) test.

3. Results

3.1. Demographics

Of the 128 children, 59.37% were male and 40.63% were female. Subjects ranged in age from 4 to 112 months (mean, 44.13 ± 23.59 months). Ninety-one percent of subjects ranged in age from 4-72 months. The age at first visit ranged from 2 to 83 months (mean, 10.52 ± 14.59 months). Table 1 shows the clinical characteristics of the two groups. All subjects were Chinese.

3.2. Genetic testing

The 128 subjects had a total of 9 mutations that were grouped into 14 genotypes. Of the 9 mutations, 5 were truncating mutations and 4 were nontruncating mutations. The most common mutation locus was c.235delC at a frequency of 63.67%. c.299delAT was found at a frequency of 19.92% and c.109G>A was found at a frequency of 8.99%. Five infrequent mutations were identified, including c.230G>A, c.257C>G, c.427C>T, c.583A>G, and c.9G>A. Of the 14 genotypes, 7 were found in children with T/

Table 1. Comparison of basic parameters of the two groups (n = 128 newborns)

group	Number	Sex: male/female	Age (months): Range (Mean)	Age at first visit (months): Range (Mean)
T/T	99	55/44	4-112 (45.44 ± 23.15)	2-77 (9.85 ± 12.81)
T/NT	29	21/8	9-112 (39.62 ± 24.92)	2-83 (10.66 ± 16.07)
Total	128	76/52	4-112 (44.13 ± 23.59)	2-83 (10.52 ± 14.59)

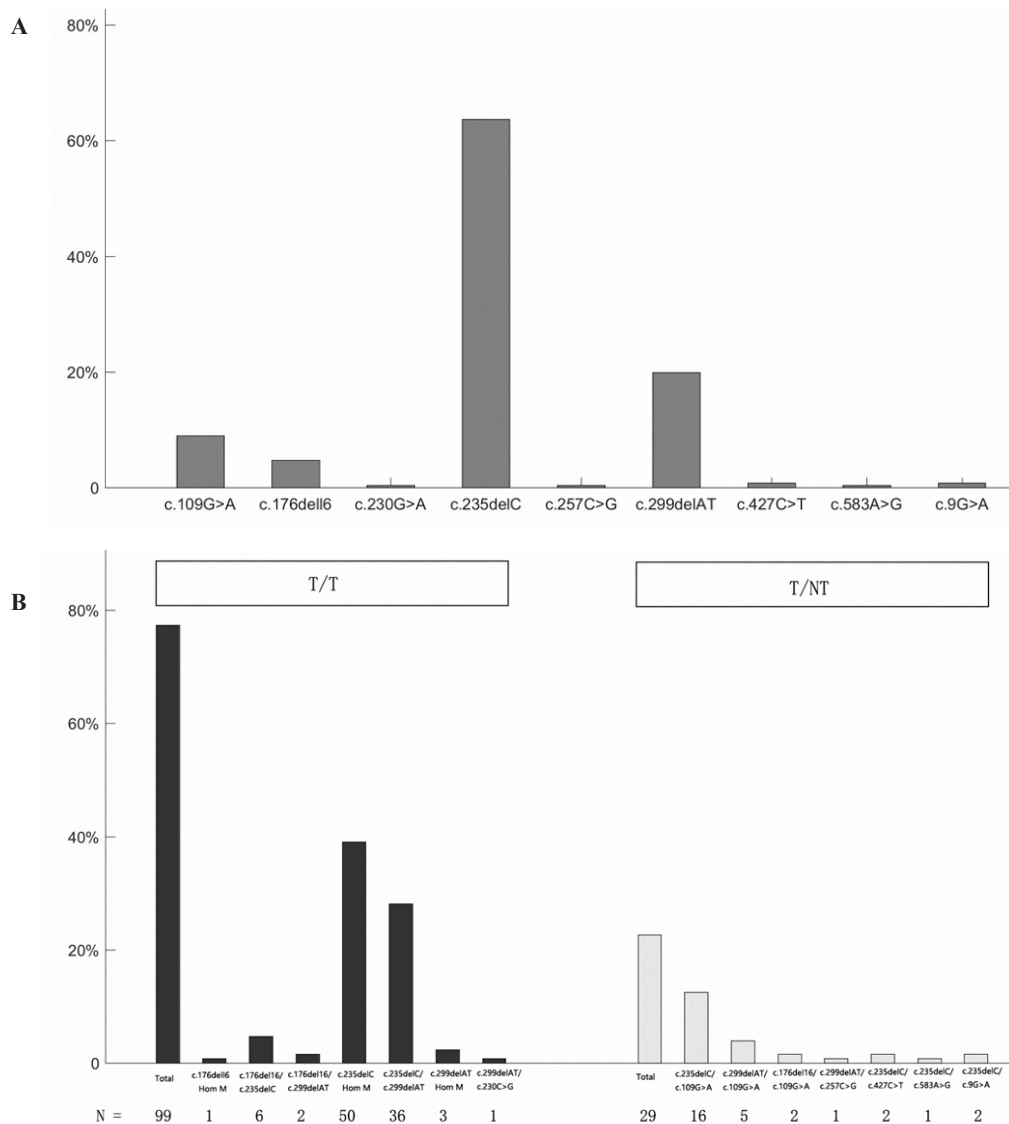


Figure 1. Results of genetic testing of subjects. (A) In total, 9 mutations were found in subjects. **(B)** Subjects had 14 genotypes, including 7 in children with T/T mutations and 7 in children with T/NT mutations. The number of subjects is shown under each subgroup. Hom M: homozygous mutation; CHM: compound heterozygous mutations.

T mutations and 7 were found in children with T/NT mutations. c.235delC Hom M was the most common genotype in children with T/T mutations (39.06%). In children with T/NT mutations, c.109G>A /c.235delC CHM was the most common genotype with a frequency of 12.50% (Figure 1).

3.3. Phenotype and UNHS

Table 2 shows the comparison of the results of UNHS for the two groups. In UNHS, 106 subjects had normal hearing, including 96 with bilateral normal hearing and 10 with unilateral passing results, whereas 22 passed UNHS. In UNHS, most subjects in both groups had bilateral normal hearing; this was true for 81.82% of children with T/T mutations and 51.72% of children with T/NT mutations (Table 2). Pair-wise comparisons of the two groups revealed significant differences ($\chi^2 = 26.05, P = 0.0038$). In addition, 22 subjects passed UNHS with at least one ear. Bilateral hearing loss was examined in those subjects, revealing 18 children with T/T mutations and 4 with T/NT mutations. In addition, 3 children with T/NT mutations were diagnosed with normal hearing in at least one ear.

3.4. Phenotype and diagnosis of audiology

3.4.1. Phenotype and the symmetrical/asymmetrical hearing loss.

Of the 128 subjects, 11 had normal hearing, 2 had

unilateral hearing loss, and 115 had bilateral hearing loss. Of subjects with bilateral hearing loss, 73 had symmetrical hearing loss and 42 had asymmetrical hearing loss. Symmetrical hearing loss was highly prevalent in children with T/T mutations (62.63%) or T/NT mutations (68.75%) (Table 3). Pair-wise comparisons of the two groups revealed no differences ($\chi^2 = 0.22, P = 0.7824$)

3.4.2. Phenotype and the degree of hearing loss

Of 258 ears, 24 were normal and 234 ears had sensorineural hearing loss. Normal ears were only noted in children with T/NT mutations (41.83%, 24/58), and genotypes in subjects with normal hearing were c.109A>G compound heterozygous mutations. Of the 234 ears with hearing loss, 96 had profound hearing loss, 61 had severe hearing loss, 56 had moderate hearing loss, and 19 had mild hearing loss. Profound hearing loss was the most common phenotype in children with T/T mutations with a frequency of 46.46%, following by severe hearing loss with a frequency of 36.77%. However, mild and moderate hearing loss were more often detected in children with T/NT mutations (with a respective frequency of 24.14% and 13.79%) (Table 4). Pair-wise comparisons of the two groups revealed significant differences ($\chi^2 = 131.87, P < 0.0001$). Table 5 shows the average hearing threshold for 14 genotypes in two groups. Subjects with T/T mutations had more severe hearing impairment, with an average hearing threshold of 75.40 ± 22.33

Table 2. Comparison of the results of UNHS in the two groups (n = 128 cases)

Group	Subjects undergoing UNHS (%)			χ^2	P
	Bilateral pass	Unilateral pass	Bilateral normal hearing		
T/T	13 (13.13)	5 (5.05)	81 (81.82)	26.05	0.0038
T/NT	9 (31.04)	5 (17.24)	15 (51.72)		
Total	22 (17.19)	10 (7.81)	96 (75.00)		

Table 3. Comparison of symmetrical/asymmetrical hearing loss in the two groups (n = 115 cases)

Group	Incidence of hearing loss (%)		χ^2	P
	symmetrical	asymmetrical		
T/T	62 (62.63)	37 (37.37)	0.22	0.7824
T/NT	11 (68.75)	5 (31.25)		
Total	73 (63.47)	42 (36.53)		

Table 4. Comparison of the degree of hearing loss in the two groups (n = 256 ears)

Group	The degree of hearing loss (%)					χ^2	P
	normal	moderate	mild	severe	profound		
T/T	0 (0)	11 (5.56)	42 (21.21)	53 (26.77)	92 (46.46)	26.05	0.0038
T/NT	24 (41.38)	8 (13.79)	14 (24.14)	8 (13.79)	4 (6.90)		
Total	24 (9.38)	19 (7.42)	56 (21.88)	61 (23.83)	96 (37.50)		

Table 5 Average hearing threshold for 14 genotypes (n = 256 ears)

Group	Genotype	Ear	Average hearing threshold (dB)	Average hearing threshold for the group (dB)		
T/T	c.176del16 Hom M	2	100.00 ± 0	75.40 ± 22.33		
	c.176del16 / c.235delC CHM	6	92.30 ± 11.20			
	c.176del16 / c.299delAT CHM	4	88.25 ± 11.61			
	c.235delC Hom M	100	77.99 ± 21.63			
	c.235delC / c.299delAT CHM	72	68.87 ± 22.42			
	c.299delAT Hom M	6	77.50 ± 26.91			
	c.299delAT / c.230C>G CHM	2	37.00 ± 1.14			
	T/NT	c.235delC / c.109G>A CHM	32		31.20 ± 19.87	39.69 ± 25.92
		c.299delAT / c.109G>ACHM	10		38.30 ± 15.75	
c.176del16/ c.109G>A CHM		4	38.00 ± 30.99			
c.299delAT/ c.257C>G CHM		2	56.50 ± 0.71			
c.235delC/ c.427C>T CHM		4	100.00 ± 0			
c.235delC/ c.583A>G CHM		2	52.50 ± 16.26			
c.235delC/ c.9G>A CHM		4	40.50 ± 24.02			

dB, and subjects with T/NT mutations a mean hearing threshold of 39.69 ± 25.92 dB.

4. Discussion

The *GJB2* gene is the main cause of hereditary nonsyndromic deafness, and its normal expression in the inner ear is required for normal development and signal transduction between inner ear sensory cells and supporting cells. Over 50% of cases of congenital autosomal recessive nonsyndromic deafness hearing loss (ARNSHL) are caused by mutations of the *GJB2* gene (12). The rates of *GJB2* mutation vary by country, and 21% of mutations have been found in Chinese patients (13). Therefore, *GJB2* mutations are a critical component of audiological screening and genetic counseling.

GJB2 gene mutations vary widely among ethnic groups. c.35delG is the most common variant in Caucasian populations (14). However, in Chinese populations, the c.235delC mutation has the highest prevalence (11.90%), followed by c.299delAT (2.22%), c.176del16 (0.65%), and c.35delG (0.27%) (4). Recent studies have indicated that the rate of the c.109G>A mutation is high in the Chinese population as well. Jiang *et al.* examined 155 patients with NSHL and reported that the incidence of c.109G>A was 9.03% (28/310) (15). Dai *et al.* performed genetic testing on 2,063 patients with NSHL and found that in the Chinese population the most common genotype of a *GJB2* gene mutation was c.235delC/c.235delC, followed by c.235delC/c.299delAT (16). A total of nine variants of the *GJB2* gene were detected in the current study, including c.235delC (63.67%), followed by c.299delAT (19.92%) and c.109G>A (8.99%). The most common genotype was c.235delC/c.235delC, and the c.35delG mutation was not detected. This finding is consistent with the results of previous studies. Five pathogenic variants (c.230G>A, c.257C>G, c.427C>T, c.583A>G, and c.9G>A) that had previously been reported were detected in the current study at lower rates.

Early studies suggested that hearing loss caused by *GJB2* gene mutations was mostly congenital and penetrant at birth and that the hearing phenotype was mainly bilateral, symmetrical, and moderate-to-profound SNHL. As research progressed, some researchers found that approximately 3.8-6.9% of children with *GJB2* gene mutations were able to pass UNHS, with delayed-onset hearing loss (17,18). This confirms that those patients had non-penetrance at birth to some extent. In the current study, 22 children had passing results on UNHS for both ears while 10 had passing results for one ear. Children with T/NT mutations had a significantly higher passing rate on UNHS than did children with T/T mutations. Wu *et al.* conducted hearing screening in combination with screening for deafness genes in 5,173 neonates, and they detected c.109G>A/c.109G>A mutations in 62 subjects, c.109G>A/c.235delC mutations in 16, and m.1555A>G mutations in 4. In that study, 46 subjects (56.1%) passed UNHS (19). In the current study, 109G>A compound heterozygous mutations were predominant in children with T/NT mutations, indicating that children with the c.109G>A mutation were more likely to pass UNHS. Subjects in both groups with bilateral SNHL had at least one ear that passed UNHS.

There are several possible reasons for this: (i) delayed-onset hearing loss, according to the study by Wu *et al.* The incidence of the c.109G>A mutation was 20% in children of Han nationality with delayed-onset hearing loss, and that rate was much higher than that in the normal hearing group, suggesting that this variant is associated with delayed-onset hearing loss. (ii) The results of UNHS were unreliable, to some extent, due to poor quality control during screening. A study indicated that approximately 11% to 31% of children with hearing loss who passed UNHS would eventually develop permanent hearing loss (20).

Three children (17.1%, 7/41) with T/NT mutations were referred for UNHS, and at least one ear was diagnosed with normal hearing in the current study. Li

et al. conducted genetic tests on 173 children who had been referred for UNHS and diagnosed with normal hearing (5). They detected the p.V37I mutation at a rate of 5.8% (10/173), which was much higher than the rate in children who passed UNHS (0.14%). Children with p.V37I compound heterozygous mutations may have subclinical or borderline slight hearing loss at birth. In addition to the reasons mentioned above, other causes could be that cochlear hair cells are relatively immature in some newborns or that middle ear effusion was present during UNHS, thus affecting the results of otoacoustic emissions. According, the sample size needs to be increased and an in-depth study needs to be conducted in the future.

A study found that hearing loss caused by *GJB2* gene mutations could be mild to profound and that patients with T/T mutations had a greater degree of hearing loss than patients with NT/T mutations (7). In the current study, children with T/T mutations mainly had severe-to-profound hearing loss (73.23%), while children with NT/T mutations mainly had normal hearing and mild-to-moderate hearing loss (79.31%). The severity of hearing loss differed significantly between the two groups. This finding was consistent with the results of previous studies. Chan *et al.* examined 52 children with *GJB2* gene mutations and found that the average hearing threshold was 100.3 dB in those with T/T mutations and 53.9 dB in those with NT/T mutations (6). In the current study, the average hearing threshold was 75.40 ± 22.33 dB in children with T/T mutations and 39.69 ± 25.92 dB in children with NT/T mutations. Both numbers were both lower than those reported by Chan *et al.* This may be due to differences in research methodologies, ethnicity, or age distribution. The subjects in the study by Chan *et al.* included Caucasians, Latinos, and Asians with an average age of 5.6 years, and the c.35delG mutation was common. However, the subjects in the current study were Chinese Han children with an average age of 3.7 years, and the c.235delC mutation was common. In the current study, the average age of enrollment was lower than that used by Chan *et al.* Therefore, patients with *GJB2* gene mutations could have progressive hearing loss (21,22), and the average hearing thresholds of the two groups in the current study were lower than those cited in the previous study by Chan *et al.* Dai *et al.* found that the *GJB2* mutation was detected at a higher rate in patients with bilateral SNHL and at a lower rate in patients with unilateral hearing loss.

Of the 117 subjects with hearing loss in this study, 2 had unilateral hearing loss and 115 had bilateral hearing loss, indicating that these subjects mainly had bilateral SNHL. Although symmetric hearing loss was predominant, 36.53% of children had asymmetric hearing loss. The number of subjects with symmetric hearing loss did not differ significantly between the two groups. This suggested that children with *GJB2*

mutations had varied levels of hearing loss, indicating a high degree of genetic heterogeneity.

5. Conclusion

Children with *GJB2* gene mutations have phenotypic variability in terms of their results on UNHS and their degree and symmetry of hearing loss. Hearing phenotypes were evident as normal hearing or mild-to-profound hearing loss. Subjects with T/NT mutations of the *GJB2* gene were more likely to pass UNHS and had milder hearing loss compared to those with T/T mutations. Symmetrical hearing loss was the main phenotype of the two groups, but 36.53% of children had bilateral asymmetric hearing loss. Therefore, parents of all subjects with sensorineural hearing loss were informed of the possibility that their child may have had a *GJB2* mutation. In addition, a small number of children (17.18%) passed UNHS despite having bilateral hearing loss, indicating that delayed-onset hearing loss may occur later on.

Acknowledgements

The authors wish to thank subjects and their family members for their participation in this study. This study was supported by the Beijing Natural Science Foundation (grant no. 7172052).

References

- Hilgert N, Smith RJH, Van Camp G. Function and expression pattern of nonsyndromic deafness genes. *Curr Mol Med.* 2009; 9:546-564.
- Kenneson A, Van NBK, Boyle C. *GJB2* (connexin 26) variants and nonsyndromic sensorineural hearing loss: A HuGE review. *Genet Med.* 2002; 4:258-274.
- Lucotte G, Diéterlen F. The 35delG mutation in the connexin26 gene (*GJB2*) associated with congenital deafness: European carrier frequencies and evidence for its origin in ancient Greece. *Genet Test.* 2005; 9:20-25.
- Ji Y, Lan L, Wang D, Zhao Y, Wang Q. Meta-analysis of epidemiological studies in the Chinese NSHL population with the *GJB2* mutation. *Journal of Audiology and Speech Pathology.* 2011; 19:323-327. (in Chinese)
- Li L, Lu J, Tao Z, Huang Q, Chai Y, Li X, Huang Z, Li Y, Xiang X, Yang J, Yao G, Wang Y, Yang T, Wu H. The p.V37I exclusive genotype of *GJB2*: A genetic risk indicator of postnatal permanent childhood hearing impairment. *PLoS One.* 2012; 7:e36621.
- Chan DK, Schrijver I, Chang KW. Connexin-26-associated deafness: Phenotypic variability and progression of hearing loss. *Genet Med.* 2010; 12:174-181.
- Snoeckx R, Huygen PLM, Feldman D, *et al.* *GJB2* mutations and degree of hearing loss: A multicenter study. *Am J Hum Genet.* 2005; 77:945-957.
- Dai Z, Sun B, Huang S, Kang D, Zhang X, Dong M, Yuan Y, Dai P. Audiological features of and genotype correlations with the *GJB2* mutation. *Chinese Journal of*

- Otology. 2014; 12:34-36. (in Chinese)
9. Kim S, Park G, Han K, Kim A, Koo J, Chang S, Oh S, Park W, Choi B. Prevalence of p.V37I variant of *GJB2* in mild or moderate hearing loss in a pediatric population and the interpretation of its pathogenicity. *PLoS One*. 2013; 8:e61592.
 10. Liu J, Huang L, Fu X, Liu H, Yang Y, Cheng X, Ni T. Audiological characteristics of large vestibular aqueduct syndrome in infants and young children. *J Clin Otorhinolaryngol Head Neck Surg (China)*. 2016; 30:1702-1709. (in Chinese)
 11. Mazzoli M, Van Camp G, Newton V, Giarbini N, Declau F, Parving A. Recommendations for the description of genetic and audiological data for families with nonsyndromic hereditary hearing impairment. *Audiol Med*. 2003; 1:148-150.
 12. Yu F, Han DY, Dai P, Kang D, Zhang X, Liu X, Zhu Q, Yuan Y, Sun Q, Xue D, Li M, Liu J, Yuan H, Yang W. Mutation of the *GJB2* gene in patients with nonsyndromic hearing impairment: Analysis of 1,190 cases. *Zhonghua Yi Xue Za Zhi*. 2007; 87:2814-2819. (in Chinese)
 13. Peterson MB, Willems PJ. Non-syndromic, autosomal-recessive deafness. *Clin Genet*. 2006; 69:371-392.
 14. Duman D, Tekin M. Autosomal recessive nonsyndromic deafness genes: A review. *Front Biosci (Landmark Ed)*. 2012; 17:2213-2236.
 15. Jiang Y, Huang S, Deng T, Wu L, Chen J, Kang D, Xu X, Li R, Han D, Dai P. Mutation spectrum of common deafness-causing genes in patients with non-syndromic deafness in the Xiamen Area, China. *PLoS One*. 2015; 10:e0135088.
 16. Dai P, Yu F, Han B, *et al.* *GJB2* mutation spectrum in 2063 Chinese patients with nonsyndromic hearing impairment. *J Trans Med*. 2009; 7:1-12.
 17. Norris VW, Arnos KS, Hanks WD, Xia X, Nance WE, Pandya A. Does universal newborn hearing screening identify all children with *GJB2* (Connexin 26) deafness? Penetrance of *GJB2* deafness. *Ear Hear*. 2006; 27:732-741.
 18. Minami SB, Mutai H, Nakano A, *et al.* *GJB2*-associated hearing loss undetected by hearing screening of newborns. *Gene*. 2013; 532:41-45.
 19. Wu CC, Tsai CH, Hung CC, Lin YH, Lin YH, Huang FL, Tsao PN, Su YN, Lee YL, Hsieh WS, Hsu CJ. Newborn genetic screening for hearing impairment: A population-based longitudinal study. *Genet Med*. 2017; 19:6-12.
 20. Lv J, Huang Z, Ma Y, Li Y, Mei L, Yang T, Xiang M, Chai Y, Li X, Li L, Wu H. Screening for delayed-onset hearing loss in preschool children. *Journal of Audiology and Speech Pathology*. 2013; 21:221-224. (in Chinese)
 21. Marlin S, Feldmann D, Blons H, *et al.* *GJB2* and *GJB6* mutations: Genotypic and phenotypic correlations in a large cohort of hearing impaired patients. *Arch Otolaryngol Head Neck Surg*. 2005; 131:481-487.
 22. Prera N, Lohle E, Birkenhager R. Progressive hearing impairment with deletion in *GJB2* gene despite normal newborn hearing screening. *Laryngorhinootologie*. 2014; 93:244-248. (in German)

(Received July 10, 2018; Revised August 7, 2018; Accepted August 10, 2018)

Surgical treatment for monolobular Caroli's disease – Report of a 30-year single center case series

Takamune Yamaguchi^{1,2}, Alessandra Cristaudi¹, Takashi Kokudo², Emilie Uldry¹, Nicolas Demartines^{1,*}, Nermin Halkic^{1,*}

¹Department of Visceral Surgery, University Hospital of Lausanne, Lausanne, Switzerland;

²Hepato-Biliary-Pancreatic Surgery Division and Artificial Organ and Transplantation Division Department of Surgery Graduate School of Medicine, The University of Tokyo, Tokyo, Japan.

Summary Congenital intrahepatic bile duct dilatation (Caroli's disease) is a rare biliary disease. Although multiple reports exist describing its surgical treatment, relatively few have provided long-term follow-up. Prospective data about 25 cases of monolobular Caroli's disease, with liver resection between 1974 and 2016, were retrospectively analyzed. Patient demographics together with postoperative outcomes and long-term follow-up were assessed. Our 25-patient cohort (average age 53.4 years (range: 27-82)) included 20 cases with disease limited to the left lobe, and 5 to the right. The average time interval between first symptoms and final diagnosis was 5 years (range: 0-34 years). The surgical procedures included left lobectomy in 11 cases, left hepatectomy in 8 cases, right hepatectomy in 3, and sub-segmentectomy in 3 cases. Biliodigestive anastomosis was performed in 7 cases. Complications were observed in 3 patients (25%). Metachronous cholangiocarcinoma was observed in one single case, 10 years after initial operation. In conclusion, surgical treatment for monolobular Caroli's disease is effective, with good short-term results and few complications. Median long-term follow-up was 18 months (range: 3-132), with favorable clinical evolution in 96% of patients.

Keywords: Caroli's disease, monolobular, liver resection

1. Introduction

Caroli's disease (CD), or congenital intrahepatic bile duct dilatation (IHBDD), is a rare congenital biliary disease, without obstruction, that corresponds to type V congenital bile duct cysts in the Todani classification of biliary cystic disease (1) (Figure 1).

CD was first described by Caroli and Couinaud in 1958 (2) as a mono or bilobar segmental cystic dilatation of the intrahepatic biliary tract without obstruction. In cases of monolobar disease, for unknown reason, the left lobe is more frequently affected. CD predisposes to biliary stasis, resulting in intrahepatic lithiasis and

possible septic complications that include recurrent episodes of cholangitis, liver abscesses, septicemia, and ultimately secondary biliary cirrhosis. Caroli's disease may also occur in association with congenital hepatic fibrosis and/or renal malformations. A disease variant, termed Caroli's syndrome, is diagnosed when dilatation is accompanied by symptoms of portal hypertension (3).

Further, CD is related to a 100-fold increase risk of developing intrahepatic cholangiocarcinoma (4). Therefore, surgical resection is recommended in cases of monolobar CD (5), although little is known about the long-term outcome.

The aim of the present study was to analyze short and long-term effects of liver resection in 25 patients with monolobar CD, which constitutes one of the largest single-center studies, covering a 30-year period.

2. Materials and Methods

Data of 25 adult patients diagnosed with CD, and treated at our Swiss tertiary center between January

Released online in J-STAGE as advance publication August 26, 2018.

*Address correspondence to:

Dr. Nicolas Demartines and Dr. Nermin Halkic, Department of Visceral Surgery, University Hospital of Lausanne, Rue du Bugnon 46, 1011 Lausanne, Switzerland.

E-mail: Demartines@chuv.ch, Nermin.Halkic@chuv.ch

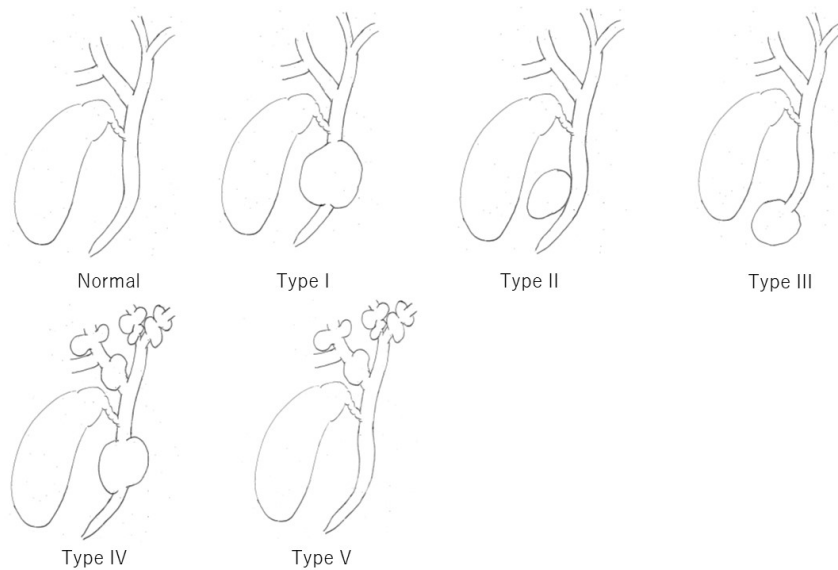


Figure 1. Todani's classification. Caroli's disease (CD) is a rare congenital biliary disease that corresponds to a type V congenital bile duct cyst according to the Todani classification.

1974 and January 2016 were collected prospectively but analyzed retrospectively. Patients' characteristics (gender, age, biological tests, etc.) are summarized in Table 1. Pre-operative imaging was, in the main, by CT, MRI, US, and cholangiography. Primary surgical outcome was our main objective. The final diagnosis of Caroli's disease was confirmed by histo-pathological analyses. The median follow-up time was 18 months (range: 3-132 months).

3. Results

Twenty-five cases of Caroli's disease were included in our analysis, 20 with disease localized to the left lobe and 5 to the right. The present cohort included 10 women and 15 men with an average age of 53.4 years (range: 27-82). The average interval between the onset of symptoms and reaching a diagnosis was 5 years (range: 0-34 years). Symptoms were nonspecific although most patients (17 cases, 68%) presented with the clinical features of cholangitis (abdominal right upper quadrant pain, fever, jaundice, or biological cholestasis). One patient presented with hepatic abscesses, and one with acute cholecystitis (associated with cholangitis due to lithiasis of the main bile duct). One patient was clinically asymptomatic with diagnosis of biological cholestasis (with elevated Gamma-GT and alkaline phosphatase (288 IU/L and 217 IU/L, respectively)) an incidental finding. Previous surgeries for this cohort included cholecystectomy (12 cases), endoscopic sphincterotomy (3 cases), biliodigestive anastomosis (3 cases), resection of a main bile duct diverticulum (1 case), and drainage of a hepatic abscess (1 case). Biliary lithiasis was identified in 20 patients (80%). For 10 (83%) of the 12 most recently treated patients, diagnoses were established by a combination

of ultrasonography, cholangiography, CT, and MRI. No detailed diagnostic data were available for earlier cases, treated between 1974 and 1997.

The surgical procedures are summarized in Table 2. Left lobectomy was performed in 10 cases, left hepatectomy in 9 cases, right hepatectomy in 3 cases, and sub-segmentectomy in 3 cases. Biliodigestive anastomosis was performed in 7 cases. This procedure was performed on the biliary convergence after resection of any bile duct tissue showing pathology up to this level.

Histopathological reports of all surgical specimens showed cystic dilatation of the segmental and subsegmental intrahepatic bile ducts, described as irregular cystic cavities ranging from a few millimeters in width to 4 cm, with thick and fibrous walls. In some cases there were also areas of stenosis between 2 adjacent cystic cavities. In all cases, cystic cavities contained black or yellow stones measuring 1 mm to 0.5 cm. In 10 cases, the hepatic parenchyma was of described as normal. In three cases, soft sections at the surface of the cystic dilatation could be depressed at finger pressure. In two cases, the liver was fibrous and pseudo-cirrhotic, which was recognized as congenital hepatic fibrosis. In one case, ectopic intrahepatic pancreatic tissue was found. The biliary epithelium was abraded, almost absent, and in some cases hyperplastic or even papillary. The portal spaces appeared fibrosed and demonstrated infiltration of inflammatory cells with newly formed bile ducts (Figure 2). In one single case (3.7%), a metachronous cholangiocarcinoma was observed 10 years after bisegmentectomy (segment V-VIII) with Roux-en-Y biliodigestive reconstruction.

In the 12 most recent cases (numbered 14 to 25), postoperative complications were rated according to the Clavien classification (6).

Table 1. Patient data and therapeutic interventions

Case	Gender, age	Year of diagnosis	Symptoms and year of onset	Year of previous interventions	Previous interventions	Gallbladder lithiasis	Site	Associated lesions	Type of resection
1	M, 34	1974	Cholangitis	1970	Cholecystectomy + choledocotomy	No	L lobe	Intrahepatic pancreatic ectopia	L lobectomy + biliojejunal anastomosis
2	M, 67	1984	Cholangitis	1977	Cholecystectomy	Yes	L lobe		L lobectomy + biliojejunal anastomosis
3	F, 45	1986	Cholangitis	1982		No	L lobe		Subsegmentectomy (III)
4	F, 68	1988	Cholangitis	1959	Cholecystectomy	Yes	L lobe		L hepatectomy
5	M, 52	1988	Cholangitis, pain		Cholecystectomy + surgical sphincterectomy	No	L lobe		L lobectomy
6	F, 68	1990	Cholangitis	1974	Cholecystectomy and resection of a diverticulum of the bile duct + biliodigestive anastomosis	No	L lobe	Diverticulum of the bile duct	L lobectomy + biliojejunal anastomosis
7	F, 30	1994	Cholangitis, pain	1994	Endoscopic sphincterectomy	Yes	L lobe		L lobectomy
8	M, 29	1994	Cholangitis	1994	Cholecystectomy	No	R lobe	Congenital hepatic fibrosis	R hepatectomy + segment I
9	M, 49	1994	None, ↑ γ-GT		None	No	R lobe		R hepatectomy (V-VI-VII)
Case	Gender, age	Year of diagnosis	Symptoms and year of onset	Year of previous interventions	Previous interventions	Gallbladder lithiasis	Site	Associated lesions	Type of resection
10	M, 62	1995	Hepatic abscess, acute pancreatitis	1984	Drainage of abscess and endoscopic sphincterectomy	Yes	L lobe		L lobectomy
11	F, 64	1996	Acute cholecystitis	1995	Cholecystectomy	Yes	R lobe	Congenital hepatic fibrosis, renal cysts	R hepatectomy + biliojejunal anastomosis
12	F, 69	1996	Cholangitis	1962	Cholecystectomy	Yes	L lobe		L lobectomy + biliojejunal anastomosis
13	F, 27	1997	Pain and recurrent jaundice	1995	Cholecystectomy + choledocotomy	No	L lobe		L lobectomy
14	M, 61	2001		2001	None	No	R lobe		Subsegmentectomy (VI-VII) + biliojejunal anastomosis
15	F, 45	2001		1999	None	No	L lobe		L lobectomy
16	M, 28	2004		1999	Cholecystectomy	Yes	L lobe		L hepatectomy
17	F, 31	2004	Cholangitis	2004	None	Yes	L lobe		L hepatectomy
Case	Gender, age	Year of diagnosis	Symptoms and year of onset	Year of previous interventions	Previous interventions	Gallbladder lithiasis	Site	Associated lesions	Type of resection
18	M, 40	2005	Cholangitis	2003	None	Yes	R lobe		Subsegmentectomy (V)
19	M, 61	2005	Cholangitis	2001	Cholecystectomy	Yes	L lobe		L hepatectomy
20	F, 29	2005		2005	None	Yes	L lobe		L lobectomy
21	M, 69	2006		2006	Cholecystectomy	Yes	L lobe		L hepatectomy
22	M, 72	2008	Cholangitis	2008	None	Yes	L lobe		L hepatectomy
23	M, 78	2008	Cholangitis	2001	Cholecystectomy	Yes	L lobe		L hepatectomy
24	M, 76	2011		2011	None	No	L lobe		L hepatectomy
25	M, 82	2015	Cholangitis	2015	None	No	L lobe		L hepatectomy

Grades 3 and 4 complication was observed in 3 patients (25%), intra-abdominal abscess, bilioma, and biliary fistula (Table 3). Post-operative 30-day mortality was zero. No precise data about complication was available for cases seen between 1974 and 1997. The median follow-up was 18 months (range: 3-132), with a favorable clinical evolution in most patients (96%).

4. Discussion

To the best of our knowledge, this present study of 25 cases collected since 1974, may be the largest monocentric series reported in Europe.

Differently as in the present series, monolobar form of CD is less commonly encountered. However, as in the present series, left lobe is more likely to be affected (8). In fact all 25 patients assessed had localized disease, with 20 patients (80%) presenting left lobe CD, and 5 patients (20%) had CD of the right lobe. The right monolobar subtype is extremely rare in the scarce literature. Without including the present cases, a literature review allowed to identify 31 cases only of right monolobar disease between 1965 and 1994 (9). In this present study, the typical CD saccular or fusiform dilatations could be observed by imaging (CT and MRI), with ultrasound (15) and CT scans thus suggesting diagnoses prior to surgery. Today, MRI is preferable for non-invasive exploration of the bile duct,

as invasive investigations like ERCP carry a risk of infection (16).

The most possible serious complication of CD is the development of cholangiocarcinoma associated with biliary stasis, in which (bile) carcinogens and chronic inflammation of the epithelium promote dysplasia. The present series describe one single case 10 year after initial CD diagnosis but a direct relation between CD and cholangiocarcinoma still need to be established. It remains hypothetical if genetic lesions in Caroli's disease patients can then ultimately lead to malignant progression.

In the present study, the average interval between becoming symptomatic and an eventual diagnosis was 5 years (range: 0-34 years). The principle clinical features of CD were atypical with abdominal pain, fever attributable to recurrent episodes of cholangitis, and jaundice. A literature review found that recurrent acute cholangitis was the most frequent mode of presentation (64% of the patients) (7,14).

In agreement with these studies, right upper quadrant pain and fever, both clinical manifestations of cholangitis, were the most frequent symptoms in our study (68%). Hepatic abscesses and recurrent episodes of jaundice (2 patients) were less commonly reported.

To explain the rarity of reports about CD, it has to be emphasized that this segmental dilatation of bile ducts has an estimated prevalence of 1/1,000,000 (7). In the absence of associated congenital hepatic fibrosis, the condition is defined as pure type Caroli's disease (2). However, a fifth of all pure CD is associated with cystic dilatation of the common bile duct, and in 6% of cases, congenital hepatic fibrosis (confirmed by histopathology), which was observed in 2 patients in the present series. Bilobar CD, affecting the entire liver, is more frequently associated with congenital hepatic fibrosis, which is responsible for portal hypertension; this condition is Caroli's syndrome and more rare, was not even observed in the present series (3).

Multiple pathogenic mechanisms have been proposed to explain CD including both embryologic and acquired factors. The bile ducts form during the 7th week of gestation following differentiation of hepatoblasts into biliary cells. These cells then envelop the vessels of the portal system to form the ductal plate. Subsequently a remodeling process takes place that separates hepatocytes and bile ducts by connective tissue, with the hepatocytes then migrating into the

Table 2. Surgical procedures

Surgical procedure	n (patients with biliojejunal anastomosis)	%
Right hepatectomy	3 (1)	12
Left hepatectomy	9 (0)	36
Left lobectomy	10 (4)	40
Subsegmentectomy	3 (1)	12

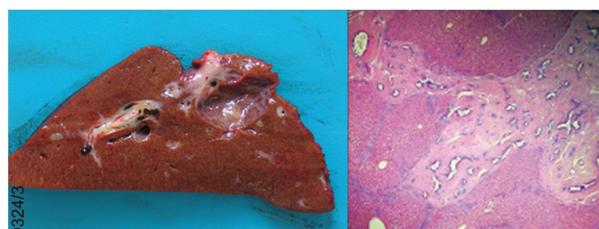


Figure 2. Pathological image. The portal spaces appear fibrosed, and demonstrate infiltration of inflammatory cells with newly formed bile ducts.

Table 3. Postoperative complications in the 12 most recent cases

Complication	Clavien-Dindo classification	Treatment	n
Intra-abdominal abscess	IIIa	Drainage	1
Bilioma	IIIa	Drainage	1
Biliary fistula	IIIa	Drainage	1
Liver hematoma	I	Observation	1
Intra-abdominal collection	II	Antibiotics	1

portal spaces. The most plausible pathologic mechanism involves an abnormality of embryonic remodeling associated with excessive cellular proliferation induced by possible genetic lesion (10).

This hypothesis is also consistent with the discontinuous and irregular dilatations of the biliary tree typical for this disease. The early onset of this genetic anomaly can result in defects in either the right or left bile ducts, or the segmental ducts (11). A later onset could induce lesion formation consistent with that seen in congenital hepatic fibrosis (12). Despite some reports of neonatal presentation (11), CD usually remains asymptomatic until early adulthood (13).

The monolobar disease types (similarly to the diffuse) are usually flagged by cholangitis aggravated by either inappropriate therapeutic interventions or opacification of the bile ducts. The discovery of an isolated lithiasis inside the bile ducts, without lithiasis of the gallbladder, or a diagnosis of cholangitis in a patient with a past history of biliary surgery, should raise a suspicion of Caroli's disease or syndrome, and prompt further investigation ideally with MRI. In the

present series, 12 patients underwent cholecystectomy before their final CD diagnosis, and in all cases the postoperative course was uneventful. There was no documented evidence of previously unrecognized damage to the common bile duct during the initial procedure, ruling out episodes of cholangitis secondary to ductal damage during surgery. The present series analysis suggests that despite its rarity, CD should be considered as differential diagnosis in case of recurrent cholangitis.

The suggested treatment for monolobar Caroli's disease remain complete resection of the affected regions. Patients with left monolobar Caroli's disease benefit from extended resection including segment IV if this segment is affected as well. For lesions in the right lobe, the extent of resection depends on the segmental anatomical distribution of the biliary ectasia. A Roux-en-Y biliodigestive anastomosis should be performed if the lesion extends to the biliary convergence, thus allowing to restore biliary discharge after surgical resection. Our institutional management algorithm for Caroli's disease is summarized in Figure 3.

While treatment of monolobar CD seems to be well defined, diffuse CD remain challenging, especially if combined approach with partial hepatectomy and biliodigestive anastomosis is impossible (17). The alternative in these advanced CD is liver transplantation as the only long-term curative option (18). However, in some well selected case, extended resection may be possible (18).

The present study has several limitations to address. The number of patients is relatively modest ($n = 25$) with a retrospective study design. However, the number of monolobar patients in this study is comparable to those detailed in some recent reports. Ulrich and Mabrut reported 40 CD (monolobar 32, bilobar 8) and 33 (monolobar 26, bilobar 7) patients, respectively (5,18).

All series with more than 20 patients with congenital intra hepatic bile duct disease treated by liver resection are summarized in Table 4 (3,5,18-20).

In conclusion, surgical resection with an observed acceptable level of post-operative morbidity and here zero mortality, should be considered treatment of choice in monolobar CD. Currently, the diagnosis of CD might be problematic and delayed, because of the complexities in accurately interpreting all symptoms. Even if rare, CD should belong to differential diagnosis of recurrent cholangitis.

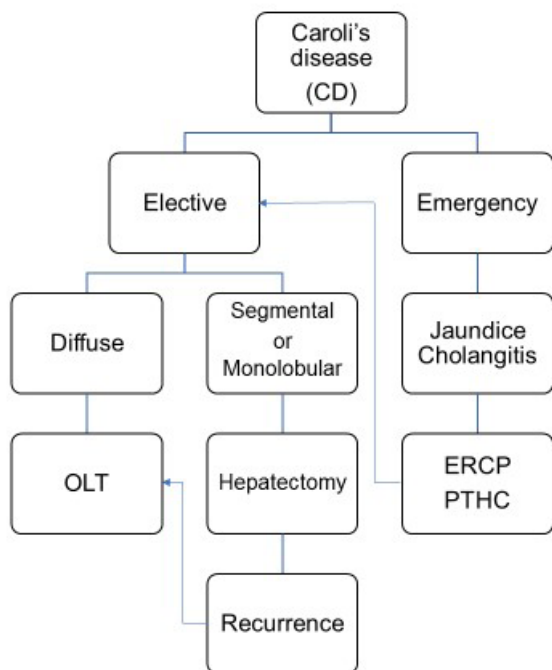


Figure 3: Treatment algorithm for Caroli's disease. ERCP: endoscopic retrograde cholangiopancreatography, PTHC: percutaneous transhepatic cholangiography, OLT: orthotopic liver transplantation

Table 4. Series exceeding 20 patients with congenital intra hepatic bile duct disease treated by liver resection

Author (year)	Patients (M/F)	Monolobar (%) (R/L)	Synchronous Carcinoma	Median follow up (months)
Kassahun <i>et al.</i> (19) (2005)	31 (15/16)	25 (81%) (13/12)	3 (9.7%)	44
Mabrut <i>et al.</i> (18) (2007)	33 (21/12)	26 (79%) (6/20)	2 (6%)	80
Ulrich <i>et al.</i> (3,5) (2002/2008)	40 (18/22)	32 (80%) (9/23)	4 (9.1%)	86.5
Mabrut <i>et al.</i> (20) (2013)	155 (89/66)	107 (69%) (16/91)	8 (5.2%)	35
Current series (2017)	25 (15/10)	25 (100%) (5/20)	0 (0%)	18

References

1. Todani T, Watanabe Y, Narusue M, Tabuchi K, Okajima K. Congenital bile duct cysts: Classification, operative procedures, and review of thirty-seven cases including cancer arising from choledochal cyst. *Am J Surg.* 1977; 134:263-269.
2. Caroli J, Couinaud C, Soupault R, Porcher P, Eteve J. A new disease, undoubtedly congenital, of the bile ducts: unilobar cystic dilation of the hepatic ducts. *Sem Hop* 1958; 34:496-502/SP. (in French)
3. Ulrich F, Steinmuller T, Settmacher U, Muller AR, Jonas S, Tullius SG, Neuhaus P. Therapy of Caroli's disease by orthotopic liver transplantation. *Transplant Proc.* 2002; 34:2279-2280.
4. Dayton MT, Longmire WP, Jr., Tompkins RK. Caroli's Disease: a premalignant condition? *Am J Surg.* 1983; 145:41-48.
5. Ulrich F, Pratschke J, Pascher A, Neumann UP, Lopez-Hanninen E, Jonas S, Neuhaus P. Long-term outcome of liver resection and transplantation for Caroli disease and syndrome. *Ann Surg.* 2008; 247:357-364.
6. Dindo D, Demartines N, Clavien PA. Classification of surgical complications: a new proposal with evaluation in a cohort of 6336 patients and results of a survey. *Ann Surg.* 2004; 240:205-213.
7. Bratu I, Laberge JM, Khalife S, Sinsky A. Regression of antenatally diagnosed localized Caroli's disease. *J Pediatr Surg.* 2000; 35:1390-1393.
8. Landen S, Bardaxoglou E, Maddern GJ, Delugeau V, Gosselin M, Launois B. Caroli's disease: A surgical dilemma. *Acta Chir Belg.* 1993; 93:224-226.
9. Benhidjeb T, Muller JM, Gellert K, Zanow J, Rudolph B. Current therapy of bile duct cysts. II. Intrahepatic cysts (Caroli syndrome). *Chirurg* 1996;67:238-243. (in German)
10. Desmet VJ. Congenital diseases of intrahepatic bile ducts: variations on the theme "ductal plate malformation". *Hepatology.* 1992; 16:1069-1083.
11. Keane F, Hadzic N, Wilkinson ML, Qureshi S, Reid C, Baker AJ, Mieli-Vergani G. Neonatal presentation of Caroli's disease. *Arch Dis Child Fetal Neonatal Ed.* 1997; 77:F145-146.
12. Waechter FL, Sampaio JA, Pinto RD, Alvares-da-Silva MR, Cardoso FG, Francisoni C, Pereira-Lima L. The role of liver transplantation in patients with Caroli's disease. *Hepatogastroenterology.* 2001; 48:672-674.
13. Longmire WP, Jr., Mandiola SA, Gordon HE. Congenital cystic disease of the liver and biliary system. *Ann Surg.* 1971; 174:711-726.
14. Caroli-Bosc FX, Demarquay JF, Conio M, Peten EP, Buckley MJ, Paolini O, Armengol-Miro JR, et al. The role of therapeutic endoscopy associated with extracorporeal shock-wave lithotripsy and bile acid treatment in the management of Caroli's disease. *Endoscopy.* 1998; 30:559-563.
15. Hara H, Morita S, Ishibashi T, Sako S, Otani M, Tanigawa N. Surgical treatment for congenital biliary dilatation, with or without intrahepatic bile duct dilatation. *Hepatogastroenterology.* 2001; 48:638-641.
16. Abdalla EK, Forsmark CE, Lauwers GY, Vauthey JN. Monolobar Caroli's Disease and cholangiocarcinoma. *HPB Surg.* 1999; 11:271-276; discussion 276-277.
17. Sans M, Rimola A, Navasa M, Grande L, Garcia-Valdecasas JC, Andreu H, Salmeron JM, Mas A, Rodés J. Liver transplantation in patients with Caroli's disease and recurrent cholangitis. *Transpl Int.* 1997; 10:241-244.
18. Mabrut JY, Partensky C, Jaeck D, Oussoultzoglou E, Baulieux J, Boillot O, Lerut J, de Ville de Goyet J, Hubert C, Otte JB, Audet M, Ducerf C, Gigot JF. Congenital intrahepatic bile duct dilatation is a potentially curable disease: Long-term results of a multi-institutional study. *Ann Surg.* 2007; 246:236-245.
19. Kassahun WT, Kahn T, Wittekind C, Mossner J, Caca K, Hauss J, Lamesch P. Caroli's disease: Liver resection and liver transplantation. Experience in 33 patients. *Surgery.* 2005; 138:888-898.
20. Mabrut JY, Kianmanesh R, Nuzzo G, et al. Surgical management of congenital intrahepatic bile duct dilatation, Caroli's disease and syndrome: Long-term results of the French Association of Surgery Multicenter Study. *Ann Surg.* 2013; 258:713-721; discussion 721.

(Received July 14, 2018; Revised August 4, 2018; Accepted August 5, 2018)

Clinical significance of respiratory compensation during exercise testing in cardiac patients

Rujie Qin¹, Akira Koike^{2,3,*}, Osamu Nagayama⁴, Yuta Takayanagi⁵, Longmei Wu³, Isao Nishi⁶, Yuko Kato⁴, Akira Sato³, Takeshi Yamashita⁴, Kazutaka Aonuma³, Masaki Ieda³

¹ Doctoral Program in Clinical Sciences, Graduate School of Comprehensive Human Science, University of Tsukuba, Tsukuba, Japan;

² Medical Science, Faculty of Medicine, University of Tsukuba, Tsukuba, Japan;

³ Department of Cardiology, Faculty of Medicine, University of Tsukuba, Tsukuba, Japan;

⁴ The Cardiovascular Institute, Tokyo, Japan;

⁵ Department of Clinical Laboratory, University of Tsukuba Hospital, Tsukuba, Japan;

⁶ Department of Cardiology, Tsuchiura Clinical Education and Training Center, University of Tsukuba, Tsuchiura, Japan.

Summary

Ventilation (VE) increases linearly with the increase of carbon dioxide output (VCO₂) during cardiopulmonary exercise testing. VE-VCO₂ slope rises in parallel with exercise intensity, reaches a turning point (called the RC point), then steepens because of respiratory compensation for lactic acidosis. While this RC point can be identified universally, it is undetectable in some patients. In this study we evaluated whether the respiratory compensation during exercise testing has clinical significance in cardiac patients. In total, 152 cardiac patients with a respiratory exchange ratio at peak exercise (peak R) of between 1.10 and 1.20 were enrolled. Cardiopulmonary parameters were compared between patients who manifested the RC point ($n = 118$) and those who did not ($n = 34$). The peak R did not significantly differ between these two groups. Compared to the patients without the RC point, those with the RC point had a higher oxygen uptake at peak exercise (peak VO₂) (20.2 ± 5.3 vs 13.6 ± 3.4 mL/min/kg, $p < 0.001$), higher anaerobic threshold (AT) (12.4 ± 3.2 vs 9.2 ± 2.3 mL/min/kg, $p < 0.001$), and lower VE-VCO₂ slope (31.7 ± 5.8 vs 37.8 ± 9.6 , $p = 0.001$). Brain natriuretic peptide (BNP) tended to be lower in the patients with the RC point (175.4 ± 364.7 vs 327.9 ± 381.1 pg/mL, $p = 0.067$). Peak VO₂, the marker of cardiopulmonary function, was found to be the independent predictor of the presence of the RC point. The present findings suggest that the phenomenon of respiratory compensation during heavy exercise indicates better cardiopulmonary function in cardiac patients within a prescribed range of effort.

Keywords: Exercise testing, respiratory compensation point, cardiac patients

1. Introduction

Cardiopulmonary exercise testing (CPX) offers clinicians the ability to obtain an abundance of information useful for the management of complex cardiovascular and pulmonary diseases (1). Five parameters noninvasively obtained from this testing

reflect the severity of heart disease and the activities of daily living in cardiac patients: the peak O₂ uptake (VO₂), anaerobic threshold (AT), rate of increase in ventilation (VE) per unit increase in CO₂ output (VCO₂) during exercise (VE-VCO₂ slope), and ratio of the increase in VO₂ to the increase in the work rate ($\Delta\text{VO}_2/\Delta\text{WR}$) (1-4). Among these parameters, the peak VO₂ reflects maximal cardiac output during exercise and is accordingly considered the main indicator of cardiopulmonary function and a gold standard in selecting patients for cardiac transplantation (1-3). However, it has a limitation and may not be accurately obtained if patients would not perform maximal effort until reaching peak exercise. The respiratory exchange

Released online in J-STAGE as advance publication August 12, 2018.

*Address correspondence to:

Dr. Akira Koike, Faculty of Medicine, University of Tsukuba, 1-1-1, Tennodai, Tsukuba, Ibaraki 305-8575, Japan.

E-mail: koike@md.tsukuba.ac.jp

ratio (R), defined as the ratio between VCO₂ and VO₂ in respiratory gas analysis, is used to evaluate a subject's effort objectively. Under current guidelines, the R of equal to or greater than 1.10 at peak exercise is generally considered an indication of excellent subject effort during CPX (1). The VE-VCO₂ slope is the rate of increase in VE per unit increase in VCO₂, and is therefore used to describe the ventilatory response to exercise.

The respiratory compensation (RC) point is an important concept in exercise physiology as it forms the boundary between the heavy and severe exercise intensity domains, a point which marks the onset of hyperventilation during incremental exercise (5,6). V-slope method is now generally used to identify the RC point (7,8). It is determined when the ratio of VE to VCO₂ starts to increase after a period of decrease or stasis, and/or when the end-tidal CO₂ pressure (PETCO₂) started to decrease after reaching a maximum level (5).

In some patients, however, no identifiable RC point is reached in the course of exercise testing, although with excellent effort. To gain further insight, we investigated whether the presence or absence of RC point during exercise testing is clinically meaningful to cardiac patients.

2. Materials and Methods

2.1. Study subjects

The subjects for this study were 416 consecutive cardiac patients who underwent CPX at the Cardiovascular Institute between January 2013 and December 2013 for the screening of cardiac disease or evaluation of exercise capacity and/or severity of heart failure. Since a peak R of equal to or greater than 1.10 is thought to reflect good exercise effort under current guidelines (1,5), we selected 152 cardiac patients with the peak R of between 1.10 to 1.20 to ensure the sufficient and similar effort by excluding patients with an R above or below that range (Table 1). The protocol and procedures for the exercise testing were approved by the Human Subjects Committee of the Cardiovascular Institute. Every patient gave his or her informed consent to participate in the study after receiving an explanation of the purposes and risks.

2.2. Exercise testing and respiratory gas analysis

An incremental symptom-limited exercise test was performed using an upright, electromagnetically braked cycle ergometer (Strength Ergo 8; Mitsubishi Electric Engineering Co., Ltd., Tokyo, Japan). The exercise test began with a 4-min rest on the ergometer followed by a 4-min warm-up at 0 or 20 W at 60 rpm. The work rate during the warm-up exercise (0 W or 20 W) was determined according to subject's habitual daily

activity. The load was then increased incrementally by 1 W every 6 s (10 W/min) or every 3 s (20 W/min). VO₂, VCO₂, and VE were measured from 4 min before the start of exercise until the end of exercise using an Aeromonitor AE-300s (Minato Medical Science, Osaka, Japan). The Aeromonitor AE-300s consists of a microcomputer, a hot-wire flow meter, and a gas analyzer composed of a sampling tube, filter, suction pump, paramagnetic oxygen cell for O₂ analysis, and infrared CO₂ analyzer. The VO₂ and VCO₂ were calculated by the Aeromonitor AE-300s breath-by-breath based on a mathematical analysis described by Beaver *et al.* (7). The concentration and flow were aligned synchronously by compensating for the time delays of the O₂ and CO₂ analyzers (flow delay from the sampling site to the analyzer plus the response time of the analyzer) with respect to the flow signal (8).

Before the parameters from the respiratory gas analysis were calculated, breath-by-breath data were interpolated to give second-by-second values. The second-by-second values thus obtained were then converted into successive 3-second averages and translated into a 5-point moving average. The peak VO₂ was calculated as the average of the values obtained during the last 15 seconds of incremental exercise. The percentage of predicted peak VO₂ (%peak VO₂) was calculated by dividing the measured peakVO₂ by the predicted peak VO₂ determined in a normal Japanese population (9). The AT was determined by V-slope analysis (7). $\Delta\text{VO}_2/\Delta\text{WR}$ was calculated by least-squares linear regression from the data recorded from 30 seconds after the start of incremental exercise to 30 seconds before the end of exercise (4). The RC point was defined as the point at which the ratio of VE to VCO₂ started to increase after a period of decrease or stasis (5). The VE-VCO₂ slope during incremental exercise was calculated from the start of incremental exercise to the RC point by least-squares linear regression, as previously described (4,5). When no RC point could be identified, the VE-VCO₂ slope was calculated from the data recorded between the start of incremental exercise to the end of the exercise (10). The left ventricular ejection fraction (LVEF) was measured by echocardiography in 139 patients (108 of whom exhibited an RC point and 31 of whom did not), and brain natriuretic peptide (BNP) was measured in 105 patients (78 of whom exhibited an RC point and 27 of whom did not).

2.3. Statistical analysis

Data are presented as the mean \pm standard deviation (SD). Student's *t* tests were used to assess differences of continuous variables between groups. χ^2 tests were used to assess differences between categorical variables. Variables were tested for their power to predict the appearance of an RC point in univariable binary logistic regression analyses. Variables with a value of $p < 0.05$

were then considered for inclusion in the multivariable models to determine independent predictors. All analyses were performed using SPSS version 22.0 software (SPSS Inc., Chicago, Illinois). A 2-sided value of $p < 0.05$ was considered statistically significant for all comparisons.

3. Results

The clinical characteristics of the study subjects are shown in Table 1. Compared to the patients who exhibited the RC point (RC group), those not exhibiting the RC point (non-RC group) were older and had lower body weight. There was no significant difference in

etiology between the two groups, and the only difference in the medications received was the prescription of diuretics. The cardiopulmonary indices of the study subjects are shown in Table 2. Compared to the non-RC patients, the RC patients had a higher peak VO₂ (20.2 ± 5.3 vs 13.6 ± 3.4 mL/min/kg, $p < 0.001$), higher %peak VO₂ (81.9 ± 19.8 vs 58.1 ± 14.8 %, $p < 0.001$), higher AT (12.4 ± 3.2 vs 9.2 ± 2.3 mL/min/kg, $p < 0.001$), and lower VE-VCO₂ slope (31.7 ± 5.8 vs 37.8 ± 9.6 , $p = 0.001$). The heart rate and blood pressure at peak exercise were also higher in the RC patients, while the BNP in the RC patients tended to be lower (175.4 ± 364.7 vs 327.9 ± 381.1 pg/mL, $p = 0.067$).

The variables were tested for their power to predict

Table 1. Clinical Characteristics of RC non-RC Patients

Characteristics	RC Patients (n = 118)	Non-RC Patients (n = 34)	p value
Age (years)	63.3 ± 12.6	69.8 ± 11.7	0.008
Male/female	99/28	25/9	NS
Height (cm)	166.9 ± 9.3	162.1 ± 7.6	0.007
Body weight (kg)	66.9 ± 13.9	58.7 ± 10.8	0.002
Body Mass Index	23.5 ± 3.5	22.2 ± 3.08	0.017
Etiology			
Valvular disease	42 (36)	16 (47)	NS
Coronary artery disease	41 (35)	12 (35)	NS
Arrhythmia	13 (11)	1 (3)	NS
Dilated cardiomyopathy	10 (8)	2 (6)	NS
Hypertrophic cardiomyopathy	4 (3)	1 (3)	NS
Other cardiovascular disease	8 (7)	2 (6)	NS
Medication			
Nitrates	14 (12)	8 (24)	NS
Calcium-channel blockers	36 (31)	12 (35)	NS
Diuretics	34 (29)	20 (59)	0.002
Digitalis	5 (4)	1 (3)	NS
β-Blockers	58 (49)	22 (65)	NS
ACEI/ ARB	23 (20)	10 (29)	NS

Data are presented as mean ± SD. NS, not significant. ACEI, angiotensin converting enzyme inhibitor; ARB, angiotensin receptor blocker.

Table 2. Cardiopulmonary Parameters

Characteristics	RC Patients (n = 118)	Non-RC Patients (n = 34)	p value
BNP (pg/mL)	175.4 ± 364.7	327.9 ± 381.1	0.067
LVEF (%)	58.0 ± 15.9	55.6 ± 19.9	NS
At rest			
Heart rate (beats/min)	74.5 ± 13.0	74.9 ± 12.5	NS
Systolic blood pressure (mmHg)	119.3 ± 16.8	117.4 ± 22	NS
Diastolic blood pressure (mmHg)	72.1 ± 12.2	68.1 ± 10.4	NS
R	0.90 ± 0.08	0.91 ± 0.06	NS
At peak exercise			
Heart rate (beats/min)	145 ± 29.3	116 ± 20.3	< 0.001
Systolic blood pressure (mmHg)	186 ± 33.6	161 ± 38.9	< 0.001
Diastolic blood pressure (mmHg)	84 ± 16.2	76 ± 13.5	0.011
R	1.15 ± 0.03	1.14 ± 0.03	NS
Peak VO ₂ (mL/min/kg)	20.2 ± 5.3	13.6 ± 3.4	< 0.001
Peak VO ₂ (%)	81.9 ± 19.8	58.1 ± 14.8	< 0.001
AT VO ₂ (mL/min/kg)	12.4 ± 3.2	9.2 ± 2.3	< 0.001
AT VO ₂ (%)	74.5 ± 18.5	55.5 ± 14.5	< 0.001
VE-VCO ₂ slope	31.7 ± 5.8	37.8 ± 9.6	0.001
ΔVO ₂ /ΔWR (mL/min/W)	9.51 ± 1.58	7.22 ± 1.56	< 0.001

Data are presented as mean ± SD. NS, not significant. BNP, brain-type natriuretic peptide; LVEF, left ventricular ejection fraction; R, gas exchange ratio; VO₂, O₂ uptake; AT, anaerobic threshold; VCO₂, CO₂ output; VE/VO₂, ventilatory equivalent for O₂; ΔVO₂/ΔWR, ratio of the increase in VO₂ to the increase in the work rate.

Table 3. Independent correlates of the RC point by logistic regression analysis

Variables	Univariable logistic regression				Multivariable logistic regression			
	OR	95% CI, Lower	95% CI, Upper	p value	OR	95% CI, Lower	95% CI, Upper	p value
Age	0.949	0.912	0.988	0.010	1.01	0.959	1.064	0.708
Height	1.060	1.015	1.107	0.009	0.959	0.883	1.041	0.319
Body weight	1.053	1.018	1.089	0.003	1.07	1.005	1.139	0.035
Peak VO ₂ (%)	1.072	1.043	1.101	<0.001	1.328	1.124	1.570	0.001
VE-VCO ₂ slope	0.886	0.832	0.943	<0.001	0.99	0.910	1.077	0.817
HR at peak exercise	1.047	1.026	1.068	<0.001	1.023	0.998	1.048	0.069
SBP at peak exercise	1.022	1.009	1.035	0.001	0.995	0.980	1.011	0.559

CI, confidence interval; OR, odds ratio. HR, heart rate; SBP, systolic blood pressure.

the appearance of the RC point. The univariable binary logistic regression analysis identified the variables of age, height, body weight, %peak VO₂, VE-VCO₂ slope, and heart rate and systolic blood pressure at peak exercise as significant prognostic indexes of the RC point (Table 3). In contrast, the multivariate logistic regression analysis identified the %peak VO₂ as a sole independent predictor of the RC point among the cardiopulmonary indices entered into the analysis.

4. Discussion

4.1. CPX and cardiopulmonary function

Parameters obtained from CPX reflect the severity of heart disease and the activities of daily living in cardiac patients (1). In 1991, Mancini *et al.* proposed that cardiac transplantation could be safely deferred in ambulatory patients with severe left ventricular dysfunction when the peak VO₂ was greater than 14 mL/min/kg (3). Since then, peak VO₂ has been considered a key index to list for cardiac transplantation. Other investigators have reported adequate evidence in support of peak VO₂ measurement for predicting prognosis (1,4). Since peak VO₂ is affected by age, sex, muscle mass and conditioning status, %peak VO₂ is suggested the superiority and widely used (1,10). The VE-VCO₂ slope, is the most widely used index of ventilatory efficiency (1,4). It ranges from approximately 24 to 34 in normal subjects and a steeper VE-VCO₂ slope is considered an indication of worse cardiopulmonary function and higher mortality (1,11). In the present study we found that the non-RC patients had a lower peak VO₂ (%) and higher VE-VCO₂ slope than the RC patients, a finding indicative of worse cardiopulmonary function and lower respiratory efficiency during exercise in the former.

4.2. VE-VCO₂ slope and respiratory compensation

Generally, as the work rate increases in a progressive exercise test, VO₂, VCO₂, and VE increase linearly with the work rate until exercise lactic acidosis develops, that is, until the AT point is reached (5). Above the AT point, VCO₂ increases more rapidly

than VO₂ because CO₂ generated by the bicarbonate buffering of lactic acid is added to the VCO₂ produced by the aerobic metabolism (5). When the work rate is increased further, the carotid bodies respond to the decreasing pH and ventilatory stimulation is intensified (12). This respiratory compensation results in a greater VE amount per VCO₂, which manifests as a steepening of the VE/VCO₂ slope and a decrease in PETCO₂. The point above which respiratory compensation occurs is referred to as the RC point (Figure 1) (5,8).

Studies of the mechanisms responsible for elevated VE-VCO₂ slope in chronic heart failure suggest that it is multifactorial (13). This steeper VE/VCO₂ slope is associated with increased ventilation-perfusion mismatching (adequate ventilation and poor perfusion) (1), reduced cardiac output during exercise (14), increased pulmonary artery and capillary wedge pressures, increased dead space/tidal volume ratio (14,15) and, more recently, an augmented chemoreceptor sensitivity (16).

4.3. The carotid body chemoreflexes and ventilatory response

The chemoreflexes are the main mechanisms of control and regulation of the ventilatory responses to the changes in arterial oxygen and CO₂ concentrations (17). The peripheral chemoreceptors located in the carotid body and aortic body, respond primarily to hypoxia via afferents to the respiratory center in the medulla oblongata and the nucleus of the solitary tract (17-19). In humans, carotid body chemosensitivity plays a dominant role in constraining variations of arterial pH in response to the acute metabolic acidosis induced by heavy exercise (19). Previous studies on chronic heart failure patients have demonstrated that the exaggerated response from peripheral chemoreceptors leads to a rapid ventilator augmentation, albeit with lower ventilatory efficiency, during exercise (18-20).

In our study, the non-RC patients showed a steeper VE/VCO₂ slope after the onset of exercise, a finding indicative of earlier and higher ventilatory response activity. Agree with Nariko Takano (21), we suppose that this hyperventilate in non-RC patients may

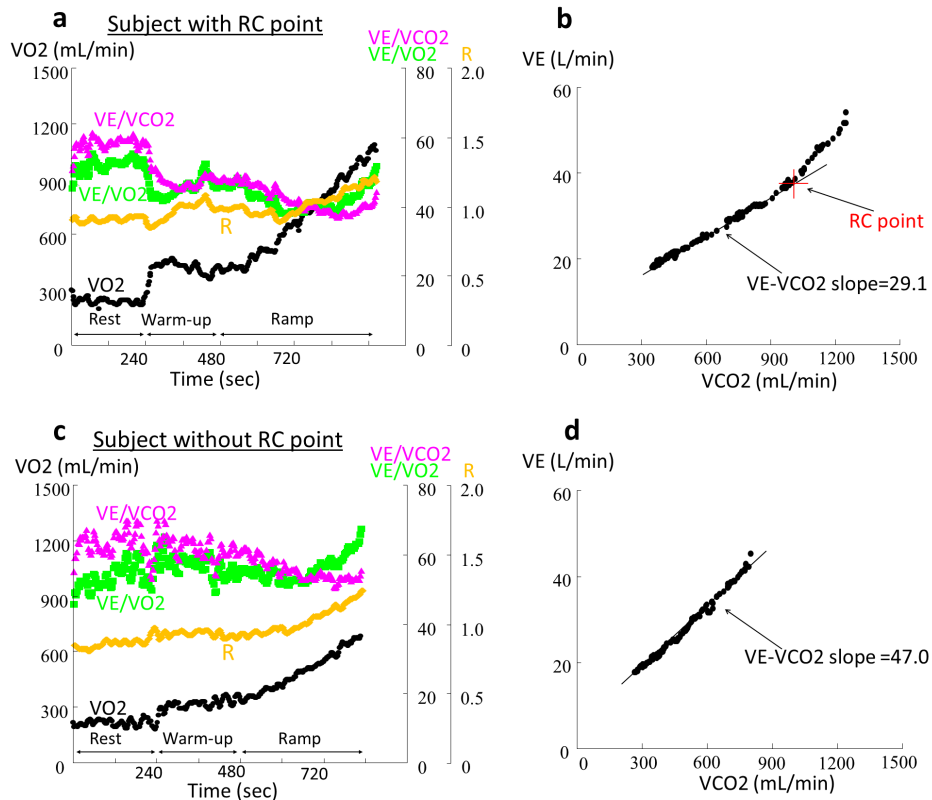


Figure 1. Panel (a) shows the parameter changes with time during incremental exercise from one RC patient; Panel (b) shows the VE/VCO₂ slope in the same patient. Panel (c) shows the parameter changes from one non-RC patient; panel (d) shows the VE-VCO₂ slope in the same patient.

attributed to the hypersensitivity of carotid body. The previous research by Nariko Takano suggest that the individuality of RC point depends partly on the rate of lactic acid increase and chemosensitivity of the carotid bodies during incremental exercise (21). The latter, in turn, may be related to sympathetic overactivity or altered central command (22,23). Animal model studies of chronic heart failure indicated that the carotid body chemoreceptors became hyperactive, resulting in an activation of the pre-sympathetic neurons in the brainstem and increases in efferent sympathetic outflow to the kidneys and heart (24,25).

Patients with worse cardiopulmonary function might tend to hyperventilate earlier before AT due to the hypersensitivity of carotid body and the lower ventilatory efficiency. Thus, in non-RC patients, their ventilatory response may not be further strengthened by carotid body during hypercapnia after AT, which might prevent them from presenting an identifiable RC point, *i.e.*, hyperventilation above the RC point.

There are several limitations to our study. According to the definition of the RC point, the appearance of the point first depends on the patient's physical effort during cardiopulmonary exercise testing. If the exercise is terminated at submaximal level, the RC point may not be reached. Thus, we selected patients with R at peak exercise in a relatively narrow range (between 1.10 to 1.20). The frequency of the appearance of respiratory

compensation must depend on the level of R achieved at peak exercise. In addition, the patients' long-term outcomes were not available for follow-up. Although our results implied the guiding significance that the absent of RC point indicates a worse cardiopulmonary function, we cannot confirm the significance of RC point in predicting mortality in cardiac patients. A further study will be worth of expecting.

In summary, the present findings suggest that the phenomenon of respiratory compensation during heavy exercise indicates better cardiopulmonary function in cardiac patients.

References

- Balady GJ, Arena R, Sietsema K, *et al.* Clinician's guide to cardiopulmonary exercise testing in adults: A scientific statement from the American Heart Association. *Circulation*. 2010; 122:191-225.
- Itoh H, Taniguchi K, Koike A, Doi M. Evaluation of severity of heart failure using ventilatory gas analysis. *Circulation*. 1990; 81:II31-II37.
- Mancini DM, Eisen H, Kussmaul W, Mull R, Edmunds LH, Wilson JR. Value of peak exercise oxygen consumption for optimal timing of cardiac transplantation in ambulatory patients with heart failure. *Circulation*. 1991; 83:778-786.
- Koike A, Itoh H, Kato M, Sawada H, Aizawa T, Fu LT, Watanabe H. Prognostic power of ventilatory responses during submaximal exercise in patients with chronic

- heart disease. *Ches*. 2002; 121:1581-1588.
5. Wasserman K, Hansen JE, Sue DY, Stringer WW, Sietsema KE, Sun XG, Whipp BJ. Principles of exercise testing and interpretation (5th ed). Lippincott Williams & Wilkins, Philadelphia, USA, 2012; pp. 85-94.
 6. Keir DA, Fontana FY, Robertson TC, Murias JM, Paterson DH, Kowalchuk JM, Pogliaghi S. Exercise Intensity Thresholds: Identifying the Boundaries of Sustainable Performance. *Med Sci Sports Exerc*. 2015; 47:1932-1940.
 7. Beaver W, Wasserman K, Whipp BJ. A new method for detecting anaerobic threshold by gas exchange. *J Appl Physiol*. 1986; 60:2020-2027.
 8. Sue DY, Hansen JE, Blais M, Wasserman K. Measurement and analysis of gas exchange during exercise using a programmable calculator. *J Appl Physiol*. 1980; 49:456-461.
 9. Itoh H, Koike A, Taniguchi K, Marumo F. Severity and pathophysiology of heart failure on the basis of anaerobic threshold (AT) and related parameters. *Jpn Circ J*. 1989; 53:146-154.
 10. Niewinski P, Engelman ZJ, Fudim M, Tubek S, Paleczny B, Jankowska EA, Banasiak W. Clinical predictors and hemodynamic consequences of elevated peripheral chemosensitivity in optimally treated men with chronic systolic heart failure. *J Card Fail*. 2013; 19:408-415.
 11. Shen Y, Zhang X, Ma W, Song H, Gong Z, Wang Q, Che L. VE/VCO₂ slope and its prognostic value in patients with chronic heart failure. *Exp Ther Med*. 2015; 9:1407-1412.
 12. Chua TP, Ponikowski P, Harrington D, Anker SD, Webb-peploe K, Clark AL, Poole-wilson PA, Coats AJS. Clinical correlates and prognostic significance of the ventilator response to exercise in chronic heart failure. *JACC*. 1997; 29:1585-1590.
 13. Sullivan MJ, Higginbotham MB, Cobb FR. Increased exercise ventilation in patients with chronic heart failure: intact ventilatory control despite haemodynamic and pulmonary abnormalities. *Circulation*. 1988; 77:552-559.
 14. Metra M, Dei Cas L, Panina G, Visioli O. Exercise hyperventilation in chronic congestive heart failure and its relation to functional capacity and hemodynamics. *Am J Cardiol*. 1992; 70:622-628.
 15. Sovijarvi AR, Naveri H, Leinonen H. Ineffective ventilation during exercise in patients with chronic congestive heart failure. *Clin Physiol*. 1992; 12:399-408.
 16. Chua TP, Clark AL, Amadi AA, Coats AJS. The relation between chemosensitivity and the increased ventilatory response to exercise in chronic heart failure. *J Am Coll Cardiol*. 1996; 27:650-657.
 17. Wasserman K, Whipp BJ, Koyal SN, Cleary MG. Effect of carotid body resection on ventilator and acid-base control during exercise. *J Appl Physiol*. 1979; 39:354-358.
 18. Barnett WH, Abdala AP, Paton JF, Rybak IA, Zoccal DB, Molkov YI. Chemoreception and neuroplasticity in respiratory circuits. *Exp Neurol*. 2017; 287:153-164.
 19. Nattie EE, Li A. Central chemoreception is a complex system function that involves multiple brainstem sites. *J Appl Physiol*. 2009; 106:1464-1466.
 20. Ciarka A, Cuyllits N, Vachery JL, Lamotte M, Degaute JP, Naeije R, van de Borne P. Increased peripheral chemoreceptors sensitivity and exercise ventilation in heart transplant recipients. *Circulation*. 2006; 113:252-257.
 21. Takano N. Respiratory compensation point during incremental exercise as related to hypoxic ventilatory chemosensitivity and lactate increase in man. *Jpn. J. Physiol*. 2000; 50:449-455.
 22. Dempsey JA, Smith CA. Pathophysiology of human ventilatory control. *Eur Respir J*. 2014; 44:495-512.
 23. Ponikowski P, Banasiak W. Chemosensitivity in chronic heart failure. *Heart Fail Monit*. 2001; 1:126-131.
 24. Despas F, Lambert E, Vaccaro A, Labrunee M, Franchitto N, Lebrin M, Galinier M, Senard JM, Lambert G, Esler M, Pathak A. Peripheral chemoreflex activation contributes to sympathetic baroreflex impairment in chronic heart failure. *J Hypertens*. 2012; 30:753-760.
 25. May CN, Yao ST, Booth LC, Ramchandra R. Cardiac sympathoexcitation in heart failure. *Auton Neurosci*. 2013; 175:76-84.
- (Received July 18, 2018; Revised August 2, 2018; Accepted August 3, 2018)

Serum cytokine profiles are altered in patients with progressive infantile hemangioma

Tomoka Yamashita, Masatoshi Jinnin*, Katsunari Makino*, Ikko Kajihara, Jun Aoi, Shinichi Masuguchi, Satoshi Fukushima, Hironobu Ihn

Department of Dermatology and Plastic Surgery, Faculty of Life Sciences, Kumamoto University, Kumamoto, Japan.

Summary Infantile hemangioma sometimes grows rapidly to a significant size around the first 2 months of life, which can be problematic and even destroy normal tissue. However, it is very difficult to predict the tumor growth at the first visit and to decide necessity of treatment. Therefore the identification of the biomarkers that can indicate a tendency to grow is clinically very important. In the present study, we evaluated the possibility that serum cytokine levels are available as the marker of hemangioma growth. Progressive hemangioma was defined as a lesion showing increased tumor size and/or coloration two weeks before and after the serum sampling, and we used membrane array to compare the twenty cytokine profiles between the sera of 3 progressive hemangioma patients and sex-/age-matched non-progressive hemangioma patients. As a result, many of the 20 cytokines were detected in the patients' sera. When a 2-fold difference in the mean levels of each group was considered meaningful, 6 of the 20 cytokines (IGF-1, IL-6, IL-8, PIGF, RANTES, TGF- β 1) were down-regulated in the progressive hemangioma group compared to the non-progressive hemangioma group, and there were statistically significant difference ($p < 0.05$): especially, IGF-1, IL-6, IL-8, PIGF, and TGF- β 1 did not expressed in all 3 progressive hemangioma patients. Accordingly, complicated cytokine network by these multiple cytokines may control the pathogenesis, and these cytokine levels may become clinically useful tumor markers. Furthermore, immunotherapy against them will be novel therapeutic approach.

Keywords: Cytokine, IGF-1, IL-8, Infantile hemangioma, RANTES

1. Introduction

Infantile hemangiomas ("strawberry marks") are a vascular tumor caused by endothelial cell proliferation, typically appear on head or face around the second week of life (1). The lesions grow till one year (proliferating phase), and slowly regress over several years (involuting phase) (2). Solitary and small lesions without cosmetic or functional problem can be managed according to 'wait and see policy' without treatment because of the

spontaneous regression. On the other hand, a part of hemangiomas grows rapidly to a significant size, which can be problematic and even destroy normal tissue (3). Such lesions cause complication (e.g. skin ulcer, a visual impairment, airway obstruction, and heart failure), or threaten life. Furthermore, larger lesions may result in the persistent scar formation, telangiectasia, fibrofatty tissue, or skin slackening (4).

As one of the clinical issues of this skin tumor, the most proliferation occurs around the first two months of life, and the majority of hemangioma growth is completed by five months of age (5). However, because the first visit to the general dermatologist may be around one month after birth, and it is very difficult to predict the tumor growth at that time and decide necessity of treatments. We often experience that a small lesion at the first visit become large and problematic at the next visit. Therefore the identification of the biomarker that can indicate a tendency to grow

Released online in J-STAGE as advance publication August 26, 2018.

*Address correspondence to:

Prof. Masatoshi Jinnin and Dr. Katsunari Makino, Department of Dermatology & Plastic Surgery, Faculty of Life Sciences, Kumamoto University, 1-1-1 Honjo, Kumamoto 860-8556, Japan.

E-mail: mjin@wakayama-med.ac.jp (MJ); katsuderma@gmail.com (KM)

Table 1. Clinical features of infantile hemangioma cases in this study

cases	age	sex	site	type	feature
1	1 month	F	cheek	superficial	progressive
2	3 month	F	eyelid	mixed	progressive
3	2 month	F	forearm	superficial	progressive
4	1 month	F	cheek	superficial	non-progressive
5	3 month	F	eyelid	deep	non-progressive
6	3 month	F	eyelid	superficial	non-progressive

is clinically very important. In the present study, we evaluated the possibility that serum cytokine levels are available as the marker of hemangioma growth using sera of patients with progressive lesions.

2. Materials and Methods

2.1. Clinical assessment and patient material

Serum samples were obtained from 3 progressive infantile hemangioma patients. Control serum samples were obtained from 3 non-progressive infantile hemangioma patients (Table 1). Progressive hemangiomas are defined as lesions showing increased tumor size and/or coloration two weeks before and after the serum sampling. Institutional review board approval and written informed consent were obtained before patients were entered into this study according to the Declaration of Helsinki. The informed consent from the guardian of the children to use the photographs for publication was also obtained.

2.2. Measurement of serum cytokine levels

Serum levels of 20 cytokines (Angiogenin, EGF, ENA-78, bFGF, GRO, IFN- γ , IGF-1, IL-6, IL-8, LEPTIN, MCP-1, PDGF-BB, PIGF, RANTES, TGF- β 1, TIMP-1, TIMP-2, Thrombopoietin, VEGF, VEGF-D) were measured with Human Angiogenesis Antibody Array-Membrane (Abcam, Cambridge, UK). Monoclonal antibody for each cytokine was precoated onto microtiter wells. Aliquots of serum were added to each well, and then incubated with cocktail of biotin-conjugated antibodies to each cytokine, after that incubated with labeled streptavidin.

2.3. Statistical analysis

Statistical analysis was carried out with Mann-Whitney's *U* test for the comparison of medians. *P* values less than 0.05 were considered significant.

3. Results and Discussion

In this study, three infants with progressive hemangioma and sex-/age-matched three non-progressive hemangioma were included: Progressive



Figure 1. Clinical pictures of infantile hemangioma patients in this study. (upper left) case 1 with progressive hemangioma at 1 month after birth; **(upper right)** case 1 with progressive hemangioma at 2 month after birth; **(lower left)** case 4 with non-progressive hemangioma at 1 month after birth; **(lower right)** case 4 with non-progressive hemangioma at 2 month after birth.

hemangiomas showed increased tumor size and color during two weeks before and after the serum sampling (Figure 1). Progressive hemangiomas were found in one-month girl on her cheek (superficial type), three-months girl on her eyelid (mixed type), and two-months girl on her forearm (superficial type). On the other hand, non-progressive hemangiomas were in one-month girl on her cheek (superficial type), three-months girl on her eyelid (deep type), and three-months girl on her eyelid (superficial type). The clinical characteristics of all patients were summarized in Table 1.

Cytokine expression profiles in sera of infantile hemangioma infants were analyzed using commercially available membrane array kits (Figure 2). Many of the 20 cytokines were detected in the patients' sera. Signal densities for each antigen-specific antibody spot were

POS	POS	NEG	NEG	angiogenin	EGF	ENA-78	bFGF
POS	POS	NEG	NEG	angiogenin	EGF	ENA-78	bFGF
GRO	IFN- γ	IGF-1	IL-6	IL-8	LEPTIN	MCP-1	PDGF-BB
GRO	IFN- γ	IGF-1	IL-6	IL-8	LEPTIN	MCP-1	PDGF-BB
PIGF	RANTES	TGF- β 1	TIMP-1	TIMP-2	TSP	VEGF	VEGF-D
PIGF	RANTES	TGF- β 1	TIMP-1	TIMP-2	TSP	VEGF	VEGF-D
BLANK	BLANK	BLANK	BLANK	BLANK	BLANK	NEG	POS
BLANK	BLANK	BLANK	BLANK	BLANK	BLANK	NEG	POS

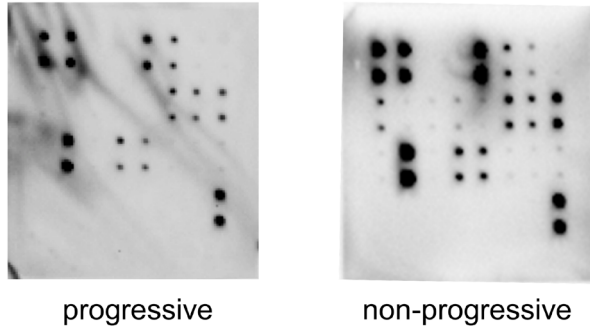


Figure 2. Results of human angiogenesis antibody array. (upper panel) array maps used in this study; (lower panel) representative membrane in each group.

obtained using 2-D densitometry, and quantitated. When a 2-fold difference in the mean levels of each group was considered meaningful, 6 of the 20 cytokines (IGF-1, IL-6, IL-8, PIGF, RANTES, TGF- β 1) were down-regulated in the progressive hemangioma group compared to the non-progressive hemangioma group, and there were statistically significant difference ($p < 0.05$, Figure 3): notably, levels of five cytokines except for RANTAS were not detected in all of progressive hemangioma group.

Various cytokine may participate in the pathogenesis of the infantile hemangioma. As an example, the involvement of VEGF, angiopoietin (6), TGF- β (7), TNF- α , and IL-1 (8) have already been reported. Furthermore, clinical significance of serum cytokine levels has also been evaluated in this disease. Serum levels of VEGF were elevated in infantile hemangioma at the proliferative or involuting phase. Serum MCP-1 and MIP-1 β can be the marker of regression (9). bFGF levels were not available for the prediction of the clinical course (10). Furthermore, Jiang *et al.* reported that angiogenin levels are increased in the sera of proliferative hemangioma (11), and suggested as the biomarker. The authors defined proliferative hemangioma or involuting hemangioma as 1-6 month age or 13-36 month age after birth, respectively, and did not describe the tendency of tumor growth. However, the duration of proliferation phase varies by individual patient.

Accordingly, the serum levels of single cytokine may not be useful to predict tumor growth, but the profile of multiple cytokines can be more sensitive tumor marker. In the present study, we tried to

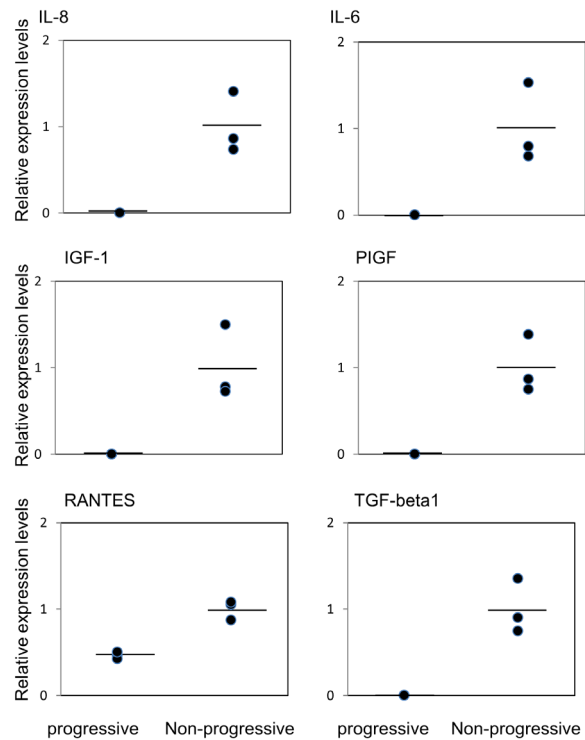


Figure 3. The cytokine expression levels measured by the array. The relative expression levels of six cytokines measured by the array using sera of progressive or non-progressive hemangioma patients are shown on the ordinate. Bars show means. * $p < 0.05$.

determine multiple serum cytokines at the same time using array experiment. Furthermore, we defined progressive hemangioma as lesions showing increased tumor size and coloration two weeks before and after the serum sampling, and compared the cytokine profiles between progressive hemangioma and non-progressive hemangioma at the similar age to really identify clinically useful tumor marker.

As a result, we demonstrated that IGF-1, IL-6, IL-8, PIGF, RANTES, and TGF- β 1 levels were significantly decreased in patient with progressive lesions: especially, IGF-1, IL-6, IL-8, PIGF, TGF- β 1 did not expressed in all 3 progressive hemangioma patients. So far, there has been no report describing involvement of IGF-1, IL-8, or RANTES in the pathogenesis of hemangioma. However, IGF-1 is reported to promote migration and tube formation of endothelial cells (12). IL-8 directly enhanced endothelial cell survival, proliferation, and regulated angiogenesis (13). RANTES is thought to have pro-angiogenic effect (14). Thus, these cytokines may positively affect tumor growth. On the other hand, IL-6 suppresses endothelial proliferation (15), whereas the expression of IL-6 is increased in tissues of proliferative hemangioma in comparison with involuting hemangioma (16). In addition, the activation of VEGF receptor 1 by PIGF promotes signal transduction of VEGF receptor 2 by VEGF and cooperatively stimulates angiogenesis. The

mRNA levels of PlGF tended to be lower in infantile hemangioma when compared to other vascular lesions (17). TGF- β 1 expresses in infantile parotid hemangioma (7), although the role are still unknown. The response of endothelial cells to TGF- β 1 is dependent upon cell types or proliferative state (18). Accordingly, complicated cytokine network by these multiple cytokines may control the pathogenesis. Unexpectedly, cytokines that positively control endothelial proliferation (IGF-1, IL-8, RANTES) is decreased in serum of the hemangioma of the proliferative phase. Although its mechanism cannot be explained by our result, for example, we speculated that negative feedback mechanism against their increased expression in tumor tissue may cause the down-regulation of serum levels.

Because this is a pilot study using small number of patient samples, larger study with increased number of cases will be necessary in future. Furthermore, immunotherapy against these cytokines may become novel therapeutic approach.

References

- Mulliken JB. A biologic approach to cutaneous vascular anomalies. *Pediatr Dermatol.* 1992; 9:356-357.
- Boye E, Yu Y, Paranya G, Mulliken JB, Olsen BR, Bischoff J. Clonality and altered behavior of endothelial cells from hemangiomas. *J Clin Invest.* 2001; 107:745-752.
- North PE, Waner M, Buckmiller L, James CA, Mihm MC Jr. Vascular tumors of infancy and childhood: beyond capillary hemangioma. *Cardiovasc Pathol.* 2006; 15:303-317.
- Jinnin M, Ishihara T, Boye E, Olsen BR. Recent progress in studies of infantile hemangioma. *J Dermatol.* 2010; 37:283-298.
- Hogeling M, Adams S, Wargon O. A randomized controlled trial of propranolol for infantile hemangiomas. *Pediatrics.* 2011; 128:e259-266.
- Yu Y, Varughese J, Brown LF, Mulliken JB, Bischoff J. Increased Tie2 expression, enhanced response to angiopoietin-1, and dysregulated angiopoietin-2 expression in hemangioma-derived endothelial cells. *Am J Pathol.* 2001; 159:2271-2280.
- Meng X, Deng CS, Wang QX, Wang TX, Liu WX. Expression and significance of pericytes and TGF- β in infantile parotid hemangioma. *Shanghai Kou Qiang Yi Xue.* 2012; 21:687-690. (in Chinese)
- Wu KQ, Muratore CS, So EY, Sun C, Dubielecka PM, Reginato AM, Liang OD. M1 Macrophage-Induced Endothelial-to-Mesenchymal Transition Promotes Infantile Hemangioma Regression. *Am J Pathol.* 2017; 187:2102-2111.
- D'Arcangelo D, Nicodemi EM, Rossi S, Giampietri C, Facchiano F, Facchiano A. Identification of serum regression signs in infantile hemangioma. *PLoS One.* 2014; 9:e88545.
- Przewratil P, Sitkiewicz A, Andrzejewska E. Serum levels of basic fibroblastic growth factor (bFGF) in children with vascular anomalies: Another insight into endothelial growth. *Clin Biochem.* 2010; 43:863-867.
- Jiang C, Lin X, Hu X, Chen H, Jin Y, Ma G, Chen D, Chen X, Gu W. Angiogenin: A potential serum marker of infantile hemangioma revealed by cDNA microarray analysis. *Plast Reconstr Surg.* 2014; 134:231e-239e.
- Bach LA. Endothelial cells and the IGF system. *J Mol Endocrinol.* 2015; 54:R1-13.
- Li A, Dubey S, Varney ML, Dave BJ, Singh RK. IL-8 directly enhanced endothelial cell survival, proliferation, and matrix metalloproteinases production and regulated angiogenesis. *J Immunol.* 2003; 170:3369-3376.
- Suffee N, Le Visage C, Hlawaty H, Aid-Launais R, Vanneaux V, Larghero J, Haddad O, Oudar O, Charnaux N, Sutton A. Pro-angiogenic effect of RANTES-loaded polysaccharide-based microparticles for a mouse ischemia therapy. *Sci Rep.* 2017; 7:13294.
- May LT, Torcia G, Cozzolino F, Ray A, Tatter SB, Santhanam U, Sehgal PB, Stern D. Interleukin-6 gene expression in human endothelial cells: RNA start sites, multiple IL-6 proteins and inhibition of proliferation. *Biochem Biophys Res Commun.* 1989; 159:991-998.
- Greenberger S, Adini I, Boscolo E, Mulliken JB, Bischoff J. Targeting NF- κ B in infantile hemangioma-derived stem cells reduces VEGF-A expression. *Angiogenesis.* 2010; 13:327-335.
- Partanen TA, Vuola P, Jauhiainen S, Lohi J, Salminen P, Pitkäranta A, Häkkinen SK, Honkonen K, Alitalo K, Ylä-Herttuala S. Neuropilin-2 and vascular endothelial growth factor receptor-3 are up-regulated in human vascular malformations. *Angiogenesis.* 2013; 16:137-146.
- Sutton AB, Canfield AE, Schor SL, Grant ME, Schor AM. 1991. The response of endothelial cells to TGF beta-1 is dependent upon cell shape, proliferative state and the nature of the substratum. *J Cell Sci.* 1991; 99 (Pt 4):777-787.

(Received May 27, 2018; Revised August 13, 2018; Accepted August 17, 2018)

Clinicopathologic characteristics of patients with tuberculosis and schizophrenia

Chao Han¹, Maoshui Wang^{2,3,*}, Yu He^{4,*}

¹Department of Geriatrics, Shandong Mental Health Center, Ji'nan, China;

²Department of Lab Medicine, Shandong Provincial Chest Hospital, Ji'nan, China;

³Department of Pediatrics, Qilu Hospital, Shandong University, Ji'nan, China;

⁴Department of Clinical Laboratory, First Affiliated Hospital of Guangxi Medical University, Nanning, China.

Summary

The clinicopathologic characteristics of patients with tuberculosis (TB) and schizophrenia are unclear. In order to facilitate early diagnosis and prompt treatment, a retrospective study was conducted in China. Subjects were 54 consecutive patients who were seen between October 2006 and December 2015. Data on demographic characteristics, underlying diseases, clinical features, and outcomes were collected from medical records using a standardized data collection form. Acid-fast bacilli were detected at a rate of 26.9%, a mycobacterial culture was positive at a rate of 35.4%, and a real-time polymerase chain reaction was positive for TB at a rate of 35%. Of the 54 patients, *i*) 44 (81.5%) had symptoms for at least 2 weeks; *ii*) 10 (18.5%) were transferred from a local psychiatric hospital, and 23 (42.6%) were transferred at least twice before arriving at this Hospital. Unfortunately, the outcome was not successful in these patients, 18 patients (33.3%) had to be retreated, 7 patients (13.0%) had their care interrupted because their schizophrenia worsened. The current study found that the management of TB in patients with schizophrenia poses several challenges. These include delays in diagnosis and treatment of TB, inefficient strategies for control of TB transmission in psychiatric hospitals, the need for a psychiatrist to be involved in care, and a high rate of retreatment.

Keywords: Tuberculosis, schizophrenia, diagnosis, treatment, outcome

Currently, tuberculosis (TB) remains one of the world's biggest threats. According to a 2017 report by the World Health Organization (WHO) (1), 10.4 million people are estimated to have contracted TB in 2016. A significant unrecognized challenge in TB care is a comorbid mental illness, such as schizophrenia, and there are several common risk factors for mental illness and TB (2).

Currently, the standard short-course chemotherapy for TB involves a 6-month regimen. Alternative

chemotherapy, which generally lasts longer than 18 months, is required for multidrug-resistant (MDR) and extensively drug-resistant TB (3,4). One major difficulty that treatment of TB shares with treatment of a mental illness is the issue of non-compliance, and especially for schizophrenics. Moreover, treatment for TB is hampered by drug interaction between antipsychotic medication and two first-line drugs (isoniazid or rifampicin) (5,6).

Improved diagnosis, treatment, and prevention of TB in patients with a mental illness will not only lower treatment costs but also help to reduce global disease transmission. In order to ascertain the clinicopathologic characteristics of patients with TB and schizophrenia, a retrospective study was conducted at Shandong Provincial Chest Hospital in China between October 2006 and December 2015. This study was approved by the ethics committee of this Hospital.

Subjects were patients diagnosed with: *i*) schizophrenia according to the Diagnostic and Statistical Manual of Mental Disorders, Fourth Ed., Text Revision

Released online in J-STAGE as advance publication August 12, 2018.

*Address correspondence to:

Dr. Maoshui Wang, Department of Lab Medicine, Shandong Provincial Chest Hospital, 46# Lishan Road, Ji'nan 250013, China.

E-mail: wangmaoshui@gmail.com

Dr. Yu He, Department of Clinical Laboratory, First Affiliated Hospital of Guangxi Medical University, Nanning 530000, China.

E-mail: heyu31@163.com

(DSM-IV-TR) or the International Classification of Diseases, 10th Revision; and *ii*) TB according to WHO criteria (7), including evaluation with chest X-rays, symptoms, microscopy, mycobacterial cultures, and a real-time polymerase chain reaction (PCR). Subjects were 54 consecutive patients (27 males, 27 females) with a mean age of 59.3 years (range, 17-90).

Data on demographic characteristics, underlying diseases, clinical features, and outcomes were collected from medical records. Due to the descriptive nature of this study, a simple description (proportion as well as mean and standard deviation) was determined for each outcome.

Table 1 shows the clinicopathologic characteristics of patients with TB and schizophrenia. Upon admission to this Hospital, 44 patients (81.5%) had symptoms for at least 2 weeks. The mean time before admission was $411 \pm 1,154$ days (range: 1 day to 20 years). Ten patients (18.5%) were transferred from a local psychiatric hospital, and 41 (75.9%) were transferred from a general hospital. A point worth noting is that 23 patients (42.6%) were transferred at least twice before arriving at this Hospital.

Acid-fast bacilli were detected at a rate of 26.9%, a mycobacterial culture was positive at a rate of 35.4%, and TB-PCR was positive at a rate of 35.0%.

Eleven patients with TB (20.4%) had diabetes mellitus. Of the 54 total patients, *i*) 11 (20.4%) had isolated extrapulmonary TB, including 6 with pleural TB; and *ii*) 43 (79.6%) had with pulmonary TB, 14 (32.6%) of whom had both pulmonary and extrapulmonary TB.

Outcomes for the 54 patients included relief of symptoms in 43 (79.6%), death in 2 (3.7%), abandonment of treatment in 2 (3.7%), and interruption of care in 7 (13.0%) because their schizophrenia worsened. Unfortunately, 18 patients (33.3%) had to be retreated.

This study yielded several important findings. First, there were delays in the diagnosis and treatment of TB in patients with schizophrenia. The healthcare facilities visited by patients may have contributed to the delay. About 20% of patients presented with symptoms (for longer than 2 weeks) at a psychiatric hospital, and close to 50% of patients were transferred at least twice before arriving at this Hospital. A point worth noting is that about 20% of patients had diabetes mellitus. In a recent study, diabetes mellitus was considered to be associated with a delay in the diagnosis of TB (8).

Second, 20% of patients were transferred from a psychiatric hospital. Close contact with such patients increases the risk of infection, especially in the event of cohabitation (9). Therefore, TB needs to be screened for and treated in a timely manner.

Third, 7 patients (13.0%) has their care interrupted because their schizophrenia worsened. This number was significantly higher than that at the local level (about

Table 1. Clinicopathologic characteristics of patients with TB and schizophrenia

Characteristics	No. of patients	%
Number	54	
Sex (male)	27	50.0
Age (years)	59.3 \pm 29.5	
HIV status (negative)	40/40	100.0
Symptoms (longer than 2 weeks)	44	81.5
Family contact of TB	8	14.8
History of smoking	12	22.2
Smoking habit (pack-years)	16.6 \pm 7.7	
Time (in days) before admission	411 \pm 1154	
Transfer		
From a local psychiatric hospital	10	18.5
From a general hospital	41	75.9
Transferred (\geq twice)	23	42.6
TB assays		
PPD (positive)	5/10	50.0
T-SPOT.TB (positive)	9/13	69.2
AFB	14/52	26.9
Mycobacterial culture	17/48	35.4
TB-PCR	14/40	35.0
Complete blood count		
White blood cell ($10^9/L$)	7.90 \pm 4.25	
Neutrophil ($10^9/L$)	5.62 \pm 3.93	
Lymphocyte ($10^9/L$)	1.37 \pm 0.75	
Monocyte ($10^9/L$)	0.75 \pm 0.44	
Eosinophil ($10^9/L$)	0.10 \pm 0.13	
Basophil ($10^9/L$)	0.01 \pm 0.01	
ESR (mm/h)	38.2 \pm 28.5	
EPTB	11/54	20.4
PTB	29/54	53.7
PTB +EPTB	14/54	25.9
Pleural	9/14	64.3
Lymph nodes	5/14	35.7
Symptoms of PTB		
Fever	23/43	53.5
Cough	33/43	76.7
Dyspnea	17/43	39.5
Abnormal imaging		
Cavitary lesions	13/43	29.5
Calcification	4/43	9.1
Outcome		
Relief of symptoms	43	79.6
Abandonment of treatment	2	3.7
Interruption of care	7	13.0
Retreatment	18	33.3
Death	2	3.7

AFB, acid-fast bacilli; EPTB, extrapulmonary tuberculosis; ESR, erythrocyte sedimentation rate; HIV, human immunodeficiency virus; PCR, polymerase chain reaction; PPD, purified protein derivative; PTB, pulmonary tuberculosis; TB, tuberculosis.

1%, data not shown). Therefore, psychiatrists need to be involved in care for TB and schizophrenia (2). Moreover, the current study indicated that patients with TB and schizophrenia have a high rate of retreatment. The overall rate of retreatment for patients with TB admitted to this Hospital was 8% (data not shown). Treatment adherence is a key factor for a positive outcome. Poor adherence is the biggest risk factor for relapse among schizophrenics and is mainly due to patients' negative attitudes towards their medication (10).

In conclusion, the current study found that treatment of TB in patients with schizophrenia poses several

challenges. These include delays in diagnosis and treatment of TB, inefficient strategies for control of TB transmission in psychiatric hospitals, the need for a psychiatrist to be involved in care, and a high rate of retreatment.

References

1. World Health Organization. Global tuberculosis report 2017. http://www.who.int/tb/publications/global_report/Exec_Summary_13Nov2017.pdf (accessed July 3, 2018).
2. Doherty AM, Kelly J, McDonald C, O'Dwyer AM, Keane J, Cooney J. A review of the interplay between tuberculosis and mental health. *Gen Hosp Psychiatry*. 2013; 35:398-406.
3. Yew WW, Lange C, Leung CC. Treatment of tuberculosis: Update 2010. *Eur Respir J*. 2011; 37:441-462.
4. Blumberg HM, Burman WJ, Chaisson RE, *et al*. American Thoracic Society/Centers for Disease Control and Prevention/Infectious Diseases Society of America: Treatment of tuberculosis. *Am J Respir Crit Care Med*. 2003; 167:603-662.
5. Angelini MC, MacCormack-Gagnon J, Dizio S. Increase in plasma levels of clozapine after addition of isoniazid. *J Clin Psychopharmacol*. 2009; 29:190-191.
6. Peritogiannis V, Pappas D, Antoniou K, Hyphantis T, Mavreas V. Clozapine-rifampicin interaction in a patient with pulmonary tuberculosis. *Gen Hosp Psychiatry*. 2007; 29:281-282.
7. World Health Organization. Case definitions: Case definitions. In: *Treatment of Tuberculosis: Guidelines* (World Health Organization, 4th edition). Geneva, Switzerland, 2010; pp. 23.
8. Chen HG, Liu M, Jiang SW, Gu FH, Huang SP, Gao TJ, Zhang ZG. Impact of diabetes on diagnostic delay for pulmonary tuberculosis in Beijing. *Int J Tuberc Lung Dis*. 2014; 18:267-271.
9. Moran-Mendoza O, Marion SA, Elwood K, Patrick D, FitzGerald JM. Risk factors for developing tuberculosis: A 12-year follow-up of contacts of tuberculosis cases. *Int J Tuberc Lung Dis*. 2010; 14:1112-1119.
10. Xiao J, Mi W, Li L, Shi Y, Zhang H. High relapse rate and poor medication adherence in the Chinese population with schizophrenia: Results from an observational survey in the People's Republic of China. *Neuropsychiatr Dis Treat*. 2015; 11:1161-1167.

(Received June 22, 2018; Revised July 3, 2018; Accepted July 23, 2018)

Erratum

DOI: 10.5582/bst.2018.E1

It has come to the authors' attention that their article entitled "The protective effects of human umbilical cord mesenchymal stem cells on damaged ovarian function: A comparative study" (*BioScience Trends. 2016; 10(4):265-276*) included an error in Figure 4 (F, H). The corrected Figure 4 is printed below.

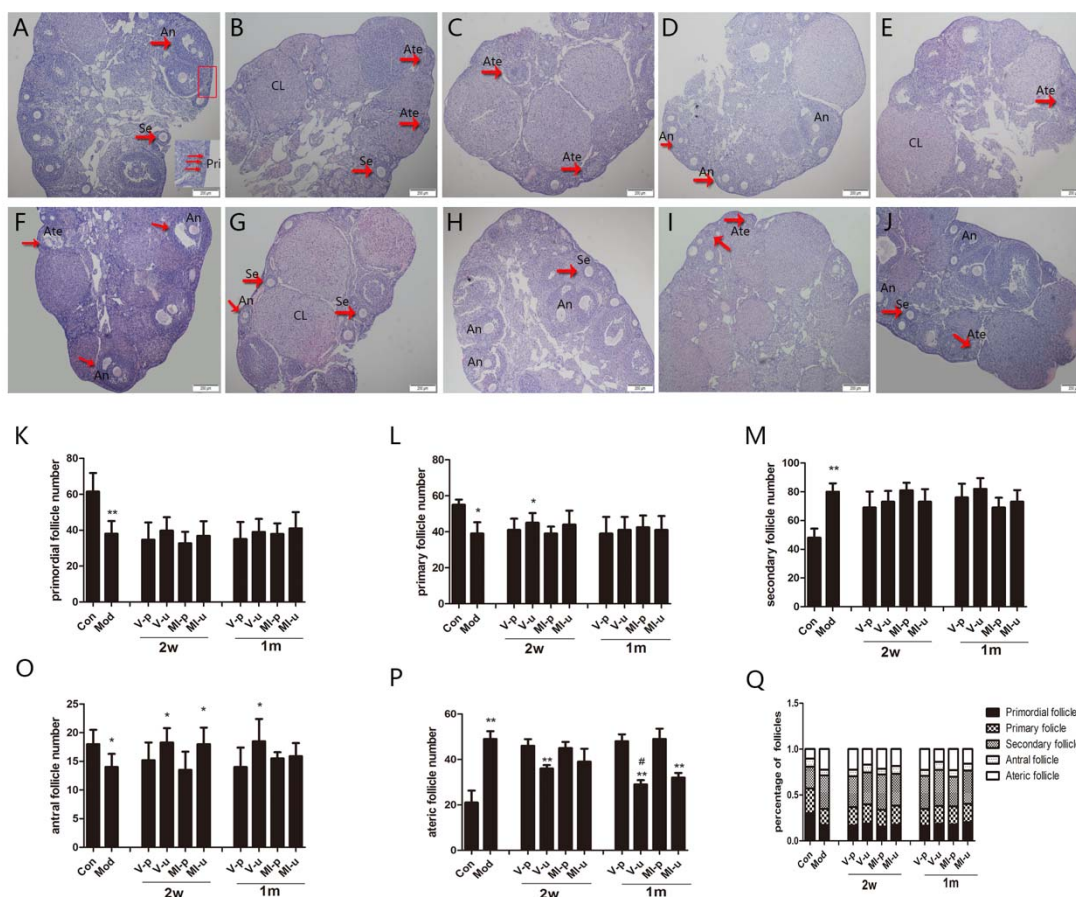


Figure 4. The effect of transplantation on follicle morphology and number in each group sequentially during various stages of development. (A-J) Representative histological images of the ovaries in each group of mice orderly (Con, Mod, v-p 2w, v-u 2w, MI-p 2w, MI-u 2w, v-p 1m, v-u 1m, MI-p 1m, MI-u 1m.). Once the model was created, the ovaries of the Mod group had fewer primordial and primary follicles compared to the NC group. However, the number of secondary follicles and atretic follicles in the Mod group increased significantly. Atretic follicles decreased and healthy antral follicles increased after treatment with hUCMSCs for 2 weeks or 1 month. Bar = 200 μ m; Pri: primordial follicles; Se: secondary follicles; An: antral follicles; Atr: atretic follicles; CL: corpus luteum. **(K-Q)** Numbers of each grade of follicles in all groups. **(K)** Primordial follicles. **(L)** Primary follicles **(M)** Secondary follicles **(O)** Antral follicles **(P)** Atretic follicles. **(Q)** The percentage of follicles in each group during various stages. The * symbol represents the Mod group versus the NC group or groups treated with hUCMSCs versus corresponding groups treated with PBS, * $p < 0.05$, ** $p < 0.01$; The # symbol represents IV-u1m group versus IV-u2w group, # $p < 0.05$.

Guide for Authors

1. Scope of Articles

BioScience Trends is an international peer-reviewed journal. BioScience Trends devotes to publishing the latest and most exciting advances in scientific research. Articles cover fields of life science such as biochemistry, molecular biology, clinical research, public health, medical care system, and social science in order to encourage cooperation and exchange among scientists and clinical researchers.

2. Submission Types

Original Articles should be well-documented, novel, and significant to the field as a whole. An Original Article should be arranged into the following sections: Title page, Abstract, Introduction, Materials and Methods, Results, Discussion, Acknowledgments, and References. Original articles should not exceed 5,000 words in length (excluding references) and should be limited to a maximum of 50 references. Articles may contain a maximum of 10 figures and/or tables.

Brief Reports definitively documenting either experimental results or informative clinical observations will be considered for publication in this category. Brief Reports are not intended for publication of incomplete or preliminary findings. Brief Reports should not exceed 3,000 words in length (excluding references) and should be limited to a maximum of 4 figures and/or tables and 30 references. A Brief Report contains the same sections as an Original Article, but the Results and Discussion sections should be combined.

Reviews should present a full and up-to-date account of recent developments within an area of research. Normally, reviews should not exceed 8,000 words in length (excluding references) and should be limited to a maximum of 100 references. Mini reviews are also accepted.

Policy Forum articles discuss research and policy issues in areas related to life science such as public health, the medical care system, and social science and may address governmental issues at district, national, and international levels of discourse. Policy Forum articles should not exceed 2,000 words in length (excluding references).

Case Reports should be detailed reports of the symptoms, signs, diagnosis, treatment, and follow-up of an individual patient. Case reports may contain a demographic profile of the patient but usually describe an unusual or novel occurrence. Unreported or unusual

side effects or adverse interactions involving medications will also be considered. Case Reports should not exceed 3,000 words in length (excluding references).

News articles should report the latest events in health sciences and medical research from around the world. News should not exceed 500 words in length.

Letters should present considered opinions in response to articles published in BioScience Trends in the last 6 months or issues of general interest. Letters should not exceed 800 words in length and may contain a maximum of 10 references.

3. Editorial Policies

Ethics: BioScience Trends requires that authors of reports of investigations in humans or animals indicate that those studies were formally approved by a relevant ethics committee or review board.

Conflict of Interest: All authors are required to disclose any actual or potential conflict of interest including financial interests or relationships with other people or organizations that might raise questions of bias in the work reported. If no conflict of interest exists for each author, please state "There is no conflict of interest to disclose".

Submission Declaration: When a manuscript is considered for submission to BioScience Trends, the authors should confirm that 1) no part of this manuscript is currently under consideration for publication elsewhere; 2) this manuscript does not contain the same information in whole or in part as manuscripts that have been published, accepted, or are under review elsewhere, except in the form of an abstract, a letter to the editor, or part of a published lecture or academic thesis; 3) authorization for publication has been obtained from the authors' employer or institution; and 4) all contributing authors have agreed to submit this manuscript.

Cover Letter: The manuscript must be accompanied by a cover letter signed by the corresponding author on behalf of all authors. The letter should indicate the basic findings of the work and their significance. The letter should also include a statement affirming that all authors concur with the submission and that the material submitted for publication has not been published previously or is not under consideration for publication elsewhere. The cover letter should be submitted in PDF format. For example of Cover Letter, please visit <http://www.biosciencetrends.com/downcentre.php> (Download Centre).

Copyright: A signed JOURNAL PUBLISHING AGREEMENT (JPA) form must be provided by post, fax, or as a scanned file before acceptance of the article. Only forms with a hand-written signature are accepted. This copyright will ensure the widest possible dissemination of information. A form facilitating transfer of copyright can be downloaded by clicking the

appropriate link and can be returned to the e-mail address or fax number noted on the form (Please visit [Download Centre](#)). Please note that your manuscript will not proceed to the next step in publication until the JPA Form is received. In addition, if excerpts from other copyrighted works are included, the author(s) must obtain written permission from the copyright owners and credit the source(s) in the article.

Suggested Reviewers: A list of up to 3 reviewers who are qualified to assess the scientific merit of the study is welcomed. Reviewer information including names, affiliations, addresses, and e-mail should be provided at the same time the manuscript is submitted online. Please do not suggest reviewers with known conflicts of interest, including participants or anyone with a stake in the proposed research; anyone from the same institution; former students, advisors, or research collaborators (within the last three years); or close personal contacts. Please note that the Editor-in-Chief may accept one or more of the proposed reviewers or may request a review by other qualified persons.

Language Editing: Manuscripts prepared by authors whose native language is not English should have their work proofread by a native English speaker before submission. If not, this might delay the publication of your manuscript in BioScience Trends.

The Editing Support Organization can provide English proofreading, Japanese-English translation, and Chinese-English translation services to authors who want to publish in BioScience Trends and need assistance before submitting a manuscript. Authors can visit this organization directly at <http://www.iacmhr.com/iac-eso/support.php?lang=en>. IAC-ESO was established to facilitate manuscript preparation by researchers whose native language is not English and to help edit works intended for international academic journals.

4. Manuscript Preparation

Manuscripts should be written in clear, grammatically correct English and submitted as a Microsoft Word file in a single-column format. Manuscripts must be paginated and typed in 12-point Times New Roman font with 24-point line spacing. Please do not embed figures in the text. Abbreviations should be used as little as possible and should be explained at first mention unless the term is a well-known abbreviation (e.g. DNA). Single words should not be abbreviated.

Title Page: The title page must include 1) the title of the paper (Please note the title should be short, informative, and contain the major key words); 2) full name(s) and affiliation(s) of the author(s), 3) abbreviated names of the author(s), 4) full name, mailing address, telephone/fax numbers, and e-mail address of the corresponding author; and 5) conflicts of interest (if you have an actual or potential conflict of interest to disclose, it must be included as a footnote on the title page of the manuscript; if no conflict of

interest exists for each author, please state "There is no conflict of interest to disclose"). Please visit [Download Centre](#) and refer to the title page of the manuscript sample.

Abstract: The abstract should briefly state the purpose of the study, methods, main findings, and conclusions. For article types including Original Article, Brief Report, Review, Policy Forum, and Case Report, a one-paragraph abstract consisting of no more than 250 words must be included in the manuscript. For News and Letters, a brief summary of main content in 150 words or fewer should be included in the manuscript. Abbreviations must be kept to a minimum and non-standard abbreviations explained in brackets at first mention. References should be avoided in the abstract. Key words or phrases that do not occur in the title should be included in the Abstract page.

Introduction: The introduction should be a concise statement of the basis for the study and its scientific context.

Materials and Methods: The description should be brief but with sufficient detail to enable others to reproduce the experiments. Procedures that have been published previously should not be described in detail but appropriate references should simply be cited. Only new and significant modifications of previously published procedures require complete description. Names of products and manufacturers with their locations (city and state/country) should be given and sources of animals and cell lines should always be indicated. All clinical investigations must have been conducted in accordance with Declaration of Helsinki principles. All human and animal studies must have been approved by the appropriate institutional review board(s) and a specific declaration of approval must be made within this section.

Results: The description of the experimental results should be succinct but in sufficient detail to allow the experiments to be analyzed and interpreted by an independent reader. If necessary, subheadings may be used for an orderly presentation. All figures and tables must be referred to in the text.

Discussion: The data should be interpreted concisely without repeating material already presented in the Results section. Speculation is permissible, but it must be well-founded, and discussion of the wider implications of the findings is encouraged. Conclusions derived from the study should be included in this section.

Acknowledgments: All funding sources should be credited in the Acknowledgments section. In addition, people who contributed to the work but who do not meet the criteria for authors should be listed along with their contributions.

References: References should be numbered in the order in which they appear in the text. Citing of unpublished results, personal communications, conference abstracts, and theses in the reference list is not recommended but these sources may be mentioned in the text. In the reference list,

cite the names of all authors when there are fifteen or fewer authors; if there are sixteen or more authors, list the first three followed by *et al.* Names of journals should be abbreviated in the style used in PubMed. Authors are responsible for the accuracy of the references. Examples are given below:

Example 1 (Sample journal reference): Inagaki Y, Tang W, Zhang L, Du GH, Xu WF, Kokudo N. Novel aminopeptidase N (APN/CD13) inhibitor 24F can suppress invasion of hepatocellular carcinoma cells as well as angiogenesis. *Biosci Trends*. 2010; 4:56-60.

Example 2 (Sample journal reference with more than 15 authors): Darby S, Hill D, Auvinen A, *et al.* Radon in homes and risk of lung cancer: Collaborative analysis of individual data from 13 European case-control studies. *BMJ*. 2005; 330:223.

Example 3 (Sample book reference): Shalev AY. Post-traumatic stress disorder: diagnosis, history and life course. In: Post-traumatic Stress Disorder, Diagnosis, Management and Treatment (Nutt DJ, Davidson JR, Zohar J, eds.). Martin Dunitz, London, UK, 2000; pp. 1-15.

Example 4 (Sample web page reference): Ministry of Health, Labour and Welfare of Japan. Dietary reference intakes for Japanese. <http://www.mhlw.go.jp/houdou/2004/11/h1122-2a.html> (accessed June 14, 2010).

Tables: All tables should be prepared in Microsoft Word or Excel and should be arranged at the end of the manuscript after the References section. Please note that tables should not be image format. All tables should have a concise title and should be numbered consecutively with Arabic numerals. If necessary, additional information should be given below the table.

Figure Legend: The figure legend should be typed on a separate page of the main manuscript and should include a short title and explanation. The legend should be concise but comprehensive and should be understood without referring to the text. Symbols used in figures must be explained.

Figure Preparation: All figures should be clear and cited in numerical order in the text. Figures must fit a one- or two-column format on the journal page: 8.3 cm (3.3 in.) wide for a single column, 17.3 cm (6.8 in.) wide for a double column; maximum height: 24.0 cm (9.5 in.). Please make sure that the symbols and numbers appeared in the figures should be clear. Please make sure that artwork files are in an acceptable format (TIFF or JPEG) at minimum resolution (600 dpi for illustrations, graphs, and annotated artwork, and 300 dpi for micrographs and photographs). Please provide all figures as separate files. Please note that low-resolution images are one of the leading causes of article resubmission and schedule delays. All color figures will be reproduced in full color in the online edition of the journal at no cost to authors.

Units and Symbols: Units and symbols

conforming to the International System of Units (SI) should be used for physicochemical quantities. Solidus notation (*e.g.* mg/kg, mg/mL, mol/mm²/min) should be used. Please refer to the SI Guide www.bipm.org/en/si/ for standard units.

Supplemental data: Supplemental data might be useful for supporting and enhancing your scientific research and BioScience Trends accepts the submission of these materials which will be only published online alongside the electronic version of your article. Supplemental files (figures, tables, and other text materials) should be prepared according to the above guidelines, numbered in Arabic numerals (*e.g.*, Figure S1, Figure S2, and Table S1, Table S2) and referred to in the text. All figures and tables should have titles and legends. All figure legends, tables and supplemental text materials should be placed at the end of the paper. Please note all of these supplemental data should be provided at the time of initial submission and note that the editors reserve the right to limit the size and length of Supplemental Data.

5. Submission Checklist

The Submission Checklist will be useful during the final checking of a manuscript prior to sending it to BioScience Trends for review. Please visit [Download Centre](#) and download the Submission Checklist file.

6. Online Submission

Manuscripts should be submitted to BioScience Trends online at <http://www.biosciencetrends.com>. The manuscript file should be smaller than 5 MB in size. If for any reason you are unable to submit a file online, please contact the Editorial Office by e-mail at office@biosciencetrends.com.

7. Accepted Manuscripts

Proofs: Galley proofs in PDF format will be sent to the corresponding author via e-mail. Corrections must be returned to the editor (proof-editing@biosciencetrends.com) within 3 working days.

Offprints: Authors will be provided with electronic offprints of their article. Paper offprints can be ordered at prices quoted on the order form that accompanies the proofs.

Page Charge: Page charges will be levied on all manuscripts accepted for publication in BioScience Trends (\$140 per page for black white pages; \$340 per page for color pages). Under exceptional circumstances, the author(s) may apply to the editorial office for a waiver of the publication charges at the time of submission.

(Revised February 2013)

Editorial and Head Office:

Pearl City Koishikawa 603
2-4-5 Kasuga, Bunkyo-ku
Tokyo 112-0003 Japan
Tel: +81-3-5840-8764
Fax: +81-3-5840-8765
E-mail: office@biosciencetrends.com

JOURNAL PUBLISHING AGREEMENT (JPA)

Manuscript No.:

Title:

Corresponding Author:

The International Advancement Center for Medicine & Health Research Co., Ltd. (IACMHR Co., Ltd.) is pleased to accept the above article for publication in BioScience Trends. The International Research and Cooperation Association for Bio & Socio-Sciences Advancement (IRCA-BSSA) reserves all rights to the published article. Your written acceptance of this JOURNAL PUBLISHING AGREEMENT is required before the article can be published. Please read this form carefully and sign it if you agree to its terms. The signed JOURNAL PUBLISHING AGREEMENT should be sent to the BioScience Trends office (Pearl City Koishikawa 603, 2-4-5 Kasuga, Bunkyo-ku, Tokyo 112-0003, Japan; E-mail: office@biosciencetrends.com; Tel: +81-3-5840-8764; Fax: +81-3-5840-8765).

1. Authorship Criteria

As the corresponding author, I certify on behalf of all of the authors that:

- 1) The article is an original work and does not involve fraud, fabrication, or plagiarism.
- 2) The article has not been published previously and is not currently under consideration for publication elsewhere. If accepted by BioScience Trends, the article will not be submitted for publication to any other journal.
- 3) The article contains no libelous or other unlawful statements and does not contain any materials that infringes upon individual privacy or proprietary rights or any statutory copyright.
- 4) I have obtained written permission from copyright owners for any excerpts from copyrighted works that are included and have credited the sources in my article.
- 5) All authors have made significant contributions to the study including the conception and design of this work, the analysis of the data, and the writing of the manuscript.
- 6) All authors have reviewed this manuscript and take responsibility for its content and approve its publication.
- 7) I have informed all of the authors of the terms of this publishing agreement and I am signing on their behalf as their agent.

2. Copyright Transfer Agreement

I hereby assign and transfer to IACMHR Co., Ltd. all exclusive rights of copyright ownership to the above work in the journal BioScience Trends, including but not limited to the right 1) to publish, republish, derivate, distribute, transmit, sell, and otherwise use the work and other related material worldwide, in whole or in part, in all languages, in electronic, printed, or any other forms of media now known or hereafter developed and the right 2) to authorize or license third parties to do any of the above.

I understand that these exclusive rights will become the property of IACMHR Co., Ltd., from the date the article is accepted for publication in the journal BioScience Trends. I also understand that IACMHR Co., Ltd. as a copyright owner has sole authority to license and permit reproductions of the article.

I understand that except for copyright, other proprietary rights related to the Work (e.g. patent or other rights to any process or procedure) shall be retained by the authors. To reproduce any text, figures, tables, or illustrations from this Work in future works of their own, the authors must obtain written permission from IACMHR Co., Ltd.; such permission cannot be unreasonably withheld by IACMHR Co., Ltd.

3. Conflict of Interest Disclosure

I confirm that all funding sources supporting the work and all institutions or people who contributed to the work but who do not meet the criteria for authors are acknowledged. I also confirm that all commercial affiliations, stock ownership, equity interests, or patent-licensing arrangements that could be considered to pose a financial conflict of interest in connection with the article have been disclosed.

Corresponding Author's Name (Signature):

Date:

